STATISTICAL ANALYSIS OF FORCE DISTRIBUTION ON THE PLANTAR FOOT DURING QUIET STANCE

A THESIS SUBMITTED TO
THE GRADUATE SCHOOL OF NATURAL AND APPLIED SCIENCES
OF
MIDDLE EAST TECHNICAL UNIVERSITY

BY

OKAN ALKAN

IN PARTIAL FULFILLMENT OF THE REQUIREMENTS
FOR
THE DEGREE OF DOCTOR OF PHILOSOPHY
IN
ENGINEERING SCIENCES

SEPTEMBER 2015

Approval of the thesis:

STATISTICAL ANALYSIS OF FORCE DISTRIBUTION ON THE PLANTAR FOOT DURING QUIET STANCE

submitted by **OKAN ALKAN** in partial fulfillment of the requirements for the degree of **Doctor of Philosophy in Engineering Sciences Department, Middle East Technical University** by,

Prof. Dr. Gülbin Dural Ünver ____________________
Dean, Graduate School of **Natural and Applied Sciences**

Prof. Dr. Murat Dicleli ____________________
Head of Department, **Engineering Sciences**

Assoc. Prof. Dr. Senih Gürses ____________________
Supervisor, **Engineering Sciences Dept., METU**

Prof. Dr. Hakan I. Tarman ____________________
Co-Supervisor, **Engineering Sciences Dept., METU**

Examining Committee Members:

Prof. Dr. Bülent E. Platin ____________________
Mechanical Engineering Dept., METU

Assoc. Prof. Dr. Senih Gürses ____________________
Engineering Sciences Dept., METU

Assoc. Prof. Dr. Ferhat Akgül ____________________
Engineering Sciences Dept., METU

Assoc. Prof. Dr. Murat Zinnuroğlu ____________________
Physical Medicine and Rehabilitation Dept., Gazi Uni.

Assoc. Prof. Dr. Bülent Cengiz ____________________
Neurology Dept., Gazi Uni.

Date: September 10, 2015

I hereby declare that all information in this document has been obtained and presented in accordance with academic rules and ethical conduct. I also declare that, as required by these rules and conduct, I have fully cited and referenced all material and results that are not original to this work.

Name, Last name: OKAN ALKAN

Signature:

ABSTRACT

STATISTICAL ANALYSIS OF FORCE DISTRIBUTION ON THE PLANTAR FOOT DURING QUIET STANCE

Alkan, Okan
Ph.D., Department of Engineering Sciences
Supervisor: Assoc. Prof. Dr. Senih Gürses
Co-Supervisor: Prof. Dr. Hakan I. Tarman

September 2015, 171 pages

In most of the posture studies, foot is considered as a single rigid body. However, recent works focused on multi-segmented kinematic foot models and ground reaction force distribution beneath the feet. This thesis presents a study on the role of the foot as a deformable body for controlling the human erect posture. A pressure-pad and a force platform were used in order to determine the distribution of ground reaction forces (GRF). Pressure distribution data beneath the feet of seven male and female right-handed subjects were analyzed. 180-second long quiet stance data was collected from the subjects during the eyes-closed and eyes-open conditions in three repetitions. Measurements from the data were computed in both time and frequency domains. The surface of the foot projected to the horizontal plane has been divided into three regions; heel region (talus and calcaneus bone included), medial longitudinal arc region (the navicular, the cuboid and three cuneiforms), and five metatarsal bones and phalanges region, respectively named as hind, mid, and front regions. In time domain, mean and the variance measurements were taken for the pressure distribution at each section of the both feet and cross correlation values of each possible combination of the three-foot regions. In frequency domain, auto and cross power spectral density estimations and coherence function between normal force distribution signals at each possible paired combination of the three-foot regions were computed. We have found that mutual interactions in between the predefined foot regions were different. Furthermore, we observed a particular load shifting behavior in time, especially between hind and

modified front foot regions, which showed substantial differences with respect to gender and left versus right foot. A mathematical model for human erect posture has been developed where a deformable foot is used in order to drive and control the human inertial body mass. The parameters of the model were estimated by analyzing the experimental data.

Keywords: Quiet Stance, Plantar pressure distribution, Ground reaction forces, Load shifting mechanism, regions of the foot.

ÖZ

SAKİN DURUŞ SIRASINDA AYAK TABANINDAKİ KUVVET DAĞILIMLARININ İSTATİSTİKSEL ANALİZİ

Alkan, Okan
Doktora., Mühendislik Bilimleri Bölümü
Tez Yöneticisi : Doç. Dr. Senih Gürses
Ortak Tez Yöneticisi: Prof. Dr. Hakan I. Tarman
Eylül 2015, 171 pages

Postür çalışmalarının pek çoğunda ayak rijit tek bir cisim olarak ele alınırdı. Bununla birlikte en son çalışmalarda çok parçalı kinematik ayak modelleri ve zemin reaksiyon kuvvetleri üzerinde odaklanılmıştır. İnsan dik duruşunun kontrol edilmesine, ayağın rolünü deforme olabilen bir cisim şeklinde ele alarak çalışmalarımıza başladık. Ayaktaki zemin reaksiyon kuvvetlerinin (GRF) belirlenmesi amacıyla Basınç-pedi ve kuvvet platformu kombinasyonu kullanılmıştır. Sağ ellerini kullanan yedi eril ve dişinin ayakları altındaki basınç dağılımı verileri analiz edildi. Şahıslardan gözleri kapalı ve açık şartlarında 180-saniye üç tekrarlı olarak veri toplandı. Alınan veriler zaman ve frekans uzayında analiz edildi. Ayağın alt yüzeyi, yatay düzleme yansıtılarak üç bölgeye ayrıldı; topuk bölgesi(talus ve kalkaneus kemikleri dahil edildi), Medial longitüdinal ark bölgesi (navikuler, küboid ve üç kuneiform), ve beş metatarsal kemikler ile parmaklar, sırasıyla arka, orta ve ön ayak bölgesi olarak isimlendirilmiştir. Zaman uzayındaki metrikler her iki ayağa ait üç bölgenin basınç dağılımının ortalaması, varyansı ve birbirlerine göre çapraz korelasyonlarıdır. Frekans uzayında ise oto ve çapraz güç izgesel yoğunluk fonksiyonları ve koherens değerleri hesaplandı. Cinsiyet farkının postürde önemli olduğu, tanımlanan ayak bölgelerinin birbirleriyle olan ilişkilerinde, eril ve dişiler arasında, sağ ve sol ayak arasında farklılar olduğu gözlemlenmiştir. Her iki ayakta ve hem erkek ve hem de dişilerde ayağın ön ve arka bölgeleri arasında dik insan postürünün kontroluna katkıda bulunabilecek, yük aktarım mekanizması diye adlandırılan fizyolojik bir mekanizma gözlemlendi.

Deneysel çalışmadan elde edilen bulgular, deforme olabilen ayak modeli kullanılarak dik postürü kontrol edebilecek şekilde matematiksel olarak modellenmiştir.

Anahtar Kelimeler: Sakin duruş postürü, ayak tabanı basınç dağılımı, Yer tepki kuvvetleri, Yük aktarma mekanizması, ayağın bölgeleri.

To my wife Didem, my daughter Duru
and my parents.

ACKNOWLEDGMENTS

I would like to express deepest gratitude to my supervisor Assoc. Prof. Dr. Senih Gürses and my co-supervisor Prof. Dr. Hakan I. Tarman for their guidance, advice, criticism, encouragements and insight throughout the research. Especially, for my supervisor Assoc. Prof. Dr. Senih Gürses, believing and constantly encouraging me when harsh times were present and when I am down thus, realizing this thesis to be possible.

I would also like to express my deepest gratitude to Prof. Dr. Bülent E. Platin, and Assoc. Prof. Dr. Ferhat Akgül, for their precious suggestions, comments and constant guidance. I would like to thank also to Prof. Dr. Kemal ÖZGÖREN, and Prof. Dr. Yalçın Mengi, for their valuable suggestions and comments.

Thanks for the Middle East Technical University, Modeling and Simulation Center (MODSIMMER) supplying laboratory and experimental environment.

Technical assistance and friendship of Emre Akçay and Roshanak Akbarifar, our Department secretaries Ms. Zehra Kabakcı and Ms. Leyla Kaya is gratefully acknowledged for their support.

I would like to express my deepest gratitude to my wife Didem Alkan; since without her indefatigable help and encouragement, I would not do that. Acknowledges goes for my daughter Duru Alkan, even in her small age, her patience to be staying away from her father, when needed most, while I work for the thesis topics in long nights and days of six years.

TABLE OF CONTENTS

LIST OF TABLES

TABLES

LIST OF FIGURES

FIGURES

LIST OF ABBREVIATIONS AND SYMBOLS

COM :	Center Of Mass
COG :	Center Of Gravity
COP :	Center Of Pressure
COP_x :	Component of COP on x-direction
COP_y :	Component of COP on y-direction
AP :	Antero - Posterior
ML :	Medio – Lateral
PA :	Plantar Aponeurosis
GRF :	Ground reaction forces
EO :	Eyes Open
EC :	Eyes Closed
M :	Male
F :	Female
LF:	Left Foot
RF:	Right Foot
L :	Left
R :	RIGHT
F :	Front Foot(Modified)
H :	Hind Foot
M :	Mid Foot
FFT	Fast Fourier Transform
ANOVA:	Analysis of Variances
5D:	Five Dimensional (in terms of ANOVA)
3D:	Three Dimensional (in terms of ANOVA)
R_{xx} :	Correlation function
R_{xy} :	Cross Correlation function
C_{xx}, C_{xy} :	Covariance function
μ_x, μ_y	Mean values of x and y
σ_X	Standard deviation

ρ_{XY}	Cross covariation function
μ_k	Spectral Moments
f	Frequency in Hz.
$G_x(f)$	Power Spectral Density function
POWER:	Total power –area of the power spectrum
CFREQ :	Centrodial Frequency
FREQD :	Frequency Dispersion
γ^2_{XY} **:**	Coherence function
A:	Ankle joint
A_x**:**	Component of force on ankle joint in x direction
A_y**:**	Component of force on ankle joint in y direction
C:	Calcaneous tuberosity
C_x**:**	Component of force on calcaneous in x direction
C_y**:**	Component of force inserted on calcaneous in y direction
M:	Metatarsals
M_x**:**	Component of force on metatarsals in x direction
M_y**:**	Component of force on metatarsals in y direction
$S(t)$**:**	Length of plantar aponeurosis as function of time
$S_{G3}(t)$**:**	Virtual distance from C to COM as function of time
T_3 **and** T_3^R**:**	Reactive Torque
T_3^1**:**	Component of Reactive Torque on l_1
T_3^2**:**	Component of Reactive Torque on l_2
α**:**	Proportion of reactive torque on link l_2
β**:**	Proportion of reactive torque on link l_1
θ_2**:**	Angle of l_2 with respect to ground
θ_{21}**:**	Angle of l_1 with respect to ground
θ_3**:**	Angle of l_3 with respect to ground
θ_{G3}**:**	Angle of S_{G3} with respect to ground
δU**:**	Virtual Work Equation
$\delta\theta_n$**:**	Virtual displacement of angle θ with respect to number n

b:	Damping coefficient of PA
k:	Stiffness coefficient of PA
bt:	Damping coefficient of reactive Torque T_3
kt:	Stiffness coefficient of reactive Torque T_3
$\boldsymbol{F_{PA}}$**:**	Tensile force on PA
$\boldsymbol{m_3}$**:**	Concentrated mass of body
$\boldsymbol{I_3}$**:**	Moment of inertia of l_3 around Ankle joint
g:	Acceleration due to gravity
$\boldsymbol{l_1}$**:**	Length of link1, from ankle joint to metatarsals
$\boldsymbol{l_2}$**:**	Length of link2, from ankle joint to calcaneous
$\boldsymbol{l_3}$**:**	Length of link3, from ankle joint to center of mass
dc:	Distance between the vertical projection of ankle from point A to calcaneous point C
dm:	Distance between the vertical projection of ankle from point A to metatarsals point M
a:	Distance between the ankle joint to ground surface
$\boldsymbol{a_{G3}^t}$**:**	Tangential component of acceleration due S_{G3}
$\boldsymbol{a_{G3}^n}$**:**	Normal component of acceleration due S_{G3}

CHAPTER 1

INTRODUCTION

In efforts to search for the answers for the questions "How is human erect posture maintained and what are the factors that affect this control mechanism?", we first investigated maintaining the posture by exploring posturography methods following force plates and contribution of pressure pads.

Review of the available literature showed that most of the previous studies considered the foot as a rigid body. Yet, this is not a correct definition. On the contrary, the foot represents the most complex bone structure of the human body, which incorporates energy storing and releasing agent with three arched structure and different types of numerous sensors beneath. These sensors, along with ligamentous curved structure and plantar aponeurosis may be sending many signals to the Central Nervous System (CNS). Accordingly, a simple deformable foot model using a truss structure is developed. In order to determine reaction forces at the heel and metatarsals, human experiments are performed. It is observed that, there is a dynamic behavior in ground reaction force transmissions, between front and hind region of the foot, due to pendulum effect (postural sway) of Center of Mass (COM) of the human body. This transfer of forces is named as the "Load Shifting Mechanism". Time and frequency domain analysis of the obtained data revealed many interesting results related to load distribution among regions of the foot, between feet, and genders. Developing a deformable foot model enabled us to fine-tune the important posture control parameters of the system. We anticipate that this study will lead to the development of better strategies in similar and relevant models.

1.1 Posture Control

Maintaining the erect posture is such an easy and automated task for healthy human individuals that they are not even aware of what kind of processes are happening behind their CNS during the process. In reality, maintaining the erect posture is a complex and developmental process/task for humans, which requires aligning body segments with respect to gravity vertically through multisensory integration of information received from different sources; such as vision, vestibular, proprioceptive and cutaneous receptors [1–4], which govern a cascade of muscular correctional movements [5]. This process is so complicated that it involves over 200 degrees of freedom powered by approximately 750 muscles [6]. A human being never stands perfectly straight, however, constant small muscular corrections take place to ensure that. Such corrections are possible only if the human have a good estimation of his/her position. Therefore, the information received from visual sensors of the eyes, vestibular sensors of the inner ears, proprioceptive sensors of the muscles, and somatosensory senses from skin receptors are constantly fed into the CNS for the determination of the correct position. Although it is well known how these systems contribute to postural control, only little of them have been understood so far on how sensory information from different senses is fused to form a unique and coherent estimate of the body's position (or self-perception) [7].

Posture describes the orientation of every body segment relative to the gravitational vector. It is an angular measure from the vertical. Balance, in general terms, describes the dynamics of body posture in order to prevent falling. It is related to the inertial forces acting on the body and the inertial characteristics of body segments. COM is the point, which represents the equivalent of the positions of total body mass in global reference system and is the weighted average of the COMs of all body segments in 3D space. It is a passive variable controlled by the balance control system. The vertical projection of the COM onto the ground is often called the Center of Gravity (COG).

Centre of Pressure (COP) is the point location of the vertical ground reaction force vector. It represents a weighted average of pressure distribution over the surface of the area in contact with the ground. It is totally independent of the COM. If one foot is on the ground, the net COP lies within that foot. If both feet are in contact with the ground, the net COP lies somewhere between the two feet, depending on the relative weight taken by each foot. Thus, when both foot are in contact with the ground there are separate COPs under each foot. If one force platform is used only the net COP is available.

1.2 Foot

In order to better understand the contribution of human foot to the control of posture, one needs to know the structure of the foot itself. However, anatomical references and planes must be introduced first. “To avoid ambiguity, all anatomical descriptions assume that the body is in the conventional ‘anatomical position’, i.e. standing erect and facing forwards, upper limbs by the side with the palms facing forwards, and lower limbs together with the toes facing forwards Figure 1-1 Descriptions are based on four imaginary planes, median, sagittal, coronal and horizontal, applied to a body in the anatomical position. The median plane passes longitudinally through the body and divides it into right and left halves. The sagittal plane is any vertical plane parallel with the median plane: although often used, ‘parasagittal’ is therefore redundant. The coronal (frontal) plane is orthogonal to the median plane and divides the body into anterior (front) and posterior (back). The horizontal (transverse) plane is orthogonal to both median and sagittal planes. Radiologists refer to transverse planes as (trans)axial: convention dictates that axial anatomy is viewed as though looking from the feet towards the head” [8].

Human foot and ankle is a strong and complex mechanical structure containing 28 separate bones including sesamoid bones, 31 joints including ankle joint and many muscles, tendons, and ligaments [8]. The 26 bones (seven tarsals, five metatarsals, and 14 phalanges) and six joints (ankle, subtalar, midtarsal, tarsometatarsal, metatarsophalangeal (MTP) and interphalangeal (IP) joints) of the foot make up its four segments: the hindfoot, the midfoot, the forefoot and the phalanges.[9]

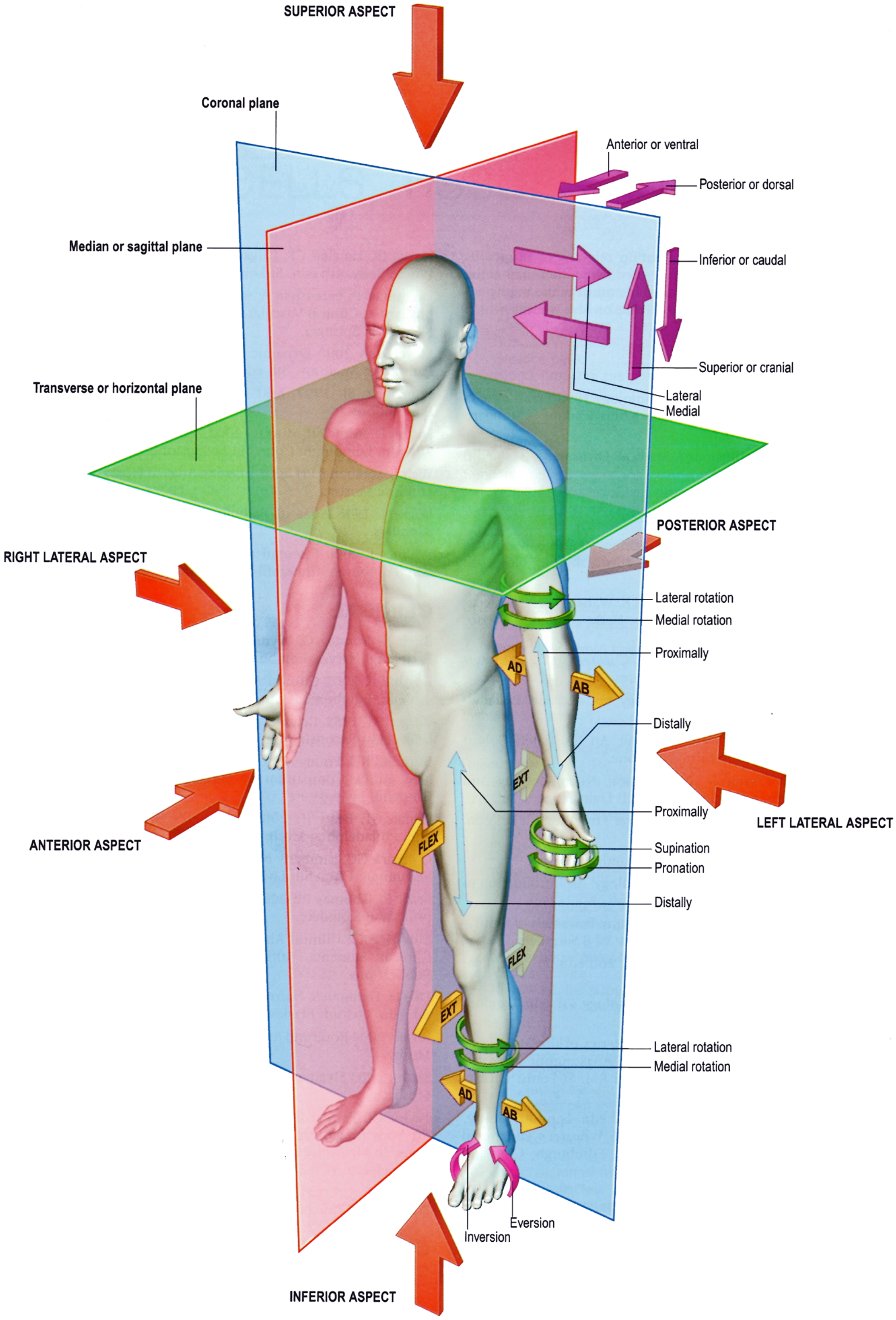

Figure 1-1 The terminology widely used in descriptive anatomy. Abbreviations shown on arrows: AD, adduction; AB, abduction; FLEX, flexion, EXT, extension [8].

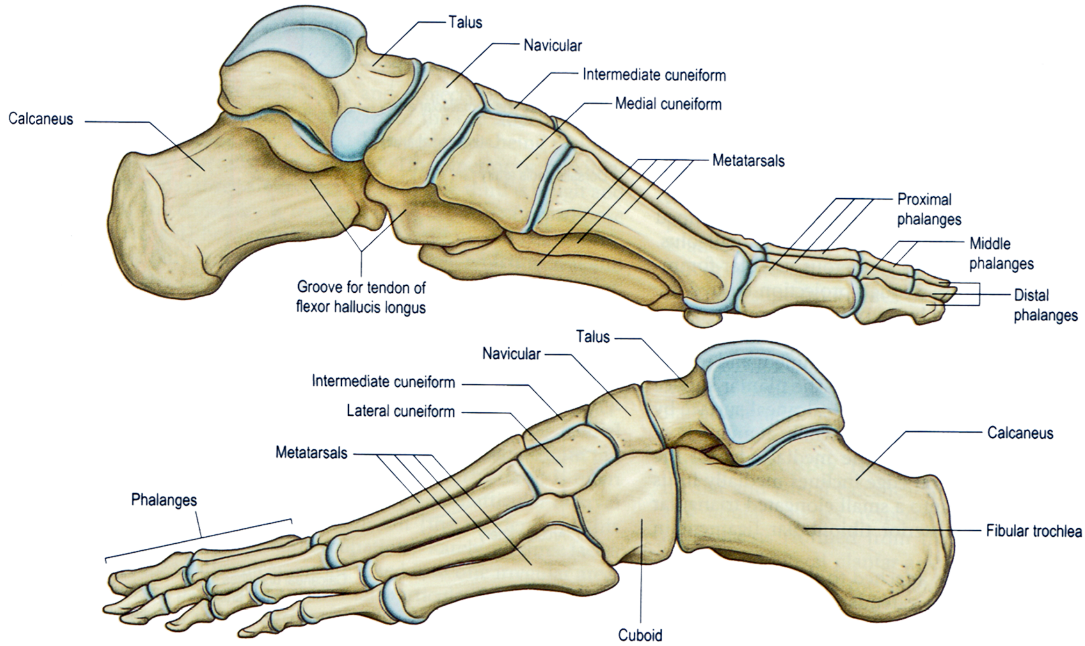

Figure 1-2 Bones of the foot from medial (above) and lateral (below) aspect [8].

1.2.1 Hindfoot

The hindfoot consists of the talus and calcaneus. The three parts of the talus (body, neck, and head) are orientated to transmit reactive forces from the foot through the ankle joint to the leg (see Figure 1-3). Lying between the calcaneus, and tibia, it communicates thrust from one to the other. The calcaneus is the largest and most posterior bone in the foot and provides a lever arm for the insertion of the Achilles tendon, which is the largest and one of the strongest tendons in the body through which gastrocnemius and soleus impart powerful plantar flexion forces to the foot. Its height, width and structure enable the calcaneus to withstand high tensile, bending and compressive forces on a regular basis without damage.[9]

1.2.2 Midfoot

The navicular, the cuboid and three cuneiforms make up the midfoot (see Figure 1-3). The navicular medial to the cuboid articulates with the head of the talus anteriorly and is the key- stone at the top of the medial longitudinal arch. The cuboid articulates with the calcaneus proximally and the fourth and fifth metatarsals distally. The three cuneiforms are convexly shaped on their broad dorsal aspect whilst the plantar surface is concave and wedge shaped so that the apex of each bone points inferiorly. The cuneiforms articulate with the first, second and third metatarsals distally. This multi-segmental configuration in conjunction with connecting ligaments and muscles contributes greatly to the stability of the midfoot. [9]

1.2.3 Forefoot

There are five metatarsals in the forefoot, these all tapered distally and articulating with the proximal phalanges (see Figure 1-3). The first metatarsal is the shortest and widest. Its base articulates with the medial cuneiform and is somewhat cone shaped. The head of the first metatarsal additionally articulates with two sesamoids on its plantar articular surface. The second metatarsal extends beyond the first proximally, and articulates with the intermediate cuneiform as well as with the medial and lateral cuneiforms in a 'key-like' configuration, which promotes stability and renders the second ray the stiffest and most stable portion of the foot. The third, fourth and fifth metatarsals are broad at the base, narrow in the shaft and have dome-shaped heads [9].

Phalanges constitute digits. The big toe (hallux) consists of two phalanges, all other toes containing three. The heads of the proximal and middle phalanges tend to be trochlear shaped allowing for greater stability. Functionally, the toes contribute to weight bearing and load distribution and also erect propulsion during the push-off phase of gait [9].

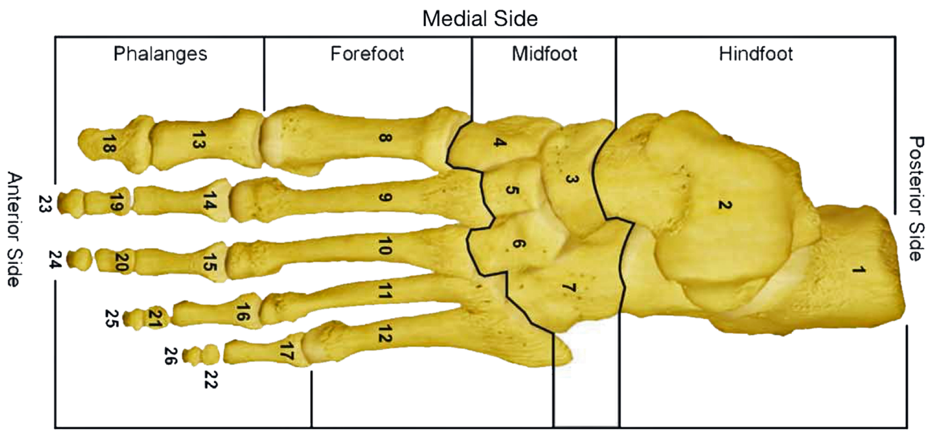

Figure 1-3 The segmentation of foot structure: four segments: hindfoot (1, 2), midfoot (3-7), forefoot (8-12), phalanges (13-26), (1) calcaneous, (2) talus, (3) navicular, (4) medial cuneiform, (5) intermediate cuneiform, (6) lateral cuneiform, (7) cuboid, (8) First metatarsal, (9) second metatarsal, (10) third metatarsal, (11) fourth metatarsal, (12) Fifth metatarsal, (13-17) proximal phalanges, , (18) distal phalange, (19-22) middle phalanges and (23-26) distal phalanges [9].

1.2.4 Arches of the foot

Three main arches are recognized in the foot. They are the medial longitudinal, the lateral longitudinal and the transverse arch.

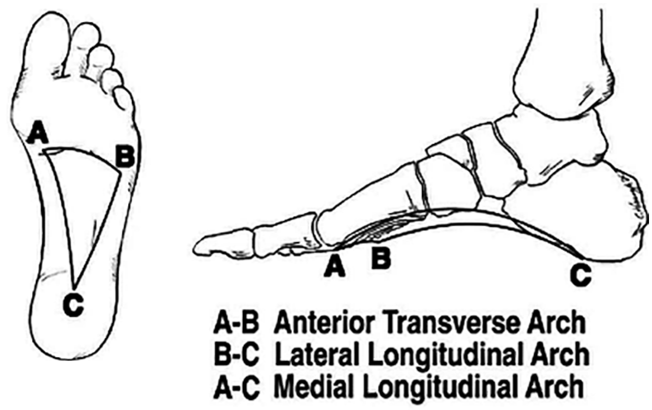

Figure 1-4 Arches of the foot ©Anonymous.

1.2.4.1 Medial longitudinal arch

The medial margin of the foot arches up between the heel proximally and the medial three metatarsophalangeal joints to form a visible arch. It is made up of the calcaneus, talar head, navicular, the three cuneiforms and the medial three metatarsals. The posterior and anterior pillars are the posterior part of the inferior calcaneal surface and the three metatarsal heads, respectively. The bones themselves contribute little to the stability of the arch, whereas the ligaments contribute significantly[8]. The most important ligamentous structure is the plantar aponeurosis, which acts as a tie beam between the supporting pillars[10]. Dorsiflexion (upward motion of foot), especially of the hallux, draws the two pillars together, thus heightening the arch: the so-called **'windlass' mechanism.**

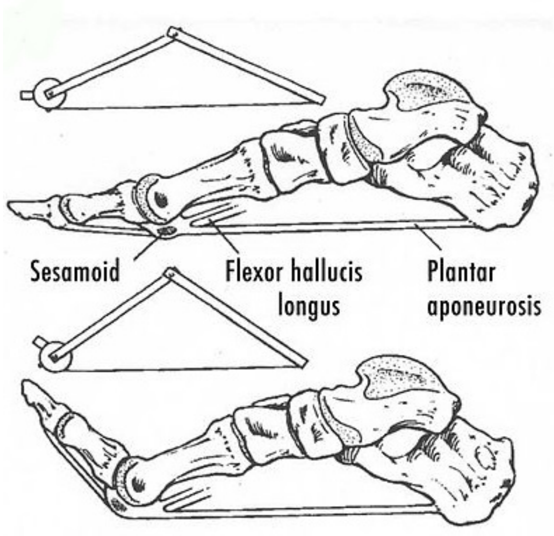

Figure 1-5 Windlass mechanism (drawing by Kosi Gramatikoff).

Next in importance is the spring ligament (plantar calcaneonavicular ligaments), which supports the head of the talus (see Figures 1-6 and 1-7). If this ligament fails, the navicular and calcaneus separate, allowing the talar head, which is the highest point of the arch, to descend. The talocalcaneal ligaments and the anterior fibres of the deltoid ligament, from the tibia to the navicular, also contribute to the stability of the arch.[8]

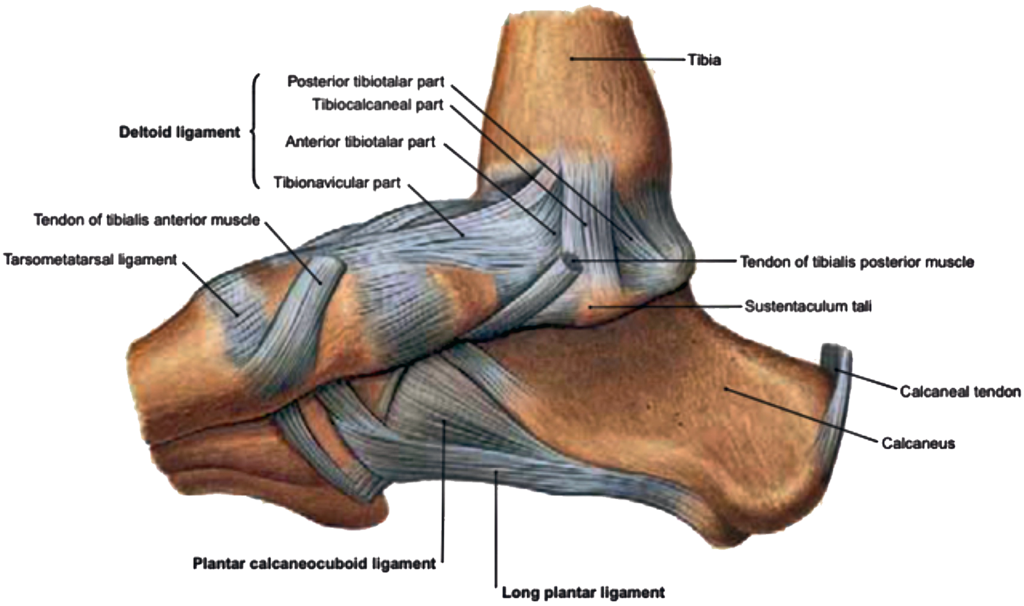

Figure 1-6 Ligaments of the Ankle and Foot: Medial View (Right Foot) [88].

Muscles play a role in the maintenance of the medial longitudinal arch. Flexor hallucis longus acts as a bowstring. Flexor digitorum longus, abductor hallucis and the medial half of flexor digitorum brevis also contribute, but to a lesser extent. Tibialis posterior and anterior invert and adduct the foot, and so help to raise its medial border. The importance of tibialis posterior is manifest by the collapse of the medial longitudinal arch that accompanies failure of its tendon [8].

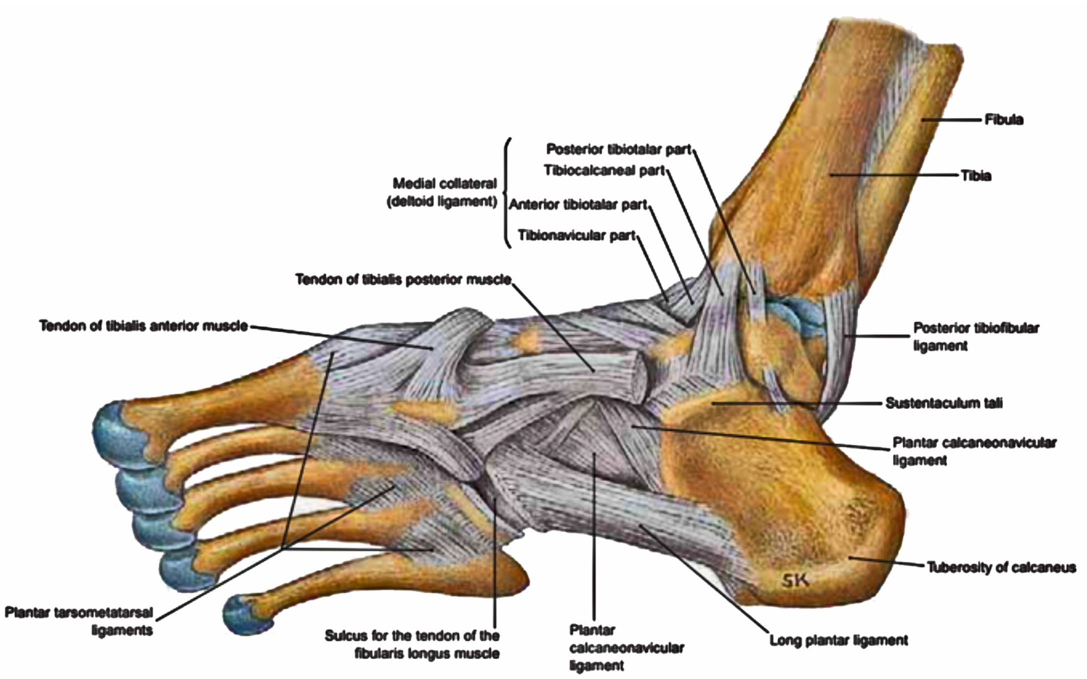

Figure 1-7 Ligaments on the Medial Aspect of the Ankle Joint and Foot [88].

1.2.4.2 Lateral longitudinal arch

The lateral longitudinal arch is much less pronounced arch than the medial one. The bones making up the lateral longitudinal arch are the calcaneus, the cuboid and the fourth and fifth metatarsals: they contribute little to the arch in terms of stability. The pillars are the calcaneus posteriorly, and the lateral two metatarsal heads, anteriorly. Ligaments play a more important role in stabilizing the arch, especially the lateral part of the plantar aponeurosis and the long and short plantar ligaments. However, the most important contribution to the maintenance of the lateral arch is made by the tendon of fibularis longus. [8] The lateral two tendons of flexor digitorum longus (and flexor accessorius), the muscles of the first layer (lateral half of flexor digitorum brevis and abductor digiti minimi) and fibularis brevis and peronius tertius also contribute to the maintenance of the lateral longitudinal arch. [8]

1.2.4.3. Transverse arch

The bones involved in the transverse arch are the bases of the five metatarsals, the cuboid and the cuneiforms. The intermediate and lateral cuneiforms are wedge-shaped and thus adapted to maintenance of the transverse arch. The stability of the arch is mainly provided by the ligaments, which bind the cuneiforms and the metatarsal bases, and also by the tendon of fibularis longus, which tends to approximate the medial and lateral borders of the foot. A shallow arch is maintained at the metatarsal heads by the deep transverse ligaments, transverse fibres that bind together the digital slips of the plantar aponeurosis, and, to a lesser extent, by the transverse head of adductor hallucis. [8]

1.2.5 Plantar aponeurosis

The plantar fascia or aponeurosis is composed of densely compacted collagen fibres orientated mainly longitudinally, but also transversely (Figure 1-8). Its medial and lateral borders overlie the intrinsic muscles of the hallux and fifth toe respectively, while its dense central part overlies the long and short flexors of the digits.

The central part is the strongest and thickest. The fascia is narrow posteriorly, where it is attached to the medial process of the calcaneal tuberosity proximal to flexor digitorum brevis, and traced distally it becomes broader and somewhat thinner. Just proximal to the level of the metatarsal heads it divides into five bands, one for each toe. As these five digital bands diverge below the metatarsal shafts, they are united by transverse fibres stratum of the plantar aponeurosis where it enters the toes (Figure 1-8). The central part of the plantar aponeurosis thus provides an intermediary structure between the skin and the osteoligamentous framework of the foot via numerous cutaneous retinacula and deep septa that extend to the metatarsals and phalanges. The central part is also continuous with the medial and lateral parts: at the junctions, two intermuscular septa, medial and lateral, extend in oblique vertical planes between the medial, intermediate and lateral groups of plantar muscles to reach bone. Thinner horizontal intermuscular septa, derived from the vertical intermuscular septa, pass between the muscle layers. [8]

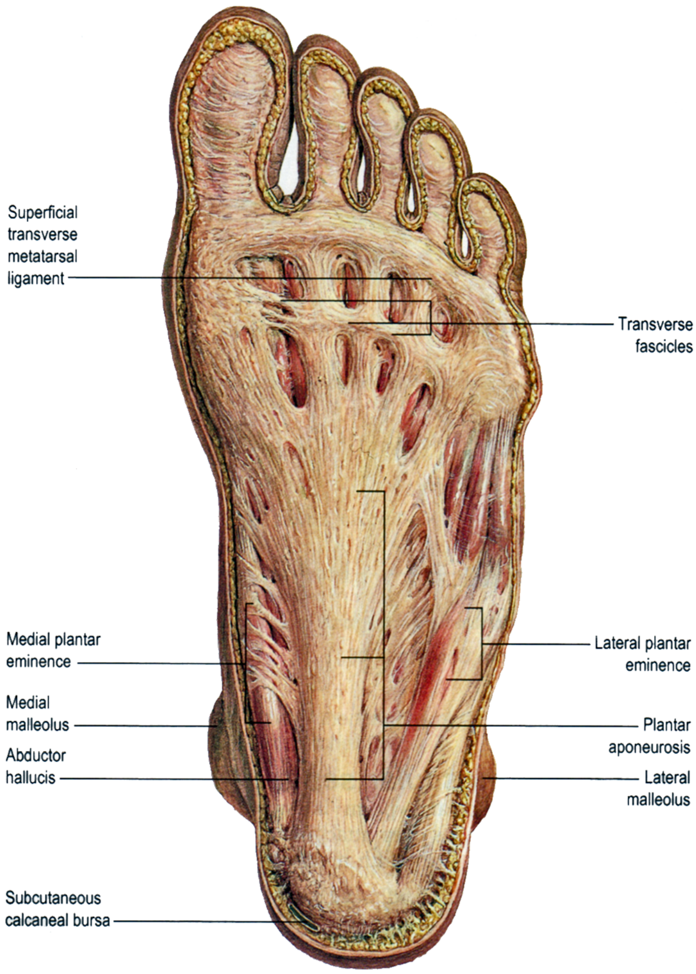

Figure 1-8 The Plantar Aponeurosis [8].

"Plantar fascia" or "plantar aponeurosis" plays an important role in load bearing and restoring effects [11–18]. During loading of the foot, the greatest amount of motion occurs in the sagittal plane around the talonavicular joint [19], which can also be described as deformation of the medial longitudinal arch. The plantar aponeurosis is shown to be the most important passive arch support during the stance phase, along with the spring ligament and the short and long plantar ligaments [20].

It has been shown experimentally, using human amputated feet loaded in a rig to simulate the weight-bearing, that strain energy is stored in the foot and largely turning into an elastic recoil, the foot behaves like a spring [21]. The plantar fascia, which is morphologically the insertion of the plantaris muscle, has been shown by Hicks (Hicks 1953) to raise the longitudinal arch when the toes are dorsiflexed; the maximum effect is on the first ray and gradually diminishes laterally **(the windlass mechanism).** This is a passive mechanism with no muscular contraction. The stretched plantar fascia also inverts the calcaneum and rotates the tibia laterally. There is also the reverse effect when the arch is flattened under body weight so that the proximal phalanges become plantarflexed and the toes are firmly opposed to the ground.

1.2.6 Arched Structures

Arches and arched structures have a wide range of uses in bridges, arched dams and in industrial, commercial, and recreational buildings. They represent the primary structural components of important and expensive structures, many of which are unique. Current trends in architecture heavily rely on arched building components due to their strengths and architectural appeal.

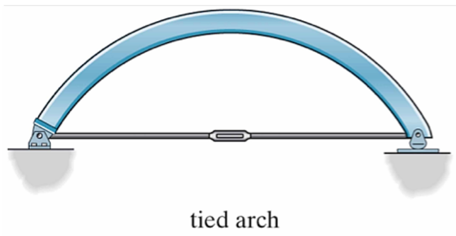

Figure 1-9 Tied arch structure (© 2009 Pearson Prentice Hall, Inc).

Arched structure of the foot also resembles to the structural configuration of beams and arches. The fundamental feature of an arched structure is that the horizontal reactions appear even if the structure is subjected to vertical loads only. If structure has a curvilinear axis but thrust does not exist then this structure cannot be treated as an arch. The
presence of thrust leads to a fundamental difference in behavior between arches and beam – the bending moments in arches are smaller than in beams of the same span

and loads. Advantages of arches over beams increase as the length of a span increases [22]. Presence of thrust demands reinforcement of the part of a structure that is subjected to horizontal force. However, the thrust may be absorbed by a tie; with this, supports of the arch are only subjected to vertical forces. In addition to the bending moments and shear forces that arise in beams, axial compressive forces are also present in arches. These forces may cause a loss of stability of the arch [22].

1.2.7. Plantar Shear Forces and Plantar Sensation in the Foot

Importance of sensation from the feet and ankles, for standing balance control has only been understood in recent decades. It is seen that more research is being conducted on the internal structure of the foot, friction forces between ground/foot and measurement of the shear forces [23–25]. It is found that horizontal frictional forces are applied to the heels, metatarsals, and toes. Therefore, ideally, sliding friction forces should be considered as the foot arch angle changes. This would likely affect the angle of the foot arch, and thus may change the weight distribution under the foot slightly [24]. The effects of the foot sole anesthesia were studied by Meyer[23] and it was found that sensory information from the foot soles is mainly used to set a relevant background muscle activity for a given posture and support surface characteristic, and consequently, is of little importance for feedback control during unperturbed stance. In general, it has been demonstrated that plantar sensation is of moderate importance for the maintenance of normal standing balance when the postural control system is challenged by unipedal stance or by closing of the eyes. The impact of reduced plantar sensitivity on postural control is expected to increase with the loss of additional sensory modalities such as the concomitant proprioceptive deficits commonly associated with peripheral neuropathies [23]. Kennedy [25], examined the location and distribution of cutaneous mechanoreceptors in the glabrous skin of the foot. They identified the receptor types and specific role of cutaneous mechanoreceptors in the foot sole in standing balance.

1.3 Foot Models

When standing quietly, human upright stance is often approximated as an inverted pendulum pivoting around the ankle [26,27]. Barin, modeled human postural dynamics in the sagittal plane as an open chain N-link inverted pendulum placed atop a triangular foot. Then, he represented system dynamics with one-link to four-link inverted pendulum models in order to search for the order of the human postural dynamics. It was seen that Ankle and Hip joints' kinematics (2-dof inverted pendulum model) constituted most of the dynamic solution [6]. Alexandrov et al. [28,29] used a three-joint (ankle, knee and hip) inverted pendulum model to account for postural responses during fast-forward bending at the waist on narrow and wide surfaces in response to platform perturbations. Ankle, hip and knee eigenmovements were derived from the mechanical properties of the body and the kinematics data collected, where each eigenmovement is named after the joint that contributes most to the eigenmovement [28,29]. Furthermore, works of Jeka and Creath [30] showed that two-linkage pendulum mechanism is sufficient to represent the whole body dynamics in the posture study.

In all of these studies, human foot is taken as a triangular non-deformable body hinged at the ankle joint. Studying the human foot shows that it is not a solid non-deformable structure [31–35]. Actually it is highly deformable and has an energy storing spring like mechanism. More complicated foot models were presented and analyzed using the Finite Element Method [36,37], however keeping the model simple is beneficial for identifying the underlying parameters.

1.4 Objective of the Thesis

Linear system approaches through inverted pendulum models with sensory feedback have been widely used in order to reveal the physiological mechanisms that control and stabilize posture in quiet stance [26,38]. Although Center of Pressure (COP) variation on the horizontal plane (xy-plane) is generally used as a summary signal for representing the dynamics of such a complex system, there exist multi-dof modeling attempts (depending on limb kinematics data per se) to understand the physiological control mechanism behind such as; two-linkage pendulum mechanism, Ankle and Hip kinematics (2-dof inverted pendulum model [39,40], three-joint (ankle, knee and hip) [28,29], and Open-chain N-link inverted pendulum [6] models. Mathematical analysis of force-stiffness characteristics of muscles in control of a single joint system [41], where dynamical characteristics and control strategies of human erect posture (against gravitational force field of the earth) has been studied thoroughly (even depending on a single dof inverted pendulum assumption) and human foot is taken as a triangular non-deformable body hinged at the ankle joint. On the other hand, complex dynamics of human postural sway has also been explored by using stochastic models and nonlinear dynamical tools [42–47] where possible sources for complexity have rarely been checked against a functioning foot; e.g., implementing a shear deformation sensor modeled as a viscoelastic body with a sensorial threshold [48].

Wright et al. [34] have recently showed that the foot arch's upwards deformation (beyond the limits that can be explained by plantar skin compression) observed by receiving data form the dorsum of the mid-foot is positively correlated with shank's sway towards posterior direction (and vice versa), which may deteriorate the classical explanation of human postural control strategies (mainly suprapedally studied) based on ankle proprioception and kinematics and torque control (generated through ankle extensors and flexors muscle activity; [41]**,** see also [49].

Furthermore, data was presented data about perturbations given to toe and metatarsals causing significant RMS changes at tibialis anterior and gastrocnemius muscles' (main ankle flexor and extensor muscles respectively) baseline activation levels, it is then found to return to baseline activation levels slowly which has been proposed (by the authors) as an indication of a switch in the surface frame of reference. On the other hand, the human foot is a complex multi-articular mechanical structure consisting of bones, joints and soft tissues, playing an extremely important role in the biomechanical function of the lower extremity and is controlled by both intrinsic and extrinsic muscles [9].

It is the end-point organ of an open kinematics chain for human biped erect posture that touches to the ground (compliant enough to sense the surface through deformations) and is the only mean to control standing (providing support and controlling balance) and locomoting (stabilizing the body and activating the propulsion; i.e., rigid enough to push the ground) through actively created ground reaction forces without which it would be impossible (from a mechanical point of view) to control the whole body posture from the ankle joint only [23,25].

Moreover, the duality (information versus action) in a functional foot; i.e., being compliant enough to sense the surface through deformations versus being rigid enough to stand for the body weight and govern the balance and propulsion respectively, has been evolutionarily succeeded by forming longitudinal (medial and lateral) and transverse arches, where tension on longitudinal arches being actively controlled by muscle activity during motion [9]; while during quiet stance body weight has been supported by the foot where the maintenance of the arch has been attributed to reactive forces at the passive tissues and the tensile strength of the plantar aponeurosis (which maintains the longitudinal arch) through the beam action of the metatarsals [10,50].

In addition, it has been shown that the tension on the plantar aponeurosis (see Figure 1-6) can actively be adjusted through a mechanism triggered by the toe extension, known as windlass effect [10,51]. Kennedy and Inglis studied the effects of mechanoreceptors in the glabrous skin of the foot sole and found that a large percentage of the skin receptors were rapidly adapting with randomly distributed receptive fields with an absence of background activity in an unloaded position [25]. Moreover, role of the plantar aponeurosis (plantar fascia) in the load bearing capacity of the human foot has been investigated by Kim and Voloshin by using a 2-dof sagittal planar model of the medial aspect of the foot (modeling the medial longitudinal arch supported by the plantar aponeurosis represented by a viscoelastic Kelvin body), where They found that (by estimating model parameters through human experiments) plantar fascia carries 14% of the body weight and in the case of release of the plantar fascia resulted 22% increase of the maximum vertical displacement of the ankle joint (and 19% increase during the steady-state phase) under the applied weight [13]. They also explored the effect of the foot geometry (by lowering the arch height in their model) and showed that lowering the height of the arch degenerated the load bearing capacity of the foot [52]. We propose based on their findings that the critical tension created at the plantar fascia is indispensable for an optimal arch height range at which human standing is enabled and is continuously monitored through mechanoreceptors [25].

It has recently been shown that actively adjusting longitudinal arch stiffness results in redistribution of the plantar pressure by mediolateral force transfer beneath the foot in standing and facilitating medial forefoot propulsion in human walking [53], which also has been proposed as an ubiquitous coupling mechanism in the human foot where lateral mid-foot compliance inversely being related to the pressure exerted by the medial metatarsals heads and hallux, which may be an indication in searching footprints of hominin bipedaility [53].

It is showed that activation of the plantar intrinsic foot muscles under loading produced significant alterations in metatarsals and calcaneous segment angles, which countered the deformation occurring owing to the initial load and ultimately increased longitudinal arch stiffness. Further, they showed that this active arch buttressing mechanism has important implications for the forces transmitted during standing as their activation enables shifting COP position both in anteroposterior and mediolateral directions (Kelly et al. 2014).

In summary, it has been proposed by researches that the windlass effect of the plantar aponeurosis, the tensile strength of the plantar ligaments, the beam effect of the metatarsals, and the joint congruity of tarsal and metatarsal bones all together provide force transmission, attenuation, and redistribution through the stress flow pathways [50] while being continuously monitored by the mechanoreceptors placed on the plantar fascia and the soft tissue beneath the foot during quiet stance [25].

In view of these important abilities of the foot in mechanics/dynamics and control of the erected posture of a human being, it becomes inevitable to consider its role as being a source of information and actuation in complex quasi-dynamics of quiet stance (against suprapedally studied postural dynamics and control). Thus, in this study, distribution of Ground Reaction Forces (GRF) in time and frequency domain for male and female subjects based on plantar pressure data is analyzed. The objective behind this work is to determine the GRF distribution beneath different regions of the foot through which the importance of deformation and/or small amplitude motion of the foot for postural control is to be revealed.

1.5 Scope of the Thesis

The objective behind this work is to determine the GRF distribution beneath different regions of the foot, through which the importance of deformation and/or small amplitude motion of the foot for postural control is to be revealed.

In order to determine the amount and characteristics of GRF on plantar foot, experiments are performed on voluntary male and female subjects at quiet stance. Matscan Tekscan pressure pad and Bertec force platform used during the experiments for collecting data. Pressure pad gave pressure distribution in terms of kPa, however that is easily converted to force distribution in Newton, since plantar areas of the regions can be calculated. Further, time and frequency domain analysis on force distribution data is accomplished in order to determine the nature of this distribution.

In Chapter 1 a review of the available literature studies of the previous researches has been presented.

In Chapter 2, in order to observe GRF of plantar foot, experiments are planned and performed on voluntary human subjects. Experimental procedures and methods are presented in this Chapter.

In Chapter 3 results of the experiments are presented, for both time and frequency method. Since ANOVA method is applied to the data, results and interpretation of the results are presented in graphical format.

In Chapter 4, a mathematical foot model combining both deformable foot and an inverted pendulum on the ankle joint is presented. This model is developed in order to better observe the parameters affecting the human erect posture. This model is run on MATLAB Simulink environment and outputs are presented.

In Chapter 5 experimental and mathematical model results are discussed with the previous works of researches. Further, improvements that can be done to the present study and suggestion for the succeeding research has been declared in this section.

CHAPTER 2

EXPERIMENTS AND METHODS

Experiments are performed in Motion Capture Laboratory at Middle East Technical University Modeling and Simulation Center (MODSIMMER).

2.1 Overview of the Subject testing and data acquisition

A group of fourteen right-handed adult 7 male (35.14 ± 3.13 years old, 875 ± 97.92 N weight, 180 ± 7.09 cm height) and 7 female (30.29 ± 4.86 years old, 627.71 ± 104.05 N, 168.57 ± 4.16 cm) subjects participated in this experiment. All subjects, with no evidence or known history of neuro-musculo-skeletal disorder, provided informed consent prior to participation in the testing protocol.

They were instructed to stand at an upright posture on the Bertec® force platform and Tekscan® Matscan pressure pad, arms relaxed at the side and the feet opened about shoulder length. Six quiet stance trials, each lasting 180 seconds, were conducted at Eyes Open (EO) and Eyes Closed (EC) conditions, with the subjects looking straight ahead with only socks on their feet. The order of testing sensory conditions, i.e., EO versus EC trials, was randomized for each of the subject. Rest periods of 60 seconds were provided between each trial. Force and moment signals at x-y-z axes were acquired at a sampling rate of 100 Hz by a force-plate (Bertec®, FP1212-25 custom made 1200×1200mm). Center-of-pressure (COP) time signals at antero-posterior (AP, COPx) and medio-lateral (ML, COPy) directions were then computed. Pressure distribution data under each foot were collected at 50 Hz using Tekscan® Pressure Pad. A representative plot is given in Figure 2-1.

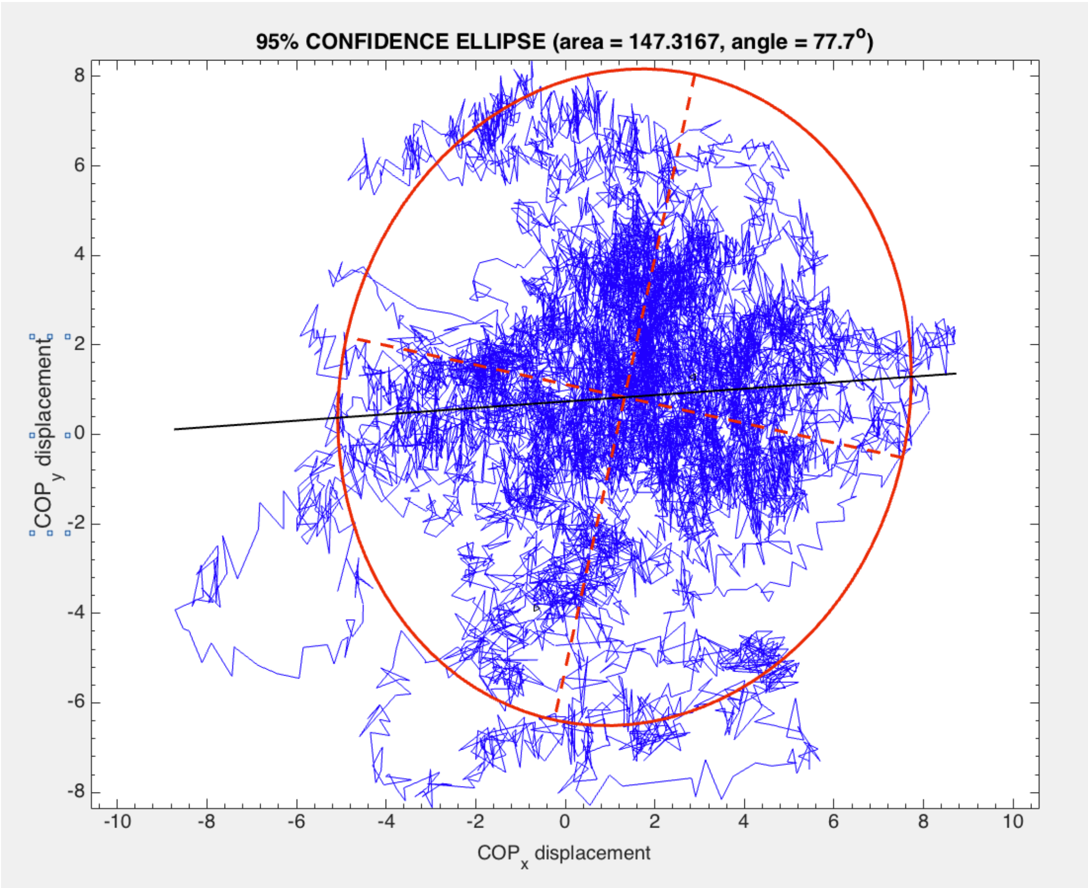

Figure 2-1 A representative male subject's plot of COPx versus COPy and its 95% confidence ellipse calculated using Principal Component Analysis (PCA)

Bertec AM6800 signal amplifier and National Instrument "NI-6221-USB" multifunction data acquisition (DAQ) modules for USB were used together for triggered collection of data. A picture is shown taken during the experiment in Figure 2-2.

Before the experiments for each subject; sex, age, used hand, weight, height, foot length, ankle height from the ground, distances from heel to metatarsals, and from ankle projection to metatarsals were recorded. The apparatus used for these measurements is shown in Figure 2-3. These recorded values were further used in verifying the mathematical model.

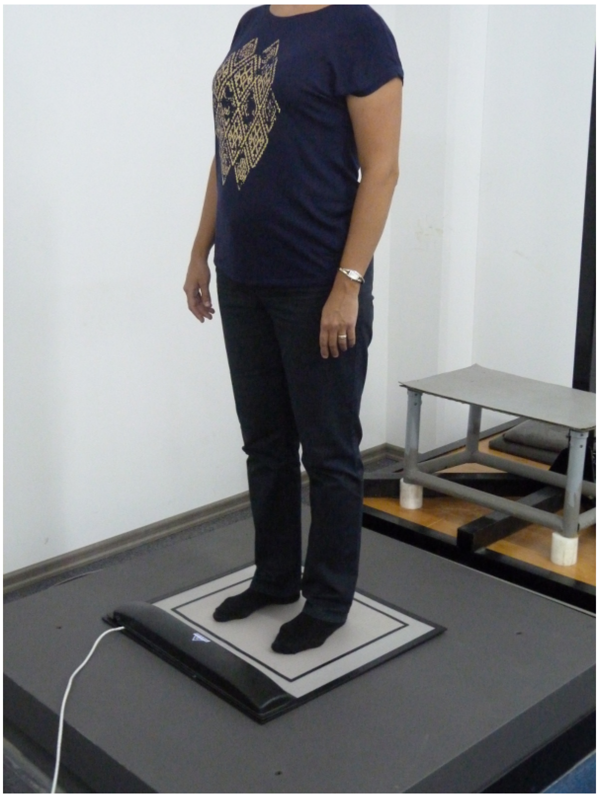

Figure 2-2 Subject on Force Platform and Pressure Pad

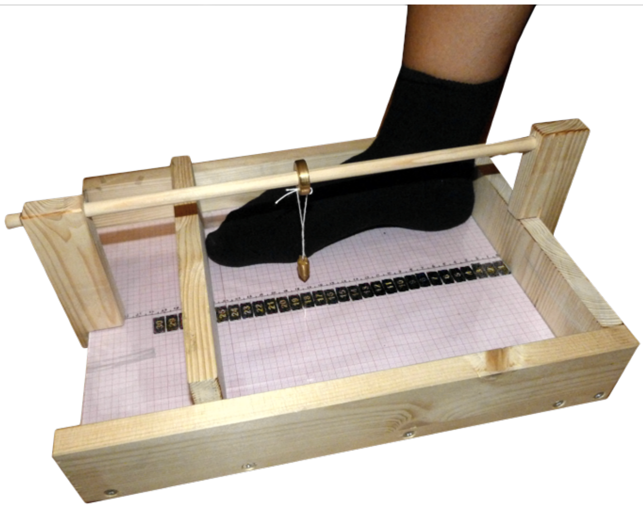

Figure 2-3 Apparatus used for measuring foot dimensions

2.2 Data Analysis

Each foot has been divided into three regions by using the predefined regions facility of **Matscan® software** based on the previous human foot model studies as shown in Figure 2-4. Selected foot regions were heel region (talus and calcaneus bone), medial longitudinal arc region (the navicular, the cuboid and three cuneiforms), and five metatarsal bones and phalanges; named as hind, mid, and front regions respectively. Foot regions were selected according to accepted partition except phalanges that were included in the forefoot region [9]. Distributed ground reaction forces at these sites were determined using "Drawing Polygons" facility of the Pressure Pad (Tekscan Matscan) software on the regions shown as in Figure 2-4. The MatScan sensor detects subject's plantar pressure. This sensor is made up of over 2288 (44×52) individual pressure-sensing locations, which are referred to as "Sensing Elements" or "Sensels." The sensels are arranged in rows and columns on the sensor. Each sensel is 70.2579 mm^2 and the output of each sensel is divided into 256 increments and displayed as a value ("Raw" sum) in the range of 0 to 255. Accordingly, pressure distribution data over pre-mentioned regions of left and right foot were obtained as a function of time. Initial mean contact areas of the three plantar foot regions for each subject in the first trial are presented in Table 2-1.

Table 2-1 Mean contact area of the three plantar foot regions

	Frontfoot [mm^2]		Midfoot [mm^2]		HindFoot [mm^2]		Total [mm^2]	
	Left (std.dev)	Right (std.dev)	Left (std.dev)	Right (std.dev)	Left (std.dev)	Right (std.dev)	Left (std.dev)	Right (std.dev)
Female	5249.29 (643.46)	5420.00 (477.12)	2188.00 (713.61)	2047.57 (504.10)	2740.14 (157.20)	2790.4 (255.42)	10177.43 (1295.88)	10258.00 (986.70)
Male	5972.00 (444.30)	6042.14 (389.09)	1897.00 (756.68)	1696.14 (475.33)	3352.43 (343.37)	3111.29 (286.04)	11221.43 (1223.96)	10849.57 (434.70)

Calibration was performed prior to taking the foot scan of each subject according to the method recommended by the MatScan manufacturer (Tekscan). The weight of the subject is measured separately with Bertec force platform and entered into the Matscan software, which is then automatically applied at an appropriate scaling to the raw outputs of the sensing elements such that the total force of the pressure pad is consistent with the weight of the subject. Normal Force signals at each region for each foot were then obtained as a function of time by averaging the pressure distribution data over its related plantar surface. Normal

Force signals at each region for each foot were named as FR, MR, HR for right foot and FL, ML, HL for left foot respectively (see Figure 2-4).

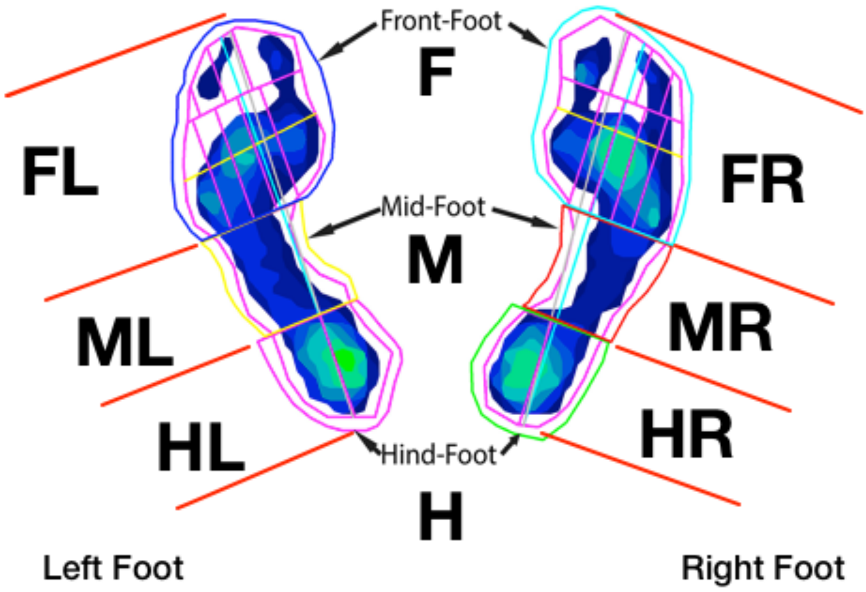

Figure 2-4 Regions of the foot and medial, longitudinal arches of the foot

2.3 Time Series Analysis

Time domain measures were: the Mean and variance of pressure distribution at each section of both feet and the Cross correlation values of each possible paired combination of the three foot-regions. Statistical measures such as the mean and variance of the pressure distribution of the foot regions in time and the correlation coefficients among the three regions were computed by using MATLAB® software (The Mathworks Inc.) standard routines. In order to reveal the correlated behavior among F, H, M regions for fourteen subjects, mean and variance of the pressure distribution in time and computed cross correlation values among 'F-H', 'F-M', and 'H-M' regions were analyzed. In order to understand how the two normal force signals are related to each other at each possible paired combination of foot regions, correlation function coefficient (normalized cross-covariance function) at $\tau = 0$ has been computed according to the equations given below.

$$R_{XX}(\tau) = \frac{1}{T}\int_0^T X(t)X(t+\tau)\,dt \tag{2.1}$$

where R_{XX} is the auto-correlation function as a function of the delay operator, *τ*; *T* is the data collection time period, *X* is the time series for normal force distribution averaged over its related plantar surface.

On the other hand, Equation 2.2 describes cross-correlation function of the two signals

$$R_{XY}(\tau) = \frac{1}{T}\int_0^T X(t)Y(t+\tau)\,dt \tag{2.2}$$

Where R_{XY} is the cross-correlation function as a function of the delay operator, *τ*; *T* is the data collection period of time, *X* and *Y* are the time series for normal force distribution averaged over its related plantar surface.

Equations 2.3 and 2.4 define covariance functions, C(τ);

$$C_{XX}(\tau) = R_{XY}(\tau) - \mu_X^2 \tag{2.3}$$

$$C_{XY}(\tau) = R_{XY}(\tau) - \mu_X \mu_Y \tag{2.4}$$

Where μ_X and μ_Y are the mean values of the respective normal force signals in time. It is important to note that, at time delay operator, τ = 0; C(0), R(0) are called as variance (σ_X^2) and mean square (ψ_X^2) in statistics as basic descriptive properties of a random time signal, respectively [55] . This fundamental statistical expression for describing random data properties can also be written as,

$$\sigma_X^2 = \psi_X^2 - \mu_X^2 \tag{2.5}$$

Finally, correlation function coefficient (normalized cross-covariance function, $\rho_{XY}(\tau)$) has been defined as

$$\rho_{XY}(\tau) = \frac{C_{XY}(\tau)}{\sqrt{C_X(0)C_Y(0)}} \tag{2.6}$$

In order to understand how the two normal force signals are related to each other at each possible paired combination of foot regions correlation function coefficient (normalized cross-covariance function) at $\tau = 0$ has been computed according to the equations given above**.** It is important to note that correlation function coefficient $\rho_{XY}(\tau)$, is always between $-1 \leq \rho_{XY}(\tau) \leq 1$

2.3 Frequency Domain Analysis

Modified Front, Mid and Hind foot region force distributions were further analyzed in the frequency domain in order to see frequency characteristics of these signals. We used MATLAB Fast Fourier Transform (FFT) routines to calculate frequency domain measures. Time series were detrended linearly before Fast Fourier Transformation. Frequency domain measures were adapted from methods described in Prieto et al. [56] and [26]. Spectral moments, $\mu(k)$ were calculated for k= 1, 2 and 3 from

$$\mu_k = \sum_{i=1}^{m} (i \times \Delta f)^k \cdot G_x(i \times \Delta f) \tag{2.7}$$

where, Δf (*1/T*; *T* being the data collection time) is the frequency resolution, *m* is Nyquist frequency (1/2 of sampling rate) divided by Δf, and $G_x(f)$ is the power spectral density function estimate as a function of frequency, *f* in [Hz] obtained by FFT [55]:

$$G_X(f) = 2\int_{-\infty}^{\infty} R_{XX}(\tau)e^{-j2\pi f\tau}\,d\tau \tag{2.8}$$

where R_{xx} is the autocorrelation function, see Equation 2.1.

The total power (POWER) is the integrated area of the power spectrum when k = 0 in Equation 2.7.

$$POWER = \mu_0 = \sum_{i=1}^{m} G_X(i \times \Delta f) \tag{2.9}$$

The 95% power frequency is the frequency below which 95% of the total power is found.

$$\sum_{i=1}^{v} G_X(i \times \Delta f) \geq 0.95 \times \mu_0 \tag{2.10}$$

where v is the smallest integer for which the equation holds.

The centroidal frequency (CFREQ) is then defined as the frequency at which the spectral mass is concentrated, which is the square root of the ratio of the second to the zeroth spectral moment (see equation 2.7)

$$CFREQ = \sqrt{\frac{\mu_2}{\mu_0}} \tag{2.11}$$

The frequency dispersion (FREQD) is a unitless measure of the variability in the frequency content of the power spectral density and is given by

$$FREQD = \sqrt{1 - \frac{\mu_1^2}{\mu_0 \times \mu_2}} \tag{2.12}$$

The frequency dispersion is zero for a pure sinusoid and increases with spectral bandwidth to a maximum of one.

Further, Cross-Spectral density estimates $G_{XY}(f)$ of normal force distribution at F-H, F-M, and H-M regions and their Coherence function values were computed from Equations 2.12-2.16. Cross Power Spectral Density Function $G_{XY}(f)$ between two discrete time signals of normal force distribution of the foot regions has been estimated by using the MATLAB® ***cpsd*** function. Then magnitude and phase angle in-between the two signals were computed through $G_{XY}(f)$ from:

$$G_{XY}(f)=2\int_{-\infty}^{\infty} R_{XY}(\tau)e^{-j2\pi f\tau}\,d\tau \tag{2.13}$$

where $R_{XY}(\tau)$ is the cross-correlation function between the two time signals.
$G_{XY}(f)$ is a complex valued function and can therefore be written as

$$G_{XY}(f)=C_{XY}(f)-jQ_{XY}(f) \tag{2.14}$$

where $C_{XY}(f)$ and $Q_{XY}(f)$ are known as the coincident spectral density function (co-spectrum) and quadrature spectral density function (quad-spectrum) respectively [55]

Then magnitude ($|G_{XY}(f)|$, Eq. 15) and phase ($\theta_{XY}(f)$, Eq. 2.16) functions of $G_{XY}(f)$ are defined as

$$\left|G_{XY}(f)\right|=\sqrt{C_{XY}^{2}(f)+Q_{XY}^{2}(f)} \tag{2.15}$$

$$\theta_{XY}(f)=\tan\theta^{-1}\left[\frac{Q_{XY}(f)}{C_{XY}(f)}\right]. \tag{2.16}$$

Finally, coherence function between the two normal force distribution signals is

$$\gamma_{XY}^{2}(f)=\left[\frac{\left|G_{XY}(f)\right|^{2}}{G_{X}(f)G_{Y}(f)}\right]. \tag{2.17}$$

Also it is important to note that $0\leq\gamma_{XY}^{2}(f)\leq 1$.

Coherence function estimates were calculated using Equation 2.17 and MATLAB® ***mscohere*** function, that finds the magnitude of the coherence estimate of the force signals by using Welch's averaged modified periodogram method. In order to better analyze the nature of the spectrum, we determined a threshold value of "**0.80**" for coherence function estimate, over which the two signals are accepted as physiologically related. Moreover, frequency spectrum has been divided into three regions based on the occurrence rate of coherence values above the threshold value; namely 0-3 Hz, (most of the higher coherence function estimates have been observed at this range), 3-10 Hz, and 10-25 Hz, which have been named as low-, mid-, and high-frequency bands, respectively. Furthermore, the frequency ranges between the first and the last frequency where coherence function estimate value was higher than 0.8 has been defined as $\Delta\omega$, in [0-3] Hz region. Maximum values of coherence, gain, and phase function estimate attained within 0-3 Hz were named as 'max_coher', 'max_gain', 'max_phase' variables respectively. Their respective frequency values were also obtained. Mean coherence and mean phase function estimate values have also been computed without using a threshold value for coherence function estimate in the frequency range of [0-3 Hz].

2.4. Statistical Analysis

5D-ANOVA (i.e., five dimensional analysis of variance) for repeated measures with a significance level of 0.05 was conducted to examine the effects of the variables Gender, Subject, Regions, Foot and Eyes. Post-hoc statistical analysis has been performed by using "Multi-comparisons" facility of Matlab® which was performed between each dimension of ANOVA afterwards. It is important to note that, although a threshold value for coherence has been used (>0.80), in some of the ANOVA cases, no coherence value above the threshold have been observed. Hence, while performing 5D-ANOVA, this case has been included into the analysis as a null set.

For the entire subjects; time domain and frequency domain plots of the obtained and calculated data are presented in APPENDIX A.

CHAPTER 3

EXPERIMENTAL RESULTS

Results obtained from the experiments are presented in this chapter. First the plantar area calculations, then time series analysis and finally frequency domain analysis results are presented. In the next chapter, results obtained from the mathematical model simulations will be presented.

3.1 Plantar Area Calculations

Tekscan Matscan pressure pad was used during the experiments. Accordingly, pressure distribution data over pre-mentioned regions of left and right foot were obtained as a function of time. Average contact area of the three plantar foot regions namely Front, Mid and Hindfoot regions are presented in Table 3-1.

Table 3-1 Average contact areas of the three plantar foot regions

	Frontfoot [mm^2]		Midfoot [mm^2]		HindFoot [mm^2]		Total [mm^2]	
	Left (std.dev)	Right (std.dev)	Left (std.dev)	Right (std.dev)	Left (std.dev)	Right (std.dev)	Left (std.dev)	Right (std.dev)
Female	5249.29 (643.46)	5420.00 (477.12)	2188.00 (713.61)	2047.57 (504.10)	2740.14 (157.20)	2790.4 (255.42)	10177.43 (1295.88)	10258.00 (986.70)
Male	5972.00 (444.30)	6042.14 (389.09)	1897.00 (756.68)	1696.14 (475.33)	3352.43 (343.37)	3111.29 (286.04)	11221.43 (1223.96)	10849.57 (434.70)

These average contact areas of plantar foot of the subjects were compared with respect to Gender, Foot and Region by using 3D ANOVA. Performing three way ANOVA on Gender, Foot and Regions of foot we have seen that, gender ($p<0.0113$), region ($p<0.00$) and gender and region interactions ($p<0.0005$) were significant. Population marginal means of male subjects, mean plantar contact area has been found to be 3679±74.19 mm^2 while female subjects' mean contact area was found to be 3406±74.19 mm^2. On the other hand, F region was found to be 5671±90.86, while H and M regions were 2999±90.86 N and 1957±90.86 N respectively. Furthermore, F regions contact surface only was significantly different with respect to gender ($p<0.0005$ Male: 6007±128.5 Female: 5335±128.5)

3.2 Time Domain Analysis

Time series of normal force distribution of a representative male and a female subject for their left and right foot are presented in Figure 3-1 and Figure 3-2. Inspection of the figures shows that, male and female subjects' dynamical behavior of normal force distribution among specified regions even for the left and right foot is different. A close correlation can be observed between F and H regions' force distribution dynamics in male subjects. Dynamics of force distribution behavior at F and H regions resembles a "mirror image" of each other (see Figure 3-1). This correlated behavior between F and H regions has been named as ***"Load Shifting Mechanism" (LSM).*** Such a correlated dynamics among F and H regions has been observed at both left and right foot in male subjects. However, similar correlated behavior among the same regions has not been observed in female subjects clearly (see Figure 3-2).

In order to see the correlated relation between modified front and hindfoot region, a regression analysis has been done. Accordingly, obtained results are plotted and shown in Figure 3-3. A correlation coefficient of $R=0.97$ is obtained for representative male subject and $R=0.71$ is obtained for representative female subject.

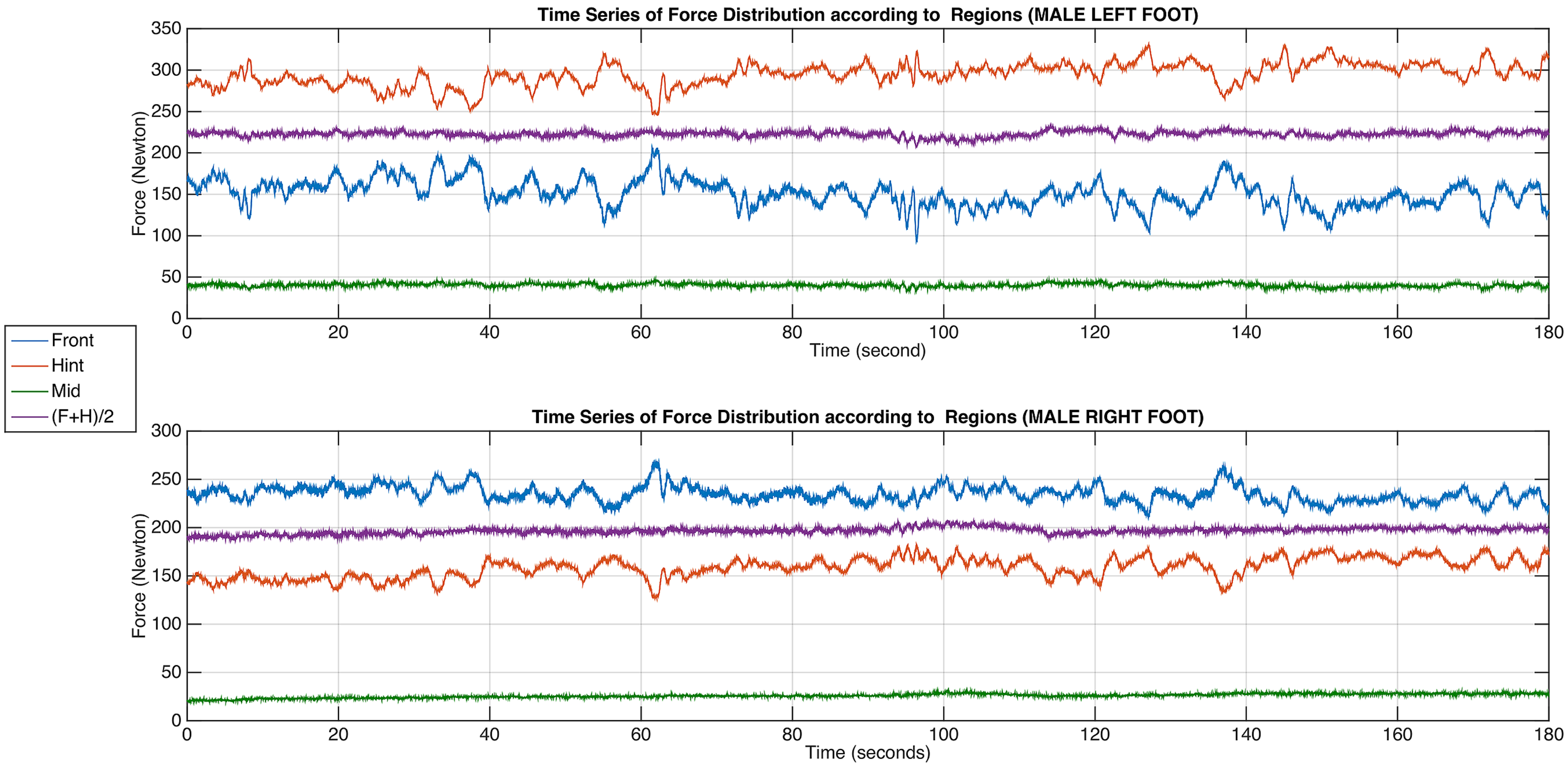

Figure 3-1 Time series of averaged normal forces at three plantar regions of left and right foot for a representative male

Figure 3-2 Time series of averaged normal forces at three plantar regions of left and right foot for a representative female

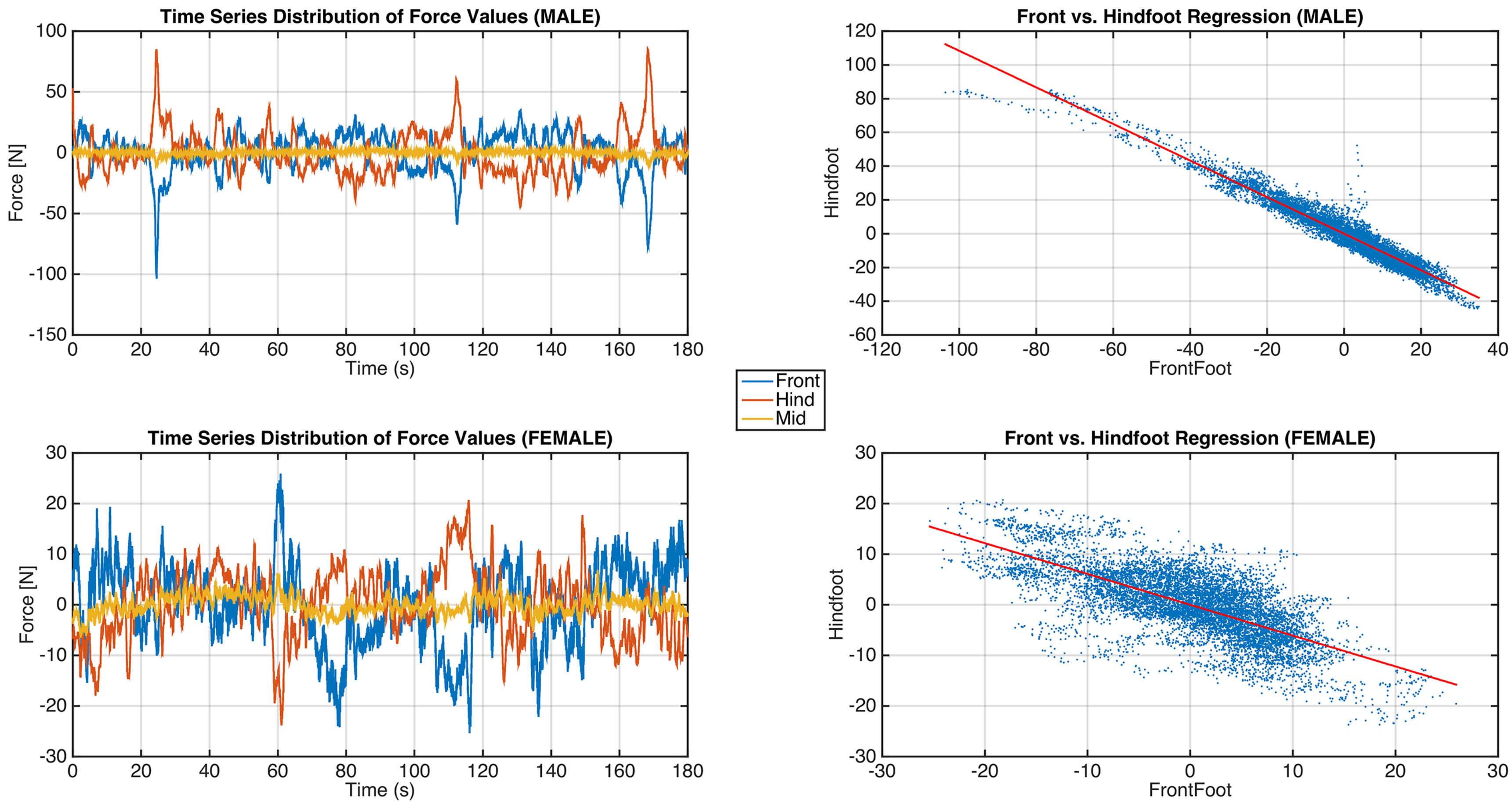

Figure 3-3 Correlated relation between Front and Hind Region can be seen clearly looking at the regression plots respectively for both male and females

Mean, variance and correlation function coefficient (normalized cross-variance function) at $\tau = 0$, (see Equation 2-6) results of normal force signals among three regions for male and female subjects are presented in Table 3-2A and 3-2B. Summary of the 5 dimensional ANOVA table is presented in Table 3-3.

Table 3-2A. Mean and variance (mean±std.dev) values of normal force distribution in Newton, where "L" stands for Left foot and "R" stands for right foot. "EC" and "EO" are for eyes closed and open conditions respectively in time series results. (R_{xy} at $\tau = 0$, Eq. 2-6)

				Region		
Gender	Foot	Eyes	Values	F	H	M
Female	L	EC	Mean [N]	127.79 ± 21.02	136.18 ± 37.10	29.82 ± 13.54
			Variance [N^2]	177.86 ± 153.70	163.66 ± 118.41	11.1 ± 10.11
		EO	Mean [N]	119.31 ± 23.75	137.0 ± 32.21	30.88 ± 10.52
			Variance [N^2]	150.5 ± 120.47	175.13 ± 112.90	12.16 ± 11.66
	R	EC	Mean [N]	147.82 ± 28.0	145.33 ± 31.37	37.56 ± 17.58
			Variance [N^2]	144.96 ± 116.30	170.43 ± 120.39	10.64 ± 7.92
		EO	Mean [N]	140.27 ± 31.84	153.1 ± 32.02	37.85 ± 16.48
			Variance [N^2]	154.4 ± 114.76	153.39 ± 110.65	16.25 ± 18.0
Male	L	EC	Mean [N]	219.19 ± 38.27	225.19 ± 45.60	42.81 ± 22.39
			Variance [N^2]	253.52 ± 147.93	281.48 ± 172.34	9.22 ± 7.43
		EO	Mean [N]	208.92 ± 33.79	232.48 ± 54.38	40.52 ± 22.66
			Variance [N^2]	213.35 ± 159.43	235.35 ± 159.37	7.07 ± 5.79
	R	EC	Mean [N]	225.6 ± 39.44	204.53 ± 31.08	33.62 ± 12.57
			Variance [N^2]	160.14 ± 92.01	195.34 ± 102.79	8.52 ± 9.32
		EO	Mean [N]	222.44 ± 27.91	200.15 ± 38.92	31.88 ± 11.62
			Variance [N^2]	134.55 ± 78.9	144.06 ± 118.54	7.14 ± 9.86

Table 3-2B Cross correlation values normal force distribution (mean±std.dev) in time series results.

				Region		
Gender	Foot	Eyes	Values	FH	FM	HM
Female	L	EC	$\rho_{XY}(\tau=0)$	-0.79 ± 0.10	0.5 ± 0.39	-0.12 ± 0.43
		EO	$\rho_{XY}(\tau=0)$	-0.6 ± 0.29	0.67 ± 0.21	-0.08 ± 0.47
	R	EC	$\rho_{XY}(\tau=0)$	-0.67 ± 0.25	0.67 ± 0.17	-0.16 ± 0.42
		EO	$\rho_{XY}(\tau=0)$	-0.55 ± 0.27	0.69 ± 0.21	-0.06 ± 0.46
Male	L	EC	$\rho_{XY}(\tau=0)$	-0.78 ± 0.17	0.61 ± 0.24	-0.26 ± 0.30
		EO	$\rho_{XY}(\tau=0)$	-0.78 ± 0.20	0.64 ± 0.22	-0.31 ± 0.37
	R	EC	$\rho_{XY}(\tau=0)$	-0.7 ± 0.15	0.51 ± 0.21	-0.03 ± 0.30
		EO	$\rho_{XY}(\tau=0)$	-0.73 ± 0.12	0.6 ± 0.18	-0.21 ± 0.25

Table 3-3 ANOVA results of mean, variance and cross correlation coefficients

Source	Means	Variances	Corr. coeff
Gender	0.0000	0.0001	0.0025
Region	0.0000	0.0000	0.0000
Foot	0.0649	0.0000	0.0341
Eyes	0.204	0.0212	0.1068
gender×region	0.0000	0.0037	0.5875
gender×foot	0.0000	0.0001	0.9542
gender×eyes	0.6019	0.0595	0.0114
region×foot	0.0000	0.0019	0.4703
region×eyes	0.0077	0.2194	0.2056

It can be seen that load has almost been carried by either hind or modified front region in both left and right foot while mid-region did not participate substantially in load carrying process. We found that average normal forces of males (see Figure 3-4) at their left foot (161.52 N) were significantly different ($p<0.00$) than their right foot (153.03 N). The average normal force values represent the group means over two feet and three regions (2×3) coming from multi-comparison statistics of 5 dimensional ANOVA. However, right foot's average normal force has been found to be significantly larger than left foot in females (110.32N vs. 96.83 N respectively, $p<0.00$). We have also found in Figure 3-5 that average force distribution for the left foot "H" region is found to be larger than "F" region while in the right foot "F" was greater than "H" ($p<0.00$). "H" is found to be significantly greater than "F" in females ($p<0.00$). We didn't observe any significant difference for eyes closed versus open conditions.

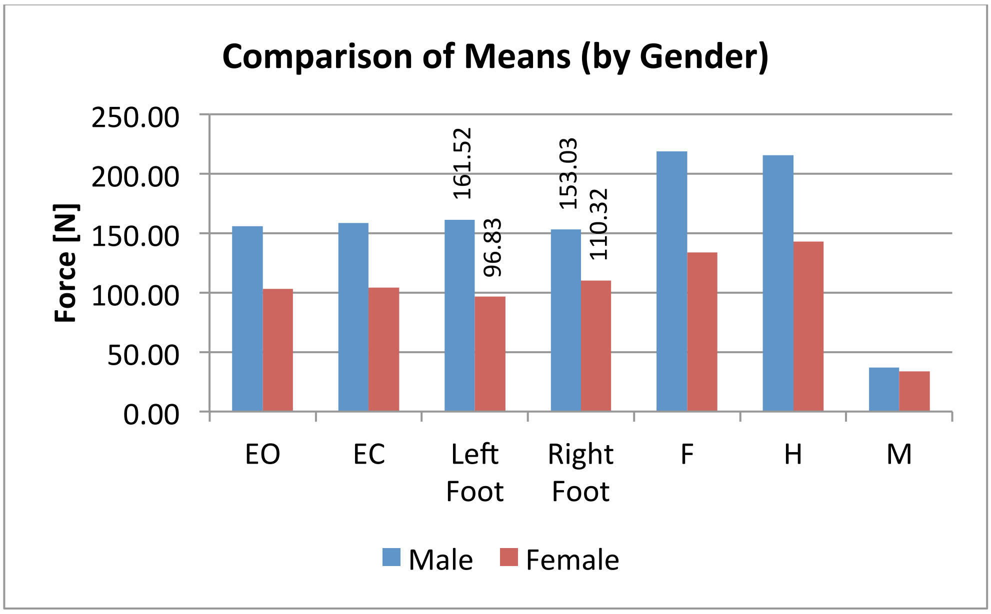

Figure 3-4 Comparison of means values by gender

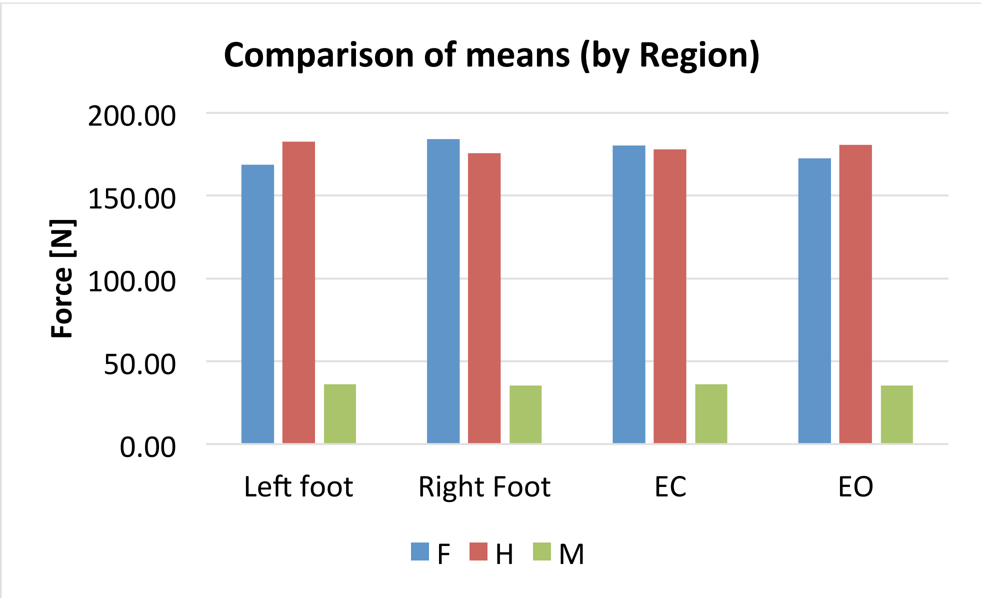

Figure 3-5 Multi-comparison results of mean by region

Variances in gender (M:137.478±6.545, F:111.706±6.545), foot (L:140.866±6.545, R:108.318±6.545), regions (F:173.660±8.016, H:189.854±8.016, M:10.261±8.016) and eyes conditions (EO:132.239±6.545, EC:116.945±6.545) were significantly different. ($p<0.00$, $p<0.00$, $p<0.00$, $p<0.02$ respectively).

Furthermore, male left foot and "H" region variance was significantly larger ($p<0.00$, $p<0.0037$).

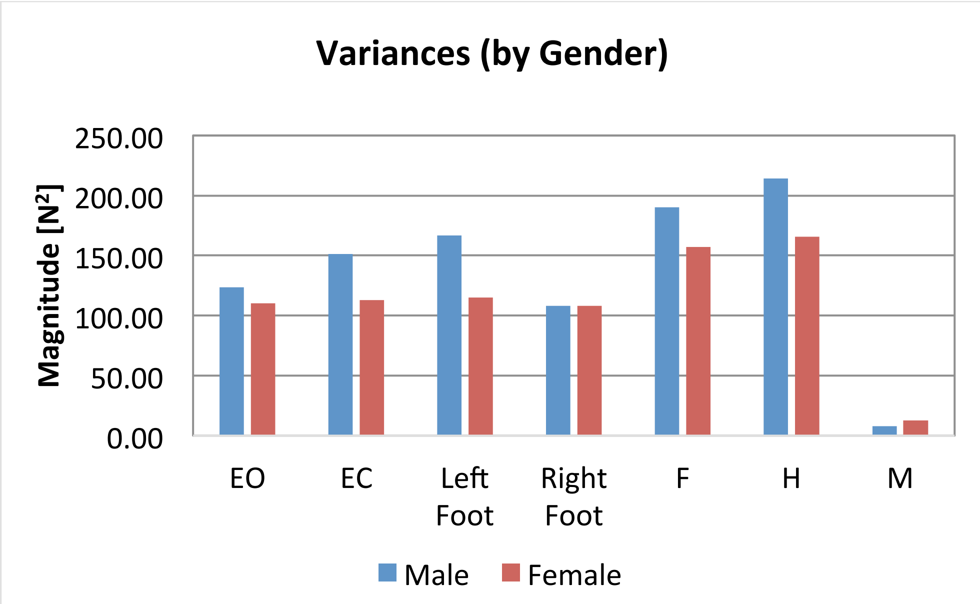

Figure 3-6 Comparison of Variances by gender

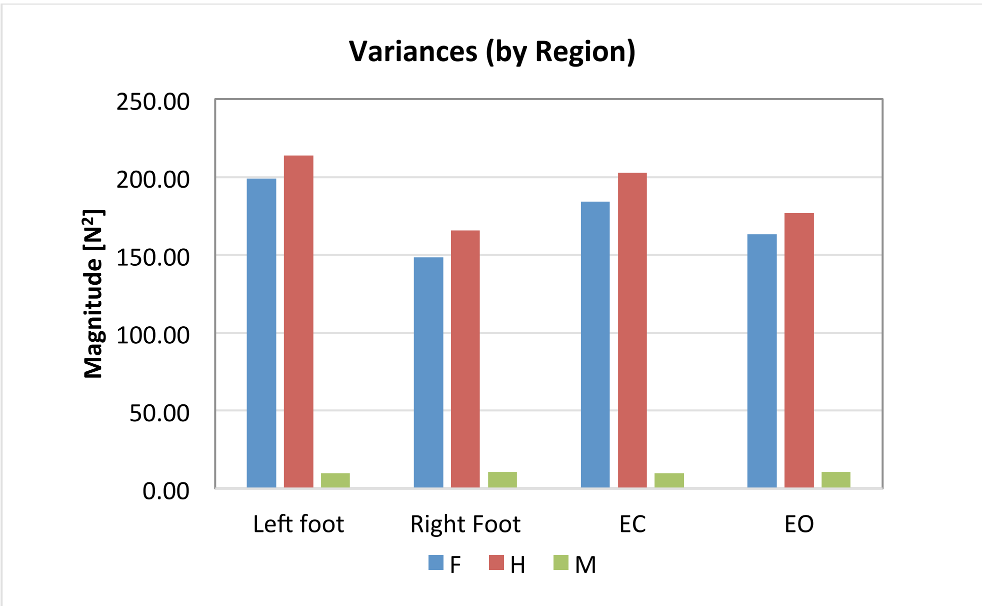

Figure 3-7 Comparison of Variances with respect to region and foot

Comparison of cross correlation coefficients among "FH", "HM" and "FM" regions demonstrated strong negative (-) relation in "FH", positive (+) relation in "FM" and slightly negative relation in "HM" region (see Table 3-2B).

The above graphs do not consider gender difference. Complementing the gender factor, though load distribution not affected, use of right and left foot is not same for both gender. Use of foot is significant and hence differs.

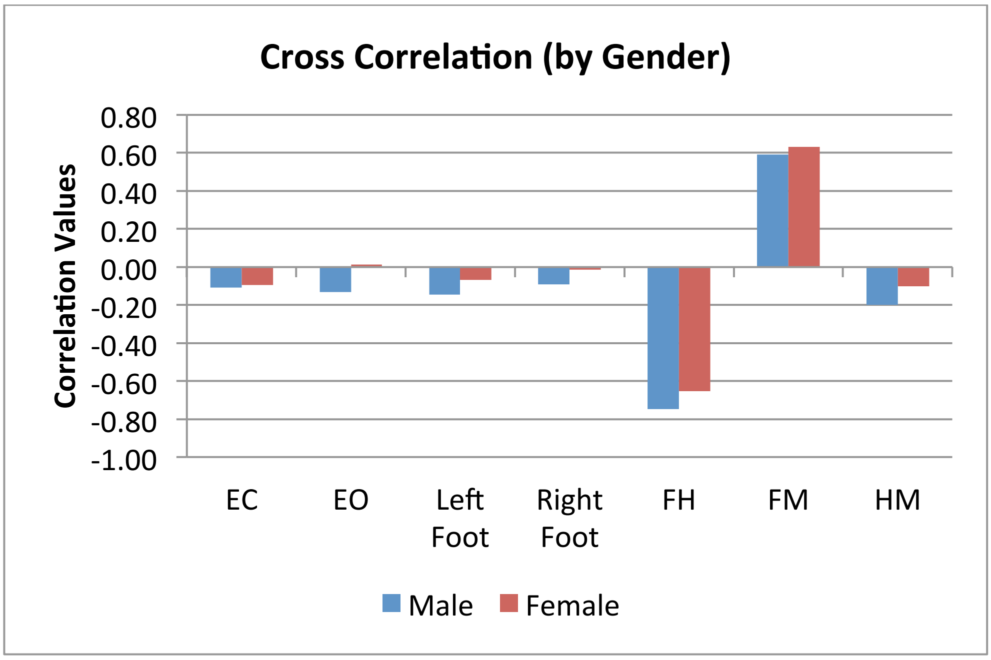

Figure 3-8 Cross Correlation values between FH, FM and HM in time domain

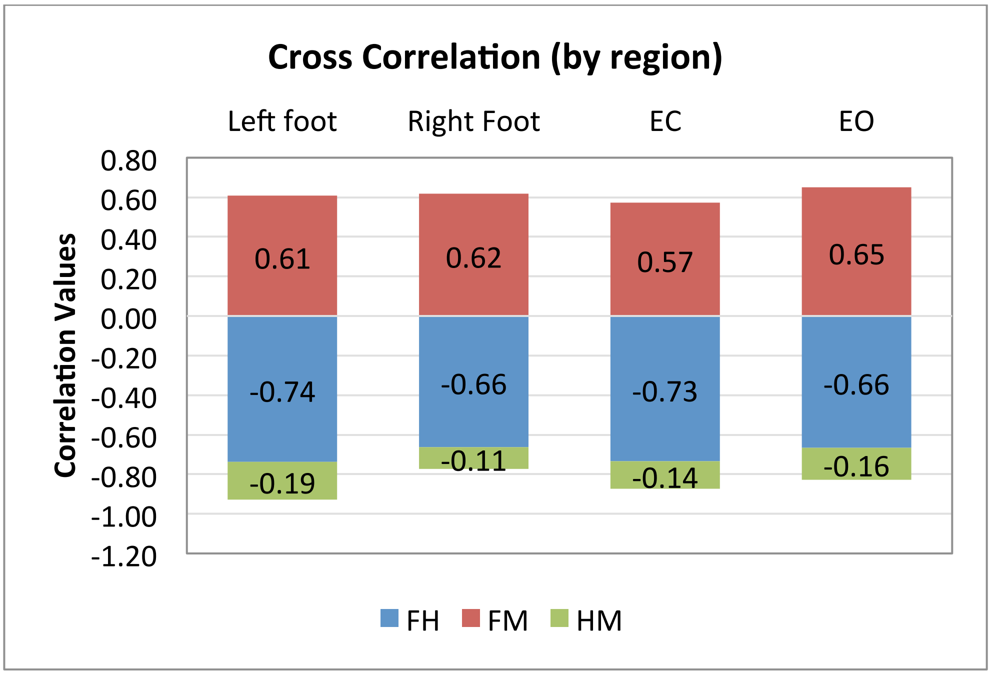

Figure 3-9 Cross Correlation values between FH, FM and HM in time domain by region

3.3 Frequency Domain And Spectral Analysis

3.3.1 Autocorrelation and Power Analysis

Magnitudes of FFT of pressure distribution over three foot regions are presented at for representative male and female subjects at Figure 3-10. Although most of the power at each foot has been collected at lower frequencies, in some of the cases (especially in male subjects) high frequencies at around 14 Hz present relatively higher magnitudes (3/7 on males and 0/7 on females a nonparametric sign test showed p=0.25 significance among males and females). Such an example is given in Figure 3-11.

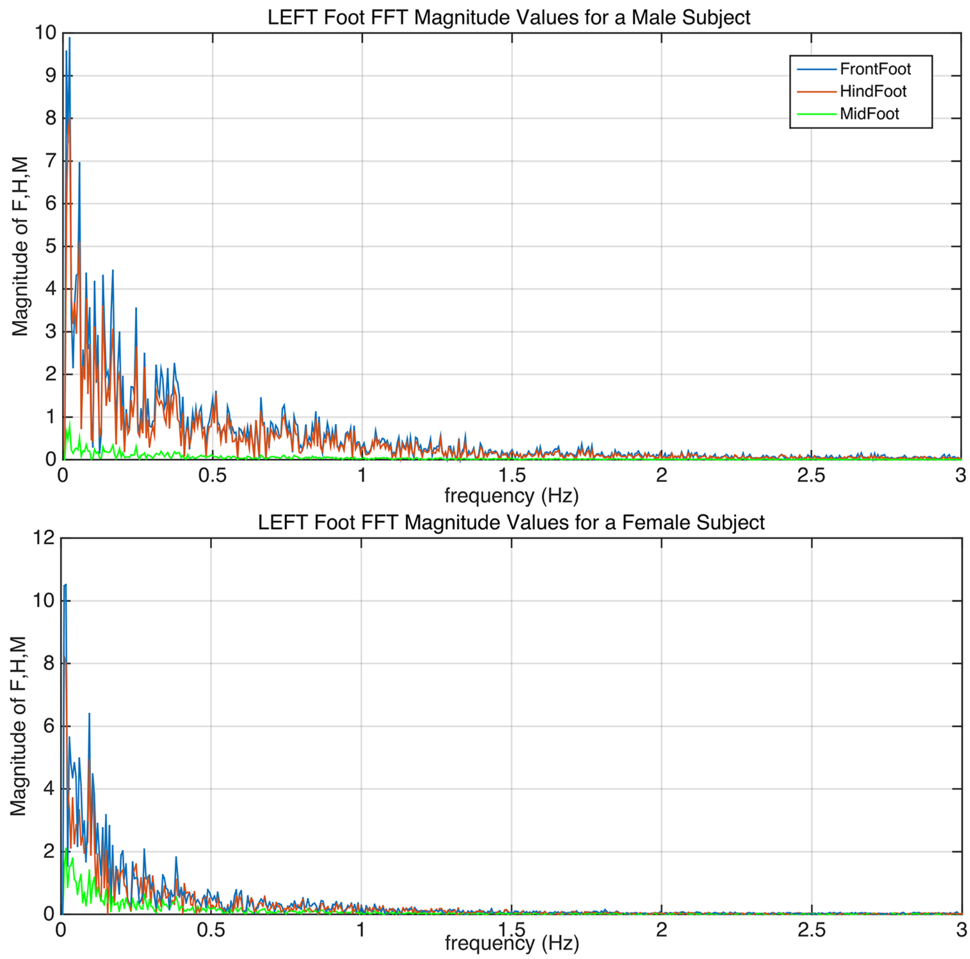

Figure 3-10 FFT plot of normal force time series for a male and female subject (left foot) at three foot-regions.

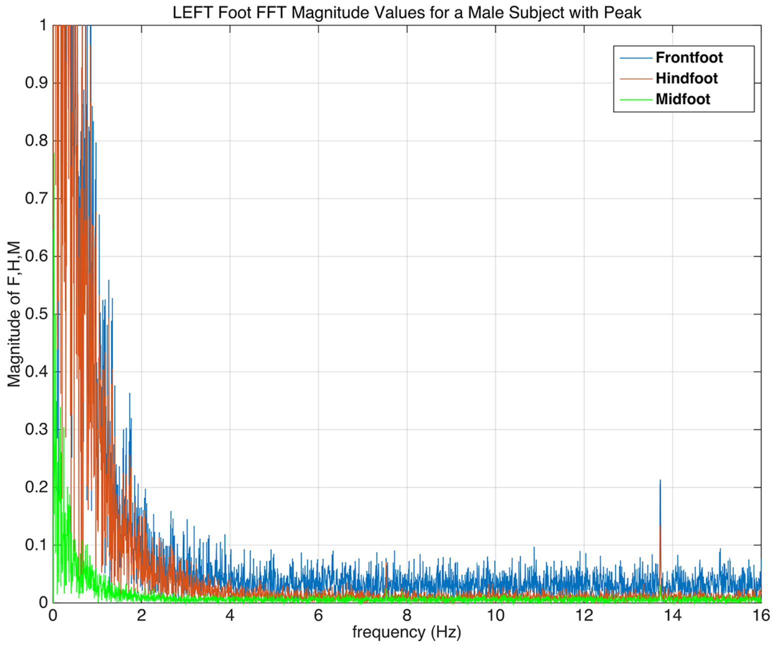

Figure 3-11 High Frequency peak at 14 Hz

Table 3-4 Power calculations data

Gender	Foot	Region	Eyes	P95	P95_frq	P50	P50_freq	CFREQ	FREQD
F	L	F	EC	284.16 ± 244.88	0.95 ± 1.14	164.05 ± 143.89	0.06 ± .04	0.18 ± .1	0.79 ± .05
			EO	218.34 ± 172.14	01.77 ± 3.28	121.91 ± 96.52	0.06 ± .03	0.26 ± .41	0.79 ± .08
		H	EC	246.55 ± 191.66	0.52 ± .17	139.98 ± 112.14	0.05 ± .04	0.15 ± .06	0.78 ± .05
			EO	210.62 ± 164.	0.45 ± .11	119.16 ± 93.17	0.06 ± .03	0.13 ± .04	0.75 ± .07
		M	EC	15.8 ± 17.3	05.05 ± 6.07	8.76 ± 9.41	0.07 ± .04	0.78 ± 1.01	0.85 ± .1
			EO	18.91 ± 19.91	04.22 ± 6.7	10.77 ± 11.21	0.06 ± .03	0.79 ± 1.5	0.83 ± .1
	R	F	EC	235.3 ± 186.09	01.17 ± 1.88	140.13 ± 124.88	0.06 ± .05	0.19 ± .17	0.79 ± .05
			EO	212.33 ± 161.57	0.82 ± 1.36	122.87 ± 96.97	0.07 ± .04	0.15 ± .11	0.79 ± .08
		H	EC	263.62 ± 204.01	0.48 ± .17	149.35 ± 118.2	0.06 ± .03	0.15 ± .08	0.78 ± .05
			EO	235.1 ± 162.8	0.44 ± .11	136.75 ± 90.37	0.06 ± .03	0.13 ± .05	0.75 ± .07
		M	EC	14.86 ± 11.15	02.67 ± 4.43	8.73 ± 7.13	0.07 ± .07	0.41 ± .62	0.85 ± .1
			EO	20.89 ± 23.44	02.09 ± 4.2	12.11 ± 13.81	0.07 ± .08	0.39 ± .9	0.83 ± .1
M	L	F	EC	415.3 ± 265.57	03.43 ± 6.55	229.77 ± 154.91	0.08 ± .05	0.83 ± 1.62	0.8 ± .07
			EO	358.23 ± 299.4	04.52 ± 7.48	202.06 ± 176.38	0.08 ± .05	01.11 ± 2.07	0.81 ± .07
		H	EC	444.22 ± 298.51	0.76 ± .38	250.02 ± 171.99	0.07 ± .04	0.19 ± .08	0.78 ± .05
			EO	353.89 ± 284.81	0.55 ± .16	205.83 ± 175.67	0.06 ± .03	0.15 ± .05	0.78 ± .06
		M	EC	11.86 ± 10.82	06.66 ± 7.49	6.79 ± 6.33	0.08 ± .07	01.35 ± 1.89	0.87 ± .09
			EO	8.29 ± 7.85	08.21 ± 7.88	4.71 ± 4.64	0.26 ± .68	01.86 ± 2.7	0.87 ± .08
	R	F	EC	261.71 ± 153.97	03.22 ± 6.08	145.88 ± 88.23	0.07 ± .03	0.68 ± 1.29	0.8 ± .07
			EO	210.11 ± 134.65	04.49 ± 6.56	115.21 ± 71.43	0.07 ± .03	0.85 ± 1.49	0.81 ± .07
		H	EC	270.07 ± 161.59	0.63 ± .32	149.65 ± 87.06	0.06 ± .04	0.15 ± .09	0.78 ± .05
			EO	190.34 ± 162.89	0.57 ± .2	104.05 ± 87.55	0.07 ± .04	0.12 ± .06	0.78 ± .06
		M	EC	6.7 ± 8.3	08.91 ± 7.22	3.92 ± 5.5	0.08 ± .07	01.6 ± 1.66	0.87 ± .09
			EO	5.11 ± 4.5	11.89 ± 7.4	2.88 ± 2.61	0.08 ± .06	02.36 ± 1.94	0.87 ± .08

Table 3-5 ANOVA results for power calculations

	P95%	P95% frq	P50%	P50% frq	CFREQ	FREQD
Gender	0.0000	0.0000	0.0002	0.278	0.0000	0.0000
Subject	0.0000	0.0000	0.0000	0.0784	0.0000	0.0000
Region	0.0000	0.0000	0.0000	0.0379	0.0000	0.0000
Foot	0.0000	0.9261	0.0000	0.1638	0.4311	1.0000
Eyes	0.0009	0.0844	0.0021	0.2308	0.029	0.0934
gender×region	0.0001	0.0000	0.0055	0.1415	0.0000	0.1355
gender×foot	0.0000	0.0008	0.0000	0.1051	0.1355	1.0000

In order to understand characteristics of the frequency content of the time series about normal force distribution at foot regions (F, H and M separately), frequency domain metrics (using equations 2.7 - 2.17 were computed (Table 3-4).

Considering the interactions of the ANOVA table (Table 3-5), by looking at multicomparisons statistics, the following observations can be made. 95% Power comparisons, which are very close to the time domain variance comparisons, reveal that gender [N^2] (M:211.317±7.510 F:164.705±7.510), foot [N^2] (L:215.514±7.510 R:160.511±7.510), regions[N^2] (F:274.434±9.198 H:276.801±9.198 M:12.802±9.198) and eyes conditions[N^2] (EC:205.845±7.510 EO:170.180±7.510) are significantly different ($p<0.00$, $p<0.00$, $p<0.00$, $p<0.0009$ respectively). In male subjects 95% power is not equally distributed over left and right foot; left being dominant where in the case of female subjects they are equally distributed over both feet. In terms of regions, F and H load is almost equally distributed. In terms of Eyes Conditions as in variances male EC condition was significantly higher.

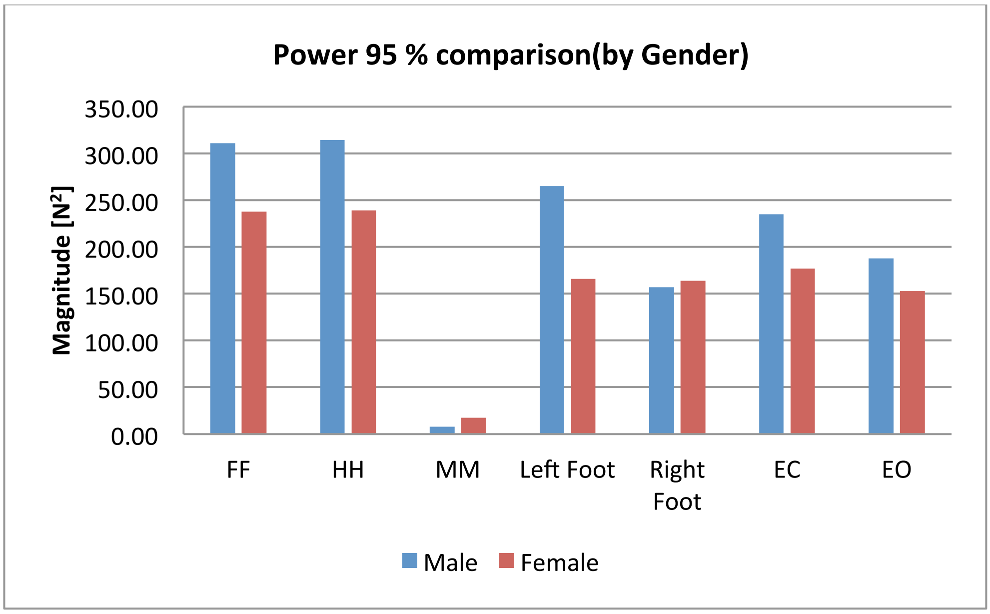

Figure 3-12 95% Power values and comparison by gender

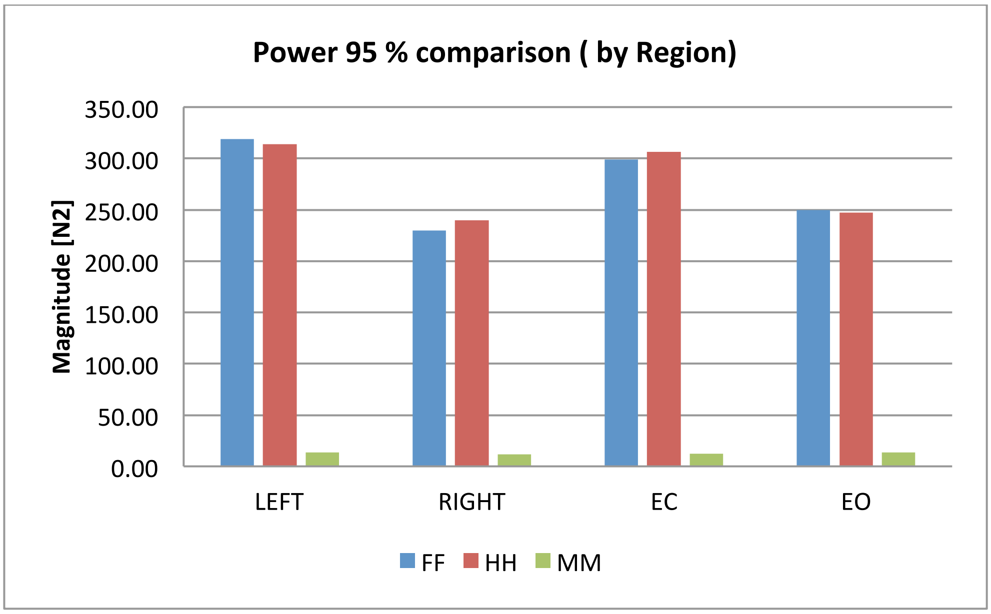

Figure 3-13 95% Power values and comparison by region

In the case of 95% power frequency, there is no significance between foots and eyes conditions. However, gender (male>female) and region comparison were significantly different ($p<0.00$). Considering regions of the foot Mid section 'M' has highest frequency range in males at about 9 Hz., where about 3.5 Hz. in females. 'F' region in males has about 3.95 Hz. and significantly higher than ‘H’ region however, females F and H region were not significantly different and were at about 0.55 Hz. This high frequency can be interpreted as high signal/noise ratio and since hindfoot region is almost static act as a support and much of the forces accumulated there, maximum power is attained at lower frequency values. Where in the case of Midfoot region, at lower amplitude maximum power is attained at higher frequencies.

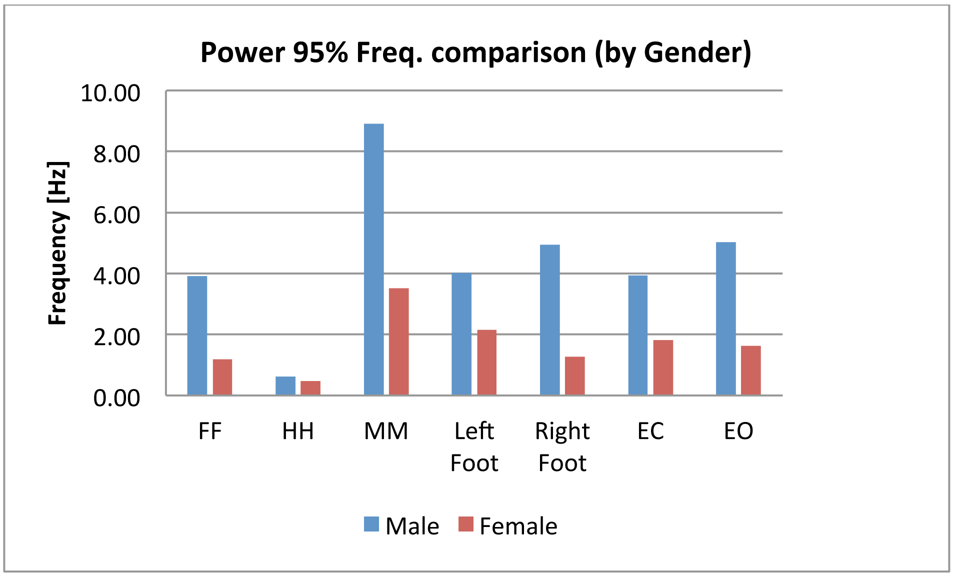

Figure 3-14 Power 95% frequency comparison by region

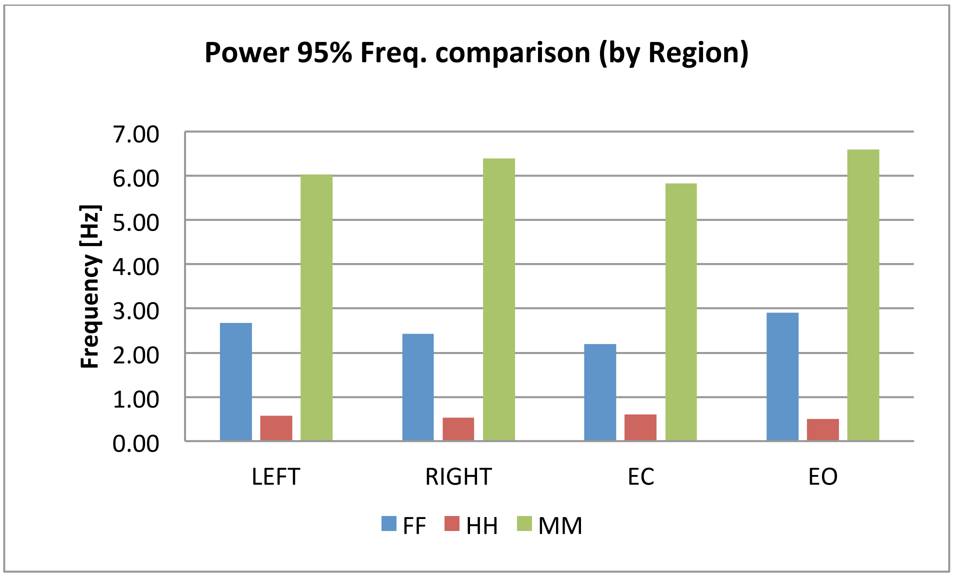

Figure 3-15 Power 95% frequency comparison by region

We could not find any significant differences when P95% magnitute estimates were compared to P50% magnitude estimates. However, behavior at P50 frequencies were different in gender and regions respectively ($p<0.0278$, $p<0.0379$) However, gender behavior at different foot regions were similar.

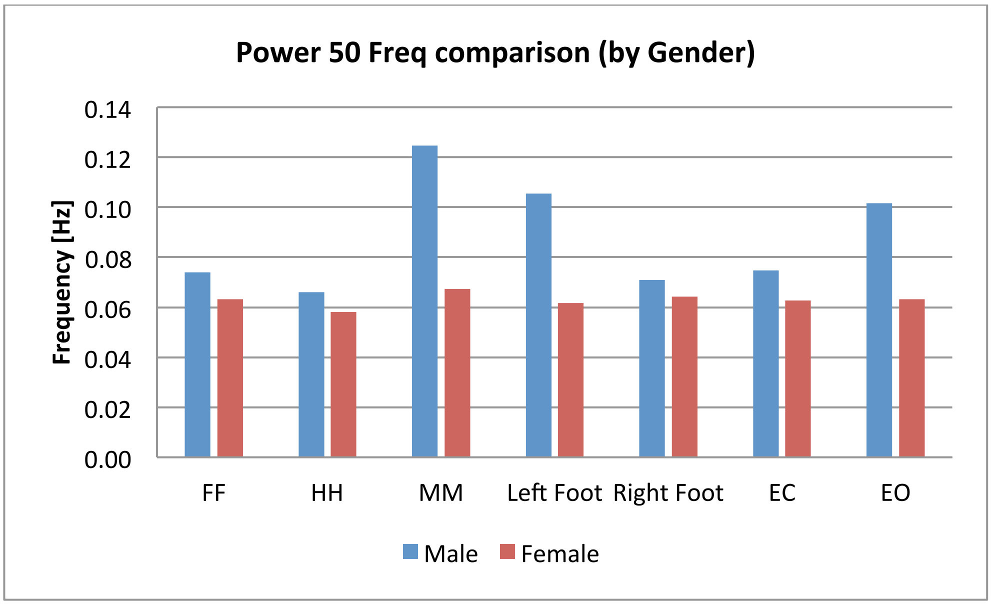

Figure 3-16 Power 50 % frequency comparison by gender

When it comes to centroidal frequency CFREQ gender (male:0.94, female:0.31 Hz), regions(F:0.53, H:0.15, M:1.20 Hz) and eyes conditions(EC:0.55, EO:0.69) were significantly different ($p<0.00$, $p<0.029$ respectively). Both feet CFREQ were about 0.60 Hz. Males "M" region CFREQ was significantly larger ($p<0.00$) at about 1.79 Hz compared to male "F" and "H" regions and females. Moreover, males "F" region and female "M" region were about 0.86 and significantly larger than male "H" and female "F" and "H" regions.

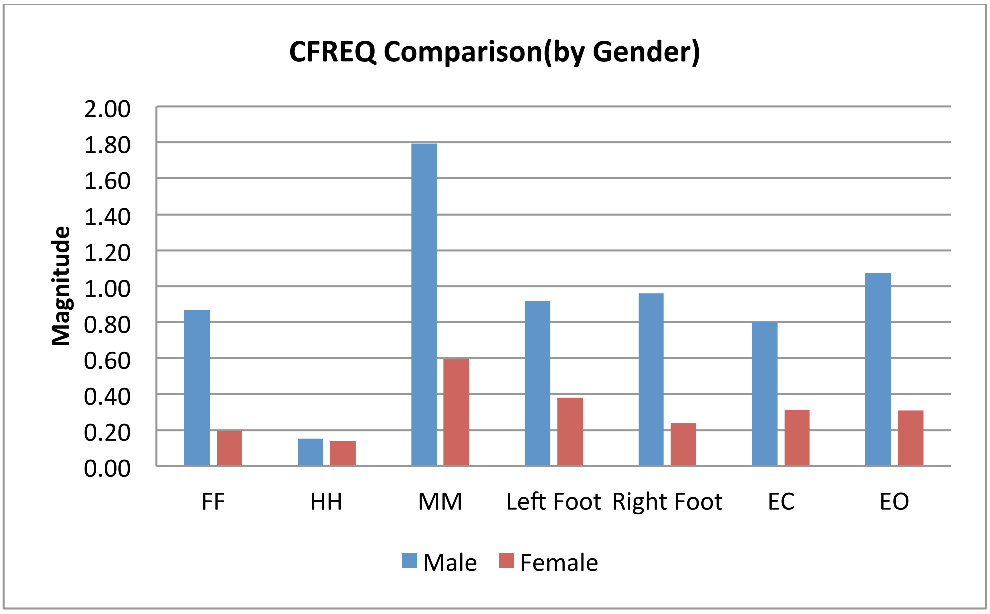

Figure 3-17 CFREQ Comparison by gender

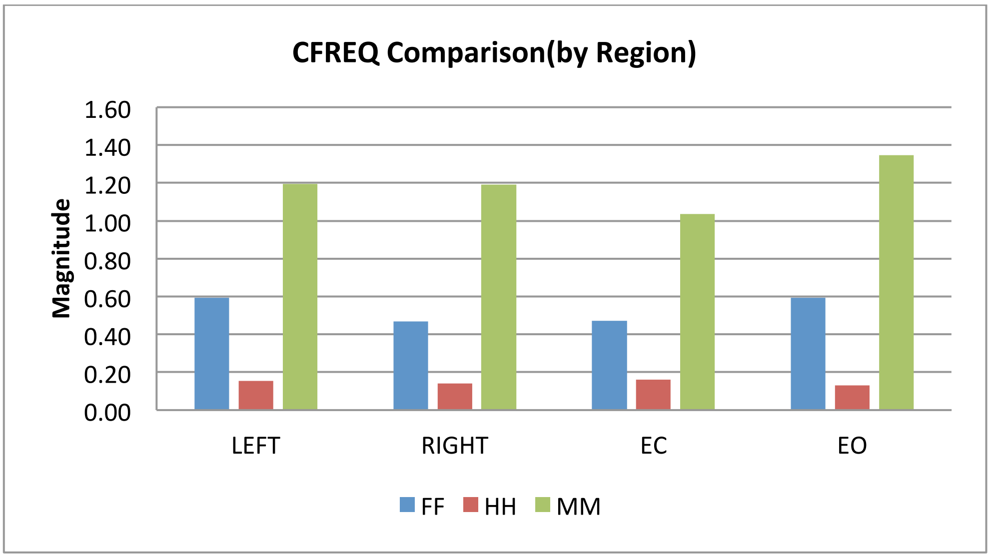

Figure 3-18 CFREQ Comparison by region

Frequency dispersion FREQD demonstrates differences in gender (male: 0.818±0.003, female: 0.796±0.003) and regions (F: 0.797±0.004, H: 0.771±0.004, M: 0.854±0.004). Furthermore, females at EO condition (0.787±0.004) were significantly smaller than EC (0.807±0.004) and males at eyes conditions ($p<0.0052$)

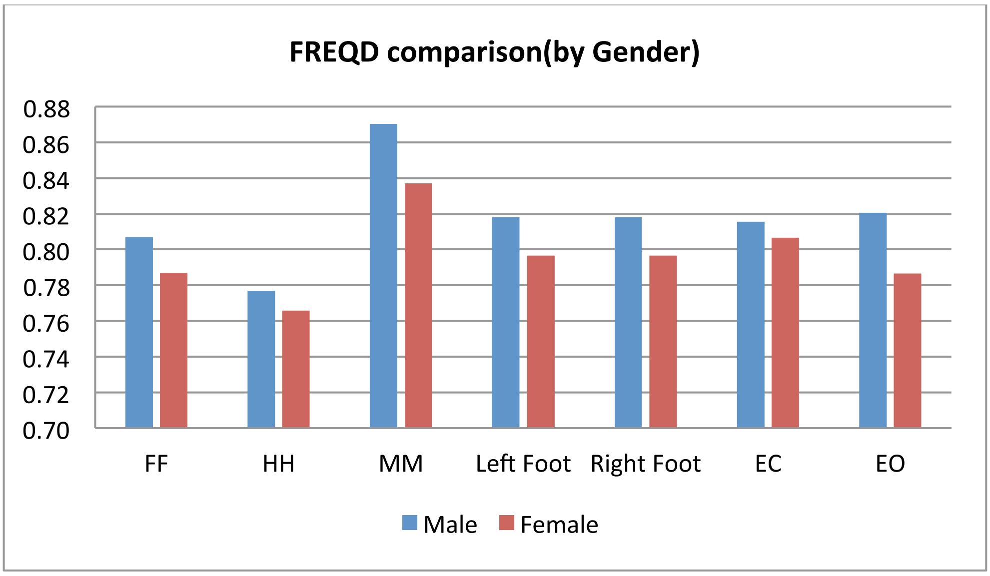

Figure 3-19 FREQD comparisons by gender

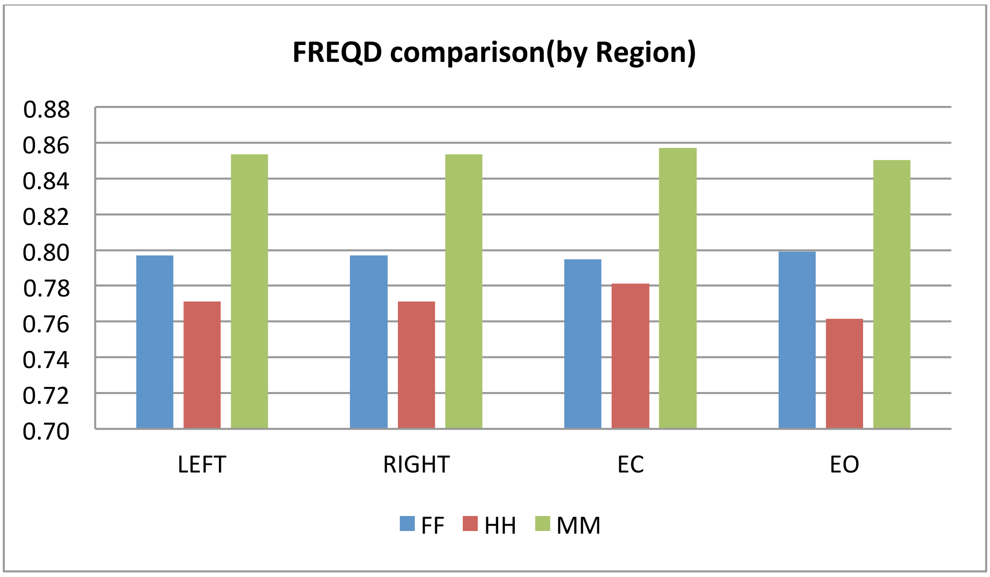

Figure 3-20 FREQD comparison by region

3.3.2 Cross Spectral density function Estimates

Cross-Spectral density function estimates of normal force distribution at F and H, F and M, and H and M regions and their 'cpsd' magnitudes or gains, coherence values of interactions and phase angles were computed (see methods). A representative male and a female subject's results are presented at Figure 3-21 and Figure 3-22 respectively.

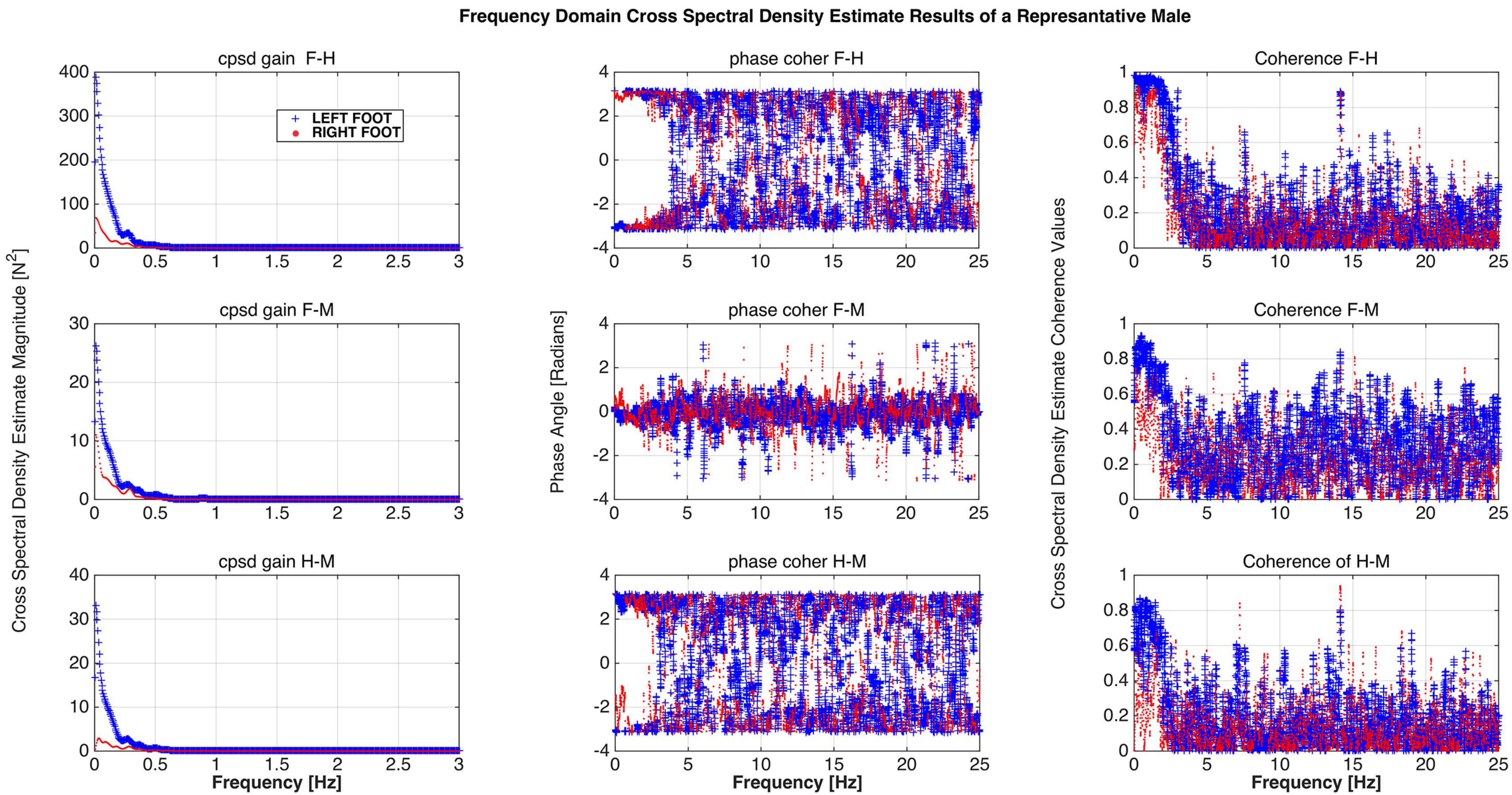

Figure 3-21 Representative Male Frequency Analysis Metrics Graphs

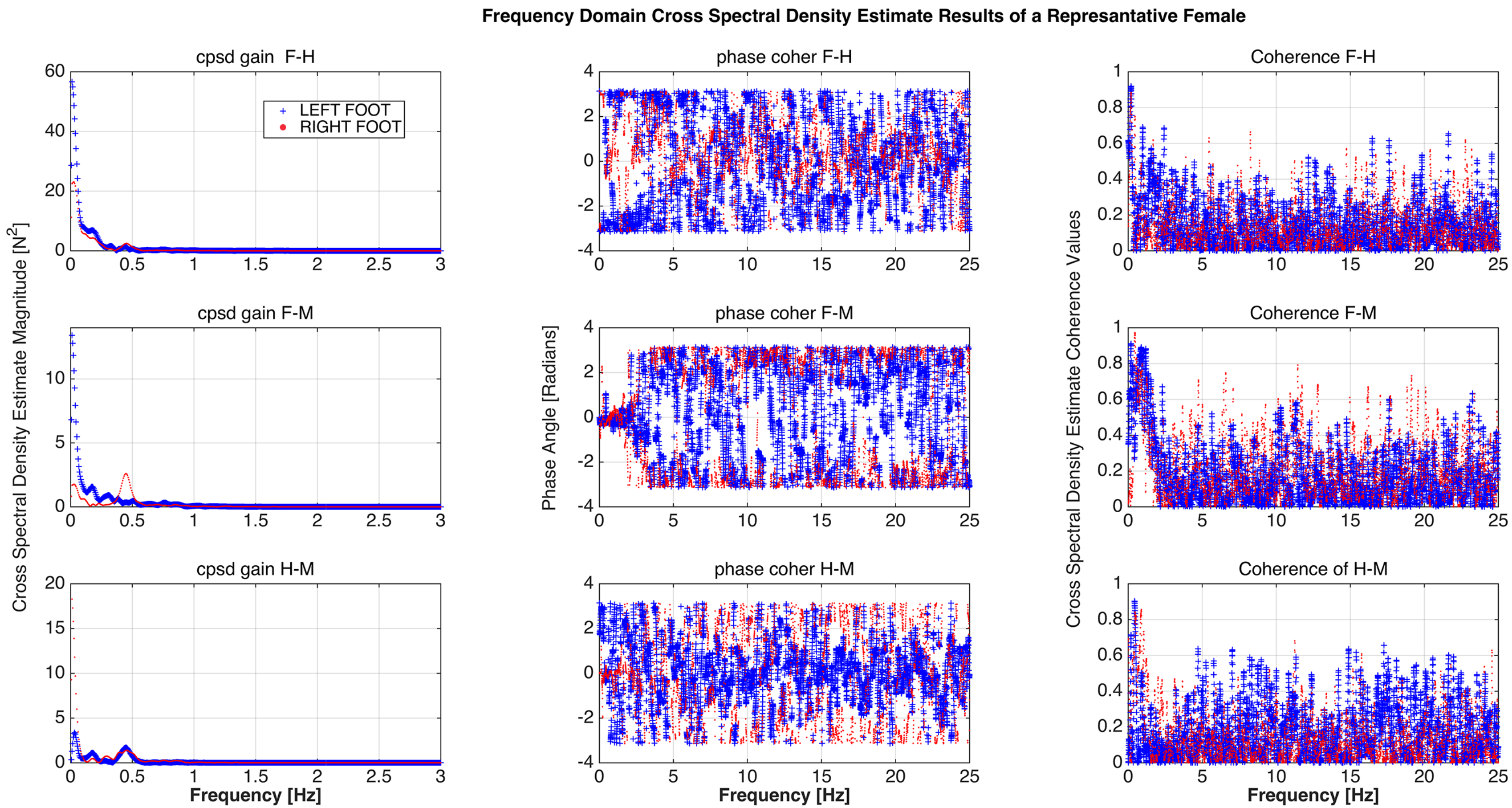

Figure 3-22 Representative Female Frequency Analysis Metrics Graphs

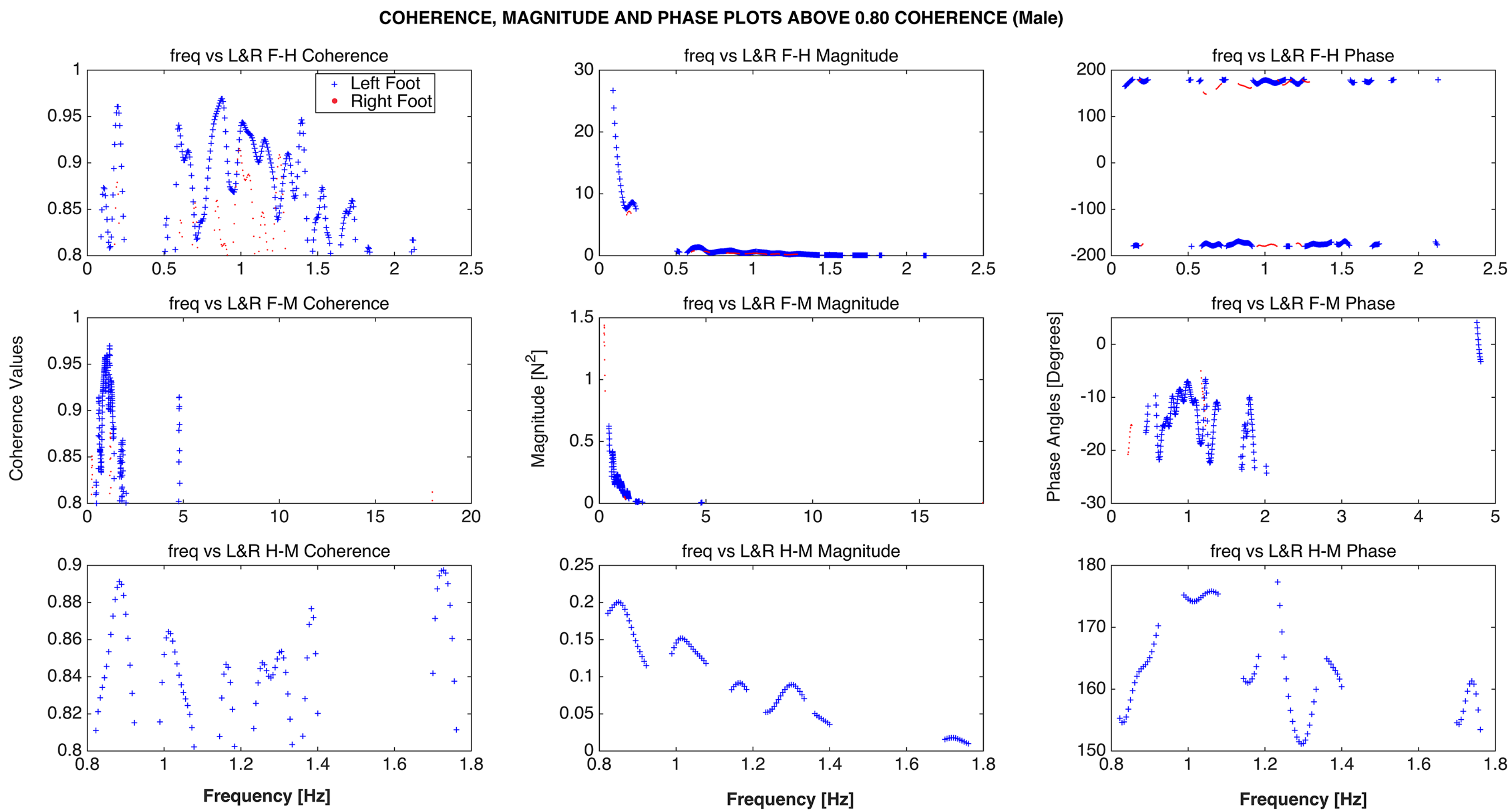

Figure 3-23 Coherence, magnitude and phase plots above 0.80 threshold coherence (males)

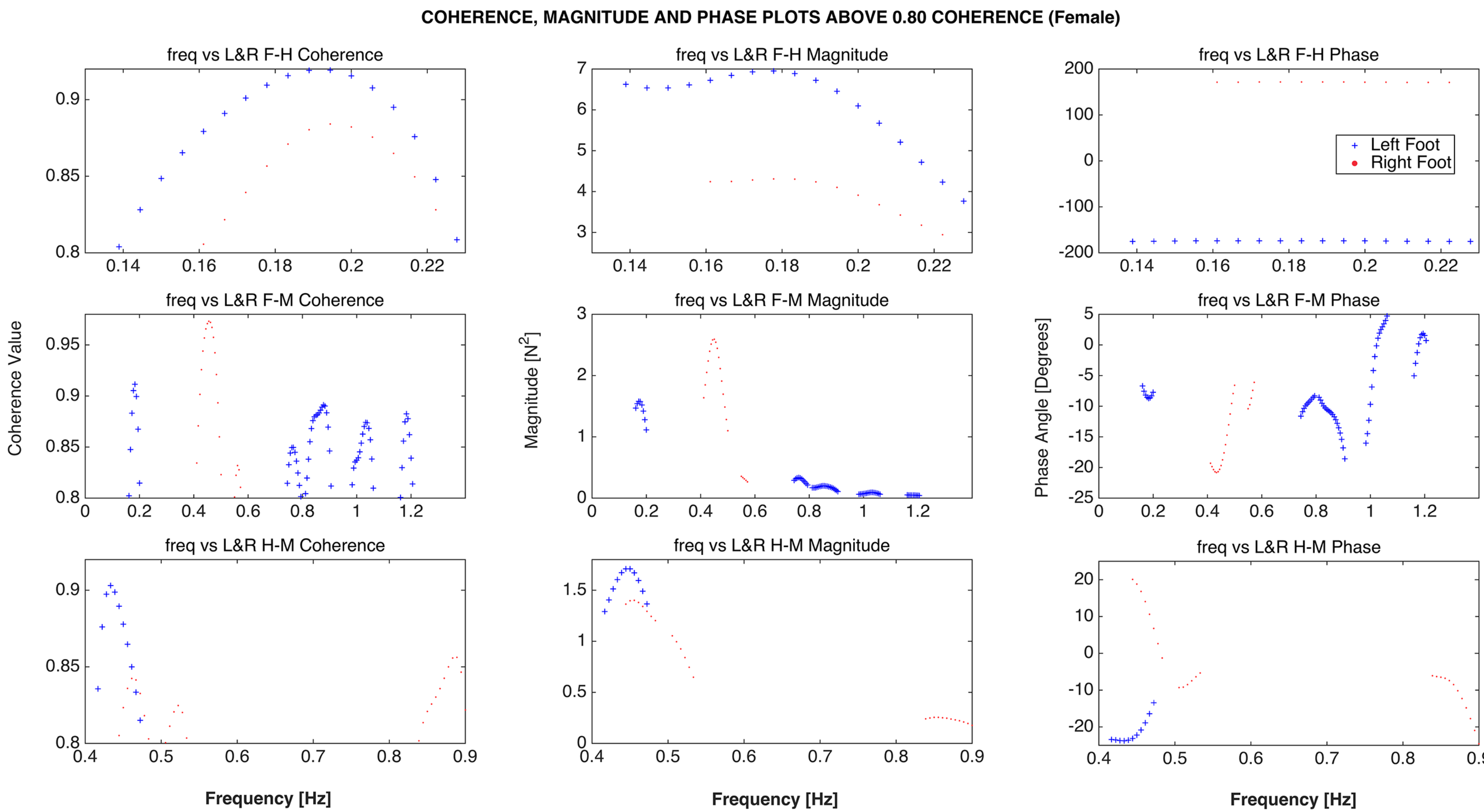

Figure 3-24 Coherence, magnitude and phase plots above 0.80 threshold coherence (females)

Since most of the coherence values are accumulated at 0-3 Hz region, and in order to better observe the correct behaviour, a 0.80 coherence value chosen. Accordingly, during the rest of the analysis data above this threshold value is considered. Representative plots over 0.80 are given in Figure 3-23 and Figure 3-24.

Frequency domain metrics; Δω (see Methods and sections), maximum coherence and its frequency (see eqns), maximum magnitude and its frequency (see eqns) at 0-3 Hz frequency region of the cross-spectrum density function computed at three foot regions were demonstrated at Table 3-6. Moreover, 5 dimensional ANOVA results have been shown on Table 3-7. Than respective metrics were analyzed. For the entire subjects; time domain and frequency domain plots of the obtained and calculated data were presented at APPENDIX A.

Table 3-6 Frequency domain analysis results (values ± standard deviations)

Gender	Region	Foot	Eyes	delta_ω	Max-coher	Max-coher_frq	Max-gain	Max-gain_frq
F	FH	L	EC	1.45 ± .84	0.89 ± .21	0.7 ± .48	80.76 ± 138.81	0.12 ± .15
			EO	1.03 ± .98	0.79 ± .33	2.56 ± 5.1	51.46 ± 84.61	2.21 ± 5.22
		R	EC	1.12 ± .82	0.83 ± .28	0.63 ± 0.51	53.35 ± 105.37	0.27 ± .37
			EO	0.68 ± .74	0.76 ± .33	2.32 ± 4.69	55.04 ± 132.02	2.05 ± 4.78
	FM	L	EC	1.07 ± .88	0.75 ± .38	2.11 ± 5.7	11.91 ± 21.63	0.39 ± .89
			EO	1.13 ± .85	0.83 ± .28	1.41 ± 3.92	20.44 ± 22.14	0.98 ± 3.98
		R	EC	1.13 ± .71	0.92 ± .05	0.67 ± 0.46	38.4 ± 72.77	0.22 ± .21
			EO	1.24 ± .74	0.91 ± .04	0.65 ± 0.55	26.85 ± 53.18	0.19 ± 0.21
	HM	L	EC	0.51 ± .72	0.56 ± .45	2.95 ± 7.03	4.32 ± 16.23	2.38 ± 5.94
			EO	0.42 ± .67	0.46 ± .45	2.26 ± 5.68	0.92 ± 1.67	0.44 ± 0.88
		R	EC	0.4 ± .64	0.63 ± .41	3.12 ± 5.67	0.52 ± 1.	2.84 ± 6.68
			EO	0.3 ± .62	0.49 ± .44	2.01 ± 3.84	4.77 ± 15.42	1.66 ± 4.05
M	FH	L	EC	2.27 ± .7	0.96 ± .04	0.86 ± .48	207.59 ± 287.97	0.1 ± 0.1
			EO	2.01 ± .8	0.96 ± .04	0.6 ± .39	218.42 ± 260.81	0.08 ± 0.13
		R	EC	1.79 ± .53	0.95 ± .03	1.44 ± 2.88	79.35 ± 131.02	0.26 ± 0.29
			EO	1.44 ± .79	0.89 ± .21	1.13 ± 2.98	54.4 ± 64.73	0.12 ± 0.14
	FM	L	EC	1.75 ± .7	0.94 ± .04	0.76 ± .41	9.62 ± 15.15	0.31 ± 0.22
			EO	1.6 ± .87	0.94 ± .05	1.48 ± 2.59	17.18 ± 26.58	1.81 ± 5.69
		R	EC	0.95 ± .94	0.74 ± .37	1.63 ± 3.25	8.91 ± 19.55	1.32 ± 3.33
			EO	0.8 ± .86	0.84 ± .2	3.73 ± 5.89	12.83 ± 23.82	2.91 ± 5.94
	HM	L	EC	1.18 ± .9	0.87 ± .21	2.29 ± 3.9	3.23 ± 7.81	1.41 ± 2.87
			EO	1.09 ± .72	0.83 ± .28	1.8 ± 3.13	3.62 ± 6.66	0.77 ± 1.44
		R	EC	0.26 ± .44	0.63 ± .41	3.21 ± 4.94	0.51 ± 1.71	2.86 ± 4.9
			EO	0.23 ± .45	0.47 ± .46	5.04 ± 7.29	0.09 ± .15	3.74 ± 6.8

Table 3-7 ANOVA table for spectral values

Source	$\Delta\omega$	Max. coherence	Max. coher.Freq.	Max.Gain	Max. Gain Freq
Gender	0.0000	0.0000	0.5193	0.0049	0.6105
Region	0.0000	0.0000	0.0004	0.0000	0.0016
Foot	0,0000	0.0049	0.154	0.002	0.0514
Eyes	0.0012	0.0611	0.2552	0.7313	0.2394
gender×subject	0.0000	0.0000	0.0034	0.0000	0.0073
gender×region	0.0000	0.0124	0.2761	0.0000	0.0195
gender×foot	0.0000	0.0000	0.0071	0.001	0.1153
gender×eyes	0.8021	0.4968	0.5287	0.7739	0.6261
region×foot	0.4744	0.0988	0.5308	0.0000	0.126
region×eyes	0.0103	0.0114	0.559	0.7818	0.0532

Considering the frequency band metric ($\Delta\omega$ [Hz]); gender(M:1.281±0.048, F:0.874±0.048), foot(L:1.293±0.048, R:0.862±0.048), regions(FH:1.475±0.058, FM:1.208±0.058, HM:0.549±0.058) and eyes conditions(EC:1.157±0.048, EO:0.998±0.048) were found to be significantly different($p<0.00$, $p<0.0187$ respectively). Furthermore, males Left foot (1.650±0.068) shows significantly higher bandwidth compared to its right foot (0.912±0.068) and females ($p<0.00$). On the other hand, when foot regions were compared with respect to gender, males' FH region was significantly higher (1.880±0.083) than it's other regions and females.

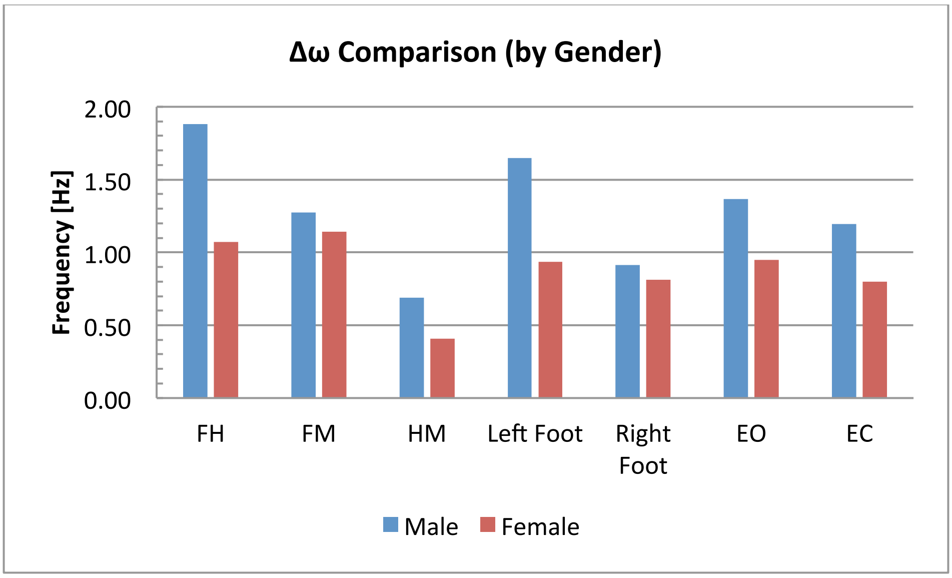

Figure 3-25 Frequency domain multi comparison based on Δω by gender

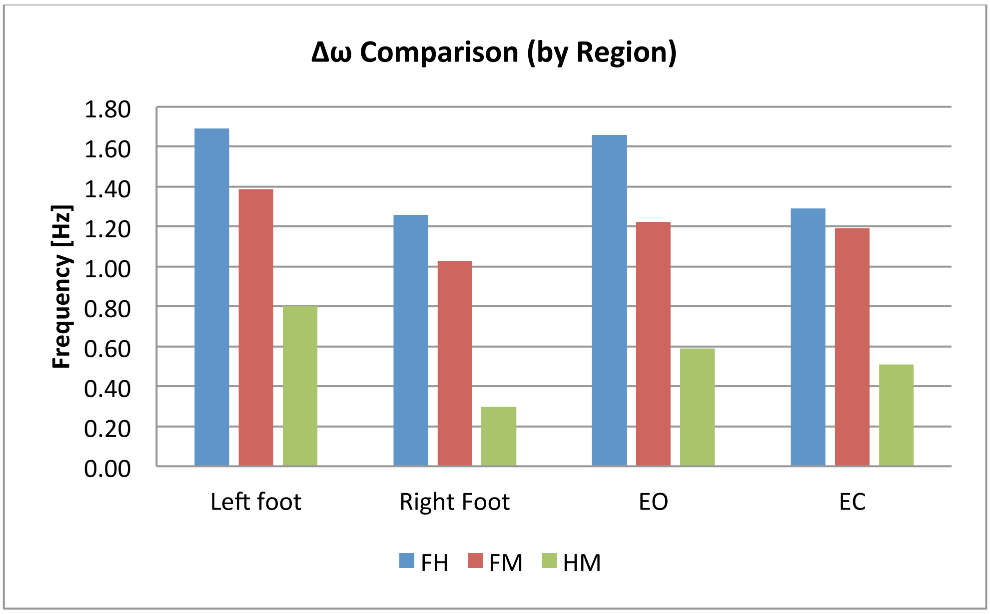

Figure 3-26 Frequency domain multi comparison based on Δω by region

Maximum Coherence in the range of [0-3Hz] showed significant differences in gender (M: 0.835±0.019, F: 0.736±0.019), foot (L: 0.815±0.019, R: 0.755±0.019), regions (FH: 0.879±0.023, FM: 0.860±0.023, HM: 0.617±0.023) ($p<0.00$).

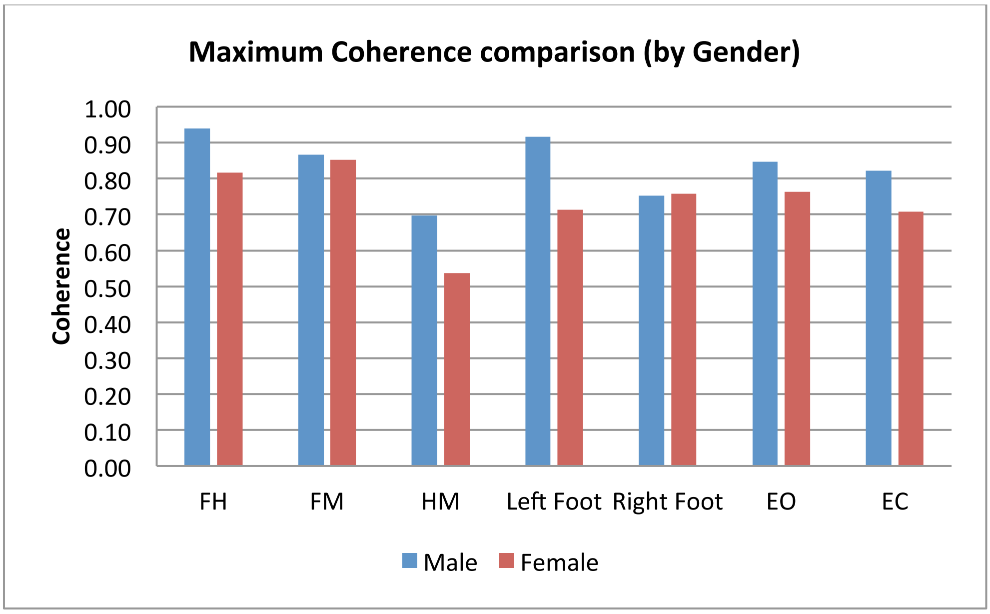

Figure 3-27 Comparison of maximum coherence by gender

Furthermore, males Left foot (0.917±0.026) shows significantly higher coherence compared to its right foot (0.753±0.026) and females ($p<0.00$). On the other hand, when foot regions are compared with respect to gender, females' HM region significantly showed lower coherence (0.537±0.032) than its other regions (FH: 0.817±0.032) and males (HM: 0.698±0.032 and FH: 0.940±0.032) ($p<0.0124$).

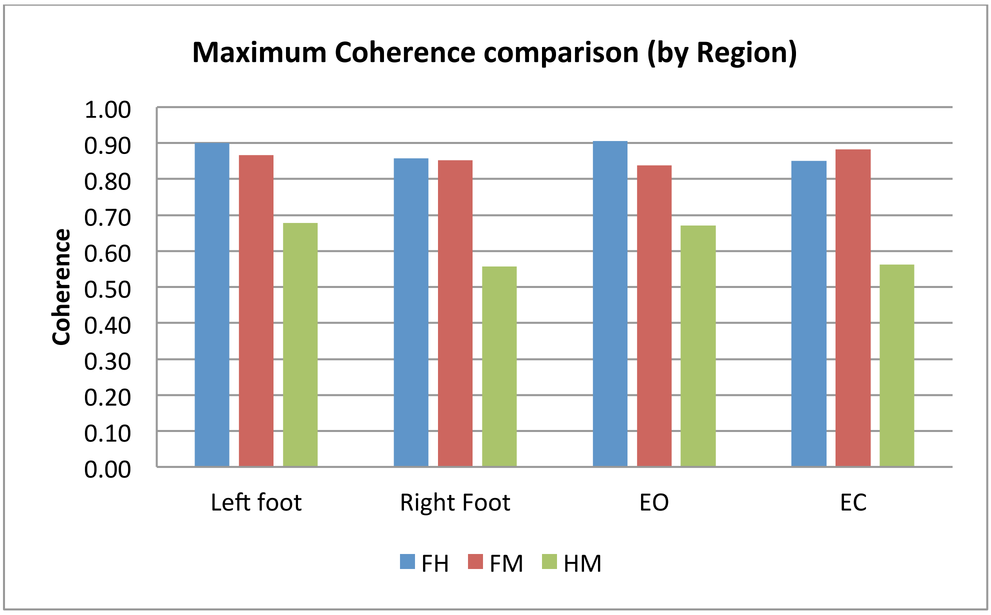

Figure 3-28 Comparison of maximum coherence by region

Maximum Coherence Frequency observed with respect to gender (at around 1.9Hz), foot (L: 1.649±0.256, R: 2.132±0.256) and eyes condition (EC: 1.698±0.256, EO: 2.083±0.256) are not significantly different. On the other hand, regions are significantly different (FH: 1.280±0.314, FM: 1.556±0.314, HM: 2.836±0.314, $p<0.0004$).

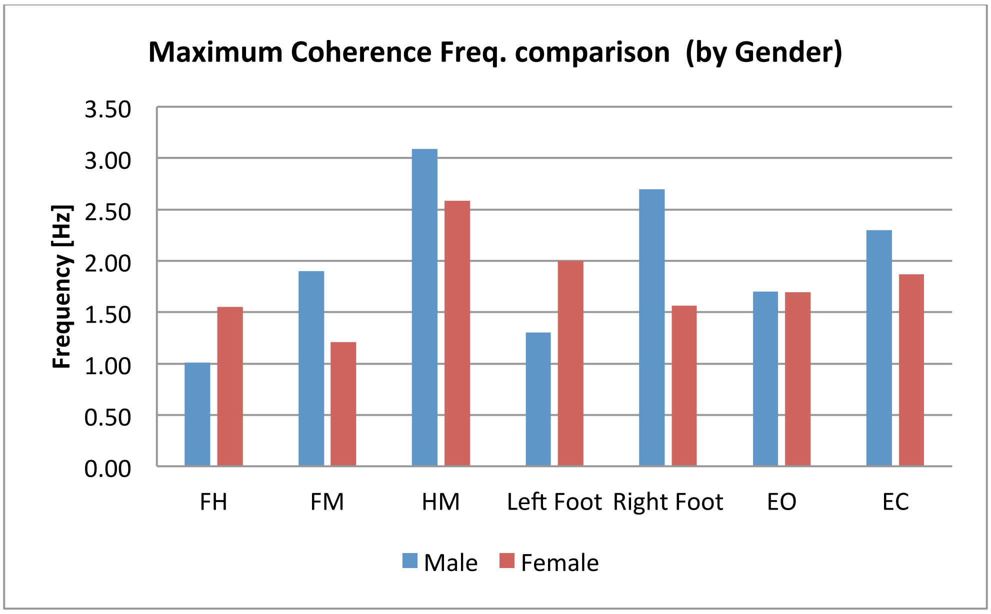

Figure 3-29 Maximum Coherence Freq. comparison by gender

Moreover, when maximum coherence frequency is observed in left foot versus right foot due to gender, right foot (2.698±0.363) of male subjects are found to be significantly higher compared to left foot (1.301±0.363, $p<0.0071$). However, female subjects did not show any significant difference with respect to foot (1.782±0.363).

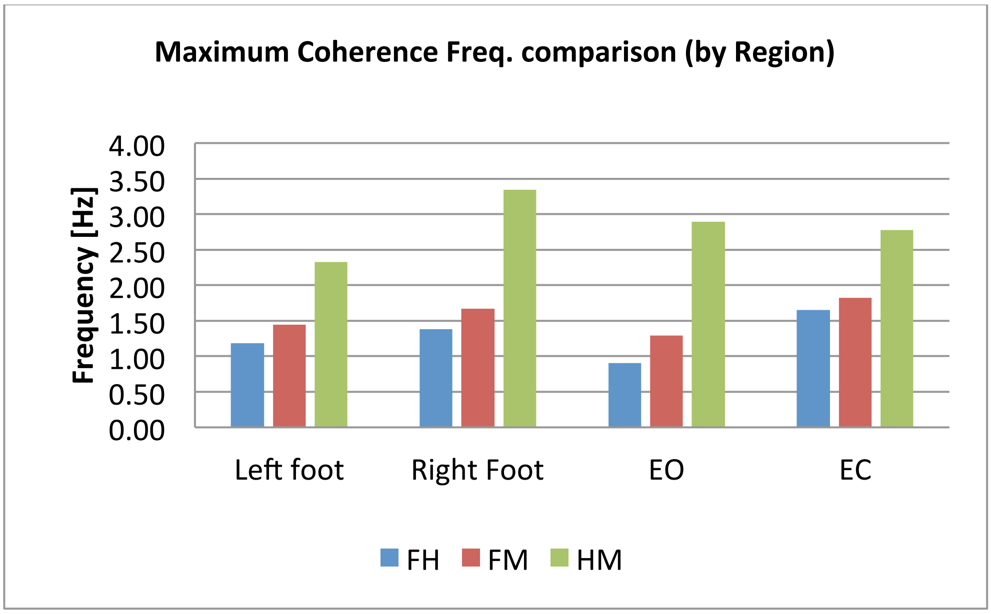

Figure 3-30 Maximum Coherence Freq. comparison by region

In terms of maximum magnitude [N^2] (gain) of cross-spectral density function (CSDF - see Methods Chapter), gender (M: 51.313±6.305 F: 29.061±6.305), foot (L: 52.455±6.305, R: 27.919±6.305) regions (FH: 100.047±7.722, FM: 18.267±7.722, HM: 2.248±7.722) are significantly different ($p<0.0049$, $p<0.00$, $p<0.002$ respectively). When variation in magnitudes of CSDF is distributed over gender versus foot, male subjects showed a significantly higher value in their left foot (76.610±8.917) compared to right foot (26.016±8.917) and females (29.050±8.917, $p<0.001$).

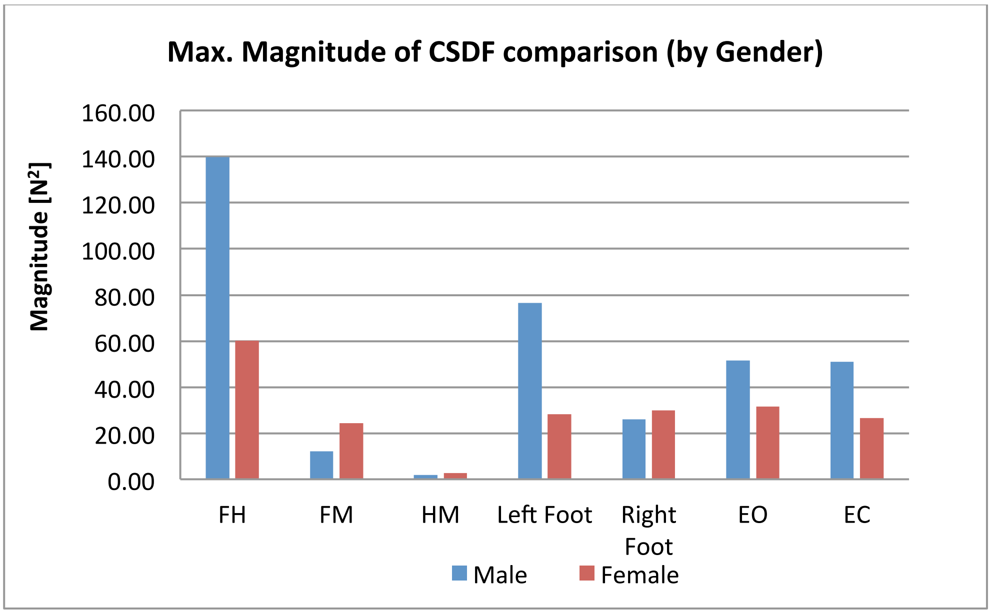

Figure 3-31 Maximum magnitude of CSDF comparison by gender

When variation in magnitudes of CSDF is distributed over gender versus foot regions, male subjects showed a significantly higher value ($p<0.00$) in FH (139.941±10.921) with respect to other regions (FM: 18.267±10.921, HM: 2.248±10.921) and females (FH: 60.153±10.921). Additionally, when CSDF magnitudes variations over foot versus foot regions are distributed FH magnitude at left foot (139.558±10.921) showed a significantly higher value ($p<0.00$) when compared to right foot (60.537±10.921) and the other regions.

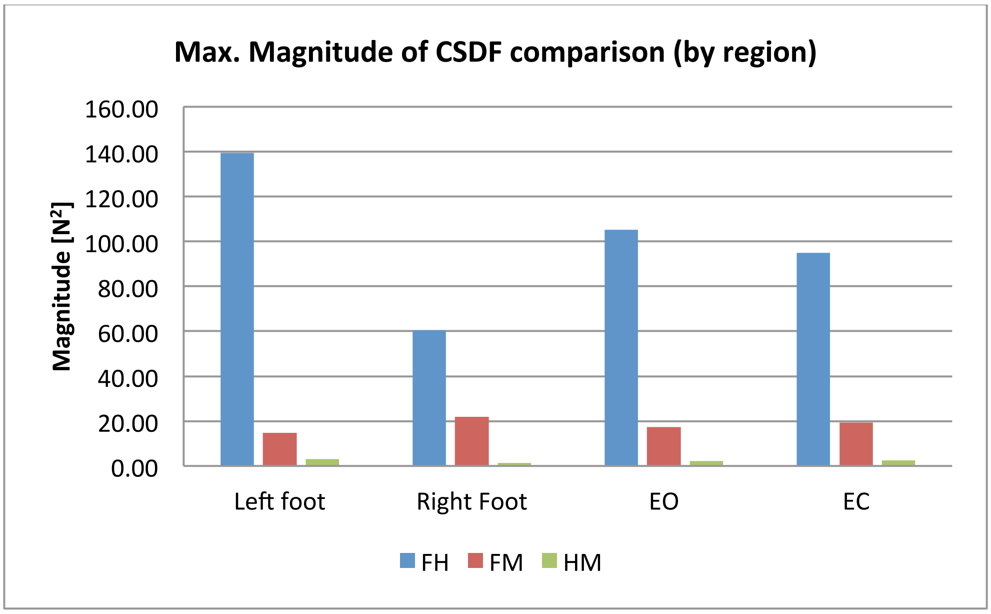

Figure 3-32 Maximum magnitude of CSDF comparison by region

Frequency of maximum CSDF showed significant difference with respect to foot regions (FH: 0.652±0.283, FM: 1.017±0.283, HM: 2.013±0.283) however, gender (1.225±0.231), foot (L: 0.917±0.231, R: 1.538±0.231), and eyes condition (EC: 1.041±0.231, EO: 1.415±0.231) are not significantly different. Furthermore, when variation at the frequency of maximum CSDF is distributed over foot region versus eyes condition HM (2.372±0.400) is found to be slightly larger than the other two-foot regions (FH: 0.188±0.400, FM: 0.562±0.400) EC condition ($p<0.0532$).

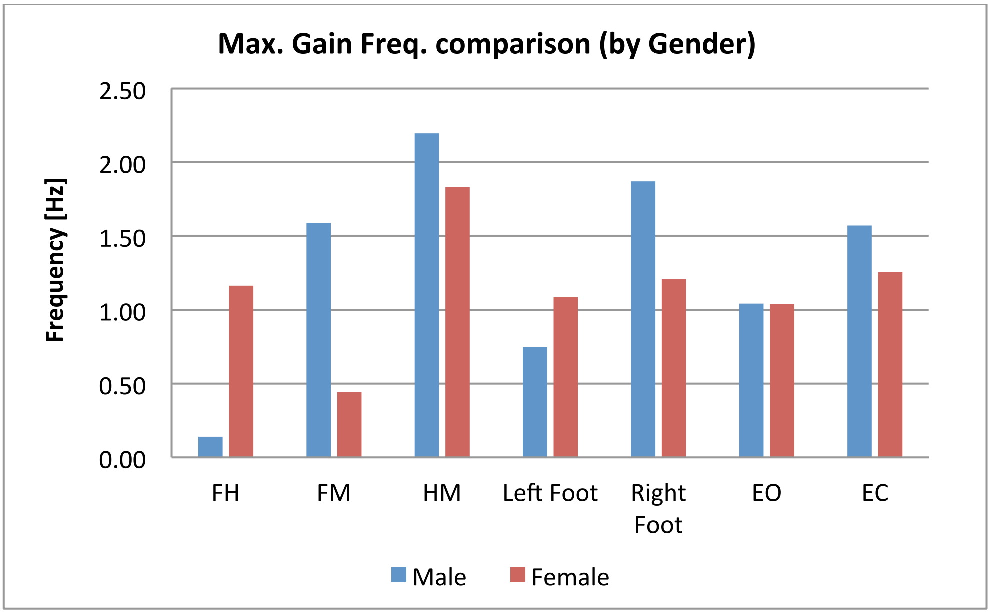

Figure 3-33 Maximum Gain Freq. comparison by gender

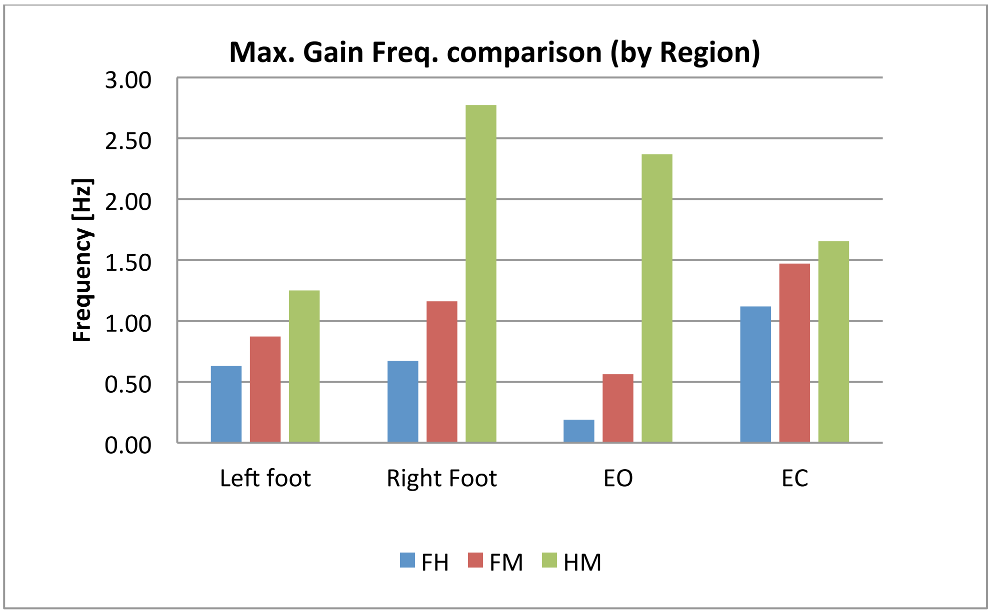

Figure 3-34 Maximum Gain Freq. comparison by gender

The above analysis is performed over 0-25 Hz region. Specific measures like maximum coherence, maximum magnitude (gain) of CSDF and its respective maximum frequency attained, maximum phase angles are all taken into account at their maximum values. It has been seen that most of the dynamics of the system observed at [0-3 Hz] region. Consequently, it has been focused on that [0-3 Hz] region and looked at the mean coherence and mean phase angles for the full bandwidth and above threshold of **0.80.** Again with obtained results ANOVA over gender, foot, region, and eyes calculated. Summary of the mean values were presented in Table 3-8.

Table 3-8 Coherence and Phase angles values and standard deviations in [0-3] Hz region. First and second columns of coherence and phase angle values are for all of the mean values of selected bandwidth. Third and fourth colums are for mean values above selected threshold value of 0.80.

Gender	Foot	Region	Eyes	Mean Coherence	Mean Phase Angles	Mean Coherence (>0.80)	Mean Phase Angles (>0.80)
Female	L	FH	EC	0.53±0.25	158.39±26.15	0.83±0.03	162.94±0.00
			EO	0.41±0.22	130.42±36.33	0.62±0.03	118.63±0.00
		FM	EC	0.47±0.23	29.21±30.48	0.78±0.03	155.67±0.00
			EO	0.49±0.24	21.33±23.36	0.61±0.02	125.71±0.00
		HM	EC	0.32±0.21	121.55±39.65	0.70±0.03	8.49±0.01
			EO	0.34±0.19	102.98±36.97	0.74±0.03	6.64±0.00
	R	FH	EC	0.47±0.24	148.89±30.69	0.86±0.03	17.60±0.00
			EO	0.36±0.21	134.89±38.47	0.85±0.03	8.83±0.00
		FM	EC	0.50±0.23	26.02±25.41	0.41±0.02	84.68±0.00
			EO	0.47±0.23	25.21±25.41	0.40±0.01	66.59±0.00
		HM	EC	0.33±0.20	117.80±37.98	0.48±0.01	78.36±0.01
			EO	0.28±0.17	102.92±40.01	0.36±0.01	50.87±0.00
Male	L	FH	EC	0.72±0.19	166.57±14.09	0.89±0.04	171.12±0.01
			EO	0.65±0.21	161.24±18.62	0.89±0.04	161.19±0.01
		FM	EC	0.63±0.21	15.63±14.75	0.87±0.04	167.60±0.01
			EO	0.61±0.22	15.02±14.24	0.83±0.04	156.41±0.01
		HM	EC	0.49±0.23	154.25±27.87	0.87±0.04	10.75±0.01
			EO	0.46±0.23	148.69±28.66	0.79±0.04	11.64±0.01
	R	FH	EC	0.59±0.23	162.43±19.05	0.61±0.02	14.10±0.01
			EO	0.52±0.24	156.28±24.20	0.65±0.02	17.83±0.01
		FM	EC	0.47±0.21	22.38±21.61	0.77±0.03	152.32±0.00
			EO	0.46±0.20	21.28±19.80	0.73±0.03	141.45±0.01
		HM	EC	0.29±0.19	134.09±42.48	0.44±0.01	104.05±0.01
			EO	0.27±0.17	130.94±40.05	0.24±0.01	67.88±0.01

Mean coherence values for the frequency range of [0-3 Hz] are found to be significantly different in Gender(M:0.514±0.01, F:0.414±0.01), Foot(L:0.51±0.01, M:0.418±0.01), Region(FH:0.532±0.012, FM:0.512±0.012, HM:0.348±0.012) ($p<0.00$ for each) and Eyes(EO:0.444±0.01 EC:0.485±0.01) ($p<0.0023$).

Furthermore, when variation in mean coherence values at frequency range of [0-3 Hz] is distributed over gender vs. foot, males left foot (0.593±0.013) is found to be significantly higher compared right foot (0.436±0.013) and females ($p<0.00$), gender vs. regions ($p<0.0002$) FH region in males (0.622±0.016) subjects are found significantly higher than females (0.443±0.016), region vs. eyes ($p<0.0189$) FH region only is significantly higher when eyes are closed (EO:0.485±0.016, EC:0.580±0.016).

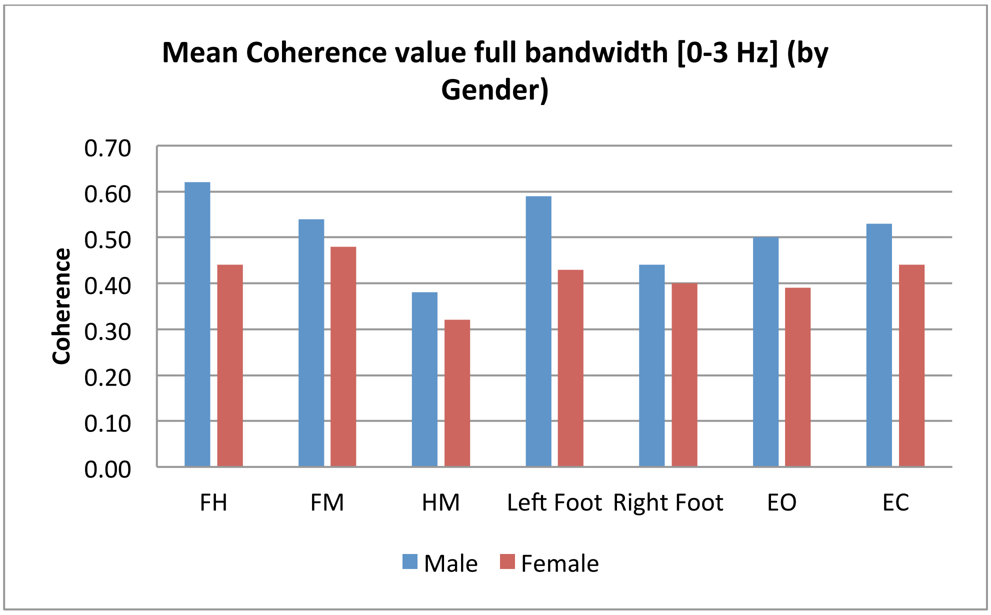

Figure 3-35 Mean coherence values on 0-3 Hz by gender

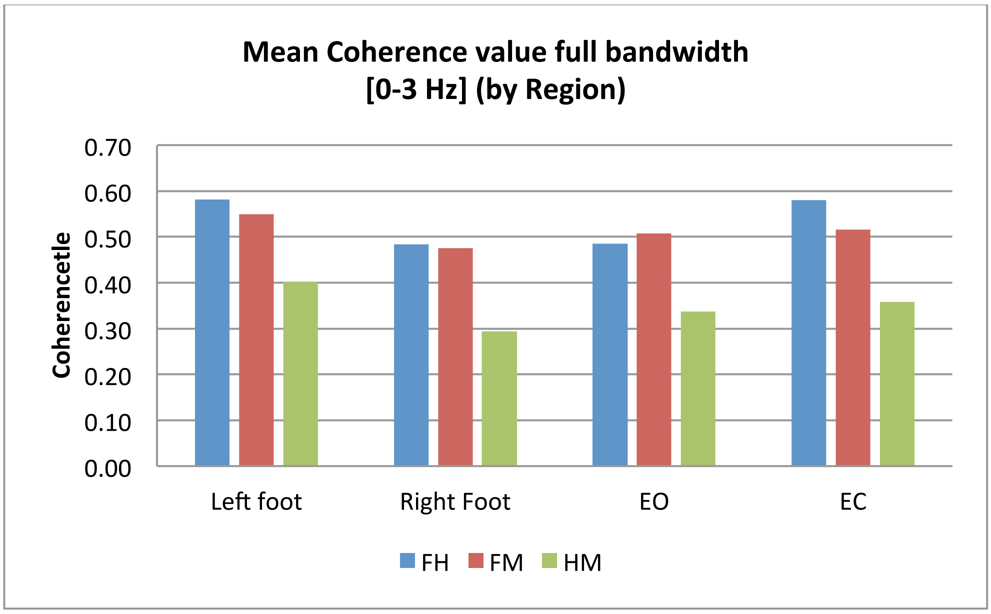

Figure 3-36 Mean coherence values on 0-3 Hz by region

On the other hand, mean coherence values above threshold are significantly different in Gender (M:0716±0.02, F:0.637±0.02), Foot(L:0.721±0.02, R:0.632±0.02), Region(FH:0.791±0.024, FM:0.759±0.024, HM:0.480±0.024), and Eyes(EO:0.643±0.02 EC:0.709±0.02) ($p<0.0046$, $p<0.00$, $p<0.0013$, $p<0.0177$ respectively).

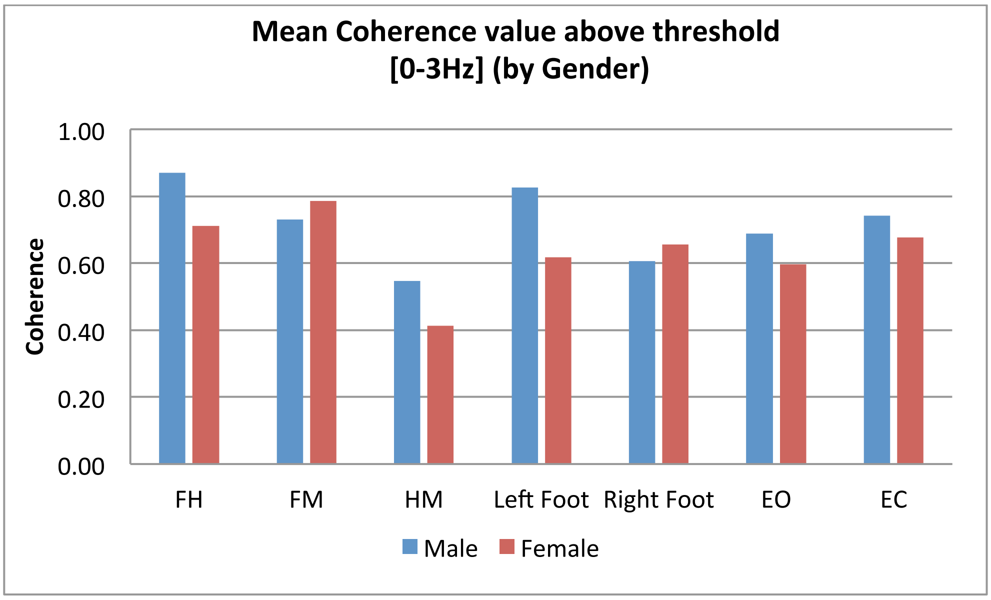

Figure 3-37 Mean coherence values above threshold on 0-3 Hz by gender

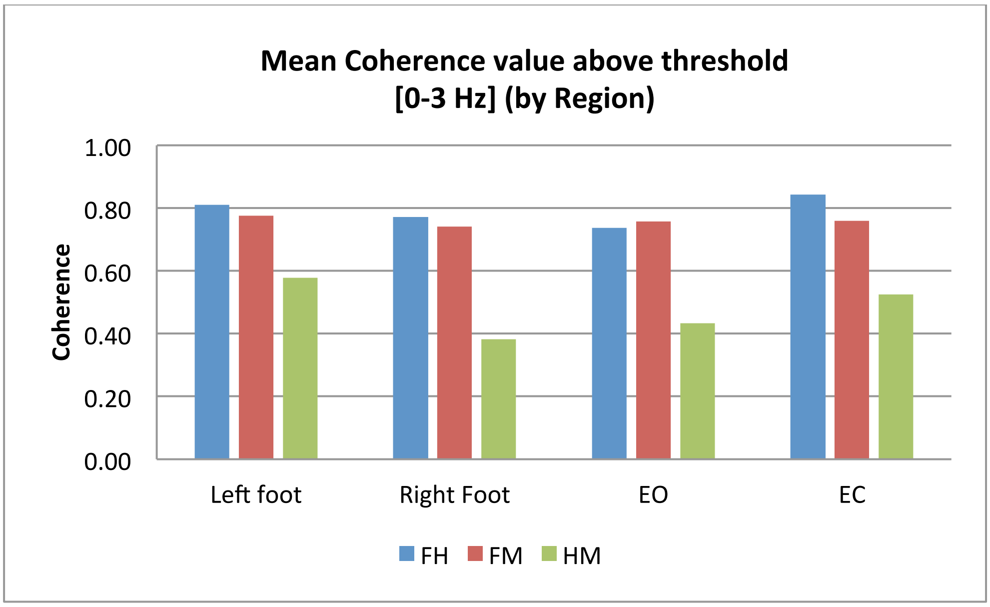

Figure 3-38 Mean coherence values above threshold on 0-3 Hz by region

Additionally, when variation in mean coherence values above threshold at frequency range of [0-3 Hz] is distributed over gender vs. foot, males left foot(0.825±0.028) is found to be significantly higher compared to right foot(0.606±0.028) and females($p<0.00$), gender vs. regions($p<0.0028$) FH region in males (0.870±0.034) are found significantly higher than females (0.711±0.034), region vs. foot($p<0.025$), only HM region at right foot(0.381±0.034) is found to be significantly lower than the left foot(0.578±0.034), region vs. eyes ($p<0.25$).

Mean phase values for the frequency range of [0-3 Hz] are found to be significantly different in Gender ($p<0.00$) (M:107.40±1.597 in degrees, F:93.301±1.597 in degrees), Foot($p<0.1206$) L:102.1107.40±1.597, R:98.6107.40±1.597), Region($p<0.00$) (FH:152.389±1.957, FM:22.01±1.957, HM:126.652±1.957) and Eyes($p<0.0001$) (EO:95.933±1.598 EC:104.768±1.598).

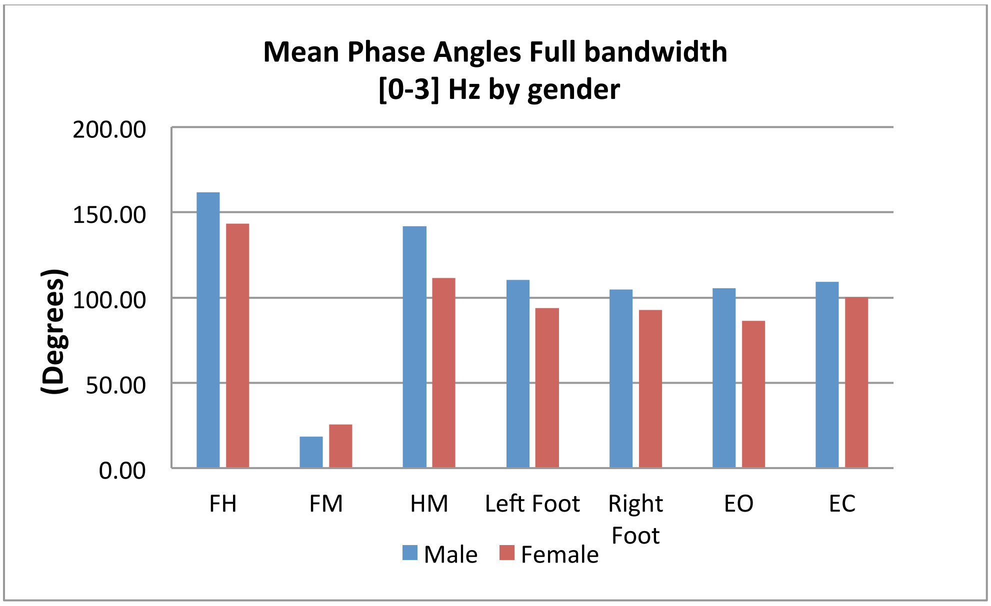

Figure 3-39 Mean phase angle values above threshold on 0-3 Hz by gender

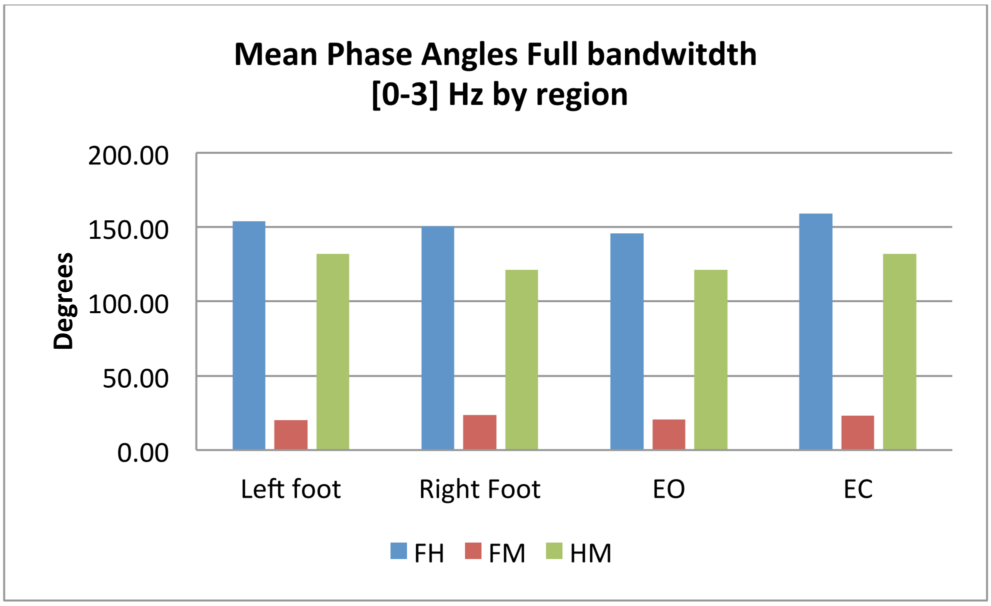

Figure 3-40 Mean phase angle values above threshold on 0-3 Hz by region

On the other hand, mean phase values above threshold were significantly different in Gender ($p<0.00$) (M:109.46±2.285, F:94.549±2.429) Foot($p<0.0703$) (L105.028±2.323:, R:98.98±2.392), Region($p<0.00$) (FH:161.58±2.708, FM:12.862±2.716, HM:131.569±3.206), and Eyes ($p<0.0011$) (EO:96.561±2.396 EC:107.447±2.311).

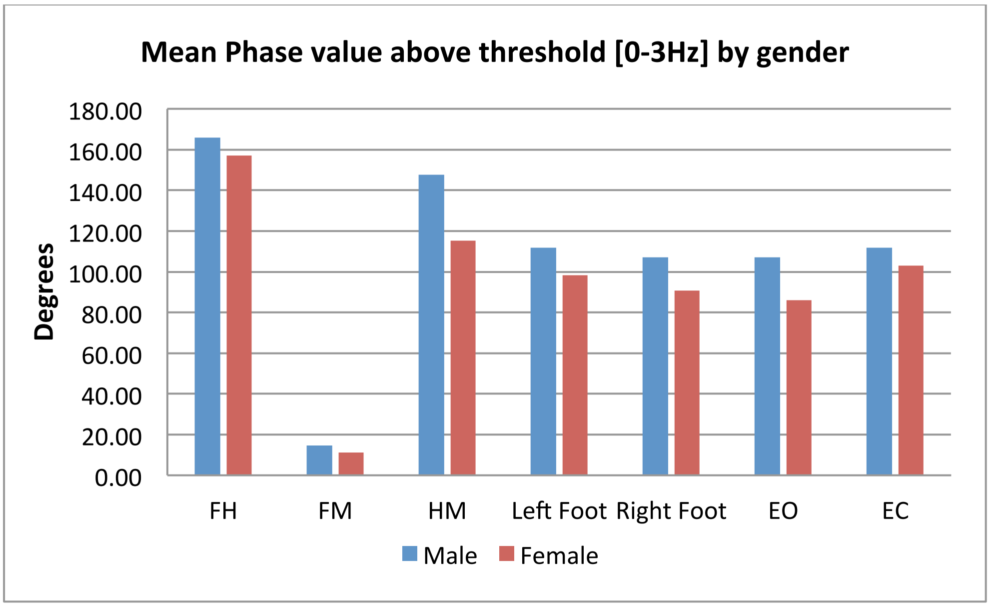

Figure 3-41 Mean Phase value above threshold [0-3Hz] by gender

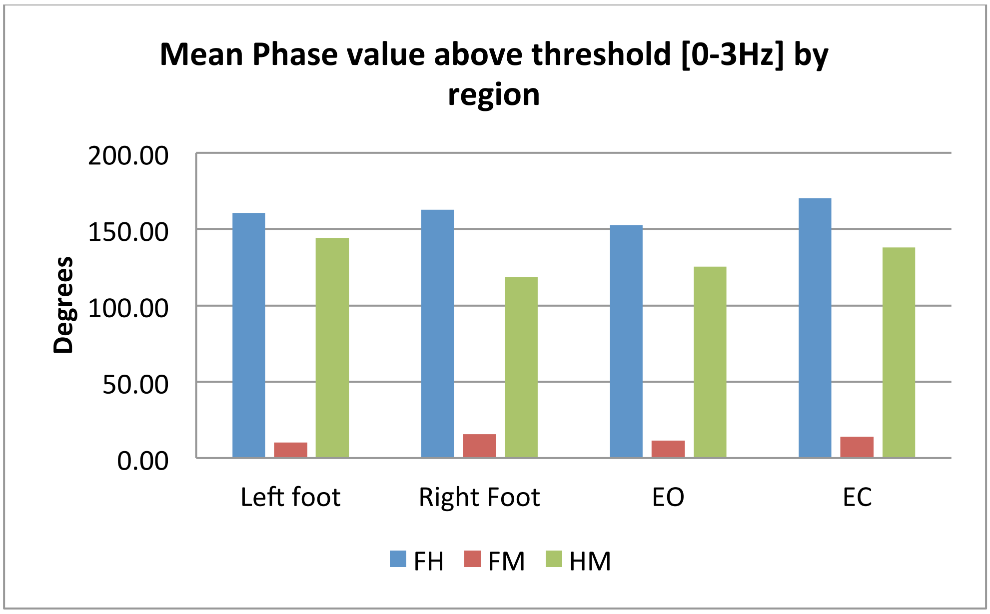

Figure 3-42 Mean Phase value above threshold [0-3Hz] by region

When variation in mean phase values at frequency range of [0-3 Hz] is distributed over gender vs. foot ($p<0.341$), gender vs. regions ($p<0.00$) FH region in males (161.630±2.767) are found significantly higher than females (143.148±2.767). Moreover, HM region is also significantly higher in males (141.99±2.767) than females(111.314±2.767). Gender vs. eyes ($p<0.0222$) EO(86.291±2.259) and

EC(100.311±2.259) condition in females are significantly lower compared to males respective eyes conditions (EO:105.575±2.259, EC:109.224±2.259).

Furthermore, when variation in mean phase values above threshold at frequency range of [0-3 Hz] is distributed over gender vs. foot ($p<0.71$), gender vs. regions ($p<0.0018$) HM region in males (147.780±4.285) subjects are found significantly higher than females (115.358±4.776), gender vs. eyes ($p<0.0566$) EO (85.958±3.486) condition in females are significantly lower than EC (103.140±3.348) condition and males. On the contrary to the mean phase angle values computed without threshold region vs. foot is found to be significantly different ($p<0.0005$ vs. $p<0.0444$). HM region in left foot is significantly higher (144.298±4.368) than HM region in Right foot (118.839±4.692).

CHAPTER 4

MATHEMATICAL MODELING FOR HUMAN ERECT POSTURE

4.1 Mathematical Foot Models

In order to understand the working mechanism and functions of the foot, various models were developed throughout the history. Early models were mostly descriptive and human foot was described as two half of a supporting column dated back to 1889 by Ellis [57]. Studies of Hicks, was a milestone for the understanding functions and capabilities, windlass effect and arched structure of the foot [10,51,58].

Most of the foot models were built considering clinical side in order to determine properties of the specific part of the foot. Namely plantar aponeurosis like Kim et al. [13], Gefen [59,60] and Cheung et al. [61] and biomechanical properties like Salathe et al. [62,63]. Some of the foot models were constructed using 3-Dimensional modeling techniques, where foot was modeled as musculoskeletal object and mostly related with gait, like works of Cheung et al. [64–66], Saraswat et al. [67], Chen et al.[68].

Incorporating a foot model for the control of human erect posture was seen mostly in posture studies as an inverted pendulum approach. Various models were introduced as stated in Chapter 1 of Introduction as Barin [6] , Winter and Prince et al. [2,69], King et al. [70], Alexandrov et al. [28,29], Mergner [3,27,71], Maurer and Peterka [26,27]. However, in most of these studies, human foot was taken as rigid non-deformable body and only ankle joint movement was emphasized. Recent studies on the other hand, were came into a conclusion that, human foot was a complex deformable body which must be taken into account as is, in posture studies [34,35].

The presented model here is among the first in mathematical foot models combining both deformable foot and an inverted pendulum on the ankle joint. Hence, posture study on deformable foot is modeled. The foot is taken as a truss structure and pillars are tied with tensional element, which is plantar aponeurosis. A reactive torque controls the inverted pendulum on ankle joint by ankle stiffness and co-contraction and reciprocal innervation of muscles. This action is simplified as torsional spring and damper for the time being and a control strategy is induced.

4.2 Model Presentation

A mathematical model for human erect posture has been developed, where a deformable foot has been used in order to drive and control the human inertial body mass and the parameters of the model were estimated by analyzing the experimental data.

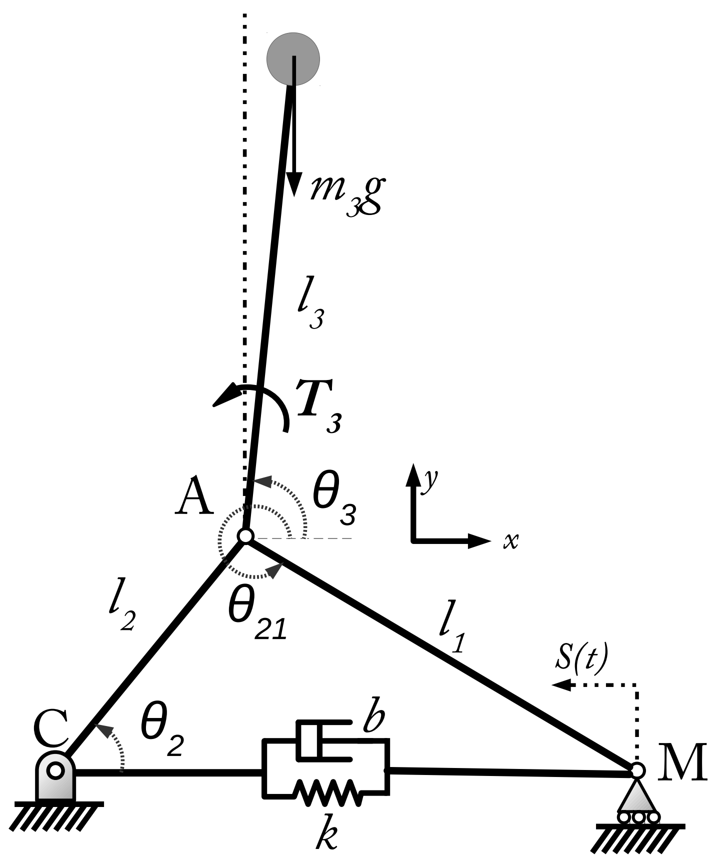

Figure 4-1 A Mathematical foot model that is presented

Reactive Torque T_3^R has been divided over l_1 and l_2 as T_3^1 and T_3^2 respectively, with a proportion of α and β according to the observations made previously. These equations are represented as;

$$T_3^R = T_3^2 + T_3^1$$
where
$$T_3^2 = \alpha T_3 \text{ and } T_3^1 = \beta T_3 \tag{4.1}$$

Sum of these proportion were taken as unity as $\alpha + \beta = 1$. While taking this proportions following assumption were made:

- Calcaneous bone has a buttress effect as discussed previously due to its strong structure
- Previous studies shows high frictional coefficient at heel region such that is treated as fixed to ground
- In such a truss structure as in Figure 4.1 since calcaneous is treated as fixed joint torque is transmitted to the least resistance to torque part of the structure. As in electrical current flowing more at lower resistance on its path.

Virtual Work equation is written according to given reference positions as

$$\begin{aligned}\delta U = -\alpha T_3\delta\theta_2 - \beta T_3\delta\theta_{21} + T_3(\delta\theta_3 + \delta\theta_2) - I_3\ddot{\theta}_3(\delta\theta_2 + \delta\theta_3) - \\ m_3 g S_{G3}\delta\theta_{G3}Cos(\theta_{G3}) - m_3 a_{G3}^t S_{G3}\delta\theta_{G3} - m_3 a_{G3}^n \delta S_{G3} + F_{PA}\delta S\end{aligned} \tag{4.2}$$

based on the notation in Figure 4-1 and Figure 4-2.

4.3 Loop Equations

For the solution of above virtual work equation, velocity and acceleration values have to be determined. In order to that vector loop equations have to be constructed. Vector loops are frequently used in kinematic analysis of mechanical linkages and the motion analysis of mechanisms is based on expressing these loops mathematically. There exist two loops in the structure, the first is being a virtual one from calcaneous C, to ankle joint A and through COM location. The second one is among calcaneous C to metatarsals M and to ankle joint A.

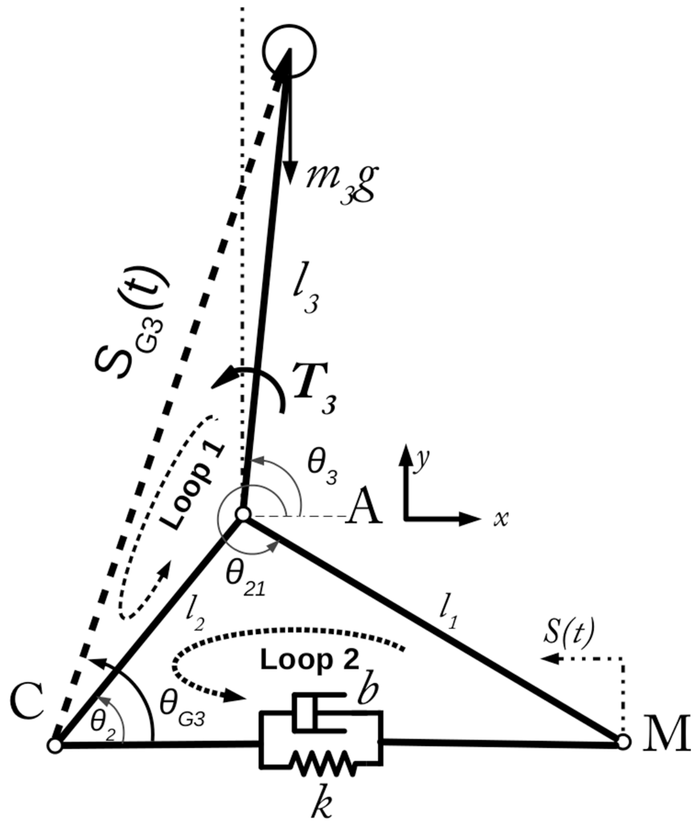

Figure 4-2 Loop equation of the model

For that reason loop equations are constructed and solved accordingly.

Loop Equation 1:

$$l_2 e^{i\theta_2} + l_3 e^{i\theta_3} = S_{G3} e^{i\theta_{G3}} \tag{4.3}$$

Taking into account real and imaginary parts;

$$\begin{aligned} &\text{Re: } l_2 \cos\theta_2 + l_3 \cos\theta_3 = S_{G3} \cos\theta_{G3} \\ &\text{Im: } l_2 \sin\theta_2 + l_3 \sin\theta_3 = S_{G3} \sin\theta_{G3} \end{aligned} \tag{4.4}$$

Squaring both sides of the equations and collecting terms

$$\begin{aligned} &l_2^2 + l_3^2 + 2 l_2 l_3 \cos(\theta_2 - \theta_3) = S_{G3}^2 \\ &\Rightarrow \\ &S_{G3} = \sqrt{l_2^2 + l_3^2 + 2 l_2 l_3 \cos(\theta_2 - \theta_3)} \end{aligned} \tag{4.5}$$

and dividing both sides of Equation 4.4

$$\tan\theta_{G3} = \frac{l_2 \sin\theta_2 + l_3 \sin\theta_3}{l_2 \cos\theta_2 + l_3 \cos\theta_3} \tag{4.6}$$

and

$$\theta_{G3} = \arctan\left(\frac{l_2 \sin\theta_2 + l_3 \sin\theta_3}{l_2 \cos\theta_2 + l_3 \cos\theta_3}\right) \tag{4.7}$$

In order to obtain velocity and acceleration terms, further differentiation of Loop Equation 1, which is Equation 4.3 to obtain velocity loop:

$$l_2\dot{\theta}_2 ie^{i\theta_2} + l_3\dot{\theta}_3 ie^{i\theta_3} = \dot{S}_{G3}e^{i\theta_{G3}} + S_{G3}\dot{\theta}_{G3}ie^{i\theta_{G3}} \tag{4.8}$$

we multiply both side of the equation with $e^{-i\theta_{G3}}$ for obtain better equations afterwards, then we obtain,

$$l_2\dot{\theta}_2 ie^{i(\theta_2-\theta_{G3})} + l_3\dot{\theta}_3 ie^{i(\theta_3-\theta_{G3})} = \dot{S}_{G3} + iS_{G3}\dot{\theta}_{G3}\,. \tag{4.9}$$

Splitting its real and imaginary parts:

$$\begin{aligned} &\text{Re: } -l_2\dot{\theta}_2 \sin(\theta_2-\theta_{G3}) - l_3\dot{\theta}_{G3}\sin(\theta_3-\theta_{G3}) = \dot{S}_{G3} \\ &\text{Im: } l_2\dot{\theta}_2 \cos(\theta_2-\theta_{G3}) + l_3\dot{\theta}_3 \cos(\theta_3-\theta_{G3}) = S_{G3}\dot{\theta}_{G3} \end{aligned} \tag{4.10}$$

The total differential of any set of system position vectors r_i, that are functions of other variables, $\{q_1, q_2, ..., q_m\}$ and time t may be expressed as follows:

$$dr_i = \frac{\partial \mathbf{r}_i}{\partial t}dt + \sum_{j=1}^{m}\frac{\partial \mathbf{r}_i}{\partial q_j}dq_j \tag{4.11}$$

If, instead, we want the virtual displacement (virtual differential displacement), then:

$$\delta \mathbf{r}_i = \sum_{j=1}^{m} \frac{\partial \mathbf{r}_i}{\partial q_j} \delta q_j \tag{4.12}$$

Accordingly, we pass to virtual displacements required for the virtual work method and rewrite the Equation 4.10:

$$\begin{aligned} &\text{Re: } -l_2\delta\theta_2 \sin(\theta_2 - \theta_{G3}) - l_3\delta\theta_{G3}\sin(\theta_3 - \theta_{G3}) = \delta S_{G3} \\ &\text{Im: } l_2\delta\theta_2 \cos(\theta_2 - \theta_{G3}) + l_3\delta\theta_3\cos(\theta_3 - \theta_{G3}) = S_{G3}\delta\theta_{G3} \end{aligned} \tag{4.13}$$

Equation 4.8 further differentiated to obtain acceleration equation as:

$$\begin{aligned} &l_2\ddot{\theta}_2 ie^{i\theta_2} - l_2\dot{\theta}_2^2 e^{i\theta_2} + l_3\ddot{\theta}_3 ie^{i\theta_3} - l_3\dot{\theta}_3^2 e^{i\theta_3} = \ddot{S}_{G3}e^{i\theta_{G3}} + S_{G3}\dot{\theta}_{G3}ie^{i\theta_{G3}} \\ &+\dot{S}_{G3}\dot{\theta}_{G3}ie^{i\theta_{G3}} + S_{G3}\ddot{\theta}_{G3}ie^{i\theta_{G3}} - S_{G3}\dot{\theta}_{G3}^2 ie^{i\theta_{G3}} \end{aligned} \tag{4.14}$$

we multiply both sides of the Equation 4.14 with $e^{-i\theta_{G3}}$ to obtain,

$$\begin{aligned} &l_2\ddot{\theta}_2 ie^{i(\theta_2-\theta_{G3})} - l_2\dot{\theta}_2^2 e^{i(\theta_2-\theta_{G3})} + l_3\ddot{\theta}_3 ie^{i(\theta_3-\theta_{G3})} - l_3\dot{\theta}_3^2 e^{i(\theta_3-\theta_{G3})} = \\ &\ddot{S}_{G3} + 2i\dot{S}_{G3}\dot{\theta}_{G3} + S_{G3}\ddot{\theta}_{G3}i - S_{G3}\dot{\theta}_{G3}^2 \end{aligned} \tag{4.15}$$

Splitting into their real and imaginary parts.

$$\begin{aligned} &\text{Re: } -l_2\ddot{\theta}_2\sin(\theta_2-\theta_{G3}) - l_2\dot{\theta}_2^2\cos(\theta_2-\theta_{G3}) - l_3\ddot{\theta}_3\sin(\theta_3-\theta_{G3}) - l_3\dot{\theta}_3^2\cos(\theta_3-\theta_{G3}) = \\ &\ddot{S}_{G3} - S_{G3}\dot{\theta}_{G3}^2 \text{ which is } a_{G3}^n \end{aligned} \tag{4.16}$$

$$\begin{aligned} &\text{Im: } l_2\ddot{\theta}_2\cos(\theta_2-\theta_{G3}) - l_2\dot{\theta}_2^2\sin(\theta_2-\theta_{G3}) + l_3\ddot{\theta}_3\cos(\theta_3-\theta_{G3}) - l_3\dot{\theta}_3^2\sin(\theta_3-\theta_{G3}) = \\ &2\dot{S}_{G3}\dot{\theta}_{G3} + S_{G3}\ddot{\theta}_{G3} \text{ which is } a_{G3}^t \end{aligned} \tag{4.17}$$

which are actually normal and tangential components of a_{G3} where tangential acceleration has also had coriolis acceleration in it.

Another loop is shown in Figure 4.1 and named as Loop 2 and it is constructed as:

$$l_2 e^{i\theta_2} + l_1 e^{i\theta_{21}} = S \tag{4.18}$$

This loop equation further split in to their real and imaginary parts as

$$\begin{aligned} &\text{Re}: l_2 \cos\theta_2 + l_1 \cos\theta_{21} = S \\ &\text{Im}: l_2 \sin\theta_2 + l_1 \sin\theta_{21} = 0 \end{aligned} \tag{4.19}$$

from the above equation θ_{21} can be taken as

$$\theta_{21} = -\arcsin\left(\frac{l_2}{l_1}\sin\theta_2\right). \tag{4.20}$$

Substitute above into Equation 4.19. Real part we can obtain *S(t)* as:

$$S(t) = l_2 \cos\theta_2 - l_1 \cos\left(\arcsin\left(\frac{l_2}{l_1}\sin\theta_2\right)\right) \tag{4.21}$$

Following these equations velocity loop equation is obtained and then separated in to real and imaginary components as:

$$l_2 \dot{\theta}_2 i e^{i\theta_2} + l_1 \dot{\theta}_{21} i e^{i\theta_{21}} = \dot{S} \tag{4.22}$$

$$\begin{aligned} &\text{Re: } -l_2 \dot{\theta}_2 \sin\theta_2 - l_1 \dot{\theta}_{21} \sin\theta_{21} = \dot{S} \\ &\text{Im: } l_2 \dot{\theta}_2 \cos\theta_2 + l_1 \dot{\theta}_{21} \cos\theta_{21} = 0 \end{aligned} \tag{4.23}$$

Equation 4.23 can be rewritten in term of virtual displacements

$$\begin{aligned}&\text{Re: } -l_2\delta\theta_2\sin\theta_2 - l_1\delta\theta_{21}\sin\theta_{21} = \delta S\\&\text{Im: } l_2\delta\theta_2\cos\theta_2 + l_1\delta\theta_{21}\cos\theta_{21} = 0\end{aligned} \tag{4.24}$$

From the above equation,

$$\delta\theta_{21} = -\frac{l_2\cos\theta_2\delta\theta_2}{l_1\cos\theta_{21}} \tag{4.25}$$

putting Equation 4.25 in to Real part of Equation 4.24

$$\delta S = l_2\left(\cos\theta_2\tan\theta_{21} - \sin\theta_2\right)\delta\theta_2 \tag{4.26}$$

can be obtained.

All of the calculated values are put into virtual work equation and following expression is obtained.

$$\begin{aligned}&\delta U = -\alpha T_3\delta\theta_2 - \beta T_3\delta\theta_{21} + T_3(\delta\theta_2 + \delta\theta_3) - I_3\ddot{\theta}_3(\delta\theta_2 + \delta\theta_3)\\&-m_3 g\left[l_2\delta\theta_2\cos(\theta_2 - \theta_{G3}) + l_3\delta\theta_3\cos(\theta_3 - \theta_{G3})\right]\cos\theta_{G3}\\&-m_3\left[l_2\delta\theta_2\cos(\theta_2 - \theta_{G3}) + l_3\delta\theta_3\cos(\theta_3 - \theta_{G3})\right]\cdot\\&\left[l_2\ddot{\theta}_2\cos(\theta_2 - \theta_{G3}) - l_2\dot{\theta}_2^2\sin(\theta_2 - \theta_{G3}) + l_3\ddot{\theta}_3\cos(\theta_3 - \theta_{G3}) - l_3\dot{\theta}_3^2\sin(\theta_3 - \theta_{G3})\right]\\&-m_3\left[l_2\delta\theta_2\sin(\theta_2 - \theta_{G3}) - l_3\delta\theta_3\sin(\theta_3 - \theta_{G3})\right]\cdot\\&\left[-l_2\ddot{\theta}_2\sin(\theta_2 - \theta_{G3}) - l_2\dot{\theta}_2^2\cos(\theta_2 - \theta_{G3}) - l_3\ddot{\theta}_3\sin(\theta_3 - \theta_{G3}) - l_3\dot{\theta}_3^2\cos(\theta_3 - \theta_{G3})\right] +\\&\left[k(S - S_0) + bl_2(\cos\theta_2\tan\theta_{21} - \sin\theta_2)\delta\theta_2\right]\end{aligned} \tag{4.27}$$

Equation 4.27 further expanded to obtain an expression in terms of $\delta\theta_2$ and $\delta\theta_3$. First, m_3 terms are for $\delta\theta_2$ expanded:

$$-m_3 l_2\delta\theta_2\begin{bmatrix}\cos(\theta_2 - \theta_{G3})\cos(\theta_2 - \theta_{G3})l_2\ddot{\theta}_2 - \cos(\theta_2 - \theta_{G3})\sin(\theta_2 - \theta_{G3})l_2\dot{\theta}_2^2\\+\cos(\theta_2 - \theta_{G3})\cos(\theta_3 - \theta_{G3})l_3\ddot{\theta}_3 - \cos(\theta_2 - \theta_{G3})\sin(\theta_3 - \theta_{G3})l_3\dot{\theta}_3^2\end{bmatrix} \tag{4.28}$$

$$-m_3 l_2 \delta\theta_2 \begin{bmatrix} \sin(\theta_2-\theta_{G3})\sin(\theta_2-\theta_{G3}) l_2\ddot{\theta}_2 + \sin(\theta_2-\theta_{G3})\cos(\theta_2-\theta_{G3}) l_2\dot{\theta}_2^2 \\ +\sin(\theta_2-\theta_{G3})\sin(\theta_3-\theta_{G3}) l_3\ddot{\theta}_3 + \sin(\theta_2-\theta_{G3})\cos(\theta_3-\theta_{G3}) l_3\dot{\theta}_3^2 \end{bmatrix} \tag{4.29}$$

and plus another term for $\delta\theta_3$

$$-m_3 l_3 \delta\theta_3 \begin{bmatrix} \cos(\theta_3-\theta_{G3})\cos(\theta_2-\theta_{G3}) l_2\ddot{\theta}_2 - \cos(\theta_3-\theta_{G3})\sin(\theta_2-\theta_{G3}) l_2\dot{\theta}_2^2 \\ +\cos(\theta_3-\theta_{G3})\cos(\theta_3-\theta_{G3}) l_3\ddot{\theta}_3 - \cos(\theta_3-\theta_{G3})\sin(\theta_3-\theta_{G3}) l_3\dot{\theta}_3^2 \end{bmatrix} \tag{4.30}$$

$$-m_3 l_3 \delta\theta_3 \begin{bmatrix} \sin(\theta_3-\theta_{G3})\sin(\theta_2-\theta_{G3}) l_2\ddot{\theta}_2 + \sin(\theta_3-\theta_{G3})\cos(\theta_2-\theta_{G3}) l_2\dot{\theta}_2^2 \\ +\sin(\theta_3-\theta_{G3})\sin(\theta_3-\theta_{G3}) l_3\ddot{\theta}_3 + \sin(\theta_3-\theta_{G3})\cos(\theta_3-\theta_{G3}) l_3\dot{\theta}_3^2 \end{bmatrix} \tag{4.31}$$

Combining Equations 4.28 - 4.31;

$$-m_3 l_2 \delta\theta_2 \left[l_2\ddot{\theta}_2 + l_3\ddot{\theta}_3 \cos(\theta_2-\theta_3) + l_3\dot{\theta}_3^2 \sin(\theta_2-\theta_3) \right] \tag{4.32}$$

$$-m_3 l_3 \delta\theta_3 \left[l_2\ddot{\theta}_2 \cos(\theta_2-\theta_3) + l_2\dot{\theta}_2^2 \sin(\theta_3-\theta_2) + l_3\ddot{\theta}_3 \right] \tag{4.33}$$

Reactive Torque T_3^R, is presented in Equation 4.1. This representation is rearranged to put in to energy equations as

$$-\alpha T_3 \delta\theta_2 - \beta T_3 \delta\theta_{21} + T_3(\delta\theta_2 + \delta\theta_3) \tag{4.34}$$

Using $\delta\theta_2$ representation in Equation 4.25 Equation 4.34 is rearranged as;

$$-\alpha T_3 \delta\theta_2 - \beta T_3 \left(-\frac{l_2\cos\theta_2}{l_1\cos\theta_{21}} \right) \delta\theta_2 + T_3(\delta\theta_2 + \delta\theta_3) \tag{4.35}$$

Rearranging Torque terms are presented as:

$$T_3\delta\theta_3 + \left(1 - \alpha + \beta\left(-\frac{l_2\cos\theta_2}{l_1\cos\theta_{21}}\right)\right)T_3\delta\theta_2 \qquad (4.36)$$

4.4 Solving Obtained Equations

Plantar Aponeurosis is modeled using a spring and damper combination and its Force representation is given simply as:

$$F_{PA} = k(S - S_0) + b\dot{S} \qquad (4.37)$$

where ***k*** is the elastic spring constant, ***b*** as damping coefficient, ***S*** distance between C and M and $\boldsymbol{S_0}$ is the initial length of the spring/damper complex. Since this model is constructed for posture analysis, when erect posture is concerned, plantar aponeurosis is taken as under compression in natural position and under corrective torque effect. Sign convention is taken accordingly. Then required $\dot{S}$ term is calculated as;

$$\dot{S} = -l_2\dot{\theta}_2\sin\theta_2 - l_1\dot{\theta}_{21}\sin\theta_{21} \qquad (4.38)$$

Where,

$$\dot{\theta}_{21} = -\frac{l_2\dot{\theta}_2\cos\theta_2}{l_1\cos\theta_{21}} \qquad (4.39)$$

Arranging terms;

$$\dot{S} = l_2\dot{\theta}_2(\cos\theta_2\tan\theta_{21} - \sin\theta_2) \qquad (4.40)$$

Finally, plantar aponeurosis force is calculated using below,

$$F_{PA} = \left[k(S - S_0) + bl_2\dot{\theta}_2(\cos\theta_2\tan\theta_{21} - \sin\theta_2)\right] \qquad (4.41)$$

Having completed required parts; all of the terms are collected with respect to $\delta\theta_2$ and $\delta\theta_3$.

$$\delta\theta_2 \begin{bmatrix} -I_3\ddot{\theta}_3 - m_3 g l_2 \cos(\theta_2 - \theta_{G3})\cos\theta_{G3} - m_3 l_2^2 \ddot{\theta}_2 - m_3 l_2 l_3 \ddot{\theta}_3 \cos(\theta_2 - \theta_3) \\ -m_3 l_2 l_3 \dot{\theta}_3^2 \sin(\theta_2 - \theta_3) + k(S - S_0)\left[l_2(\cos\theta_2 \tan\theta_{21} - \sin\theta_2)\right] + \\ \left(1 - \alpha + \beta \dfrac{l_2 \cos\theta_2}{l_1 \cos\theta_{21}}\right) T_3 \end{bmatrix} = 0 \qquad (4.42)$$

and

$$\delta\theta_3 \begin{bmatrix} T_3 - I_3\ddot{\theta}_3 - m_3 g l_3 \cos(\theta_3 - \theta_{G3})\cos\theta_{G3} - m_3 l_3^2 \ddot{\theta}_3 - m_3 l_2 l_3 \ddot{\theta}_2 \cos(\theta_2 - \theta_3) \\ -m_3 l_2 l_3 \dot{\theta}_2^2 \sin(\theta_3 - \theta_2) \end{bmatrix} = 0 \quad (4.43)$$

These equations were solved for $\ddot{\theta}_2$ and $\ddot{\theta}_3$ using Cramer's Law and put in a matrix form as shown below:

$$\underbrace{\begin{bmatrix} I_{11} & I_{12} \\ I_{21} & I_{22} \end{bmatrix}}_{\substack{\text{Inertia Terms} \\ A}} \underbrace{\begin{bmatrix} \ddot{\theta}_2 \\ \ddot{\theta}_3 \end{bmatrix}}_{\substack{\ddot{\theta}\text{ terms} \\ C}} = \underbrace{\begin{bmatrix} T_1 \\ T_2 \end{bmatrix}}_{\substack{\text{Torque terms} \\ B}} \qquad (4.44)$$

Putting the values in:

$$\begin{bmatrix} m_3 l_2^2 & I_3 + m_3 l_2 l_3 \cos(\theta_2 - \theta_3) \\ m_3 l_2 l_3 \cos(\theta_2 - \theta_3) & I_3 + m_3 l_3^2 \end{bmatrix} \begin{bmatrix} \ddot{\theta}_2 \\ \ddot{\theta}_3 \end{bmatrix} =$$

$$\begin{bmatrix} -I_3\ddot{\theta}_3 - m_3 g l_2 \cos(\theta_2 - \theta_{G3})\cos\theta_{G3} - m_3 l_2^2 \ddot{\theta}_2 - m_3 l_2 l_3 \ddot{\theta}_3 \cos(\theta_2 - \theta_3) \\ -m_3 l_2 l_3 \dot{\theta}_3^2 \sin(\theta_2 - \theta_3) + k(S - S_0)\left[l_2(\cos\theta_2 \tan\theta_{21} - \sin\theta_2)\right] + \\ \left(1 - \alpha + \beta \dfrac{l_2 \cos\theta_2}{l_1 \cos\theta_{21}}\right) T_3 \\ T_3 - I_3\ddot{\theta}_3 - m_3 g l_3 \cos(\theta_3 - \theta_{G3})\cos\theta_{G3} - m_3 l_3^2 \ddot{\theta}_3 - m_3 l_2 l_3 \ddot{\theta}_2 \cos(\theta_2 - \theta_3) \\ -m_3 l_2 l_3 \dot{\theta}_2^2 \sin(\theta_3 - \theta_2) \end{bmatrix} \tag{4.45}$$

Using $C = \dfrac{B}{A}$ matrix operation following angular acceleration terms are obtained using MATLAB© MuPAD solver:

$$\begin{pmatrix} \dfrac{(I_3 + l_2 l_3 m_3 \cos(\theta_2 - \theta_3))\sigma_4}{\sigma_1} - \dfrac{(m_3 l_3^2 + I_3)\sigma_3}{\sigma_1} \\ -\dfrac{l_2 \sigma_4}{\sigma_2} + \dfrac{l_3 \cos(\theta_2 - \theta_3)\sigma_3}{\sigma_2} \end{pmatrix} \tag{4.46}$$

Where,

$$\sigma_1 = -l_2^2 l_3^2 m_3^2 \cos(\theta_2 - \theta_3)^2 + l_2^2 l_3^2 m_3^2 + I_3 l_2^2 m_3 - I_3 l_2 l_3 m_3 \cos(\theta_2 - \theta_3) \tag{4.47}$$

$$\sigma_2 = -l_2 m_3 l_3^2 \cos(\theta_2 - \theta_3)^2 + l_2 m_3 l_3^2 - I_3 l_3 \cos(\theta_2 - \theta_3) + I_3 l_2 \tag{4.48}$$

$$\sigma_3 = \begin{pmatrix} \alpha + l_2(k(\sigma_6 - S_0 + l_2\cos\theta_2)) - b l_2 \dot{\theta}_2 \sigma_5)\sigma_5 - \dfrac{\beta l_2 \cos\theta_2}{\sigma_6} \\ + l_2 l_3 m_3 \dot{\theta}_3^2 \sin(\theta_2 - \theta_3) + m_3 g l_2 \cos\theta_{G3} \cos(\theta_2 - \theta_{G3}) - 1 \end{pmatrix} \tag{4.49}$$

$$\sigma_4 = -T_3 + l_2 l_3 m_3 \dot{\theta}_2^2 \sin(\theta_3 - \theta_2) + m_3 g l_3 \cos\theta_{G3} \cos(\theta_3 - \theta_{G3}) \tag{4.50}$$

$$\sigma_5 = \sin\theta_2 - \tan(\theta_{21}) \tag{4.51}$$

$$\sigma_6 = l_1 \cos\left(-\arcsin\left(\frac{l_2}{l_1}\sin\theta_2\right)\right) = l_1 \cos\theta_{21} \tag{4.52}$$

can be found.

These calculations are modeled using MATLAB© Simulink and results are obtained.

4.5 Calculation of Reaction Forces

For the calculation of reaction forces at point C and M where they refer to Calcaneous and Metatarsal reaction forces. Dynamic equilibrium equations are written as for the upper link:

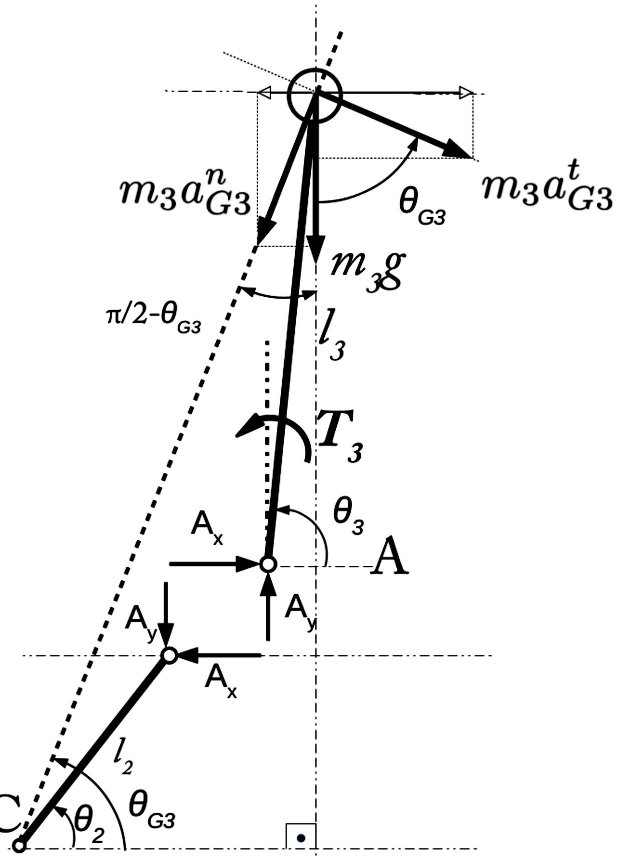

Figure 4-3 Upper link of the model

$$\xrightarrow{+} \sum F_x : A_x + m_3 a^t_{G3} \sin\theta_{G3} - m_3 a^n_{G3} \sin\left(\frac{\pi}{2} - \theta_{G3}\right) = 0$$
$$\Rightarrow \boxed{A_x = m_3 a^n_{G3} \cos\theta_{G3} - m_3 a^t_{G3} \sin\theta_{G3}} \tag{4.53}$$

$$+\uparrow \sum F_y : A_y - m_3 g - m_3 a_{G3}^t \cos\theta_{G3} - m_3 a_{G3}^n \cos\left(\frac{\pi}{2} - \theta_{G3}\right) = 0$$
$$\Rightarrow \boxed{A_y = m_3 g + m_3 a_{G3}^t \cos\theta_{G3} + m_3 a_{G3}^n \sin\left(\theta_{G3}\right)} \tag{4.54}$$

For the Lower link:

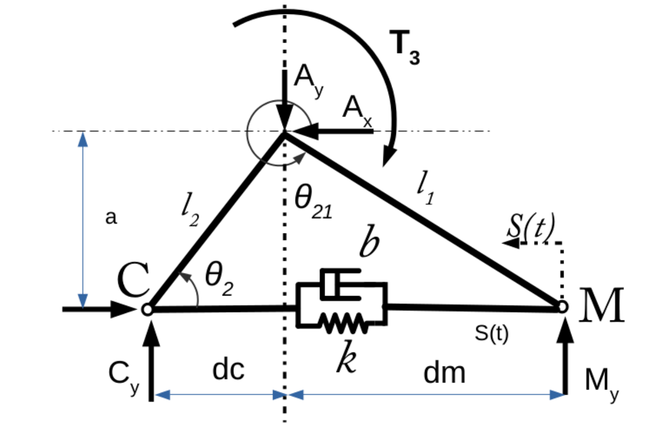

Figure 4-4 Lower Link of the foot model for reaction forces calculation

$$T_3 = k_t\left(Th - \theta_3\right) + b_t \dot{\theta}_3 A_y - m_3 g \tag{4.55}$$

Here a threshold value (Th) around 90°, which is introduced as a corrective action of the pendulum.

$$\xrightarrow{+} \sum F_x = 0 : \boxed{A_x = C_x} \tag{4.56}$$

$$+\uparrow \sum F_y = 0 : \boxed{A_y = M_y + C_y} \tag{4.57}$$

$$\sum M_C = 0 : \boxed{M_y S - A_y d_c + A_x a - T_3 = 0} \tag{4.58}$$

where

$dc(t) = l_2 \cos\theta_2(t)$ and $a(t) = l_2 \sin\theta_2(t)$

Therefore;

$$\Rightarrow M_y = \frac{T_3 - A_x a(t) + A_y dc(t)}{S(t)} \tag{4.59}$$

When this formulation has been completed a Matlab Simulink model was constructed and simulation was performed. The model representation is presented below in Figure 4-5. Proceeding, corresponding subgroup figures are presented.

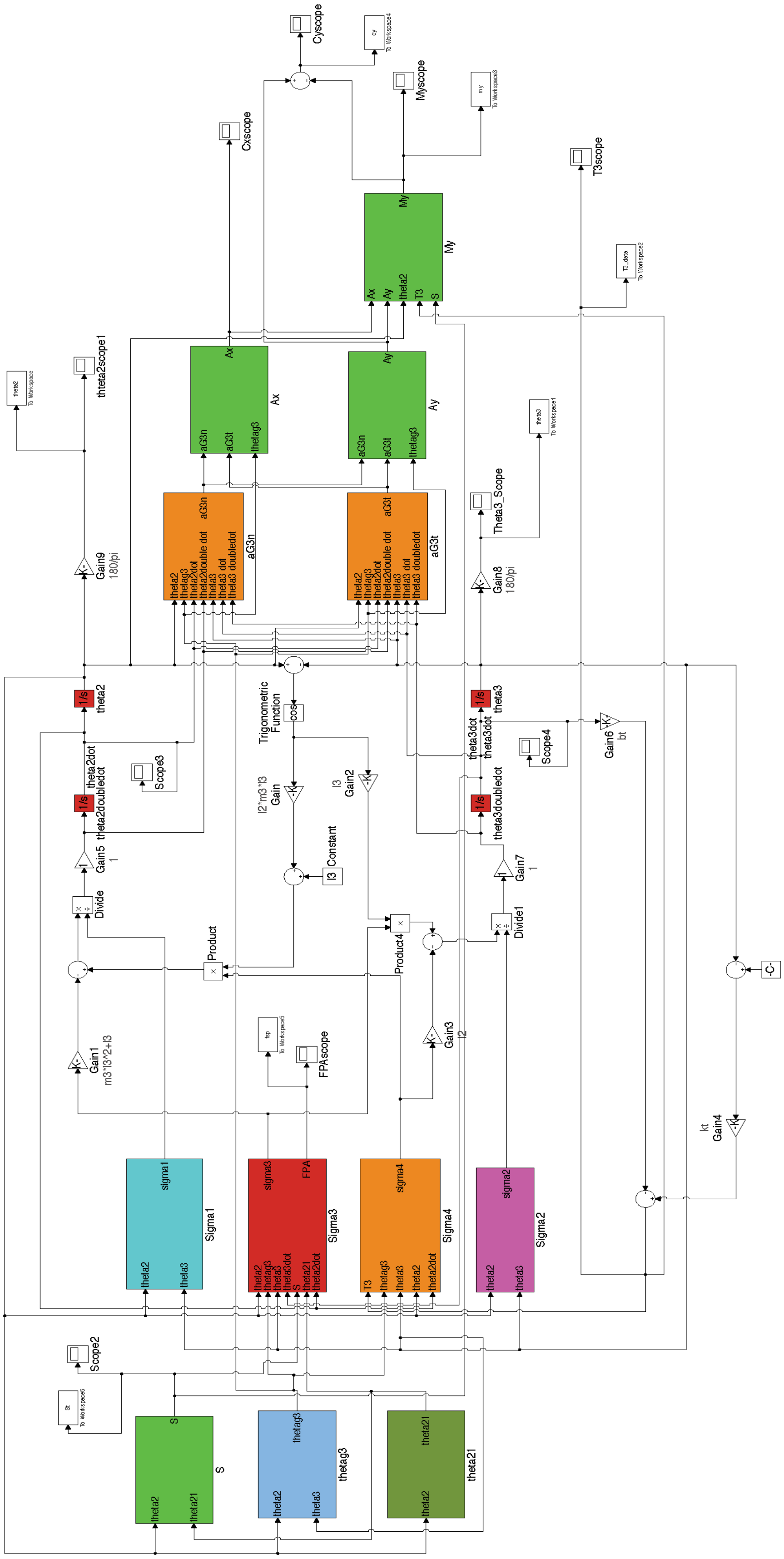

Figure 4-5 Matlab Simulink model representation

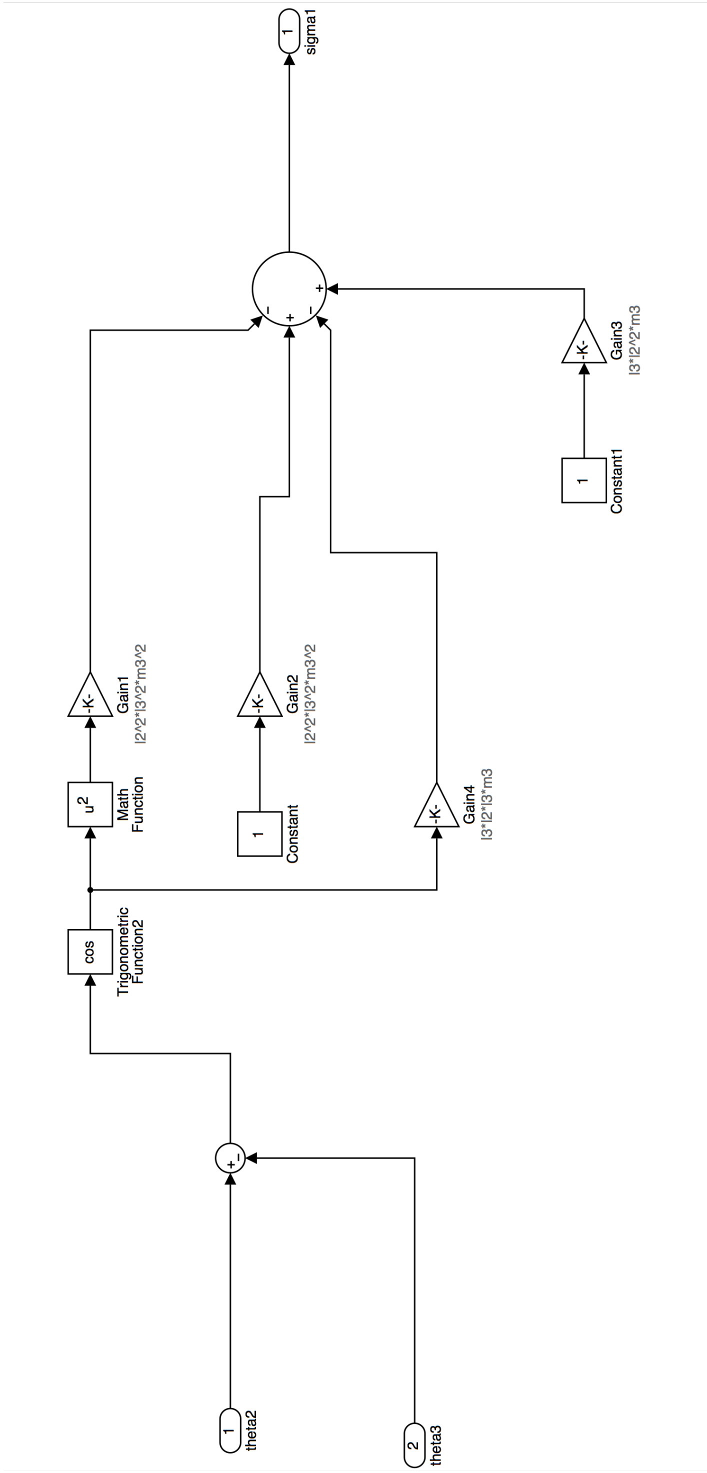

Figure 4-6 Sigma-1 subgroup

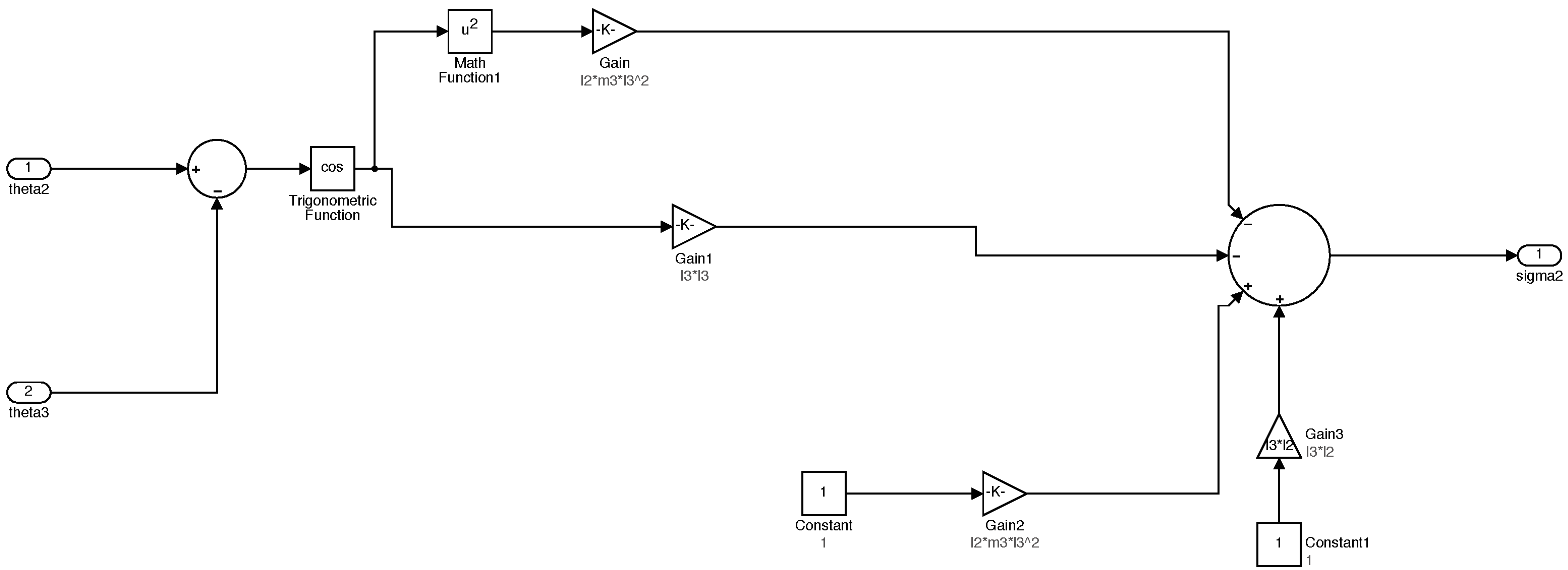

Figure 4-7 Sigma-2 Subgroup

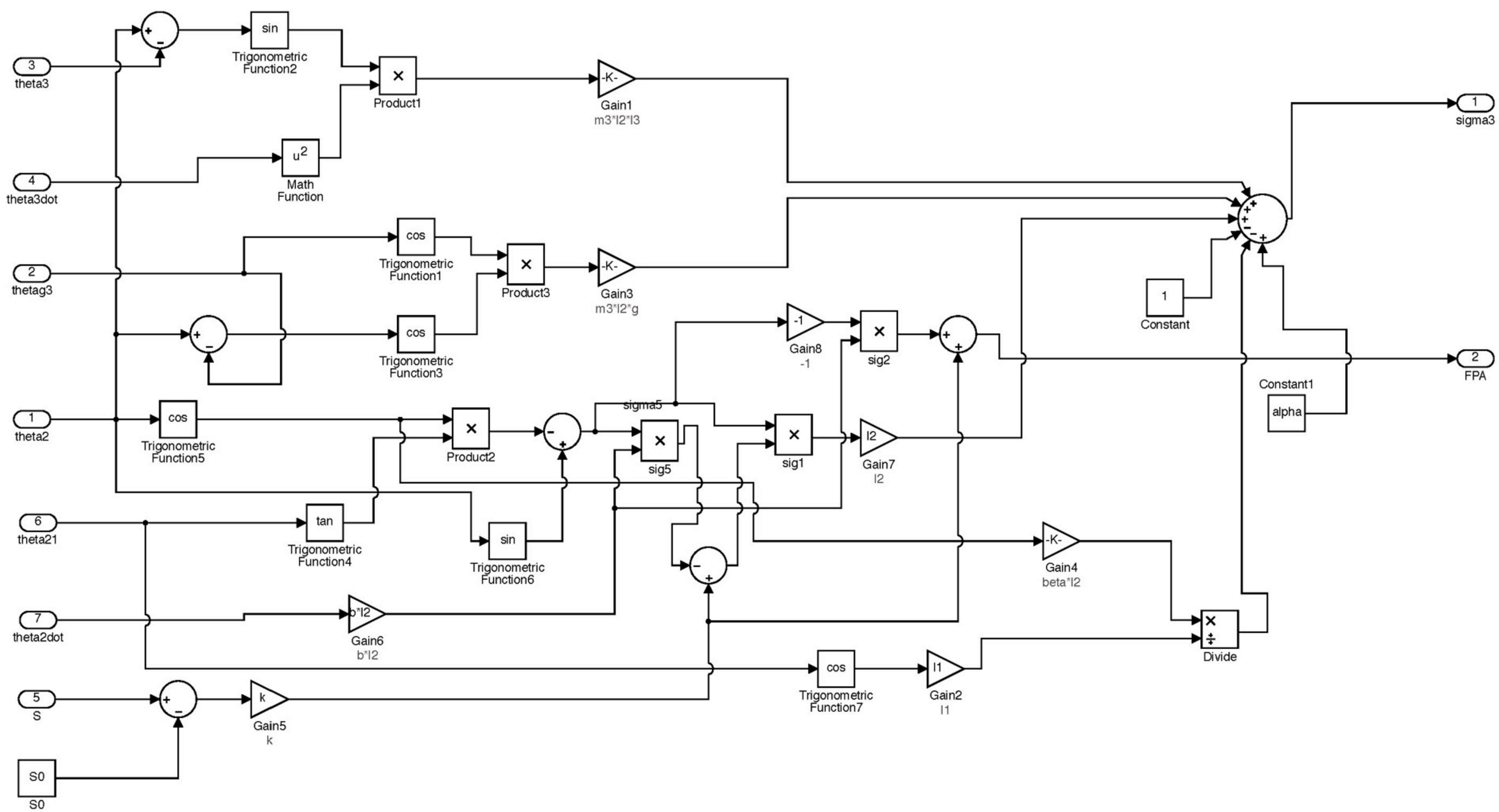

Figure 4-8 Sigma-3 subgroup

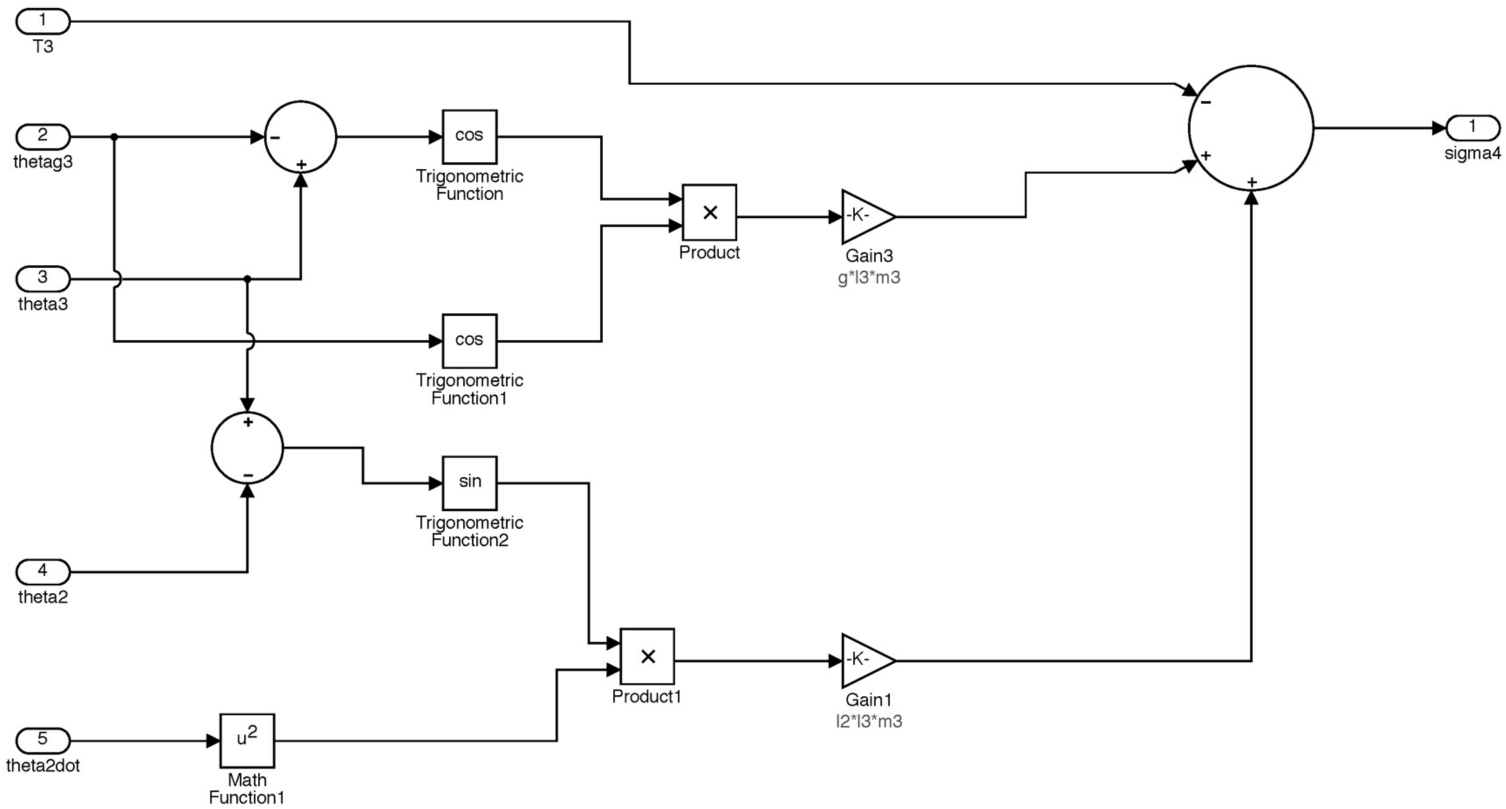

Figure 4-9 Sigma-4 subgroup

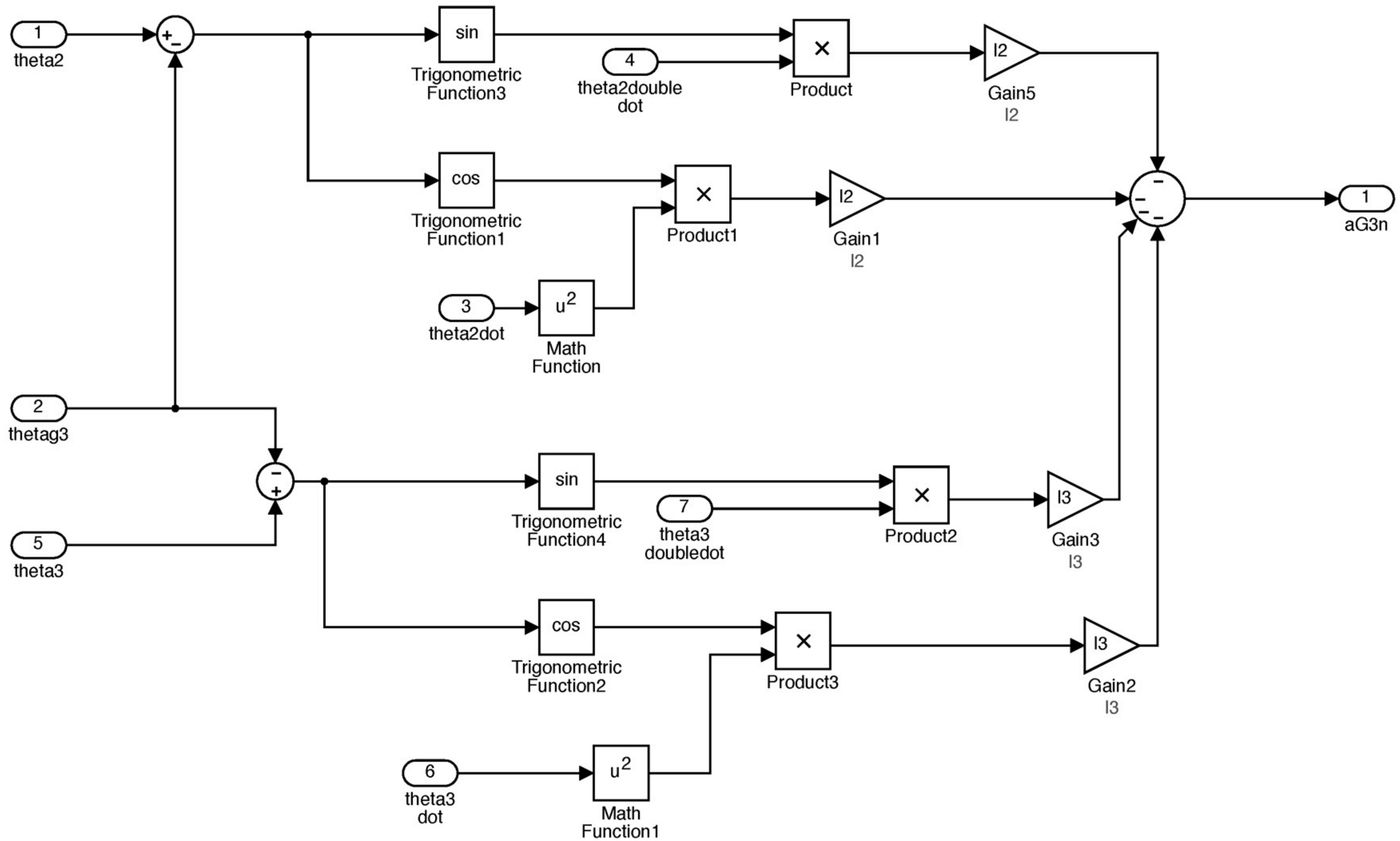

Figure 4-10 Normal component of acceleration subgroup

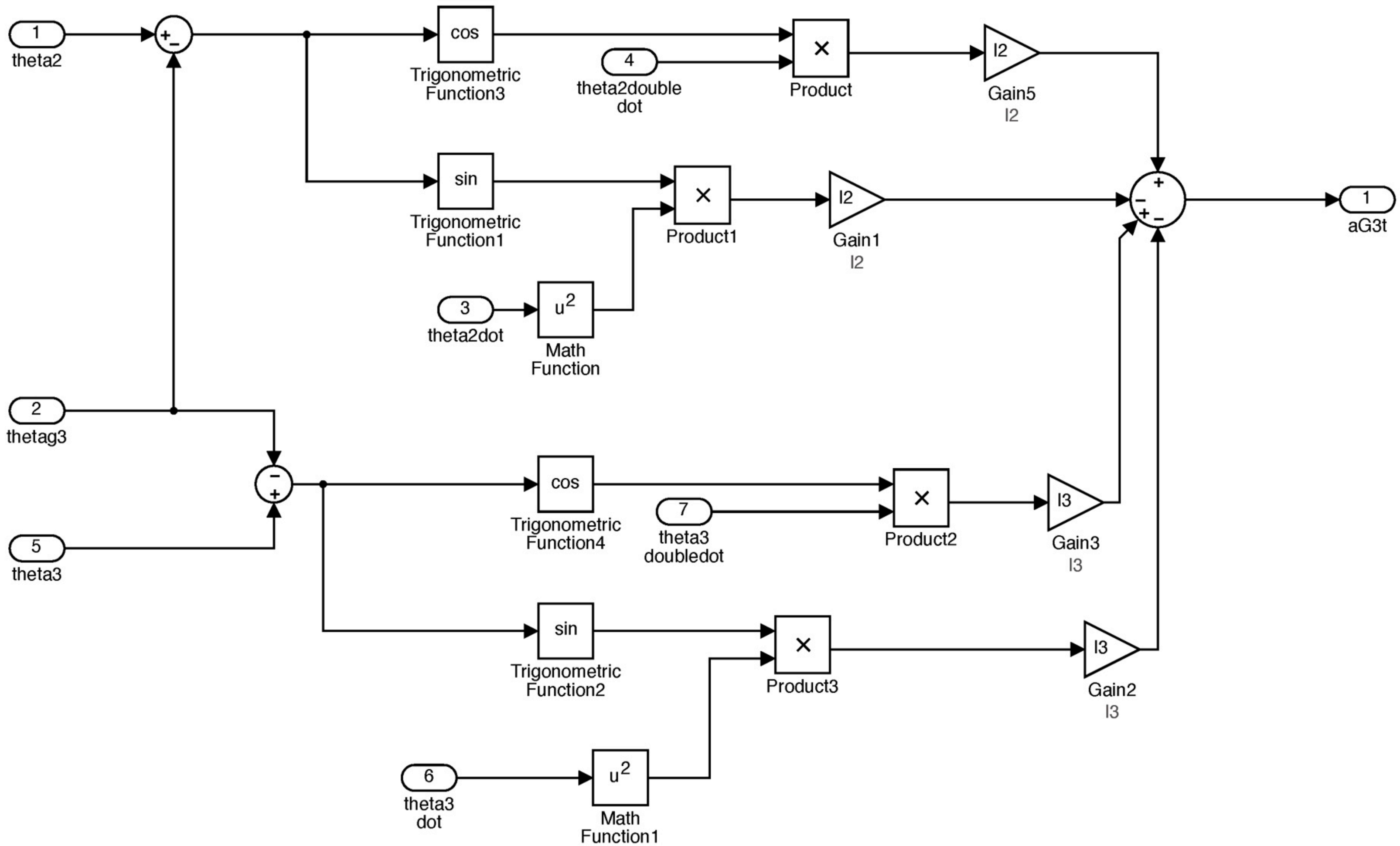

Figure 4-11 Tangential component of acceleration subgroup

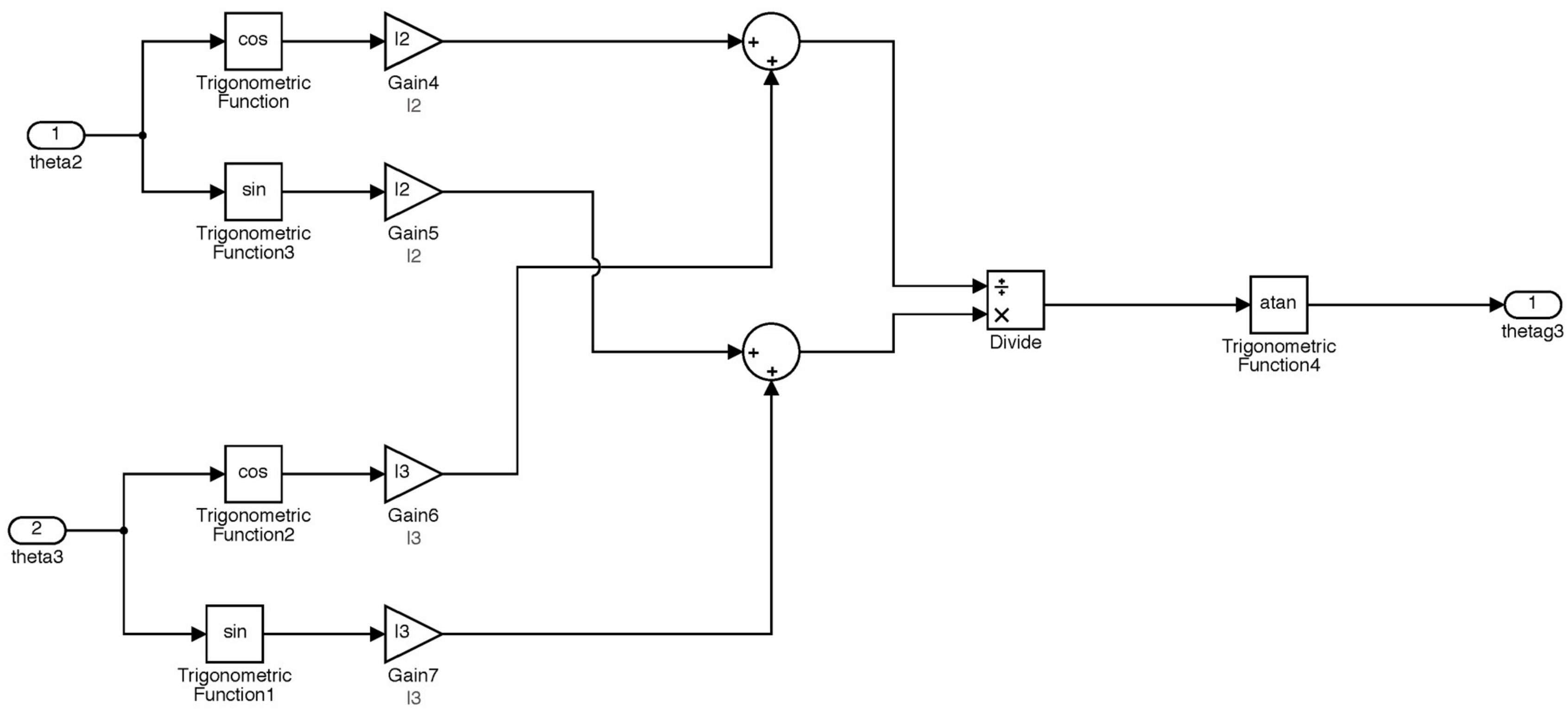

Figure 4-12 Theta_G3 subgroup

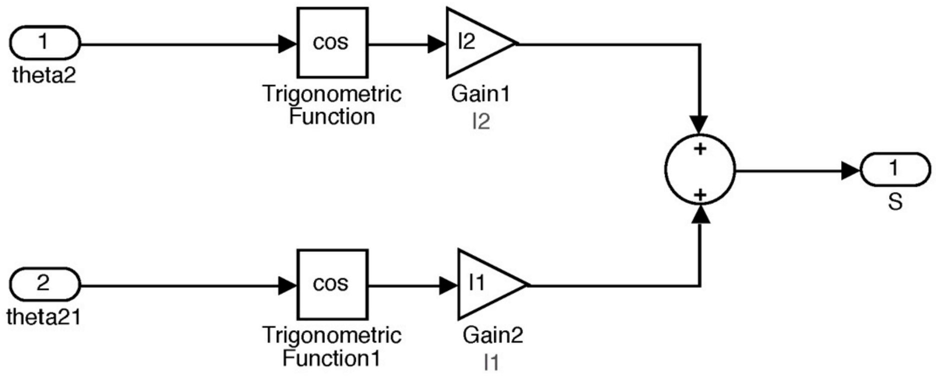

Figure 4-13 S subgroup

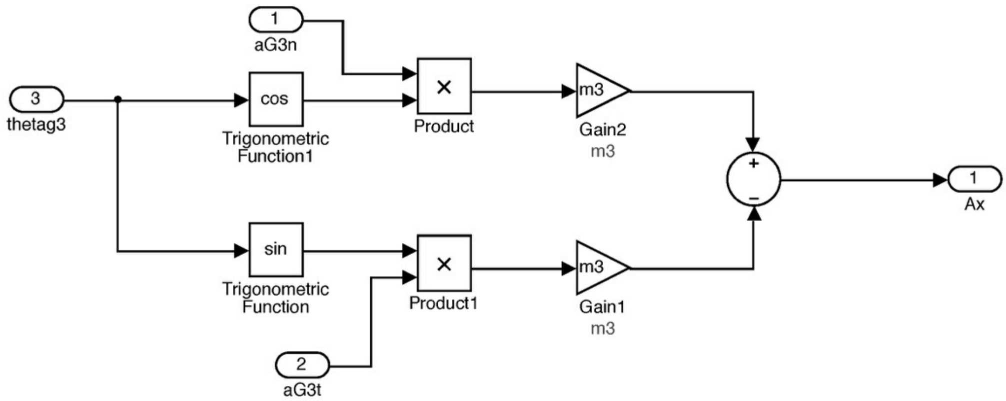

Figure 4-14 Ax component of reaction forces subgroup

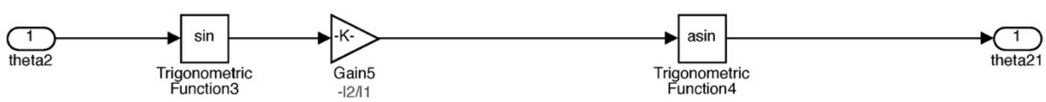

Figure 4-15 Theta_21 subgroup

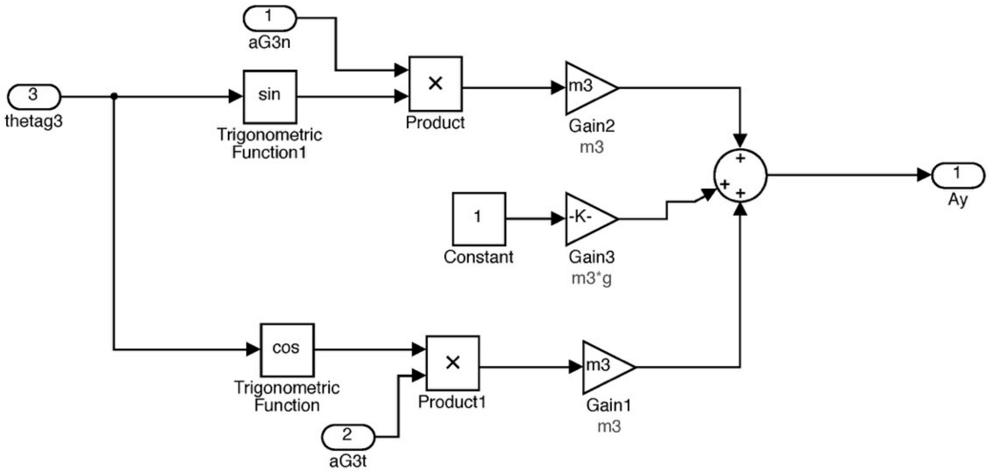

Figure 4-16 Ay component of reaction forces subgroup

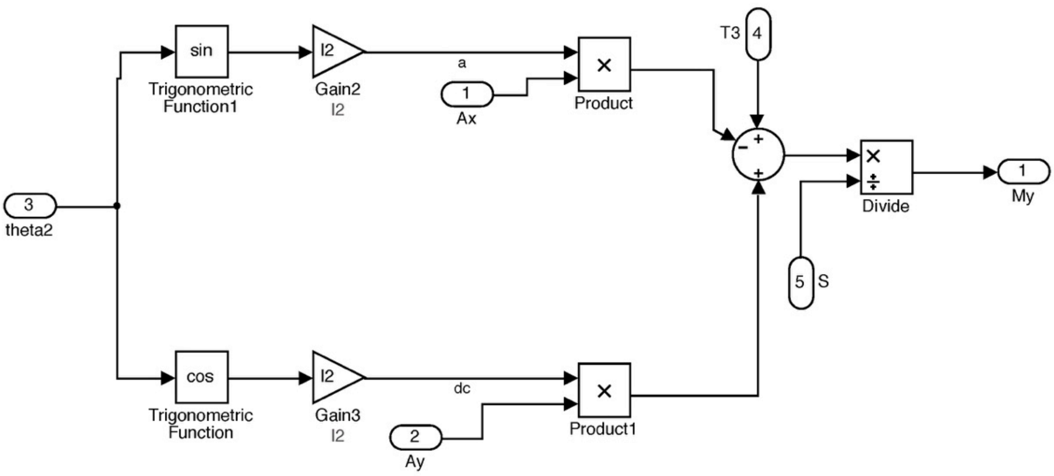

Figure 4-17 My component of reaction forces subgroup

.

4.6 Simulation Results

Deformable foot mathematical model and formulation are presented in the previous sections. Here in this section, simulation results that are run on the MATLAB® Simulink module, are presented.

4.6.1 Simulink Simulation Results

Simulation is performed using ode45 (Dormand-Prince) variable-step type solver with 0-5000 seconds time option. Other configuration settings are taken as default. Before beginning of each experiment basic dimensions of subjects' foot are recorded. They are whole foot length, from tuberosity of calcaneous to metatarsals region above sesamoid bone, tuberosity of calcaneous to downward projection of ankle joint and height of the ankle joint from plantar face of foot using a specially designed apparatus. Representative male subject measurements are shown in Figure 4-18.

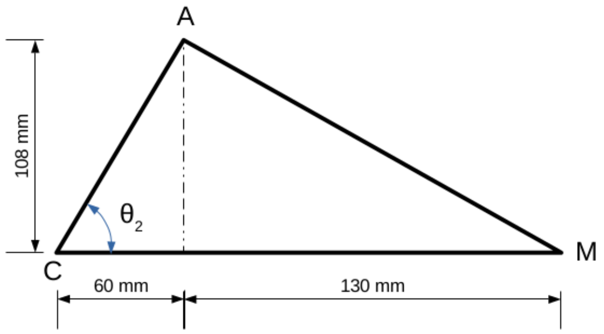

Figure 4-18 A representative male subject measurements

4.6.2 Results for a Representative Male

Accordingly performing the basic calculations parameters required for the mathematical model are calculated. For a male subject data presented in Figure 4-18 where weight of the subject is 873 N which is 89 kg in mass, height of 178 cm, where height of center of gravity is taken as 0.55-0.575 of body height [72] about 0.98 cm from ground and about 0.88 cm from the ankle joint. l_1 and l_2 calculated as approximately 170 and 124 mm respectively (see Figure 4-18). θ_2 is then found to be 61 degrees and taken as initial conditions. Moreover for θ_3 initial value taken 88 degrees. According to anthropometric studies of human foot and ankle by Isman et al. θ_2 is defined as "angle between axis of talocalcaneal joint and horizontal plane".

It's value ranges between 20-68 degrees and mean value is 41±9 degrees as in Figure 4-19 [73].

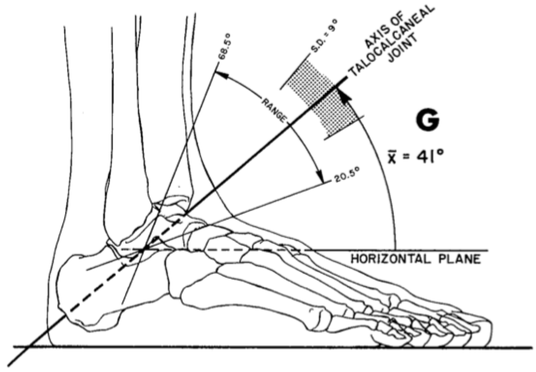

Figure 4-19 Angle between axis of talocalcaneal joint and horizontal plane.

Reactive torque T_3^R torsional stiffness k_t (see Equation 4.55) is taken as 2000 Nm/rad. α and β values are taken 0.2 and 0.8 since these values are found to be the best values for stable region. Moment of Inertia of the single pendulum model is taken simply as $I_3 = m_3 l_3^2$. Although many different suggestions are presented this simple representation suffices for the model. Parameters used for these calculations are shown on Table 4-1 and output of the simulation is given in Figure 4-19 –21

Table 4-1 Simulation parameters of a representative male

Parameters	**Case 1**	**Case 2**	**Case 3**
α	0.2	0.2	0.2
β	0.8	0.8	0.8
θ_2 [deg]	61	61	61
θ_3 [deg]	88	88	88
k_t [N/m]	2000	**1500**	**1200**
b_t [Ns/rad]	5	**20**	20
k [N/m]	15000	**10000**	**10000**
b [Ns/m]	100	**125**	125
Th [deg]	91	91	**90**
m_3 [kg]	89	89	89
I_3 [kgm2]	68	68	68
l_1 [m]	0.17	0.17	0.17
l_2 [m]	0.12	0.12	0.12
l_3 [m]	0.87	0.87	0.87

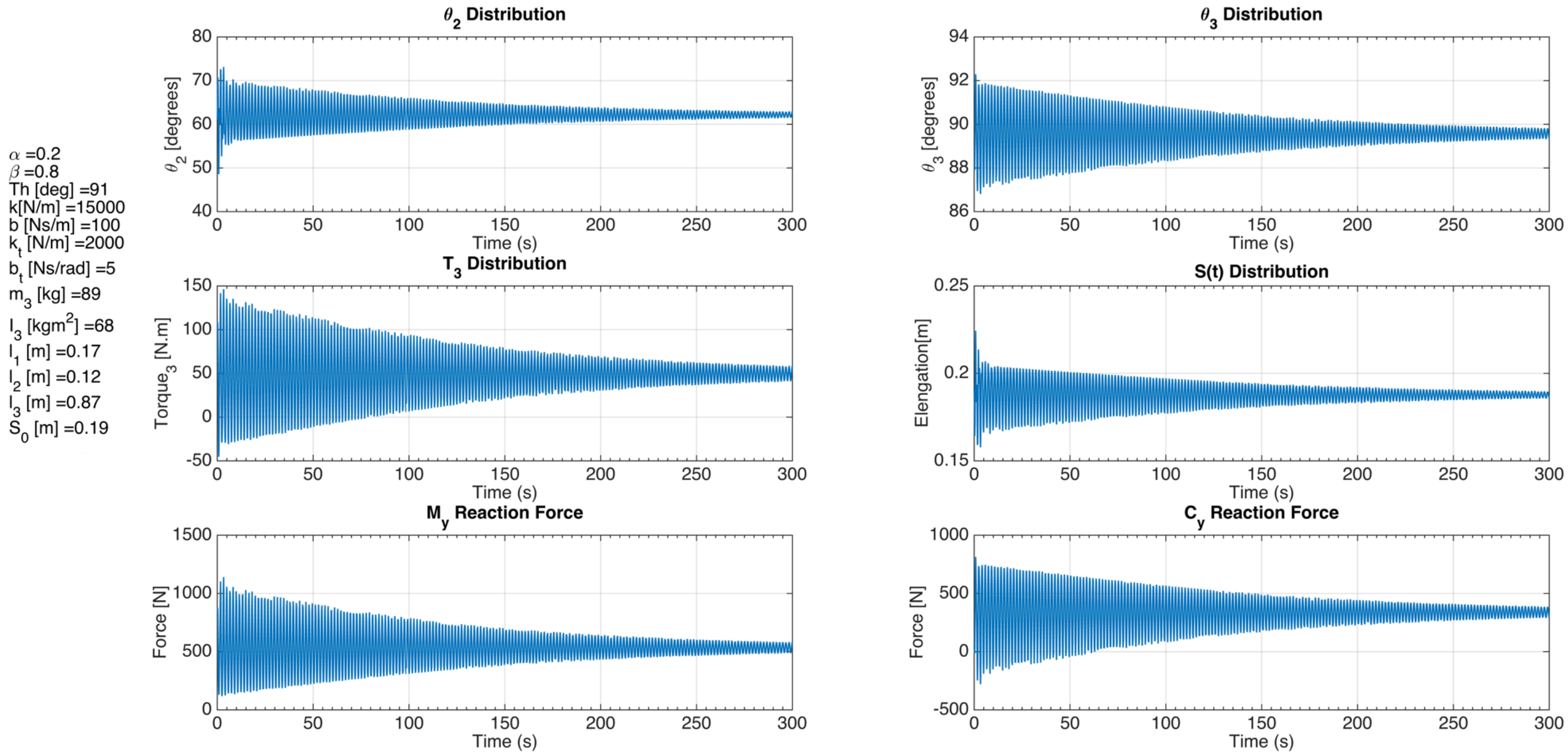

Figure 4-20 Simulation output of a representative male subject case-1

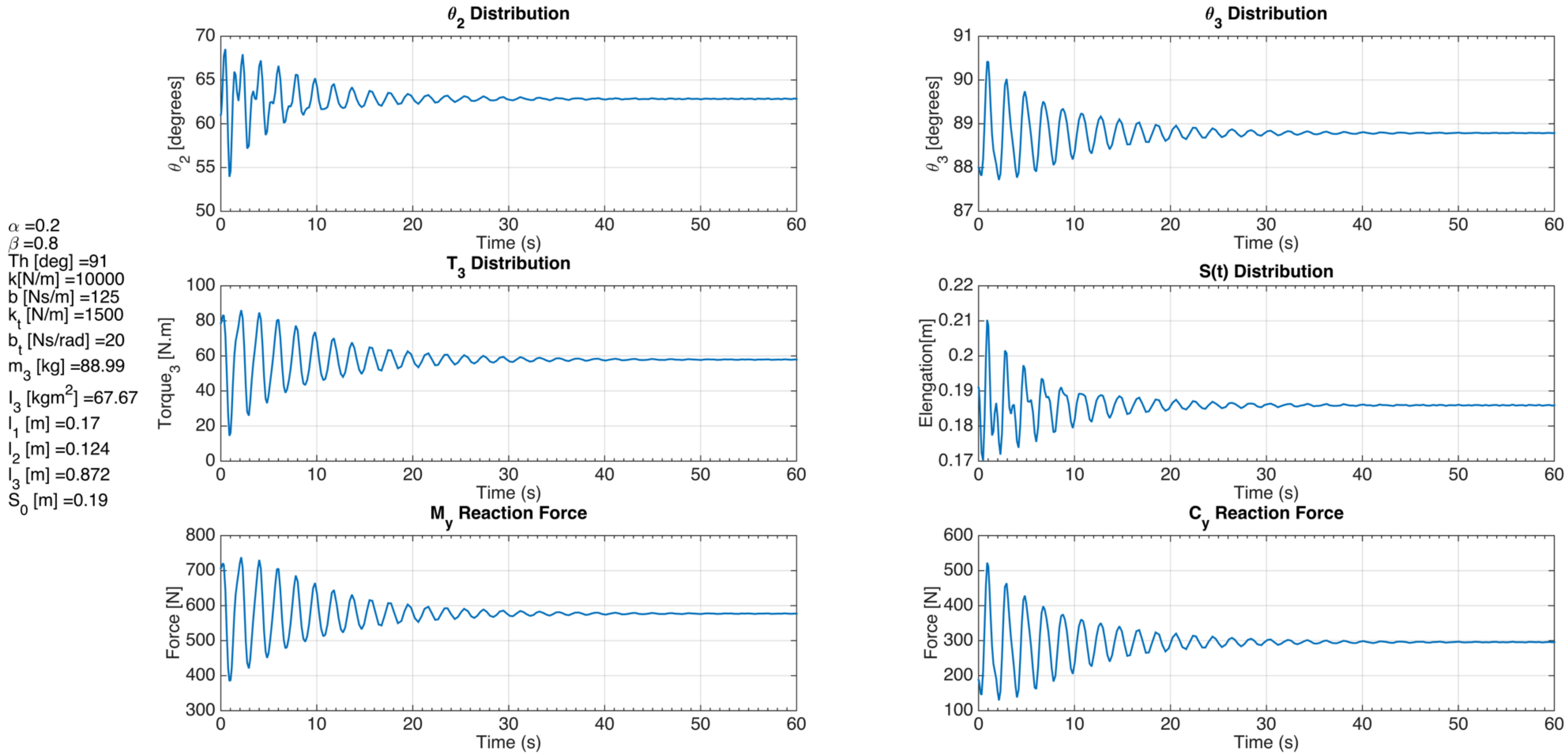

Figure 4-21 Simulation output of a representative male subject case -2

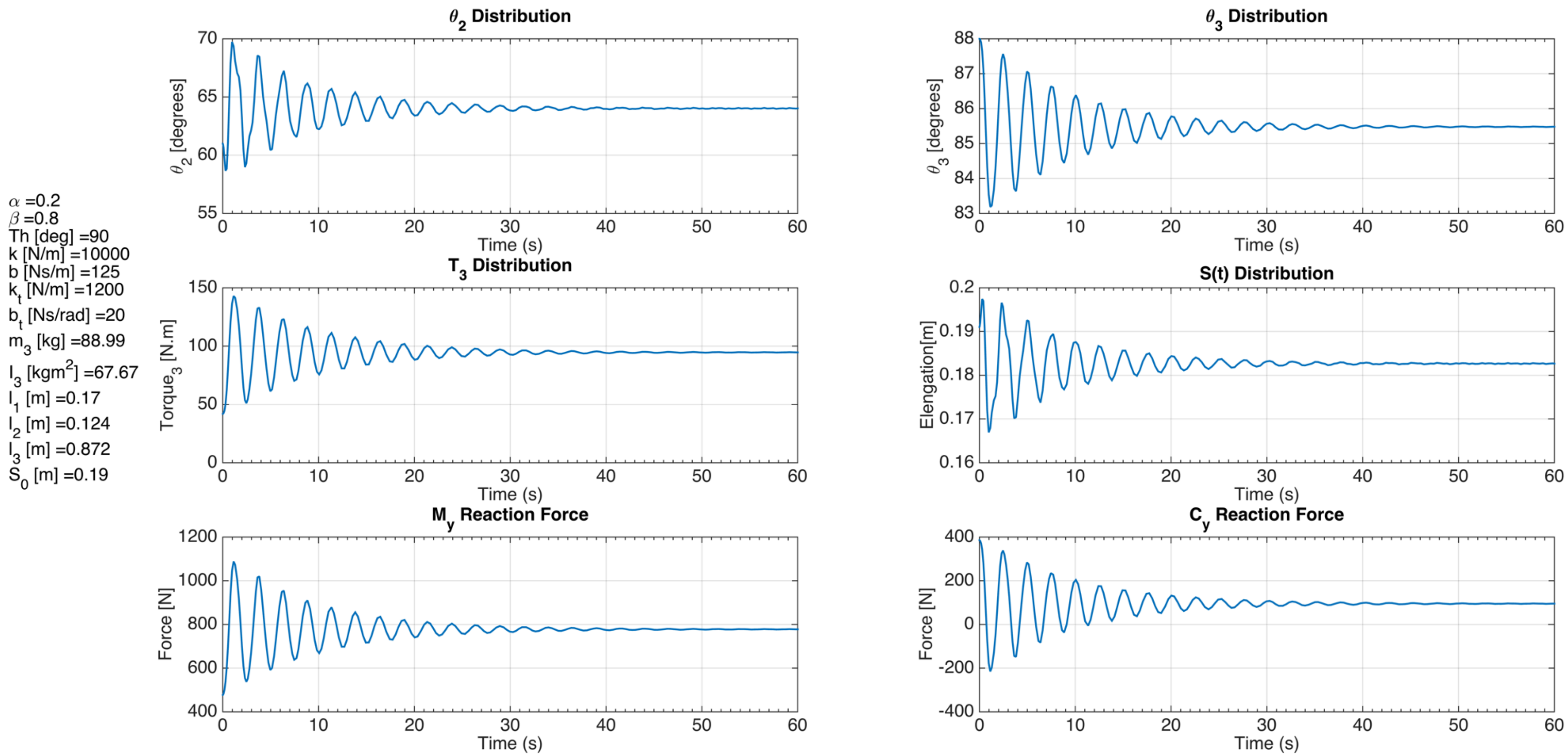

Figure 4-22 Simulation output of a representative male subject case-3

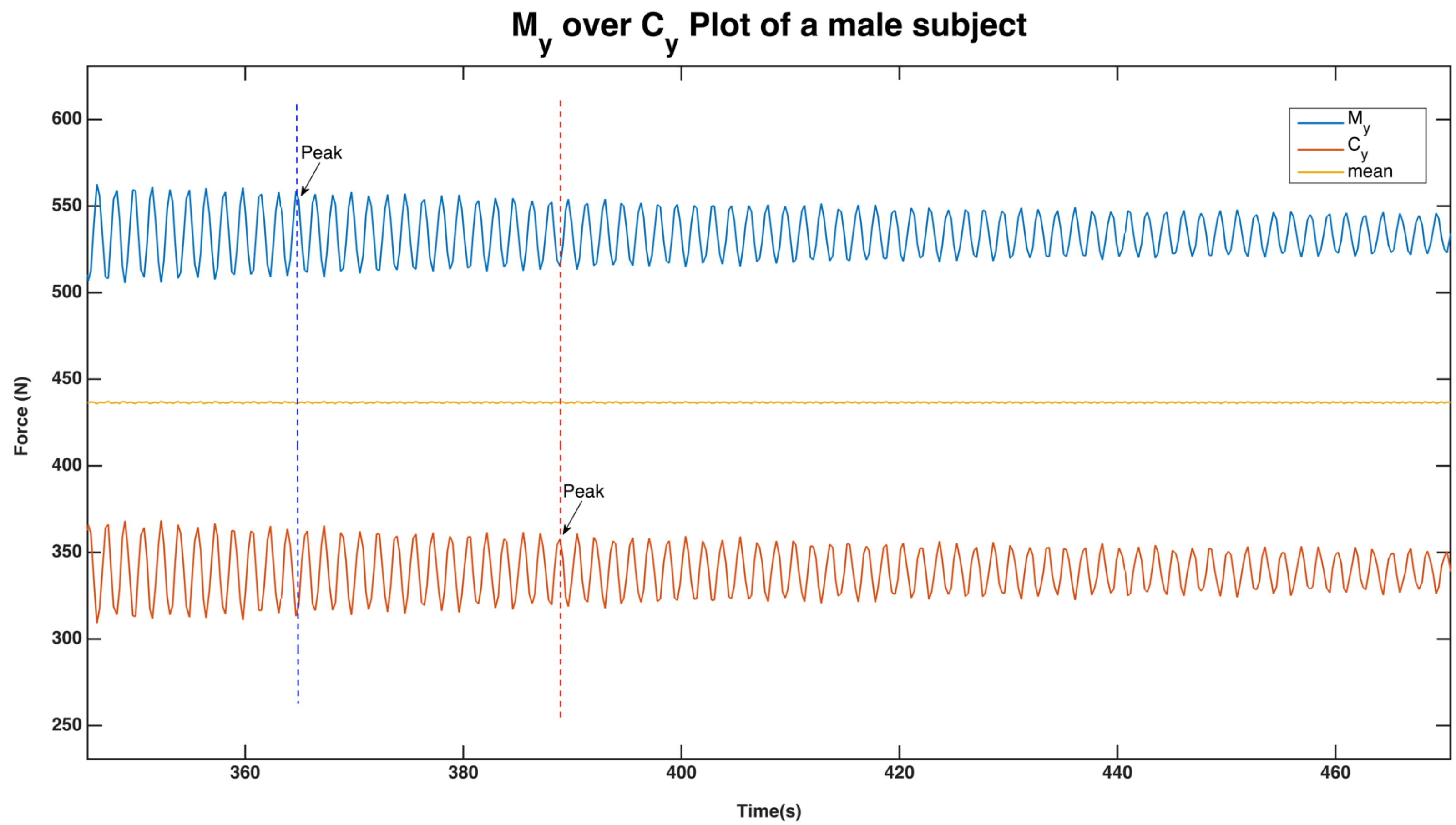

Figure 4-23 Load Shifting Mechanism can be seen in upper and lower peak values.

4.6.3 Results for a Representative Female

For a representative female subject following results are obtained. Measured dimensions of a subject are presented in Figure 4-24.

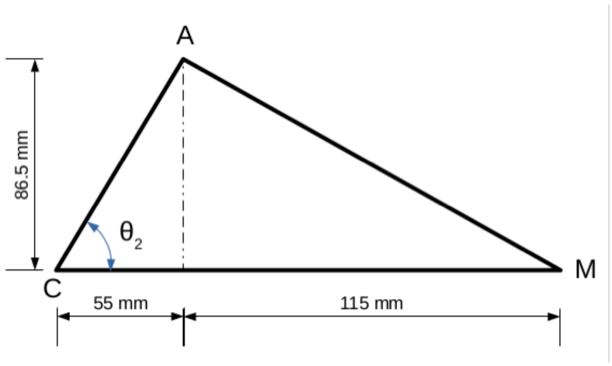

Figure 4-24 A representative female subject measurements

Table 4-2 Simulation parameters of a representative female

Parameters	**Case 1**	**Case 2**	**Case 3**
α	0.2	0.2	0.2
β	0.8	0.8	0.8
θ_2 [deg]	57.5	57.5	57.5
θ_3 [deg]	88	88	88
k_t [N/m]	2000	2000	**1200**
b_t [Ns/rad]	5	20	20
k [N/m]	17500	**15000**	**10000**
b [Ns/m]	100	100	**125**
Th [deg]	90	90	90
m_3 [kg]	57.5	57.5	57.5
I_3 [kgm^2]	44.5	44.5	44.5
l_1 [m]	0.14	0.14	0.14
l_2 [m]	0.10	0.10	0.10
l_3 [m]	0.88	0.88	0.88

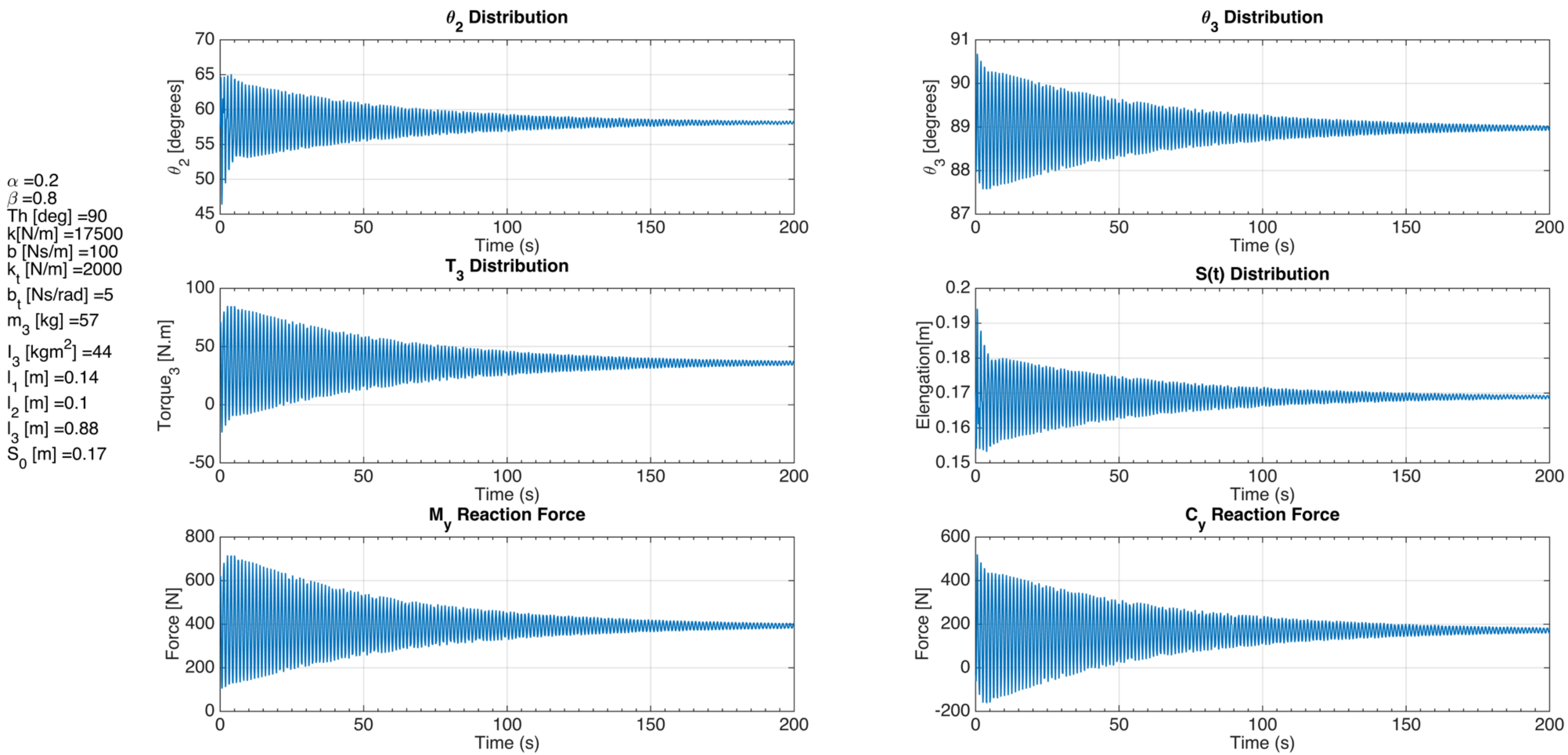

Figure 4-25 Simulation output of a representative female subject case-1

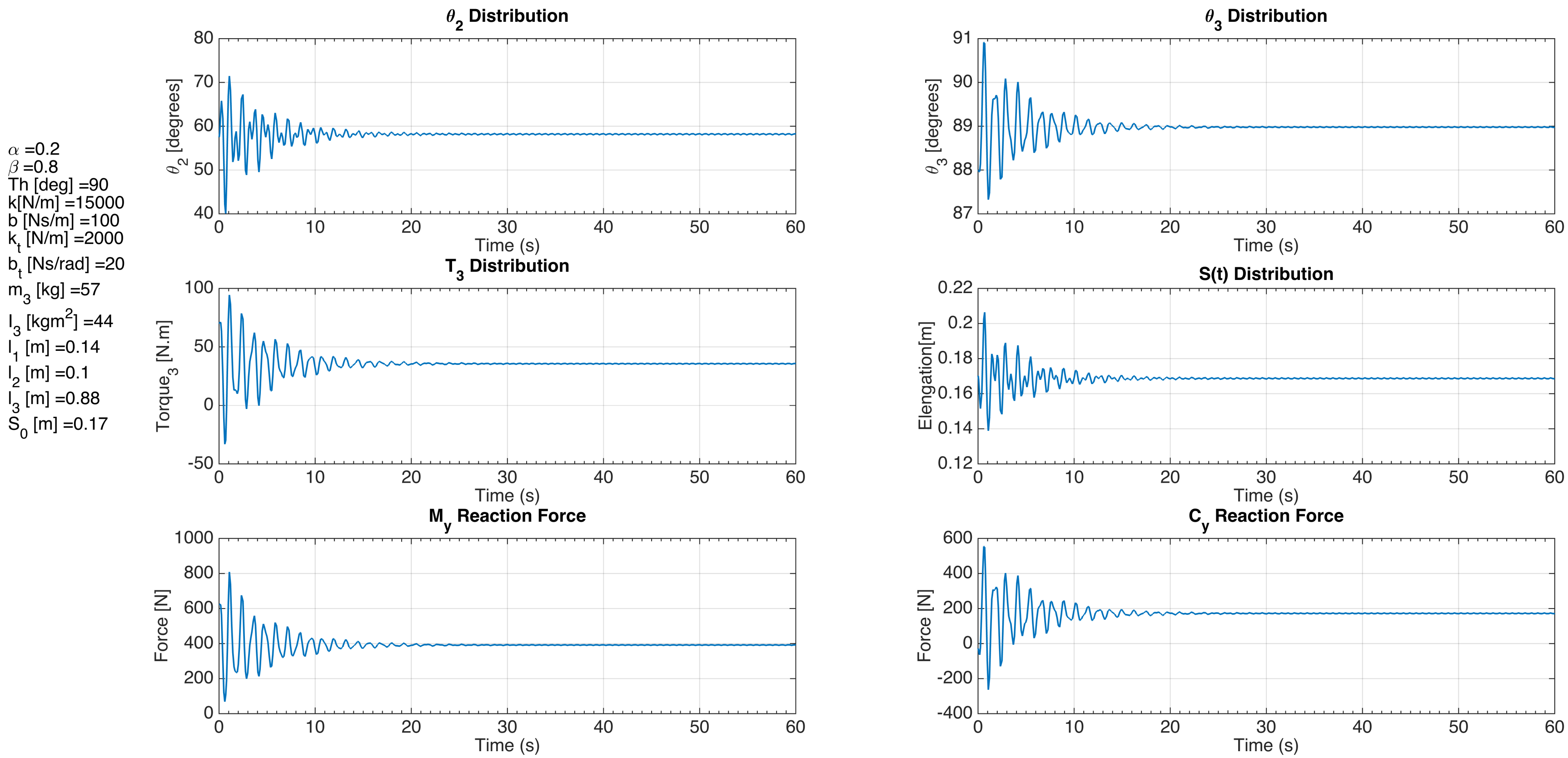

Figure 4-26 Simulation output of a representative female subject case-2

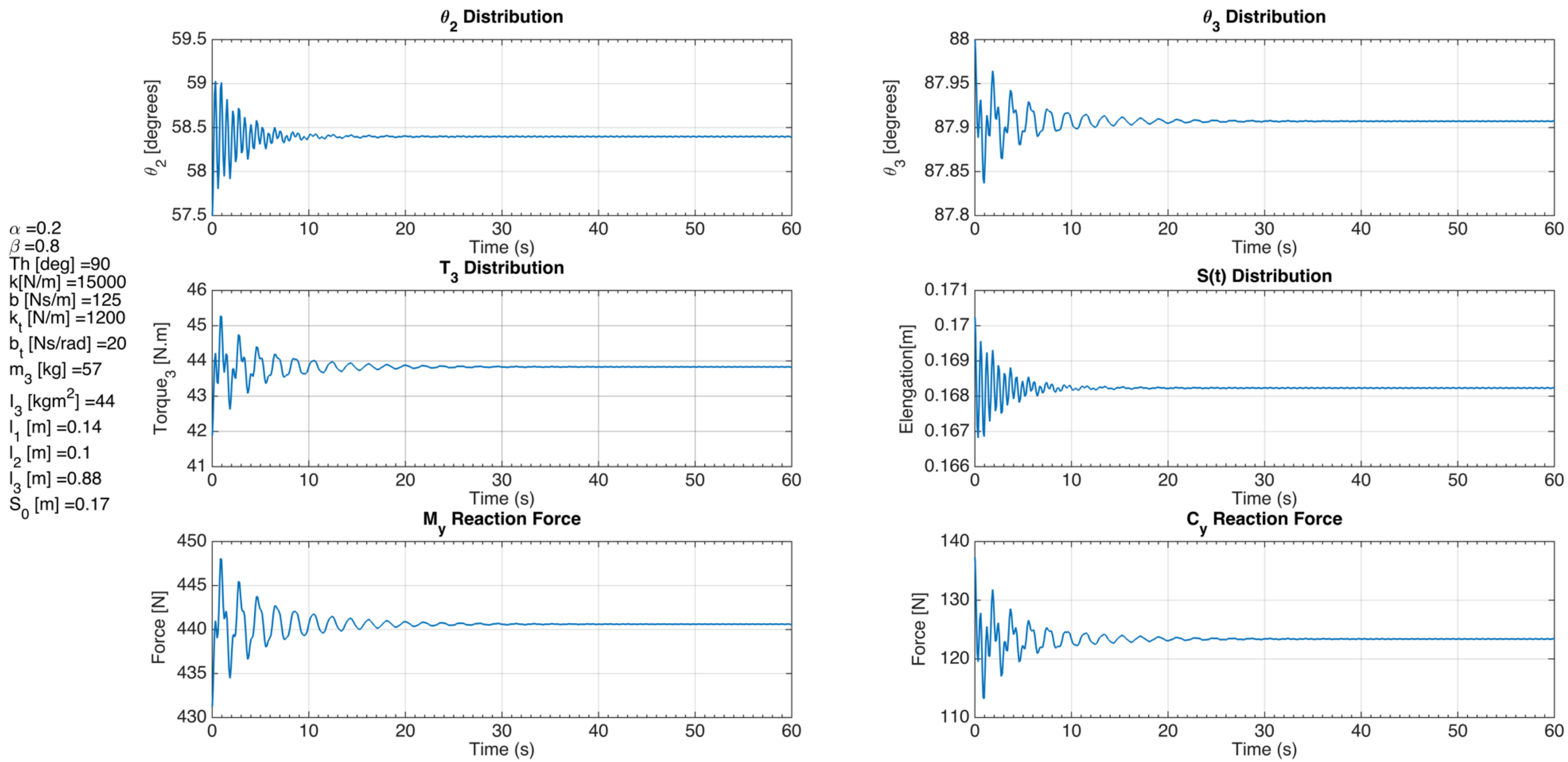

Figure 4-27 Simulation output of a representative female subject case-3

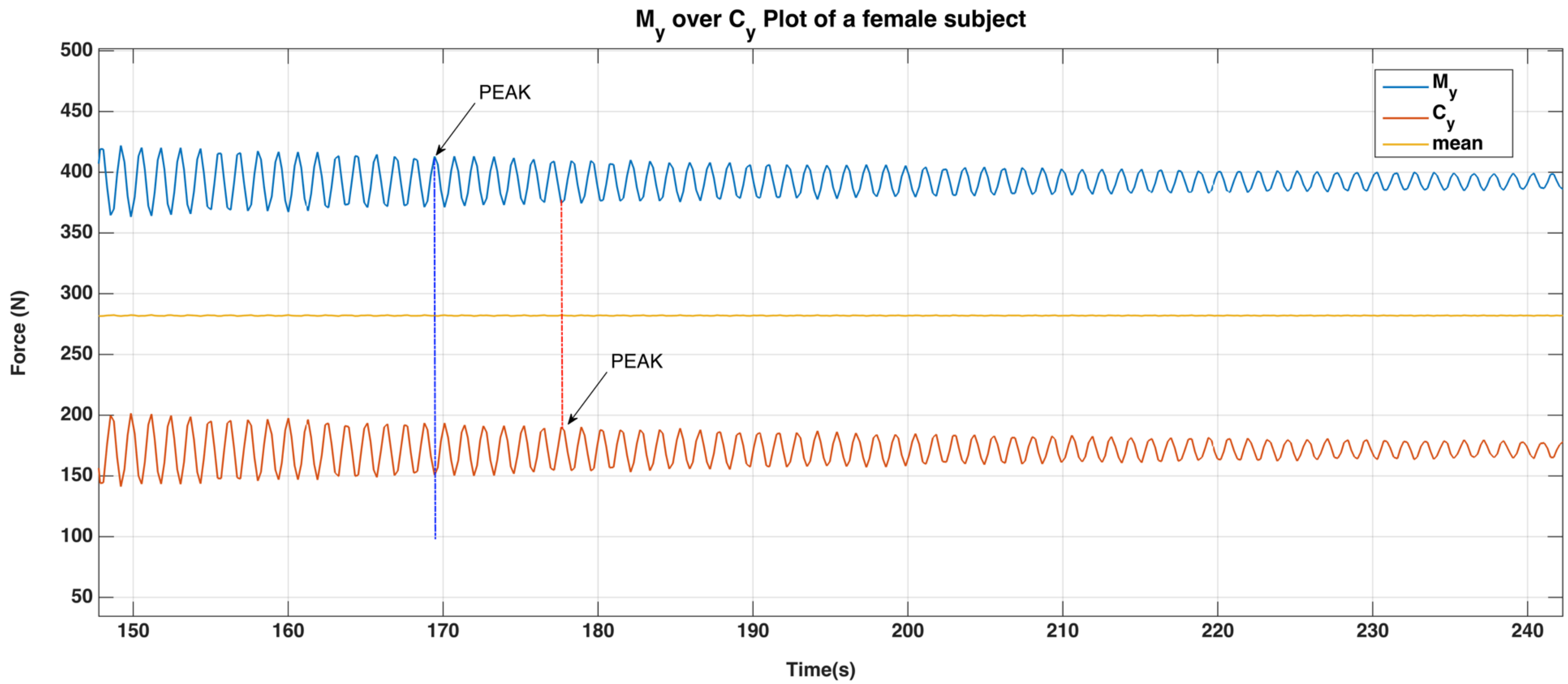

Figure 4-28 Load Shifting Mechanism can be seen in upper and lower peak values.

It can be observed examining the simulation outputs of male and female subjects that, change of critical variables like torsional stiffness and damping coefficients “k_t”, “b_t”, plantar aponeurosis (PA) stiffness and damping coefficients, “k”, “b” and threshold angle “Th” effects the simulation output dramatically. The values of these variables are taken mostly from the works of Kim et al. [13], Gefen[60] and Gürses [48].

In the male subject of “case-1” with reactive torque components k_t = 2000 N/m and b_t=5 Ns/rad. PA components k=15000 N/m and b=100 Ns/m, then the system came to rest or stability at about 300 seconds. For a real human body this must be maintained in milliseconds. Rearranging the variables and increasing b_t= 20 Ns/rad, decreasing k_t=1500 N/m and increasing PA b=125 Ns/m and decreasing k=10000 N/m the system stability is reduced 10 times to 30 seconds in “case-2”. Similar observation can be seen in female subject. It is clear that 30 seconds does not represent the real human behavior, however response of the model to change of variables can be observed. When the correct values are given to the system we may see the real human performance. The correct values of these variables differ from person to person actually. The working ranges of the variables are to be determined from human experiments specifically designed for the variable in subject. Figures 4-23 and 4-28 shows the LSM for both male and females as in the real case, due to sway of the inverted pendulum.

CHAPTER 5

DISCUSSION AND CONCLUSION

5.1 Discussion

Many deductions can be reached based on examining and interpreting the results of the experiments. In all of the interactions there is a single fact that; males and females are different in every aspect of using their feet. Utilization of left and right foot, using F, M and H regions and co-ordination of F-H, F-M and H-M force-couples, emphasizes the "Load Shifting Mechanism (LSM)".

Firstly, average contact areas of male and females were different. Forefoot and hindfoot areas of males were larger than females. Meanwhile midfoot mean contact area was larger in females. Putti et al. has expressed his findings as “the contact area is greater in males than in females, however there are no significant differences between gender in the peak pressure characteristics of the feet” [74], but it is not so in our case.

Secondly, average normal force on males' left foot is significantly larger than their right foot and the vice versa for females. Considering the fact that all of the subjects are right-handed, a question of laterality arises. This topic has taken many interests in research [75–79] and importance of laterality on posture and gait was emphasized. Even at early dates by Hirasawa [80], the importance of laterality on standing posture that uses left foot as support and supplementary function of right foot was found. It was also stated that there was a significant difference between male and female subjects. In our study it has been seen that, on males left foot dominance and LSM is clearly observed, but it is not so clear, in females.

In time domain analysis it is observed that F-M regions are acting together. A positive (+) correlation has been found between them. Meanwhile, there is a negative (-) correlation between F and H regions. In frequency domain analysis, auto and cross correlations were analyzed and looked for coherence, gain and phase values. Considering phase angles, F force and M force are in phase at zero degree, F and H forces are out of phase at 180 degrees.

Having completed phase considerations, cross correlations of FH, FM & HM and their coherence values (above 0.80) are analyzed. It has been observed that, most of the posture dynamics occurred at lower frequencies around 0-5 Hz regions. There were also high-frequency values 7 Hz, 14 Hz even 20-25 Hz. However, their reason of presence could not be determined at this time, whether they are a kind of control signal or not. Maximum correlation was observed at FH and FM regions, and minimum at HM region. In male subjects, left foot and FH region dominance is observed. Meanwhile, in female subjects slightly larger FM dominance is seen. FH region used the maximum frequency bandwidth and maximum coherence in males, while the FM region of females used slightly larger bandwidth and maximum coherence.

Considering the 95% power calculations of force regions, a significant difference between genders and feet was clearly revealed. Moreover, it is observed that in the mid-foot section, high-frequency activities take place. Accordingly, an order of frequency distribution was determined for H – F – M regions respectively from lower to higher. High frequency value observations may be a consequence of plantar fascia interaction or high signal/noise ratio at M region.

Gender difference is a major separation point and lateralization of foot is another important aspect. It is observed in both Power (P95%, P50%) and frequency domain calculations; gender difference among subjects is significant. As for the use of feet, left foot is more frequently used among right-handed subject set. Left foot dominance is observed mainly in males, whereas foot usage is almost equal in females. In addition, in terms of regions, FH correlation is dominant in males, whereas FM correlation is more dominant in females.

Foot pressure distributions between males and females were studied before. [74,81] However, except for the anatomical differences due plantar area, no difference is found. As a matter of fact, there are many differences. These differences may result from stiffness variability in plantar aponeurosis between male and female, affecting the mediolateral arch height[82]. Therefore, considering the arch index and arch height can be a good correlation point.

5.2 Conclusion

Mathematical model constructed has been solved analytically and simulation results are obtained. However, parameter identification and determination of stability points must be calculated. When looking at the load distribution; although inverted pendulum is stabilized at expected region, metatarsals have been carrying more weight than hind foot region. Contrary hindfoot carries more weight than metatarsals in experimental results. Since, COM line of action to ground always passing through modified front side of the model, that is θ_3 around 85-89.5° and including moment arms, metatarsals carry more weight than hind foot region. In such a truss model the hardest part of the problem is to maintain virtual arch height where most of the job is on stiffness of plantar aponeurosis. However, considering the model as a "tied curved arched" shape instead of a "truss model" solves half of the problem. Due to arched structure, an internal stiffness is induced. Then, at ankle joint location an inverted pendulum can be constructed. Since COM is more close to hind foot region, due arched nature load can be distributed as in the real human foot. This type of arched structure was already suggested by Hicks, and Wright et al., [34,58].

Further analysis can be made using nonlinear analysis methods or principal component analysis, coupling force data with center of pressure (COP) movement, where COP distribution can be enclosed in an ellipsoid. Hence, principal directions are determined and force fields are coupled accordingly by comparing the actual results.

Since, human nature is actually a nonlinear and chaotic system, application of a nonlinear control strategy for the control torque would be a better alternative for a more realistic foot model.

During the experiments, we worked on anterior-posterior axis, so media-lateral axis can be considered and cross correlations can be taken into account. In fact, higher coherence values are observed at cross sides of foot, like left foot-front and right foot-hindfoot regions.

It has also been observed that the emotional state of the subjects, directly affects the distribution of the load signals. Further improved experiments are suggested in order to better clarify such situations.

Posturography is based on the resultant COP signals. Recent works mostly concentrated on analyzing left and right foot COP signals separately [83–85]. Therefore, further analysis based on combining the foot and its application of posture metrics like COP variances (the data was already collected in our case) can deliver more promising results in the future.

To conclude, there is no better ending line for this study other than the statement made by the early 20th century anatomist, Frederick Wood Jones: "Man's foot is all his own. It is unlike any other foot. It is the most distinctly human part of his whole anatomical makeup. It is a human specialization and, whether he be proud of it or not, it is his hall-mark and so long as Man has been Man and so long as he remains Man, it is by his feet that he will be known from all other members of the animal kingdom" [86,87]

BIBLIOGRAPHY

[1] Massion J. Postural control system. Curr Opin Neurobiol 1994;4:877–87. doi:10.1016/0959-4388(94)90137-6.

[2] Prince F, Winter D a., Archer SE. Assessment of postural control during quiet stance with different foot configurations. Gait Posture 1995;3:110. doi:10.1016/0966-6362(95)93513-C.

[3] Mergner T, Maurer C, Peterka RJ. A multisensory posture control model of human upright stance. Prog Brain Res 2003;142:189–201. doi:10.1016/S0079-6123(03)42014-1.

[4] Schweigart G, Mergner T. Human stance control beyond steady state response and inverted pendulum simplification. Exp Brain Res 2008;185:635–53. doi:10.1007/s00221-007-1189-4.

[5] Nait-Ali A. Advanced Biosignal Processing. Berlin, Heidelberg: Springer Berlin Heidelberg; 2009. doi:10.1007/978-3-540-89506-0.

[6] Barin K. Evaluation of a generalized model of human postural dynamics and control in the sagittal plane. Biol Cybern 1989;61:37–50.

[7] Oie KS, Kiemel T, Jeka JJ. Multisensory fusion: simultaneous re-weighting of vision and touch for the control of human posture. Brain Res Cogn Brain Res 2002;14:164–76.

[8] Standring S. Gray’s Anatomy Fortieth edition. Churchill Livingstone 2008.

[9] Abboud R. Relevant foot biomechanics. Curr Orthop 2002;16:165–79. doi:10.1054/cuor.2002.0268.

[10] Hicks JH. The mechanics of the foot: I. The joints. Journal of Anatomy, 1955; 87(Pt 4), 345.

[11] Yavuz M, Botek G, Davis BL. Plantar shear stress distributions : Comparing actual and predicted frictional forces at the foot – ground interface 2007;40:3045–9. doi:10.1016/j.jbiomech.2007.02.006.

[12] Gefen A. Stress analysis of the standing foot following surgical plantar fascia release. J Biomech 2002;35:629–37. doi:10.1016/S0021-9290(01)00242-1.

[13] Kim W, Voloshin AS. Role of plantar fascia in the load bearing capacity of the human foot. Journal of biomechanics,1995; 28(9), 1025-1033.

[14] Rouhani H, Favre J, Crevoisier X, Aminian K. Ambulatory assessment of 3D

ground reaction force using plantar pressure distribution. Gait Posture 2010;32:311–6. doi:10.1016/j.gaitpost.2010.05.014.

[15] Kirby KA. Ten Biomechanical Functions of the Plantar Fascia Plantar Aponeurosis Consists of Three Components : Medial , Central and Lateral Anatomy of Plantar Mechanical Functions of Plantar Aponeurosis Role of Plantar Fascia in Truss Structure of Foot Mechanics of 2012:1–8.

[16] Bolgla L a, Malone TR. Plantar fasciitis and the windlass mechanism: a biomechanical link to clinical practice. J Athl Train 2004;39:77–82.

[17] Lekkala J, Kaistila T, Laine H. Plantar pressure distribution measurements : an approach to different methods to compute a pressure map. XIX IMEKO World Congress Fundamental and Applied Metrology 2009:1770–4.

[18] Ledoux, W. R. A biomechanical model of the human foot with emphasis on the plantar soft tissue 1999.

[19] Bencke J, Christiansen D, Jensen K, Okholm A, Sonne-Holm S, Bandholm T. Measuring medial longitudinal arch deformation during gait. A reliability study. Gait Posture 2011;35:400–4. doi:10.1016/j.gaitpost.2011.10.360.

[20] Schleip R. Fascial plasticity – a new neurobiological explanation Part 2. J Bodyw Mov Ther 2003;7:104–16. doi:10.1016/S1360-8592(02)00076-1.

[21] Ker RF, Bennett MB, Bibby SR, Kester RC, Alexander RM. The spring in the arch of the human foot. Nature n.d.;325:147–9. doi:10.1038/325147a0.

[22] Karnovsky IA. Theory of Arched Structures. Boston, MA: Springer US; 2012. doi:10.1007/978-1-4614-0469-9.

[23] Meyer PF, Oddsson LIE, De Luca CJ. The role of plantar cutaneous sensation in unperturbed stance. Exp Brain Res 2004;156:505–12. doi:10.1007/s00221-003-1804-y.

[24] Humphrey LR, Hemami H. A computational human model for exploring the role of the feet in balance. J Biomech 2010;43:3199–206. doi:10.1016/j.jbiomech.2010.07.021.

[25] Kennedy PM, Inglis JT. Distribution and behaviour of glabrous cutaneous receptors in the human foot sole 2002:995–1002. doi:10.1013/jphysiol.2001.013087.

[26] Maurer C, Peterka RJ. A new interpretation of spontaneous sway measures based on a simple model of human postural control. J Neurophysiol 2005;93:189–200. doi:10.1152/jn.00221.2004.

[27] Maurer C, Mergner T, Peterka RJ. Multisensory control of human upright stance. Exp Brain Res 2006;171:231–50. doi:10.1007/s00221-005-0256-y.

[28] Alexandrov a V, Frolov a a, Massion J. Biomechanical analysis of movement strategies in human forward trunk bending. II. Experimental study. Biol Cybern 2001;84:435–43.

[29] Alexandrov a V, Frolov a a, Massion J. Biomechanical analysis of movement strategies in human forward trunk bending. I. Modeling. Biol Cybern 2001;84:425–34.

[30] Jeka J, Kiemel T, Creath R, Horak F, Peterka R. Controlling human upright posture: velocity information is more accurate than position or acceleration. J Neurophysiol 2004;92:2368–79. doi:10.1152/jn.00983.2003.

[31] Mits S De, Segers V, Woodburn J, Elewaut D, Clercq D De, Roosen P. A Clinically Applicable Six-Segmented Foot Model 2012:655–61. doi:10.1002/jor.21570.

[32] Bruening DA. A Kinetic Multi-Segment Foot Model With Preliminary Applications by University of Delaware. 2009.

[33] Michelle C. A Technique for Assessing Foot Kinematics and Plantar Surface Characteristics During Stance for Varying Arch Structures Drexel University Dissertation Thesis 2010.

[34] Wright WG, Ivanenko YP, Gurfinkel VS. Foot anatomy specialization for postural sensation and control. J Neurophysiol 2012;107:1513–21. doi:10.1152/jn.00256.2011.

[35] Wrbaskić N, Dowling JJ, Wrbaškić N, Dowling JJ. An investigation into the deformable characteristics of the human foot using fluoroscopic imaging. Clin Biomech (Bristol, Avon) 2007; 22:230–8. doi:10.1016/j.clinbiomech.2006.09.006.

[36] Cheung JT-MM, Zhang M, Leung AKL, Fan Y-BB. Three-dimensional finite element analysis of the foot during standing--a material sensitivity study. J Biomech 2005;38:1045–54. doi:10.1016/j.jbiomech.2004.05.035.

[37] Tao K, Wang D, Wang C, Wang X, Liu A, Nester CJ, et al. An In Vivo Experimental Validation of a Computational Model of Human Foot. J Bionic Eng 2009;6:387–97. doi:10.1016/S1672-6529(08)60138-9.

[38] Winter DA, Patla AE, Prince F, Ishac M, Gielo-Perczak K. Stiffness control of balance in quiet standing. J Neurophysiol 1998;80:1211–21. doi:10.1016/S0966-6362(97)83378-4.

[39] Creath R, Kiemel T, Horak F, Peterka R, Jeka J. A unified view of quiet and perturbed stance: simultaneous co-existing excitable modes. Neurosci Lett 2005;377:75–80. doi:10.1016/j.neulet.2004.11.071.

[40] Creath R, Kiemel T, Horak F, Jeka JJ. The role of vestibular and somatosensory systems in intersegmental control of upright stance. J Vestib Res 2008;18:39–49.

[41] Shadmehr R, Arbib M a. A mathematical analysis of the force-stiffness characteristics of muscles in control of a single joint system *. Biol Cybern 1992;477:463–77. doi:10.1007/BF00204111.

[42] Oie KS, Kiemel T, Jeka JJ. Human multisensory fusion of vision and touch: detecting non-linearity with small changes in the sensory environment. Neurosci Lett 2001;315:113–6.

[43] Collins JJ, De Luca CJ. Open-loop and closed-loop control of posture: a random-walk analysis of center-of-pressure trajectories. Exp Brain Res 1993;95:308–18.

[44] Bottaro A, Yasutake Y, Nomura T, Casadio M, Morasso P. Bounded stability of the quiet standing posture: an intermittent control model. Hum Mov Sci 2008;27:473–95. doi:10.1016/j.humov.2007.11.005.

[45] Stella F. Donker MR, Donker SF, Roerdink M, Greven AJ, Beek PJ. Regularity of center-of-pressure trajectories depends on the amount of attention invested in postural control. Exp Brain Res 2007;181:1–11. doi:10.1007/s00221-007-0905-4.

[46] Duarte M, Harvey W, ZatsiorskyVM. Stabilographic analysis of unconstrained standing. Ergonomics 2000;43:1824–39. doi:10.1080/00140130050174491.

[47] Gurses S, Celik H. Correlation dimension estimates of human postural sway. Hum Mov Sci 2013;32:48–64. doi:10.1016/j.humov.2012.07.007.

[48] Gürses S. Postural dynamics and stability. Middle East Technical University, Ph.D. Thesis 2002.

[49] V. S. Gurfinkel, Yu P. Ivanenko, Yu S. Levik IAB. Kinesthetic Reference For Human Posture. Neuroscience 1995;68:229–43.

[50] Donatelli R a. Normal biomechanics of the foot and ankle. J Orthop Sports Phys Ther 1985;7:91–5.

[51] Hicks JH. The mechanics of the foot: II. The plantar aponeurosis and the arch." Journal of anatomy 88, no. Pt 1 (1954): 25..

[52] Teyhen DS, Stoltenberg BE, Collinsworth KM, Giesel CL, Williams DG, Kardouni CH, et al. Dynamic plantar pressure parameters associated with static arch height index during gait. Clin Biomech 2009;24:391–6. doi:10.1016/j.clinbiomech.2009.01.006.

[53] Bates KT, Collins D, Savage R, McClymont J, Webster E, Pataky TC, et al. The evolution of compliance in the human lateral mid-foot. Proc Biol Sci 2013;280:20131818. doi:10.1098/rspb.2013.1818.

[54] Kelly L a, Cresswell AG, Racinais S, Whiteley R, Lichtwark G. Intrinsic foot muscles have the capacity to control deformation of the longitudinal arch. J R Soc Interface 2014;11:20131188. doi:10.1098/rsif.2013.1188.

[55] Bendat, J. S. and Piersol AG. Random Data: Analysis and Measurement Procedures. Fourth Edi. John Wiley & Sons, Inc., Hoboken, NJ, USA.; 2010. doi:10.1002/9781118032428.ch11.

[56] Prieto TE, Myklebust JB, Myklebust BM. Characterization and modeling of postural steadiness in the elderly: a review. IEEE Trans Rehabil Eng 1993;1:26–34. doi:10.1109/86.242405.

[57] Ellis TS. The Human Foot: Its Form and Structure, Functions and Clothing. . JA Churchill, 1889.

[58] Hicks JH. The foot as a support. Cells Tissues Organs 25.1 (1955): 34-45.

[59] Gefen A. Plantar soft tissue loading under the medial metatarsals in the standing diabetic foot. Med Eng Phys 2003;25:491–9. doi:10.1016/S1350-4533(03)00029-8.

[60] Gefen A. The in vivo elastic properties of the plantar fascia during the contact phase of walking. Foot Ankle Int / Am Orthop Foot Ankle Soc [and] Swiss Foot Ankle Soc 2003;24:238–44.

[61] Cheung JT-M, Zhang M, An K-N. Effects of plantar fascia stiffness on the biomechanical responses of the ankle-foot complex. Clin Biomech (Bristol, Avon) 2004;19:839–46. doi:10.1016/j.clinbiomech.2004.06.002.

[62] Salathe EP, Arangio G a., Salathe EP. The foot as a shock absorber. J Biomech 1990;23:655–9. doi:10.1016/0021-9290(90)90165-Y.

[63] Salathé EP, Arangio G a, Salathé EP. A biomechanical model of the foot. J Biomech 1986;19:989–1001. doi:10.1016/0021-9290(86)90116-8.

[64] Jt-m AC, Zhang MA. A 3-Dimensional Finite Element Model of the Human Foot and Ankle for Insole Design 2005;86. doi:10.1016/j.apmr.2004.03.031.

[65] Cheung JTM, Zhang MA, Jt-m AC, Zhang MA. A 3-dimensional finite element model of the human foot and ankle for insole design. Arch Phys Med Rehabil 2005;86:353–8. doi:10.1016/j.apmr.2004.03.031.

[66] Cheung JT-M, Zhang M, An K-N. Effect of Achilles tendon loading on plantar fascia tension in the standing foot. Clin Biomech (Bristol, Avon) 2006;21:194–203. doi:10.1016/j.clinbiomech.2005.09.016.

[67] Saraswat P, Andersen MS, MacWilliams B a. A musculoskeletal foot model for clinical gait analysis. J Biomech 2010;43:1645–52. doi:10.1016/j.jbiomech.2010.03.005.

[68] Chen Y-N, Chang C-WC-H, Li C-T, Chang C-WC-H, Lin C-F. Finite Element Analysis of Plantar Fascia During Walking: A Quasi-static Simulation. Foot Ankle Int 2014;36:90–7. doi:10.1177/1071100714549189.

[69] Winter DA. Human balance and posture standing and walking control during. Gait Posture 1995;3:193–214.

[70] King DL, Zatsiorsky VM. Extracting gravity line displacement from stabilographic recordings. Gait Posture 1997;6:27–38.

[71] Mergner T. A neurological view on reactive human stance control. Annu Rev Control 2010;34:177–98. doi:10.1016/j.arcontrol.2010.08.001.

[72] Winter D a D a. D a. BIOMECHANICS AND MOTOR CONTROL OF Fourth Edition. vol. 2nd. 2009. doi:10.1002/9780470549148.

[73] Isman R, Inman V. Anthropometric Studies of the Human Foot and Ankle. Foot Ankle 1969;11:97–129.

[74] Putti a. B, Arnold GP, Abboud RJ. Foot pressure differences in men and women. Foot Ankle Surg 2010;16:21–4. doi:10.1016/j.fas.2009.03.005.

[75] Peters M. Footedness: asymmetries in foot preference and skill and neuropsychological assessment of foot movement. Psychol Bull 1988;103:179–92. doi:10.1037/0033-2909.103.2.179.

[76] Sadeghi H, Allard P, Prince F, Labelle H. Symmetry and limb dominance in able-bodied gait: A review. Gait Posture 2000;12:34–45. doi:10.1016/S0966-6362(00)00070-9.

[77] Sadeghi H. Local or global asymmetry in gait of people without impairments. Gait Posture 2003;17:197–204. doi:10.1016/S0966-6362(02)00089-9.

[78] Bacelar AM, Teixeira LA. Footedness across ages: Distinction between mobilization and stabilization tasks. Laterality Asymmetries Body, Brain

Cogn 2015;20:141–53. doi:10.1080/1357650X.2014.924959.

[79] Kalaycioğlu C, Kara C, Atbasoğlu C, Nalçaci E. Aspects of foot preference: differential relationships of skilled and unskilled foot movements with motor asymmetry. Laterality 2008;13:124–42. doi:10.1080/13576500701701704.

[80] Hirasawa Y. An observation on standing ability of Japanese males and females. J.of Anthr Soc Nippon 1979;87:81–92.

[81] Periyasamy R, Mishra a., Anand S, Ammini a. C. Preliminary investigation of foot pressure distribution variation in men and women adults while standing. Foot 2011;21:142–8. doi:10.1016/j.foot.2011.03.001.

[82] Zifchock RA, Davis I, Hillstrom H, Song J. The effect of gender, age, and lateral dominance on arch height and arch stiffness. Foot Ankle Int / Am Orthop Foot Ankle Soc [and] Swiss Foot Ankle Soc 2006;27:367–72. doi:10.1177/107110070602700509.

[83] Kilby MC, Newell KM. Intra- and inter-foot coordination in quiet standing: Footwear and posture effects. Gait Posture 2012;35:511–6. doi:10.1016/j.gaitpost.2011.11.018.

[84] Wang Z, Molenaar PMC, Newell KM. The effects of foot position and orientation on inter- and intra-foot coordination in standing postures: A frequency domain PCA analysis. Exp Brain Res 2013;230:15–27. doi:10.1007/s00221-013-3627-9.

[85] Wang Z, Jordan K, Newell KM. Coordination patterns of foot dynamics in the control of upright standing. Motor Control 2012;16:425–43.

[86] Browner BD. Skeletal trauma: basic science, management, and reconstruction. vol. 1. Elsevier Health Sciences; 2009.

[87] Griffin NL, Miller C, Schmitt D, D'Août K. Understanding the evolution of the windlass mechanism of the human foot from comparative anatomy: insights, obstacles, & future directions. Am J Phys Anthr 2015;10:1–10. doi:10.1002/ajpa.22636.

[88] Clemente CD. Anatomy: A Regional Atlas of the Human Body. Williams & Wilkins, Baltimore, 2011.

APPENDIX A

TIME AND FREQUENCY DOMAIN PLOTS OF THE EXPERIMENTAL DATA

In this part time and frequency domain plots of individuals namely 7 males and 7 females are presented. Since analysis are performed in both time and frequency domain, there are many figures to be presented. These figures are divided into two for each person. In the first part force distribution of Left and Right Foot F, H, M in time domain in its natural form and detrended signals are plotted. Then, Fast Fourier Transform (FFT) of the force signals of Left/Right foot are taken and plotted as the third plot. Frequency axis of FFT plot is restricted at 3 Hz, because except for the 3 male subjects, no significant value over that value exists.

In the Frequency domain part of the analysis, Cross Power Spectral Density (CPSD) of the FH, FM and HM interactions are taken into account. Accordingly, CPSD magnitude or gain, Phase angles and Coherence plots of those interactions are plotted. Magnitude or Gain Plots frequency axis is restricted to 1 Hz, because over that value, signal values mostly goes to zero. Phase Angles and Coherence plot frequency axis are divided into three frequency ranges, 0-3 Hz as “Low”, 3-10 Hz as “Mid” and 10-25 Hz as “High” regions where their reason was mentioned in the context.

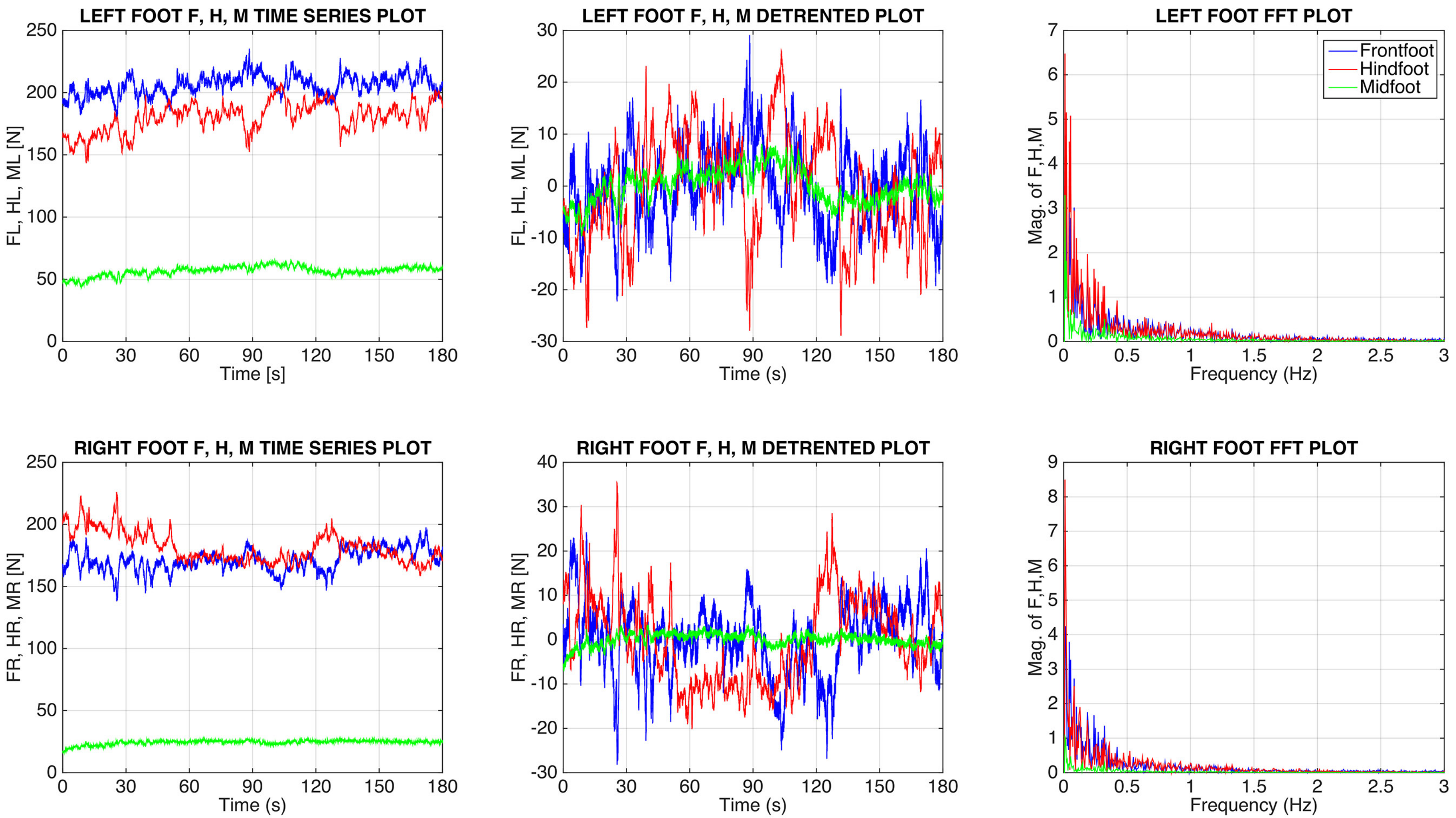

Figure A-1 Force Distribution on Time and Frequency Domain of a male subject-1

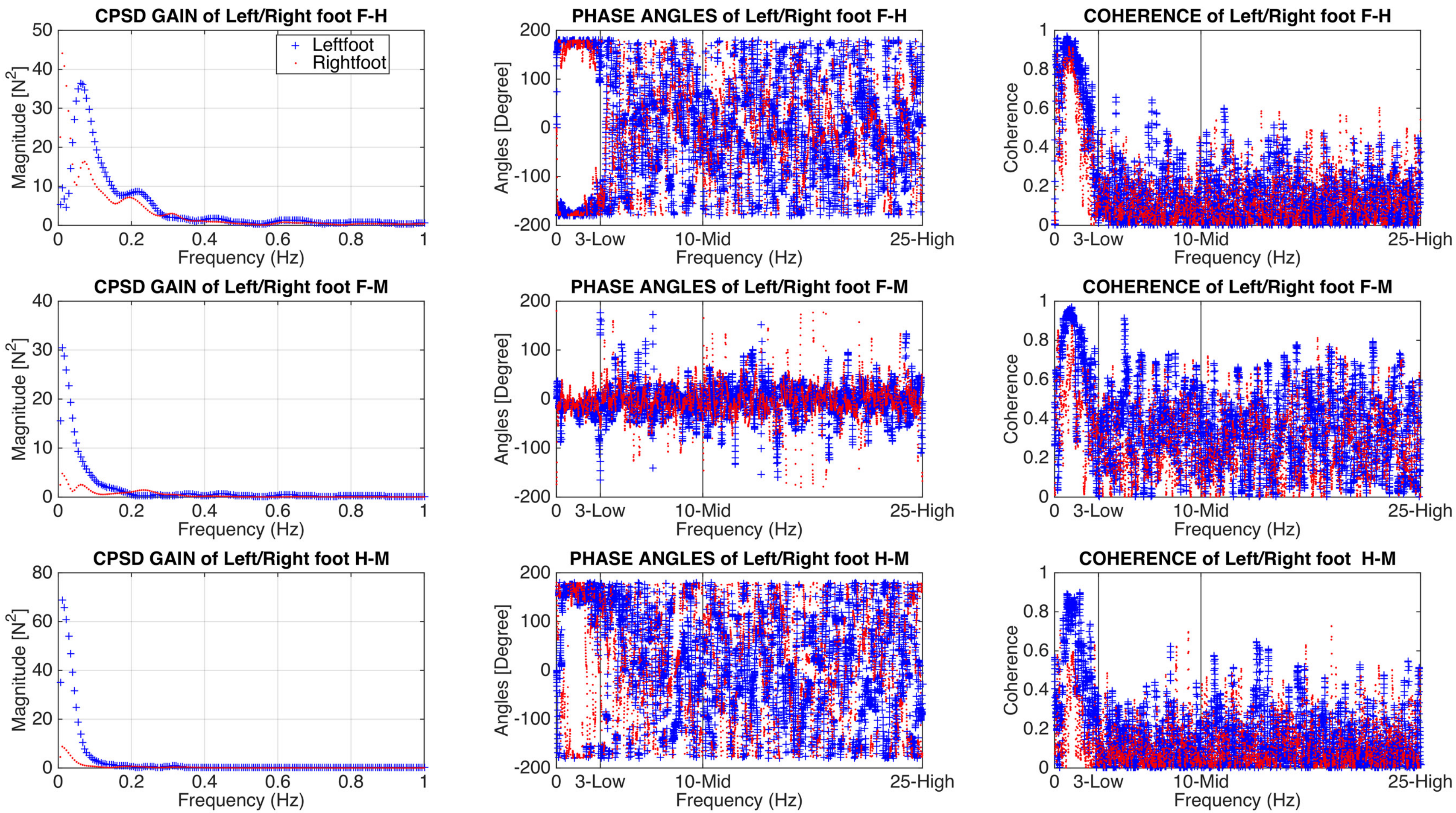

Figure A-2 Frequency Domain CPSD Magnitude, Phase Angle and Coherence plots of male subject-1

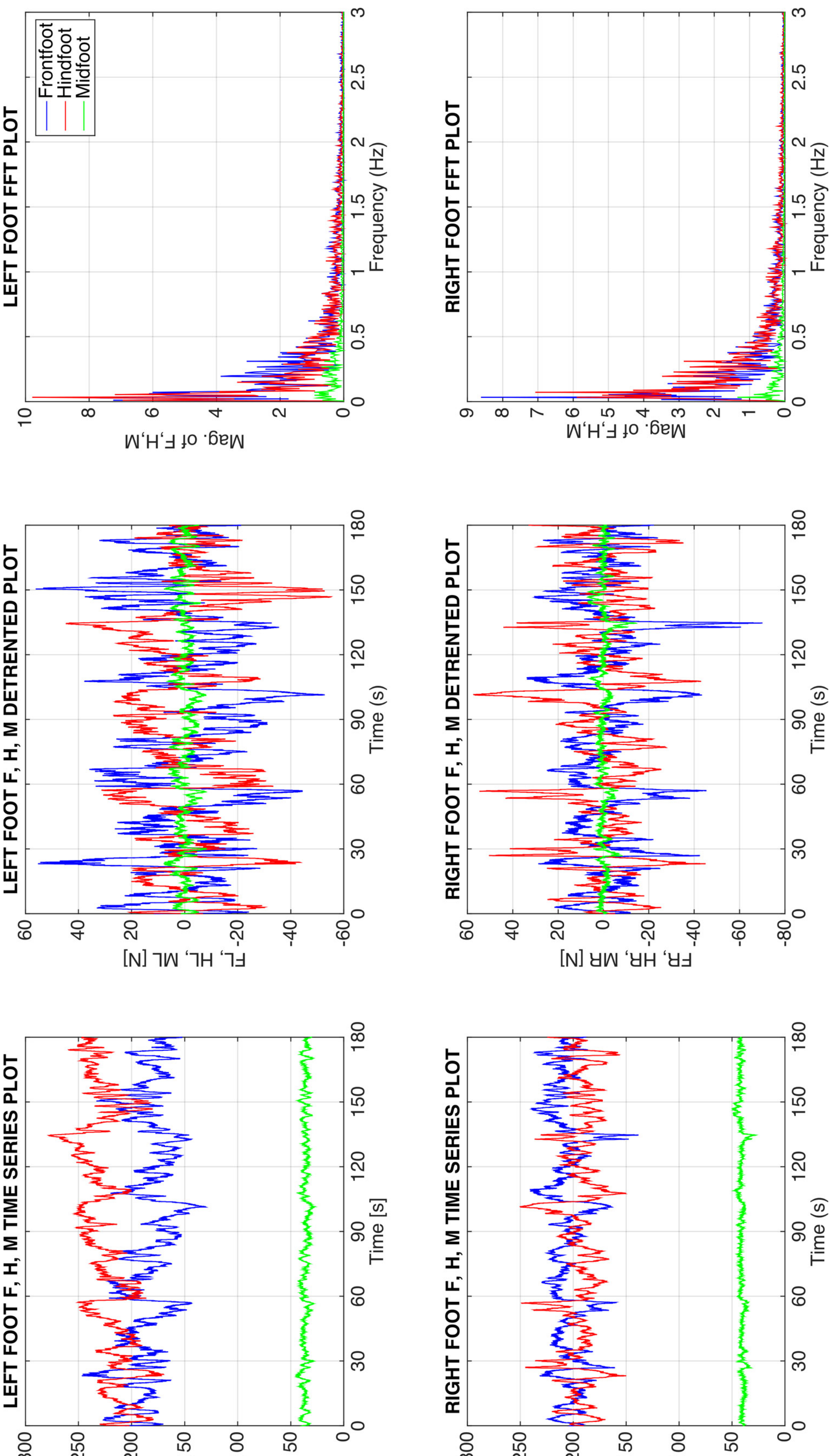

Figure A-3 Force Distribution on Time and Frequency Domain of a male subject-2

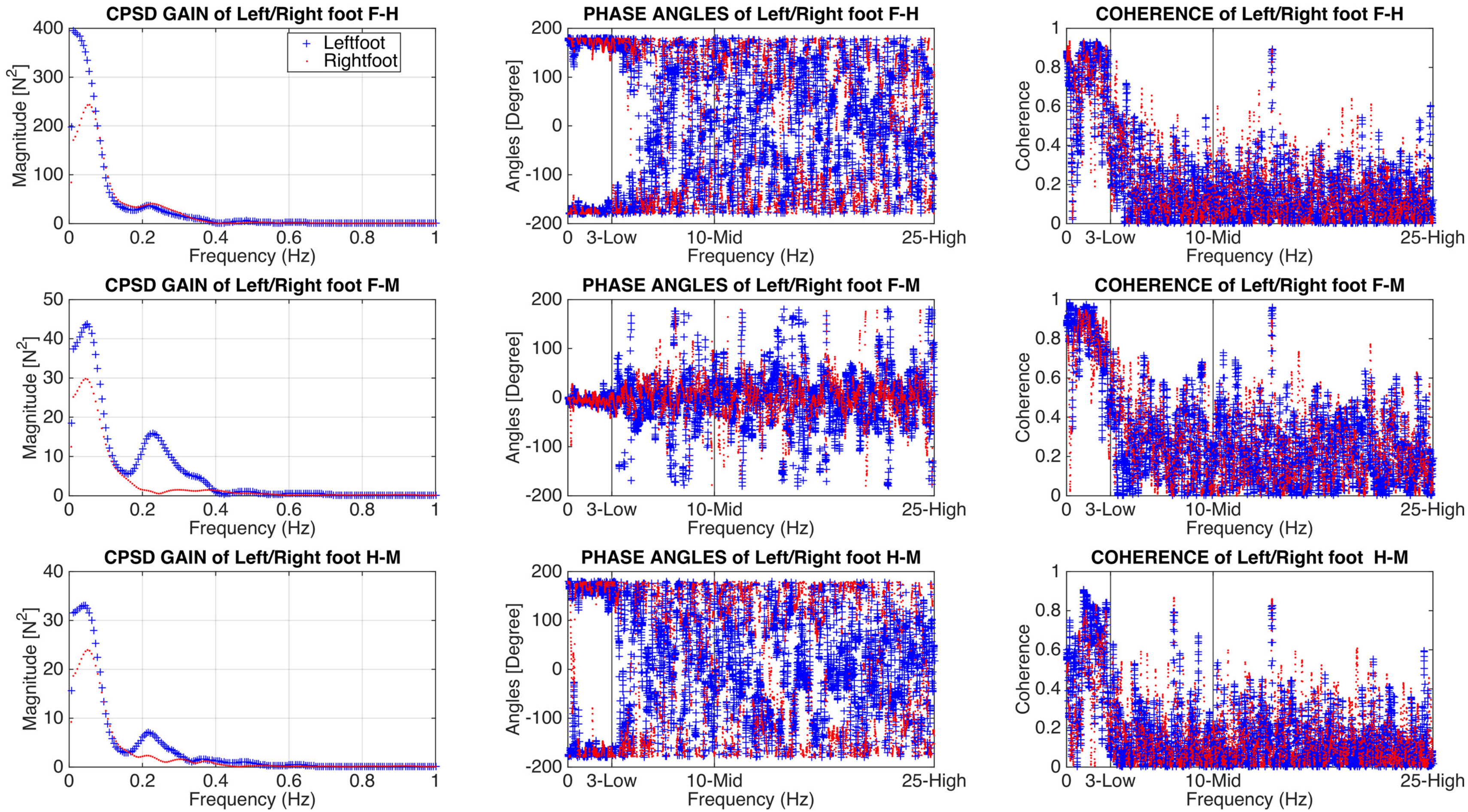

Figure A-4 Frequency Domain CPSD Magnitude, Phase Angle and Coherence plots of male subject-2

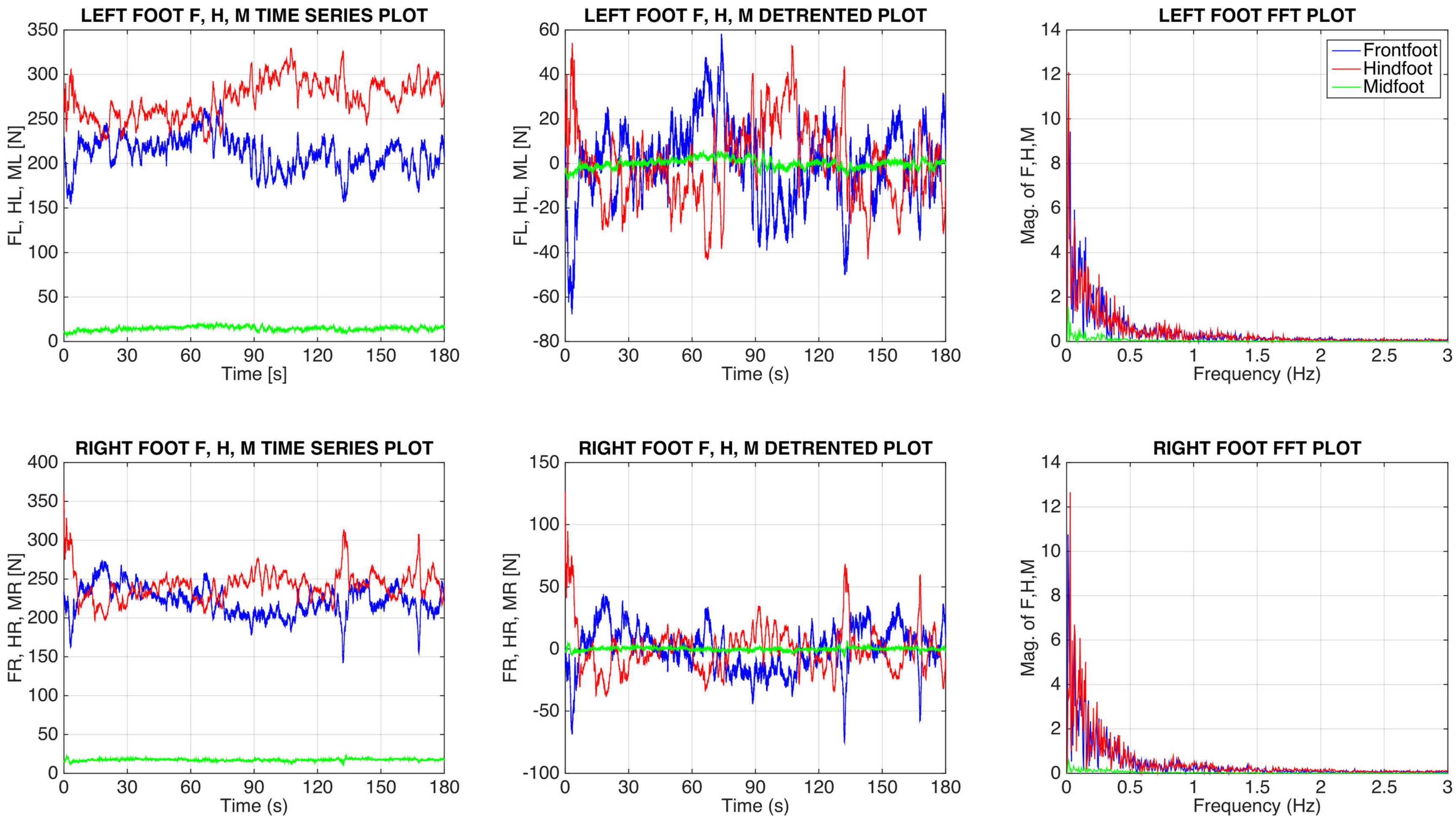

Figure A-5 Force Distribution on Time and Frequency Domain of a male subject-3

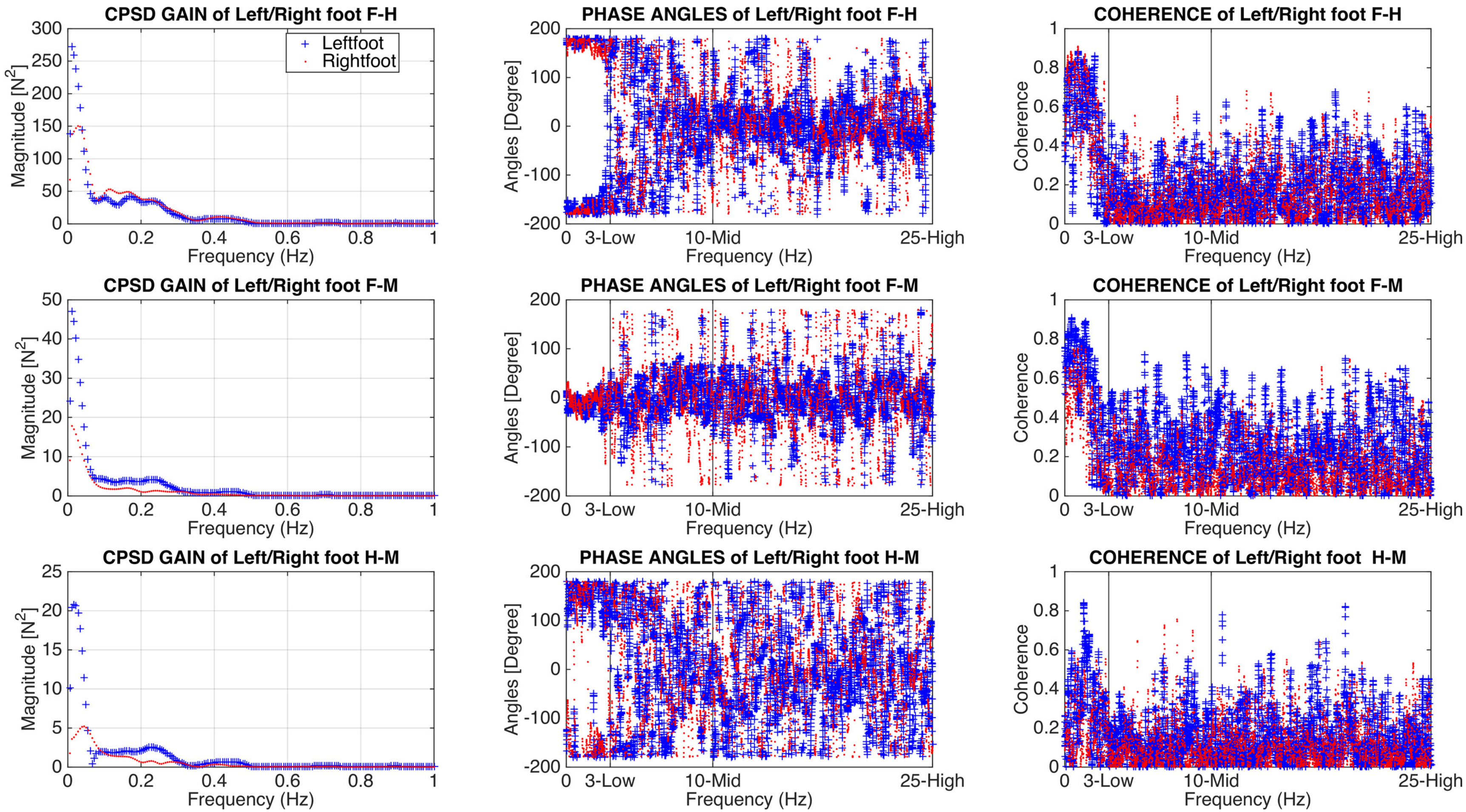

Figure A-6 Frequency Domain CPSD Magnitude, Phase Angle and Coherence plots of male subject-3

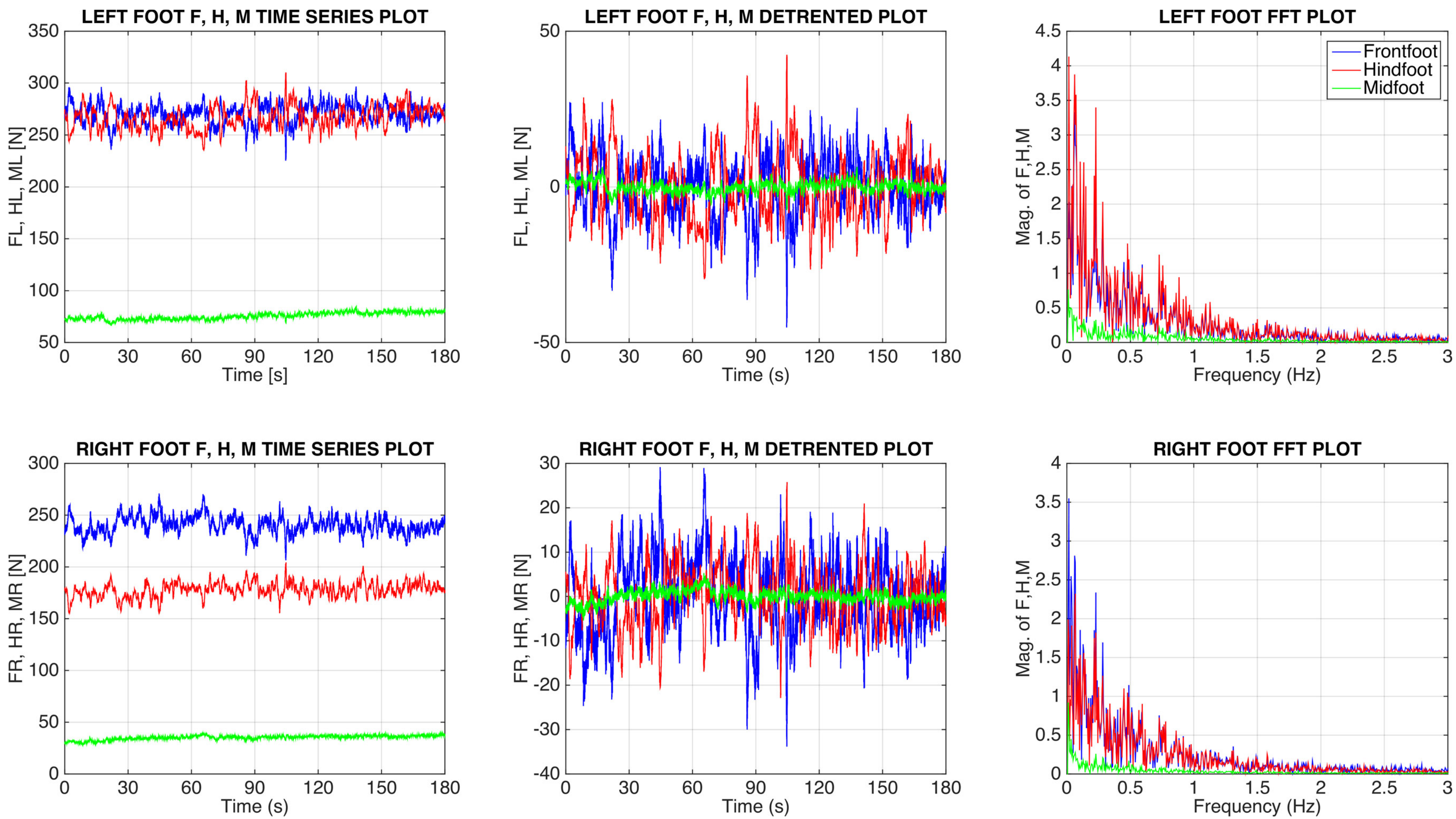

Figure A-7 Force Distribution on Time and Frequency Domain of a male subject-4

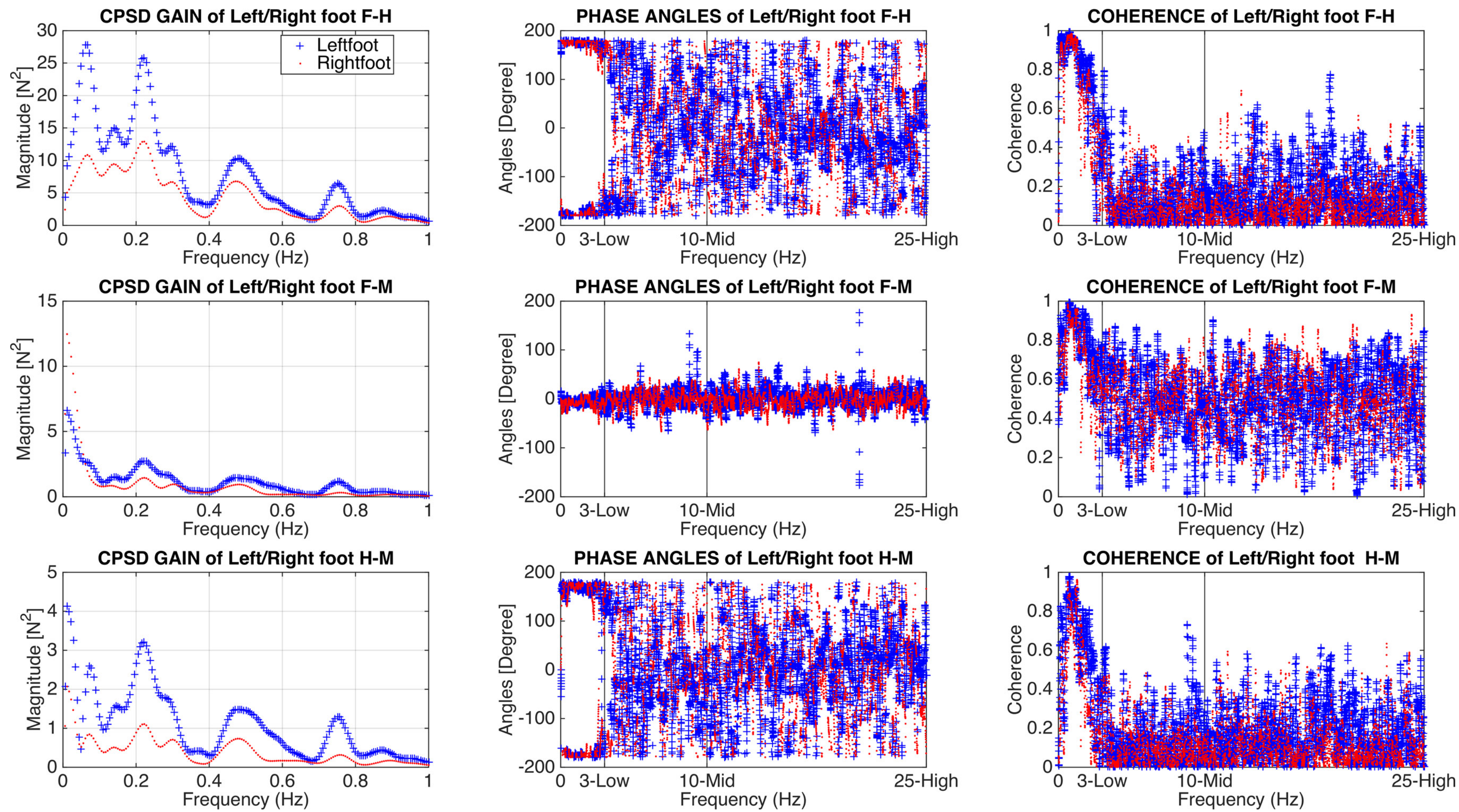

Figure A-8 Frequency Domain CPSD Magnitude, Phase Angle and Coherence plots of male subject-4

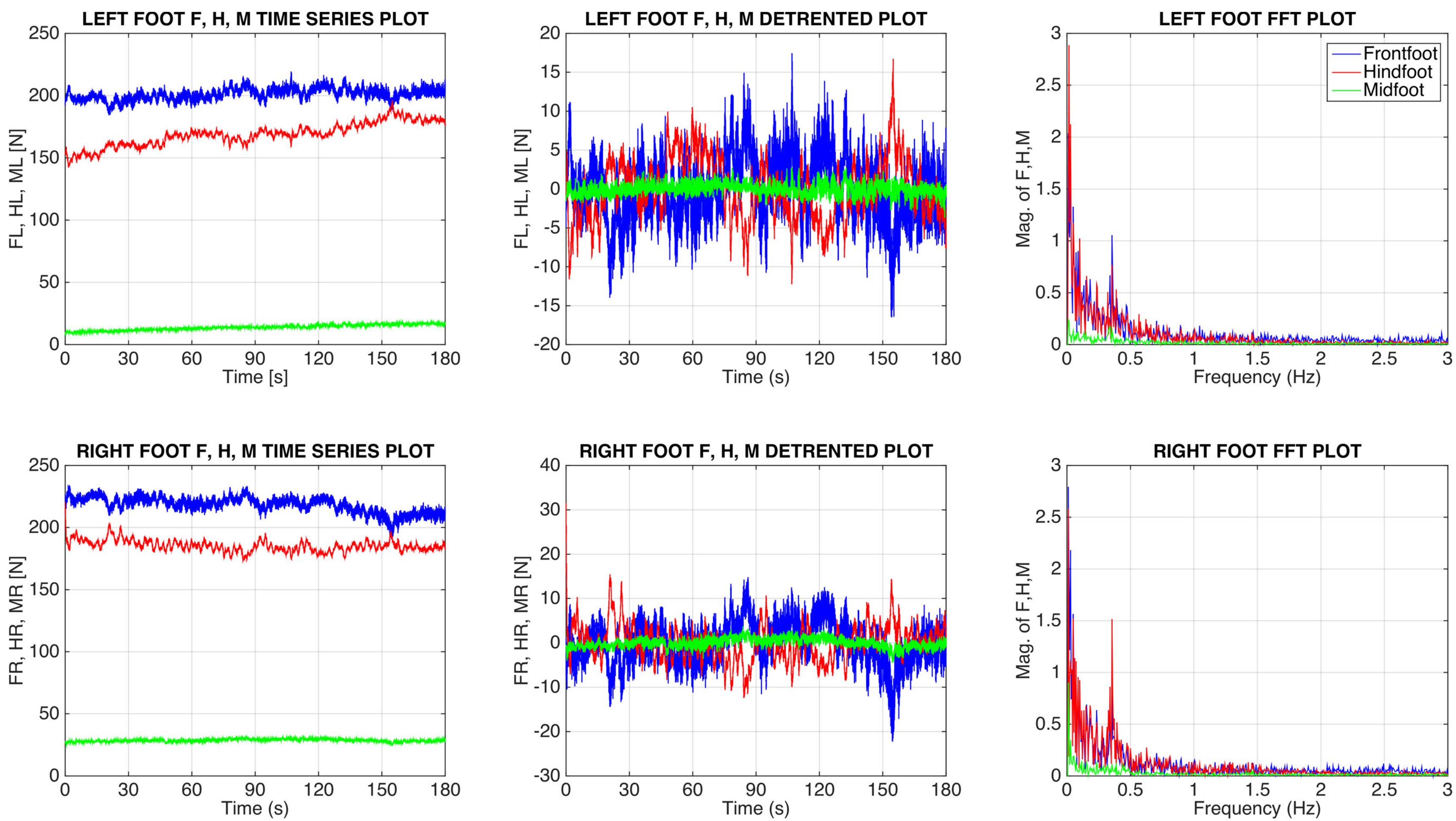

Figure A-9 Force Distribution on Time and Frequency Domain of a male subject-5

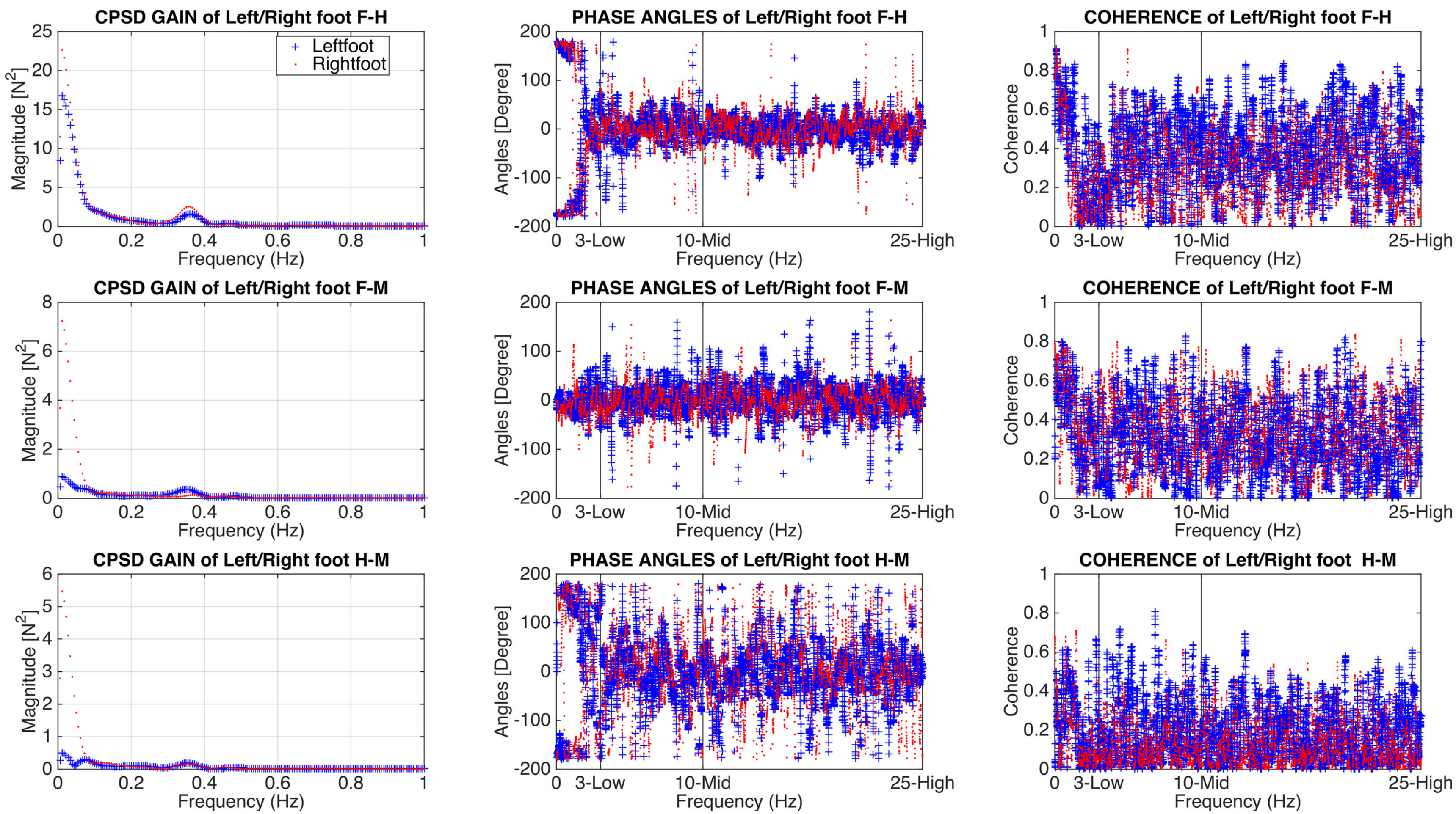

Figure A-10 Frequency Domain CPSD Magnitude, Phase Angle and Coherence plots of male subject-5

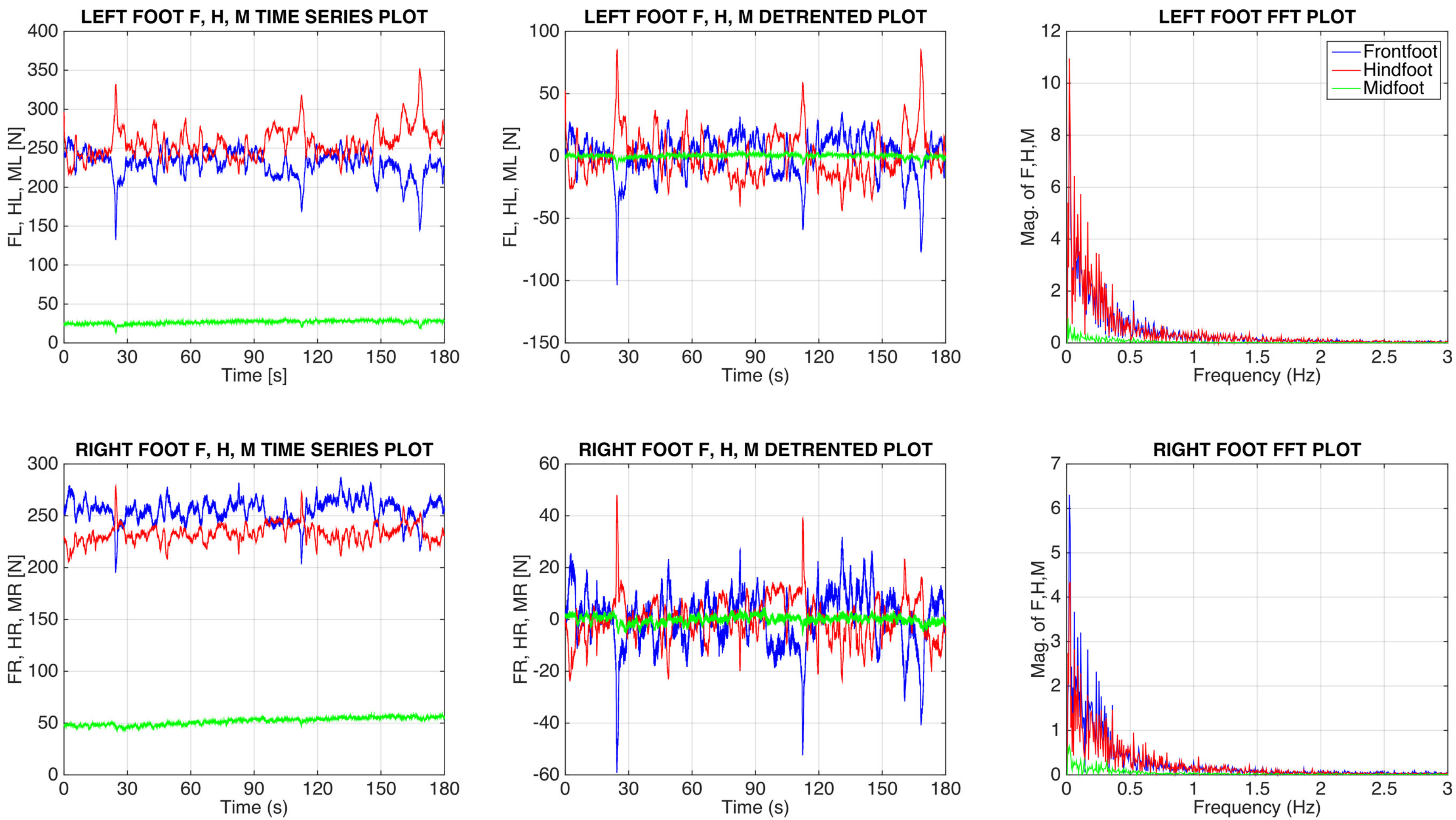

Figure A-11 Force Distribution on Time and Frequency Domain of a male subject-6

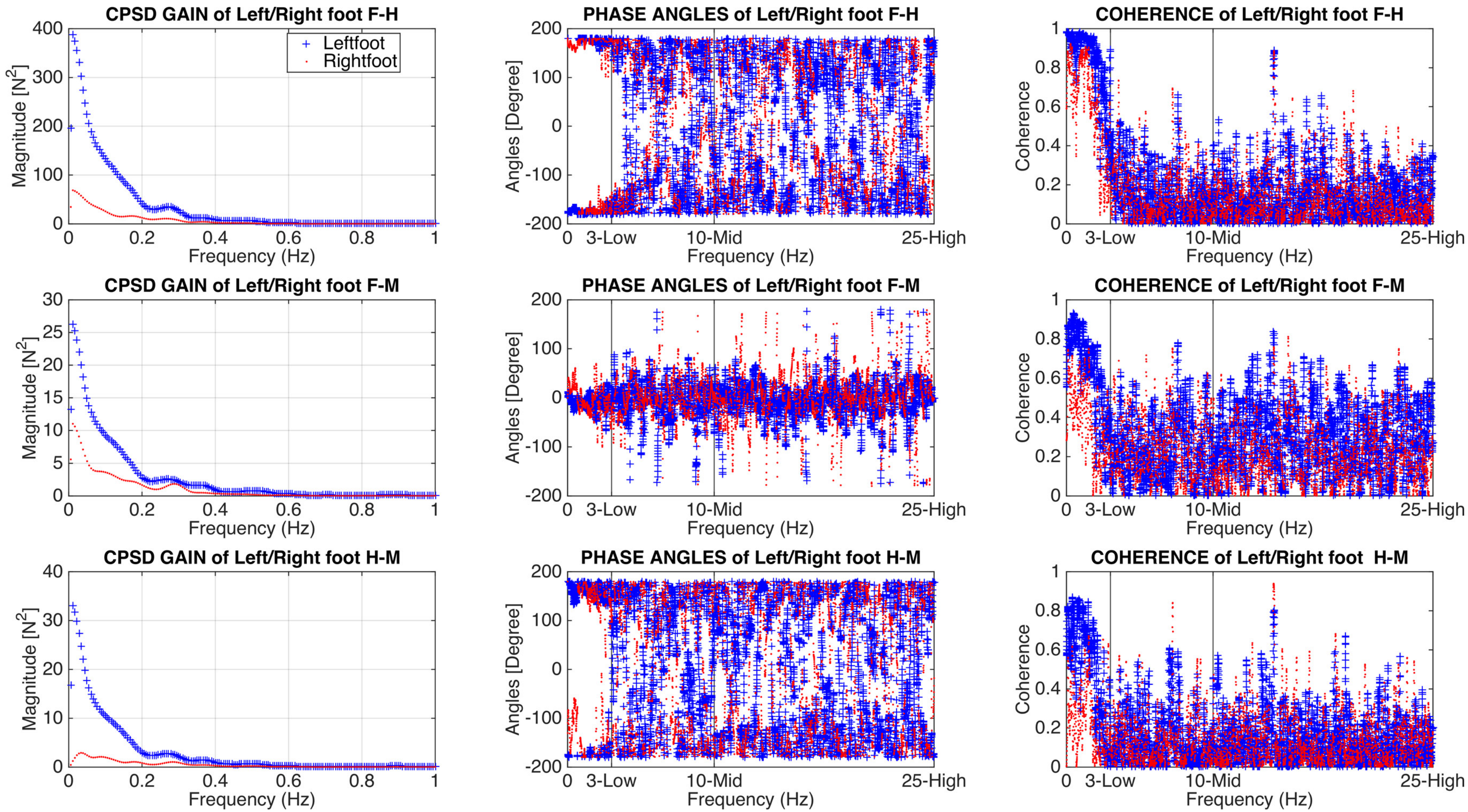

Figure A-12 Frequency Domain CPSD Magnitude, Phase Angle and Coherence plots of male subject-6

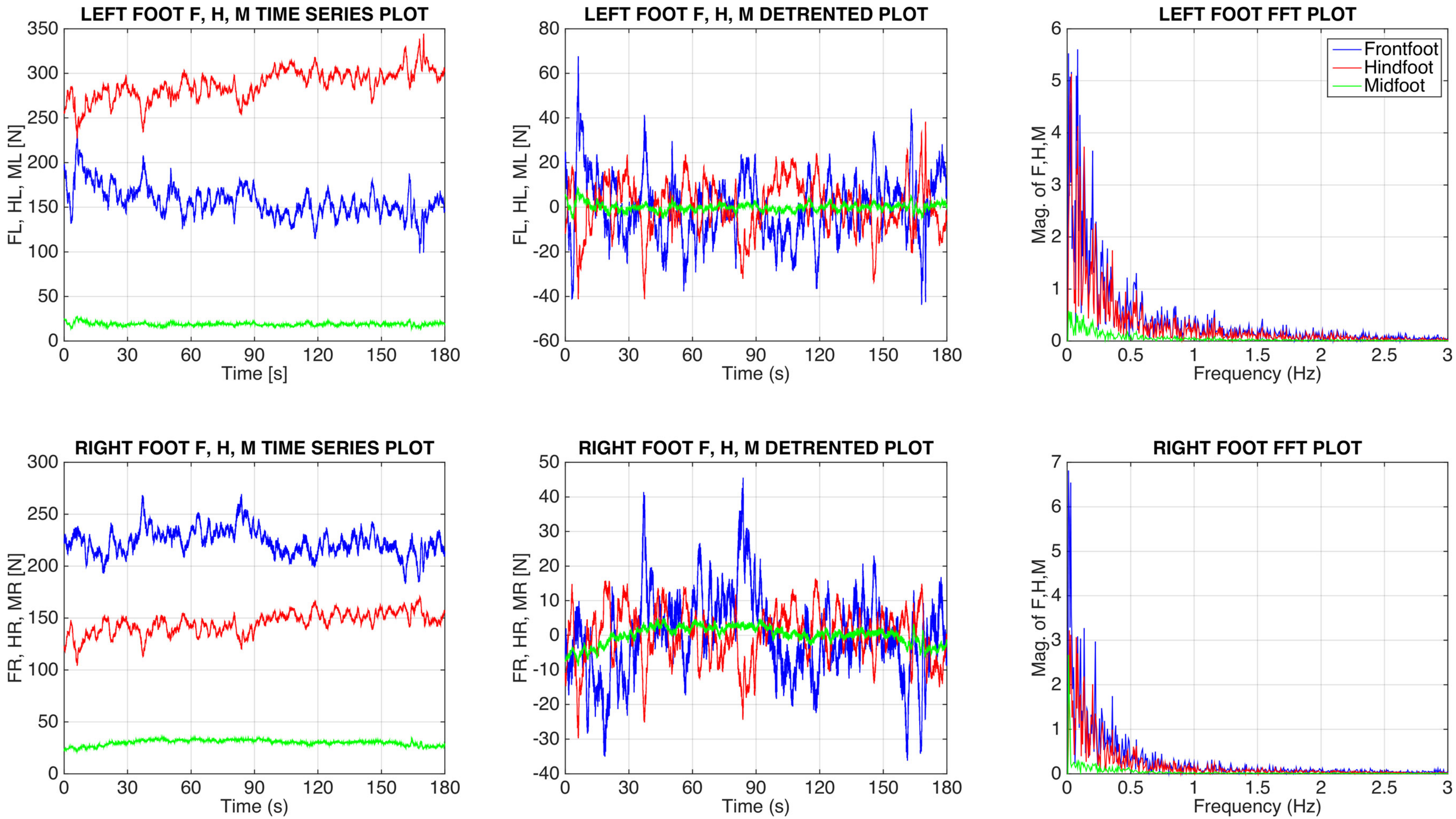

Figure A-13 Force Distribution on Time and Frequency Domain of a male subject-7

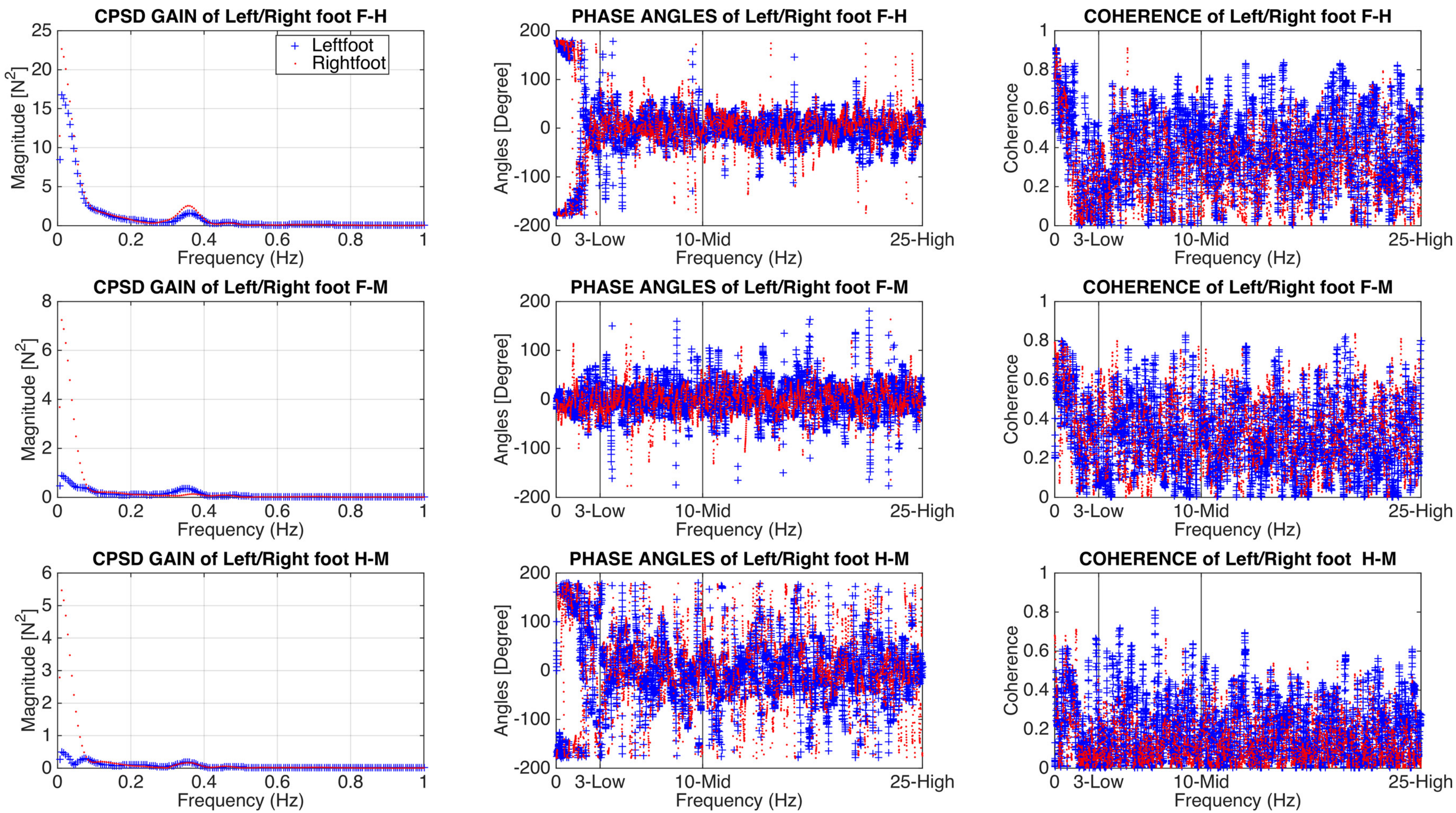

Figure A-14 Frequency Domain CPSD Magnitude, Phase Angle and Coherence plots of male subject-7

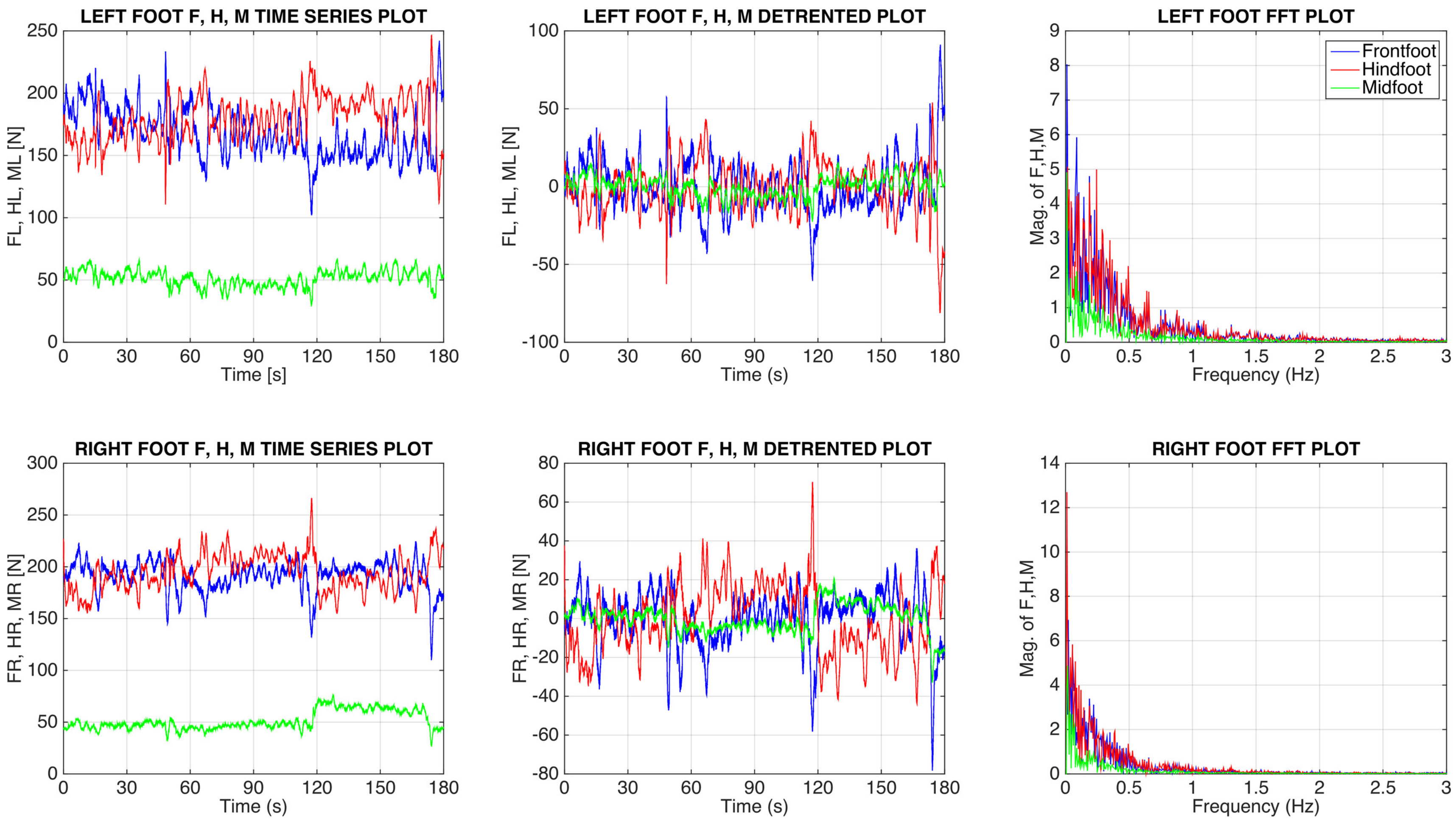

Figure A-15 Force Distribution on Time and Frequency Domain of a female subject-1

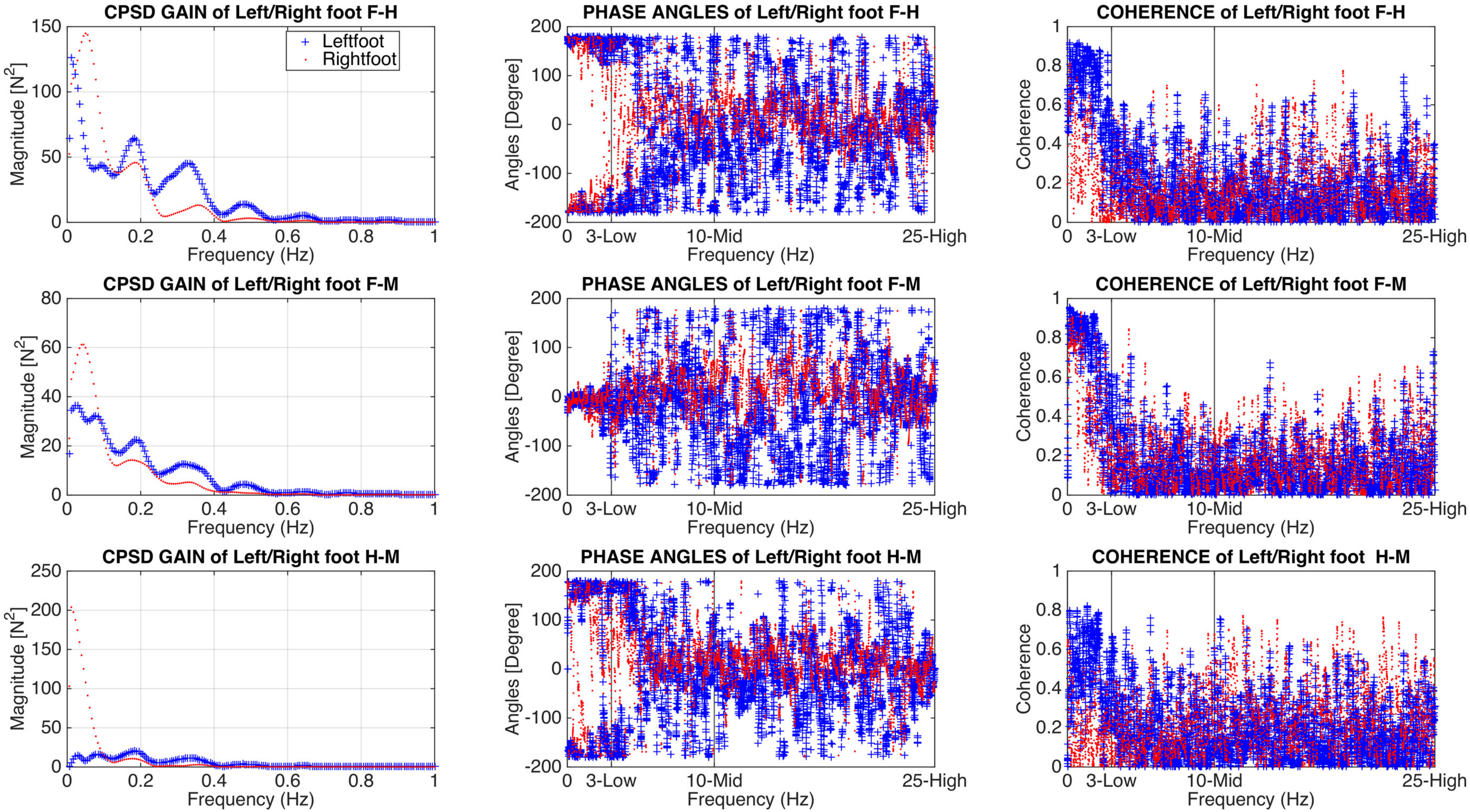

Figure A-16 Frequency Domain CPSD Magnitude, Phase Angle and Coherence plots of female subject-1

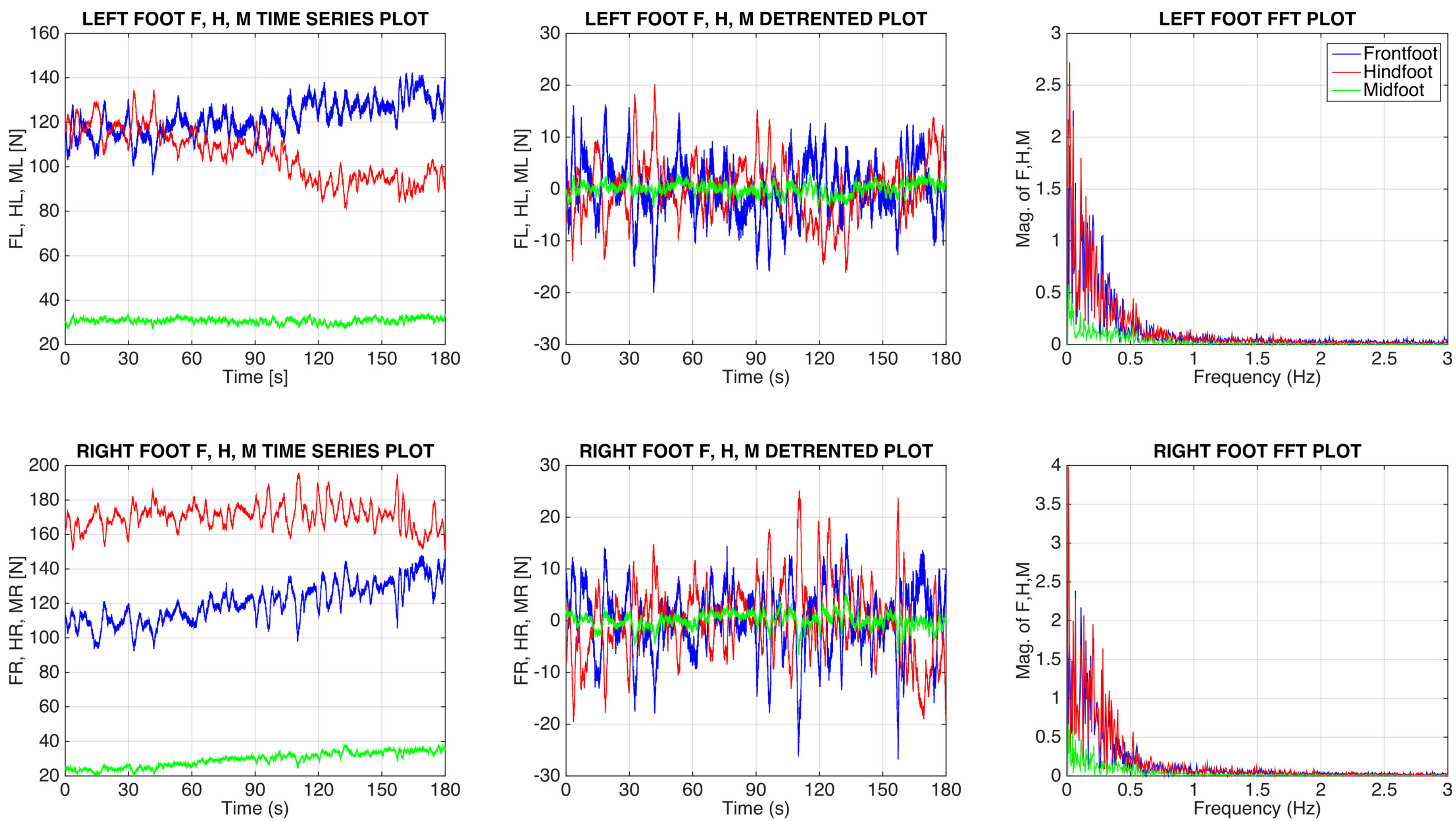

Figure A-17 Force Distribution on Time and Frequency Domain of a female subject-2

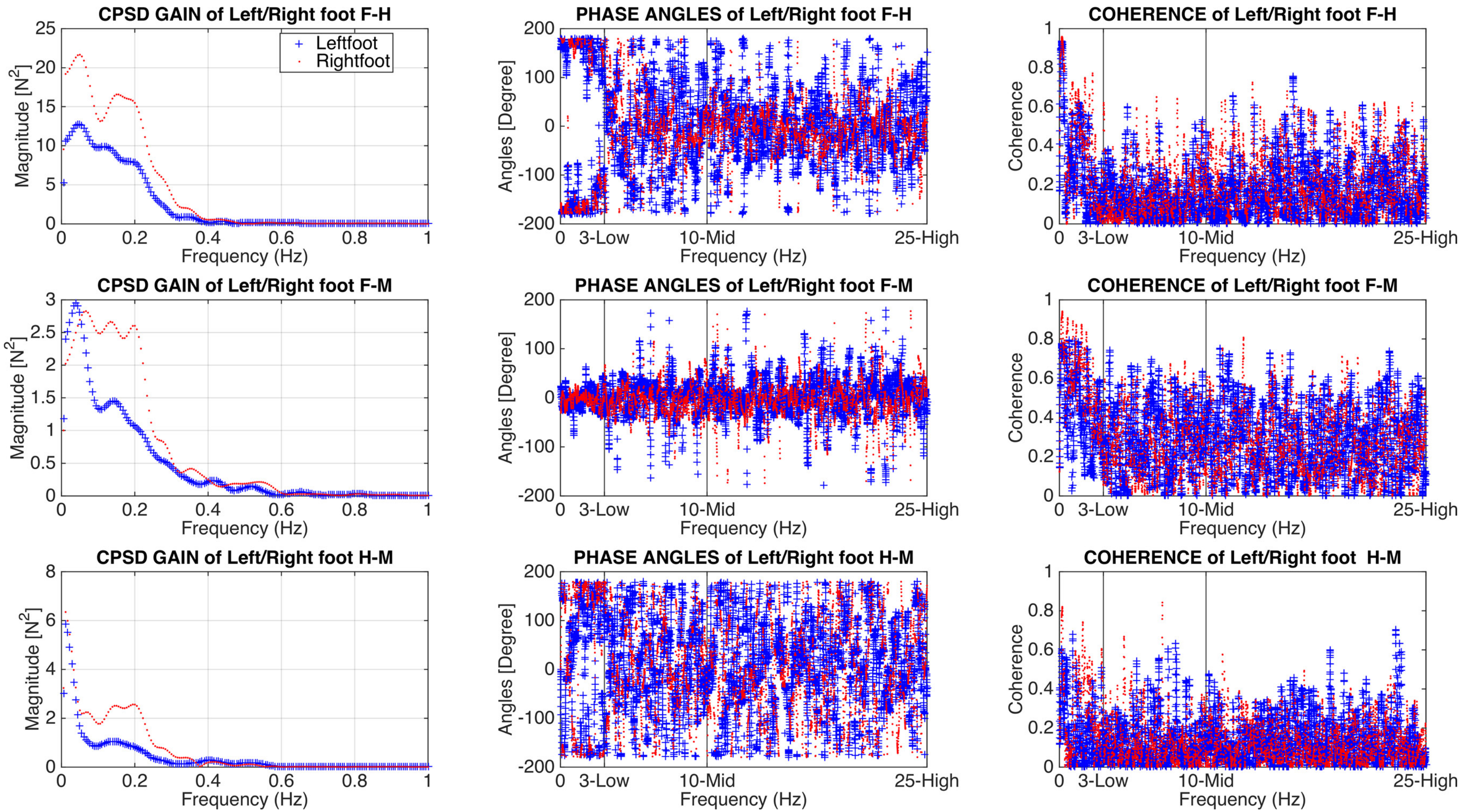

Figure A-18 Frequency Domain CPSD Magnitude, Phase Angle and Coherence plots of female subject-2

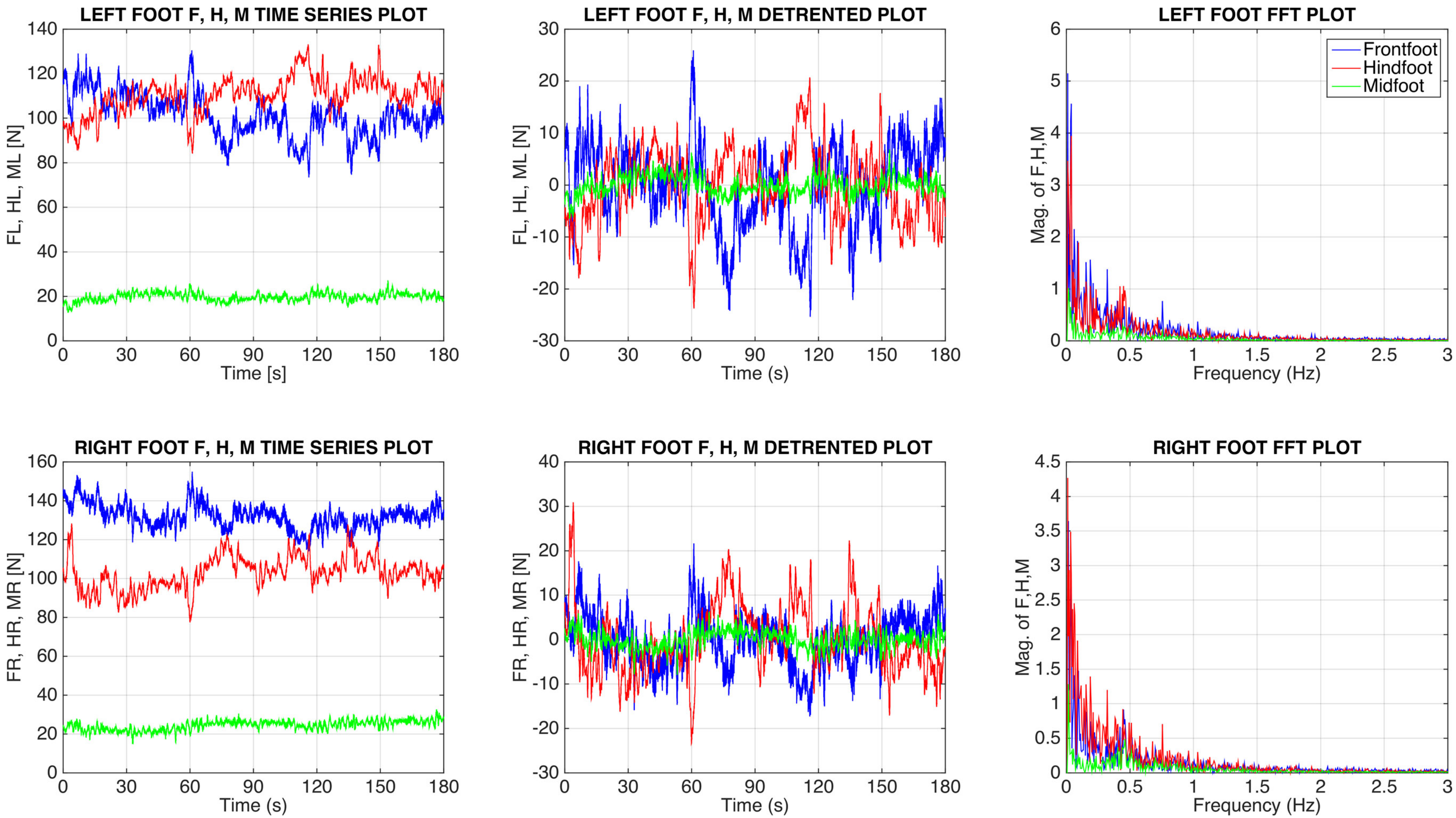

Figure A-19 Force Distribution on Time and Frequency Domain of a female subject-3

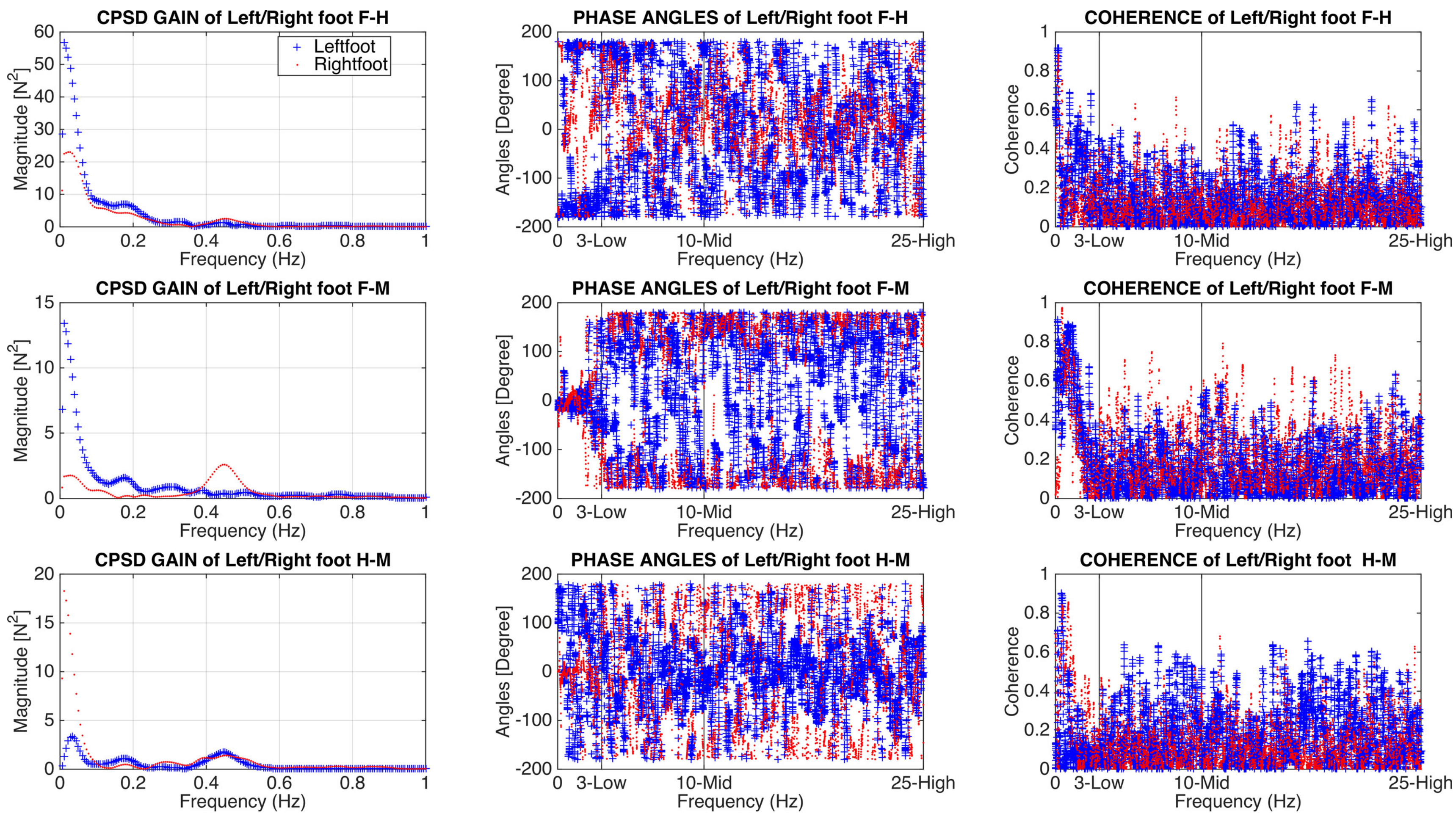

Figure A-20 Frequency Domain CPSD Magnitude, Phase Angle and Coherence plots of female subject-3

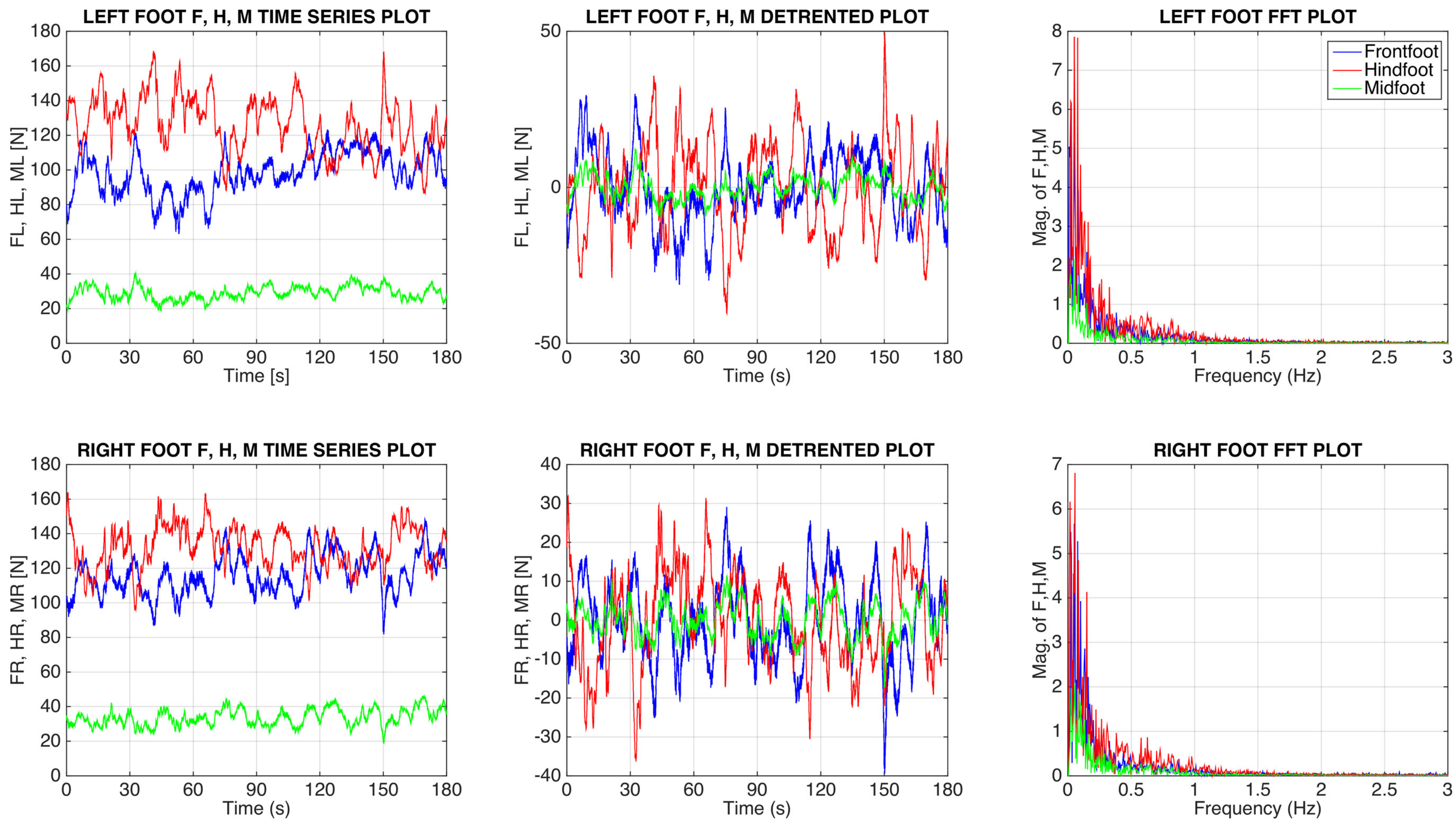

Figure A-21 Force Distribution on Time and Frequency Domain of a female subject-4

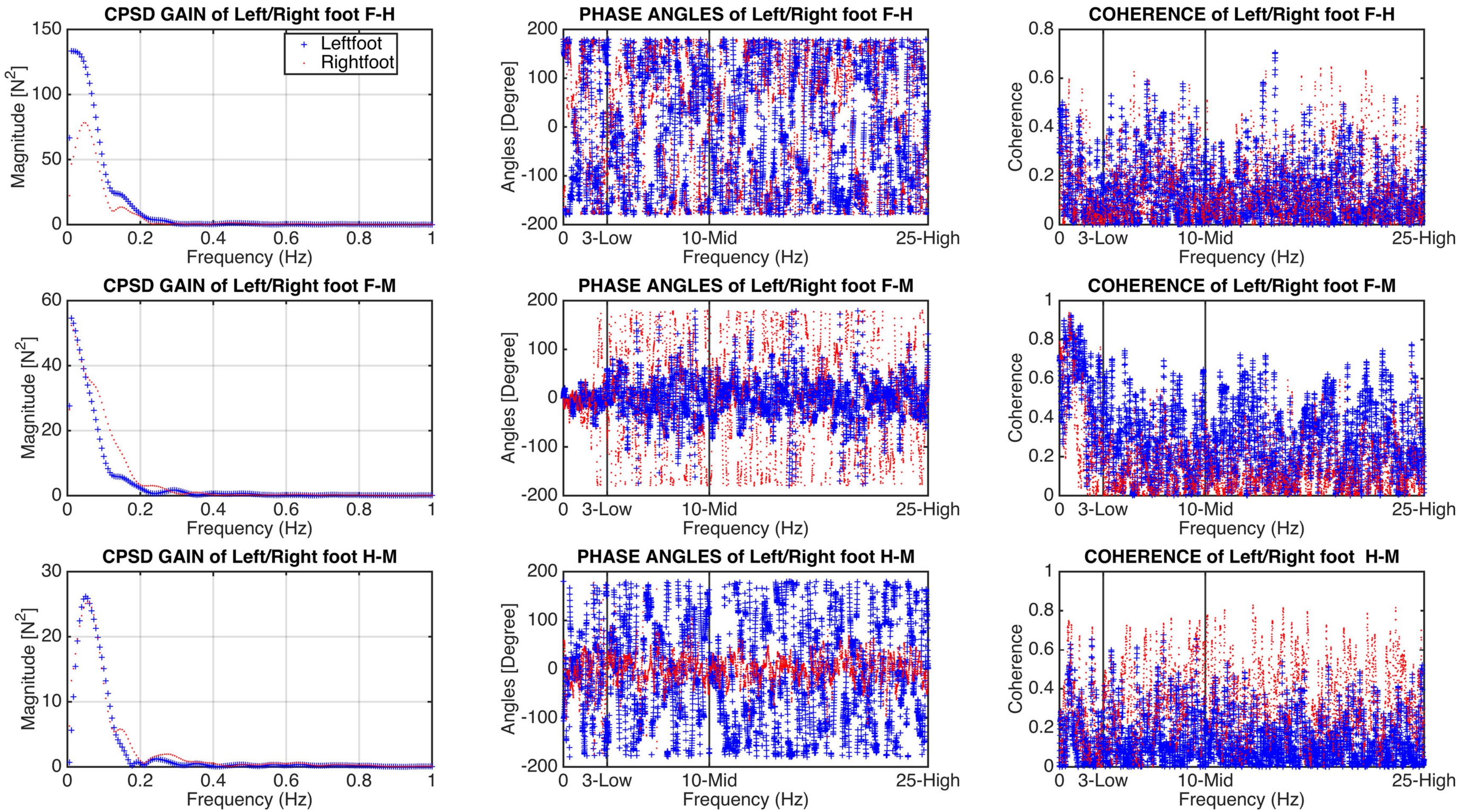

Figure A-22 Frequency Domain CPSD Magnitude, Phase Angle and Coherence plots of female subject-4

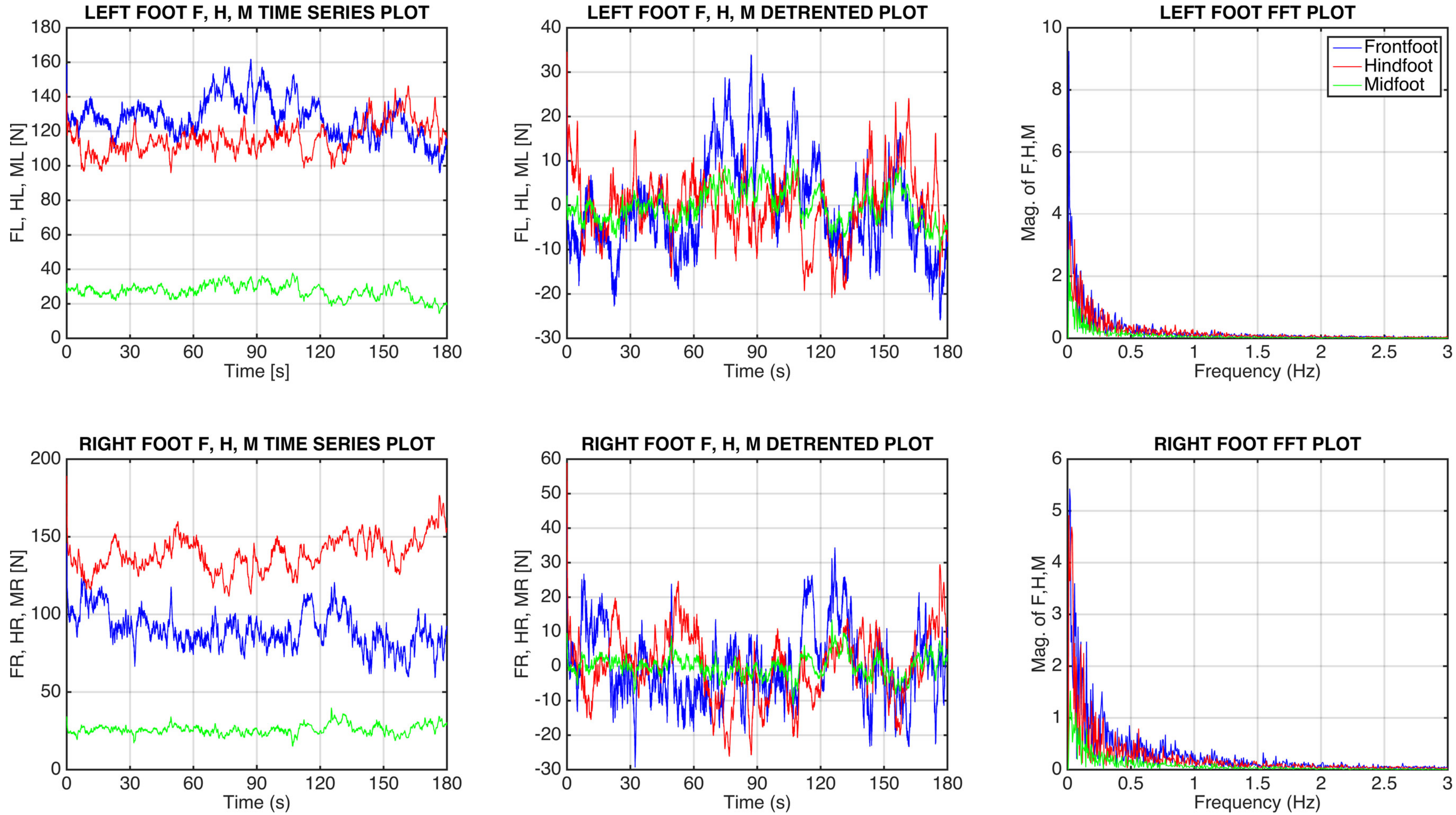

Figure A-23 Force Distribution on Time and Frequency Domain of a female subject-5

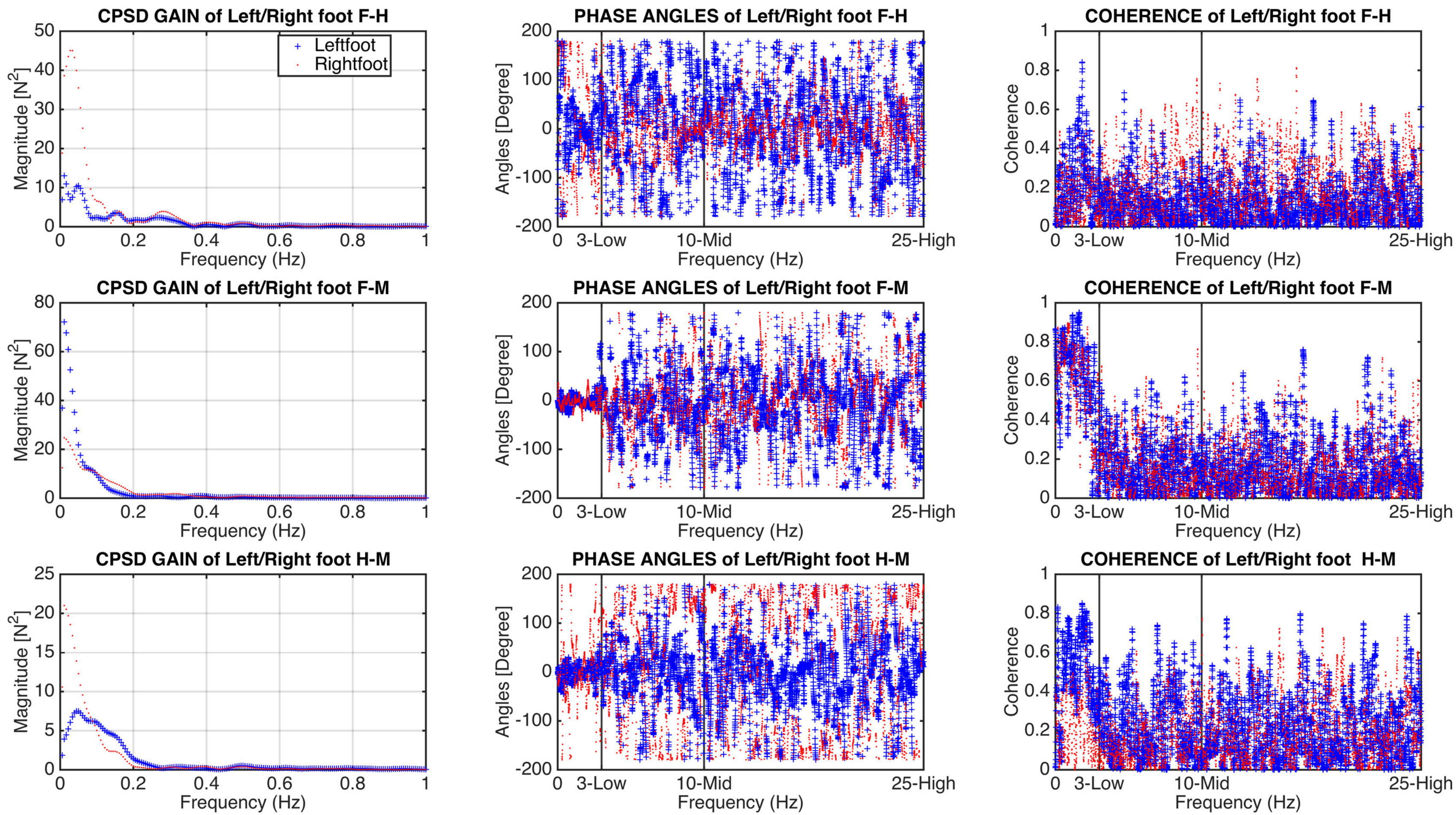

Figure A-24 Frequency Domain CPSD Magnitude, Phase Angle and Coherence plots of female subject-5

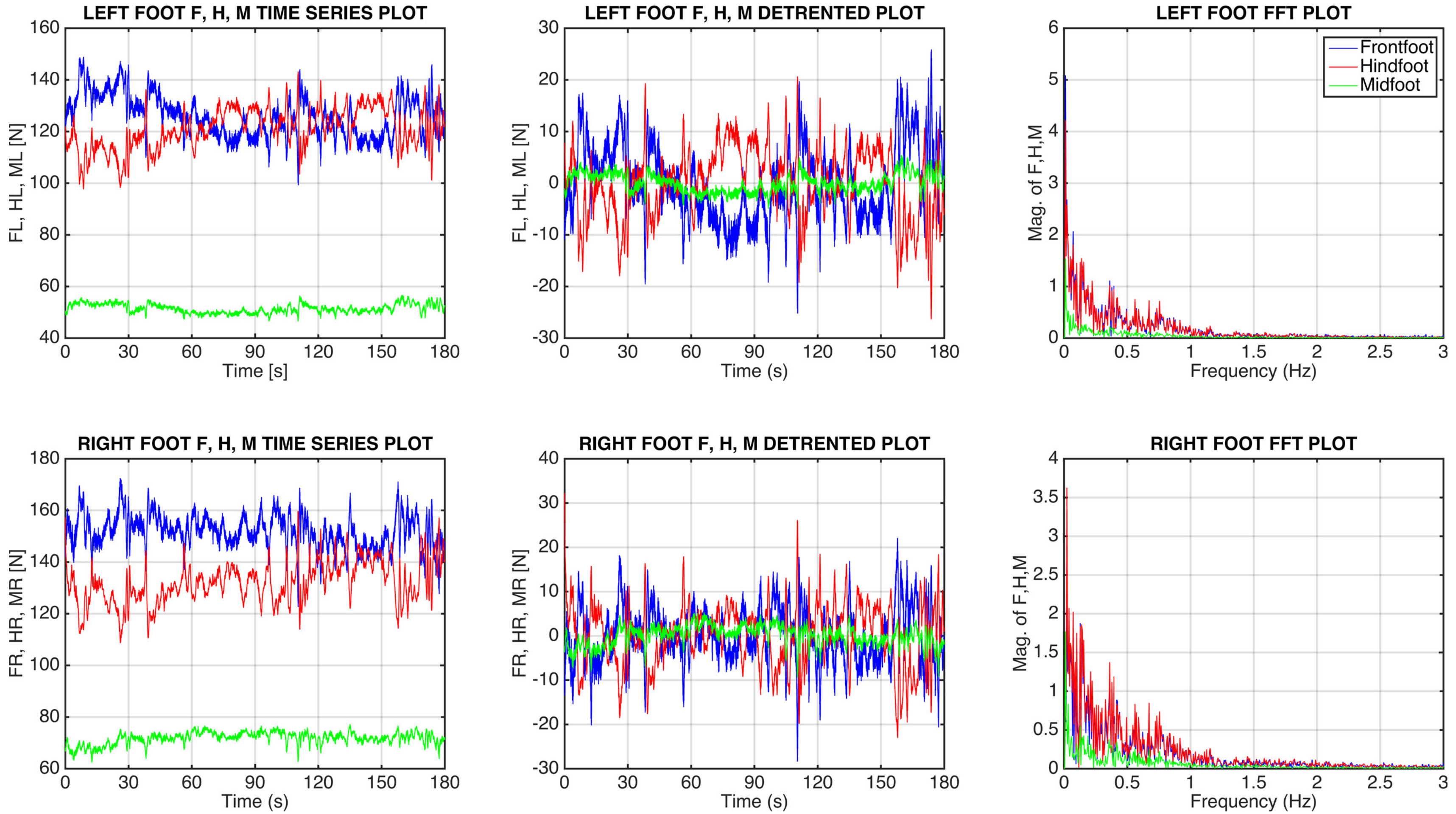

Figure A-25 Force Distribution on Time and Frequency Domain of a female subject-6

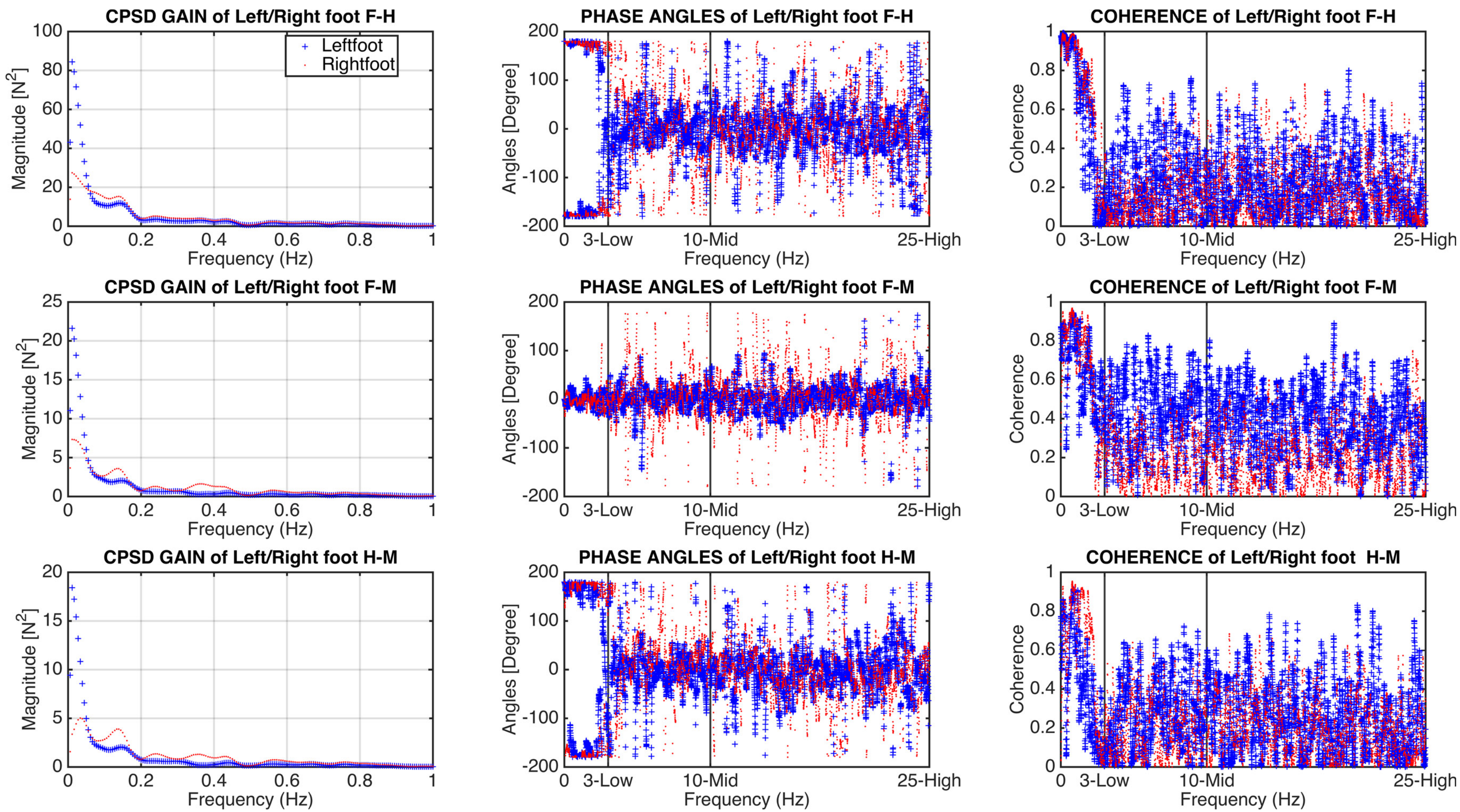

Figure A-26 Frequency Domain CPSD Magnitude, Phase Angle and Coherence plots of female subject-6

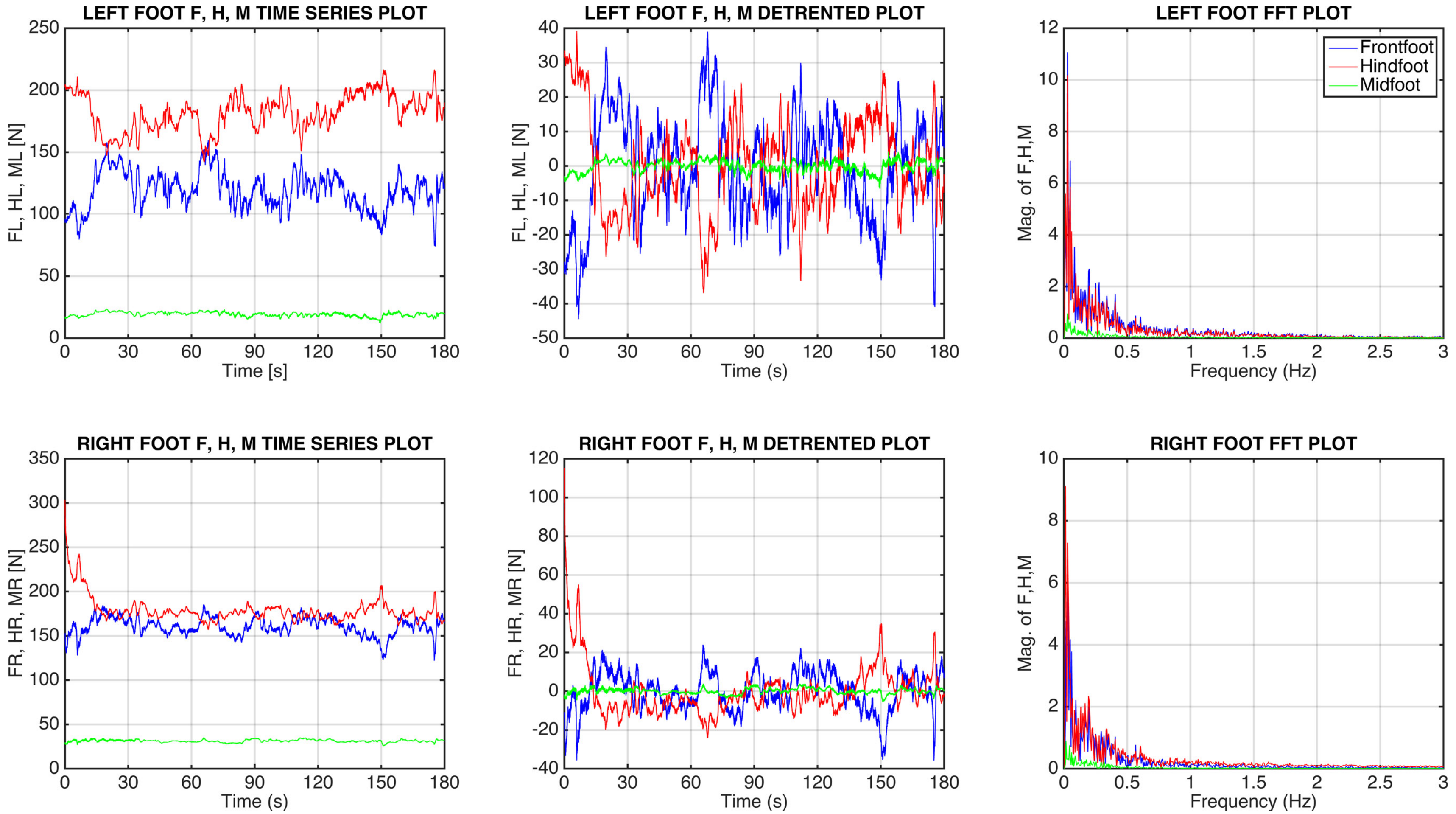

Figure A-27 Force Distribution on Time and Frequency Domain of a female subject-7

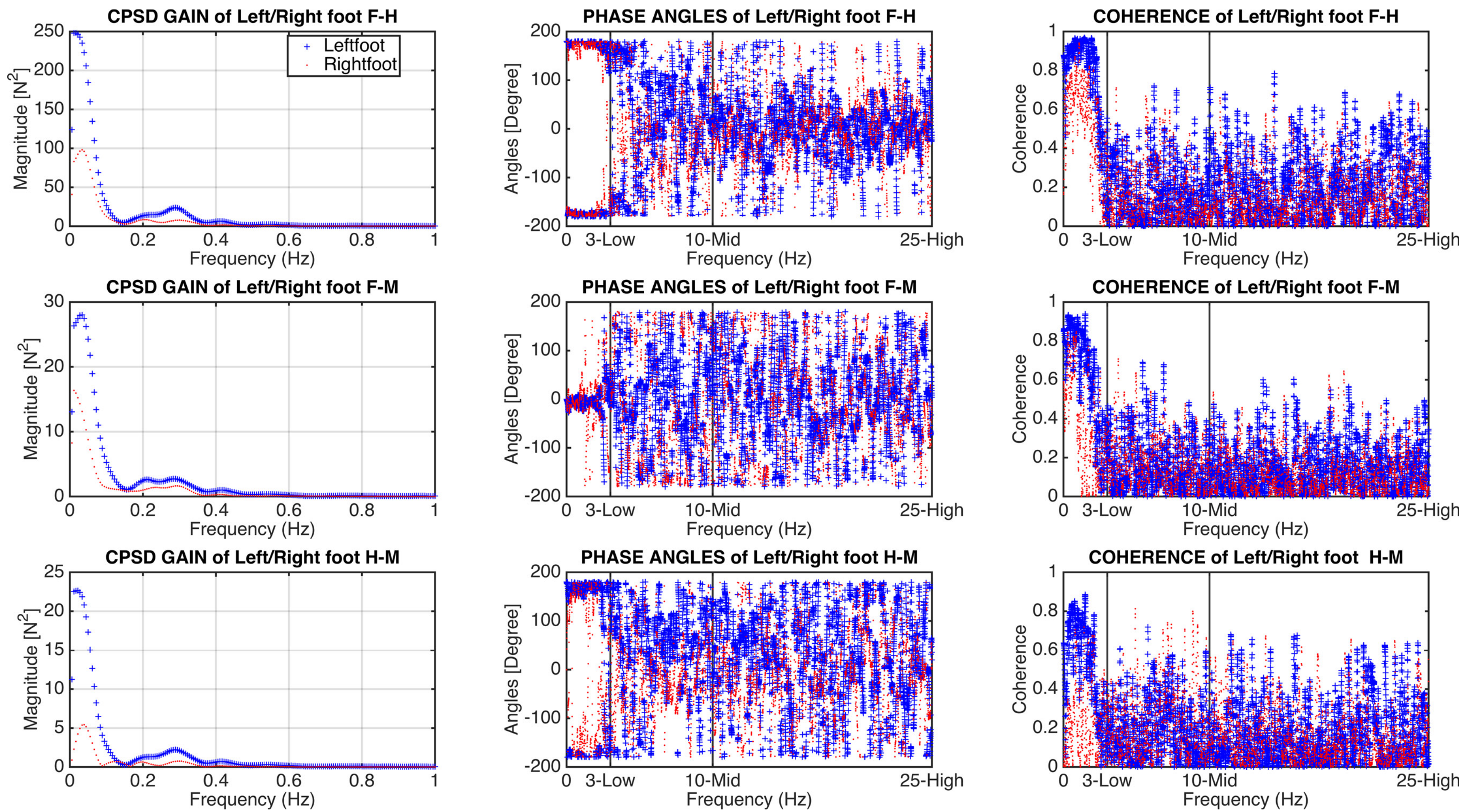

Figure A-28 Frequency Domain CPSD Magnitude, Phase Angle and Coherence plots of female subject-7

APPENDIX B

MATLAB CODES FOR THE EXPERIMENTAL DATA ANALYSIS

MATLAB codes of the experimental data are presented here. It consists of firstly, time series analysis codes and secondly frequency domain analysis codes. Additional functions created are presented at the end of the related code.

B-1 Time Domain Analysis Codes:

%% Used to process all mat files of subjects' trials process and plot their % respective figures and regressions%

```
clear all;

pathname='/Pressure_Pad_Exp//male_mats/';
cd(pathname);
files=dir('*.mat');
```

% Read txt files into Matlab. Since data is collected at 50 Hz. There are 9000 data points

```
time_lower_range=1;
time_upper_range=9000;

file_header(1,1:14)={'Filename','Foot','meanF','meanH','meanM','varF','varH','varM',
'r','m','b','F-H','F-M','H-M'}; % CSV text file header is determined.

dlmcell('results.txt',file_header,',');

for i=1:2:size(files)
filename = (files(i).name);
filelength=length(files(i).name);
k=filename(1:filelength-8);
k=filename(1:filelength-5);

leftfile=strcat(pathname,k,'L.mat'); %Left foot file is read
leftf=strcat(k,'L.mat');
rightfile=strcat(pathname,k,'R.mat');  %Right foot file is read
rightf=strcat(k,'R.mat');

load(leftfile);
load(rightfile);
```

```
% LEFT Foot Force values

t=t(time_lower_range:time_upper_range);
FL=FL(time_lower_range:time_upper_range);
HL=HL(time_lower_range:time_upper_range);
ML=ML(time_lower_range:time_upper_range);

% Right Foot Force values

FR=FR(time_lower_range:time_upper_range);
HR=HR(time_lower_range:time_upper_range);
MR=MR(time_lower_range:time_upper_range);

%Required mean values of forces are calculated below
meanFL=mean(FL); meanFR=mean(FR);
meanHL=mean(HL); meanHR=mean(HR);
meanML=mean(ML); meanMR=mean(MR);

%Required variance values of forces are calculated below
varFL=var(FL);varFR=var(FR);
varHL=var(HL);varHR=var(HR);
varML=var(ML);varMR=var(MR);

[rL,mL,bL]=regression(FL,HL,'one');
[rR,mR,bR]=regression(FR,HR,'one');

%plot of data
  figure('units','normalized','outerposition',[0 0 1 1])
  subplot(2,2,1);
  plot(t,FL,'b');hold;
  plot(t,HL,'r');
  plot(t,ML,'g');
  plot(t,(FL+HL)/2,'cyan');
  title('Left foot');
  xlabel('Time (seconds)');
  ylabel('Force (Newtons)');
  grid on;
  legend('Forefoot','Hindfoot','Midfoot','Mean of F-H','Location', 'Best');
  axis([0 180 0 350]);
  subplot(2,2,3);
  scatter(FL,HL,25,'b','.');
  lsline;
  title(['Reg=',num2str(rL,2), '  Y=',num2str(mL,2),'x +', num2str(bL,2)]);
  xlabel('F (Newtons)');
  ylabel('H (Newtons)');
```

```
   subplot(2,2,2);
   plot(t,FR,'b');hold;
   plot(t,HR,'r');
   plot(t,MR,'g');
   plot(t,(FR+HR)/2,'cyan');
   title('Right foot');
   xlabel('Time (seconds)');
   ylabel('Force (Newtons)');
   grid on;
   legend('Forefoot','Hindfoot','Midfoot','Mean of F-H','Location', 'Best');
   axis([0 180 0 350]);

   subplot(2,2,4);
   scatter(FR,HR,25,'b','.');
   lsline;
   title(['Reg=',num2str(rR,2), '  Y=',num2str(mR,2),'x +', num2str(bR,2)]);
   xlabel('F (Newtons)');
   ylabel('H (Newtons)');

figname=horzcat('Figures of  ',filename(1:filelength-8));
suptitle(figname);

saveas(gcf,k,'fig');

close all;
```

% Cross Correlation values are calculated here

```
[C1L,LAGS]=xcorr(detrend(FL),detrend(HL),'coeff');
[C2L,LAGS]=xcorr(detrend(FL),detrend(ML),'coeff');
[C3L,LAGS]=xcorr(detrend(HL),detrend(ML),'coeff');

sz=size(LAGS);
szf=(sz(1,2)-1)/2;

r1L=C1L(szf);
r2L=C2L(szf);
r3L=C3L(szf);



[C1R,LAGS]=xcorr(detrend(FR),detrend(HR),'coeff');
[C2R,LAGS]=xcorr(detrend(FR),detrend(MR),'coeff');
[C3R,LAGS]=xcorr(detrend(HR),detrend(MR),'coeff');

r1R=C1R(szf);
r2R=C2R(szf);
r3R=C3R(szf);
```

```
Cellarr(1,1:14)={rightf,'R',meanFR,meanHR,meanMR,varFR,varHR,varMR,rR,mR,
bR,r1R,r2R,r3R};
Cellarr(2,1:14)={leftf,'L',meanFL,meanHL,meanML,varFL,varHL,varML,rL,mL,bL
,r1L,r2L,r3L};

dlmcell('results.txt',Cellarr,',','-a');
% all of the values are written into a CSV text file to be processed later.

disp('OK');
end

% End of the program.
%*************************************************************
```

B-2 Frequency Domain, FFT and Autocorrelation - Power Calculations

```
clear all; close all;


pathname='/Pressure_Pad_Exp/female_mat/';

cd(pathname);
files=dir('*.mat');
```

%read mat files into matlab

%Constructing file header for the output CSV file

```
file_header(1,1:32)={'Filename','Foot','Power F','P50_F','P50_F-
freq','P95_F','F_95_frq','mu0_F','mu1_F','mu2_F','Power H', 'P50_H','P50_H-
freq','P95_H','H_95_fr','mu0_H','mu1_H','mu2_H','Power M','P50_M','P50_M-
freq','P95_M','M_95_fr','mu0_M','mu1_M','mu2_M','CFREQ_F','CFREQ_H','CFRE
Q_M','FREQD_F','FREQD_H','FREQD_M'};

dlmcell('Freq-domain-results.csv',file_header,',');


  for i=1:2:size(files)

  filename = (files(i).name);
  filelength=length(files(i).name);
  k=filename(1:filelength-8);

  k=filename(1:filelength-5);

  leftfile=strcat(pathname,k,'L.mat');
```

```
  leftf=strcat(k,'L.mat');
  rightfile=strcat(pathname,k,'R.mat');
  rightf=strcat(k,'R.mat');

  load(leftfile);
  load(rightfile);
```

%********************* LEFT FOOT FFT **************************

```
freq_2=1/180:1/180:9000*1/180; % arrange according to step size

freq=freq_2(1:4500); %25 Hz frequency

FL_new=detrend(FL,1);
HL_new=detrend(HL,1);
ML_new=detrend(ML,1);
```

% FFT Calculations

```
coeff_F=fft(FL_new);
coeff_H=fft(HL_new);
coeff_M=fft(ML_new);
```

%Nyquist frequency reducing one half to 25 Hz

```
magnitude_FL=abs(coeff_F(1:4500))/4500;
magnitude_HL=abs(coeff_H(1:4500))/4500;
magnitude_ML=abs(coeff_M(1:4500))/4500;
```

%Calculating Full Powers

```
pow_F_L=(magnitude_FL.^2);
pow_H_L=(magnitude_HL.^2);
pow_M_L=(magnitude_ML.^2);

powFL=sum(pow_F_L);
powHL=sum(pow_H_L);
powML=sum(pow_M_L);
```

% 50 percent power calculations pow_50 function is used

```
[pow50_FL,FL_50_fr]=pow_50(pow_F_L,freq);
[pow50_HL,HL_50_fr]=pow_50(pow_H_L,freq);
[pow50_ML,ML_50_fr]=pow_50(pow_M_L,freq);
```

% 95 percent power calculations pow_95 function is used

```
[pow95_FL,FL_95_fr]=pow_95(pow_F_L,freq);
[pow95_HL,HL_95_fr]=pow_95(pow_H_L,freq);
[pow95_ML,ML_95_fr]=pow_95(pow_M_L,freq);
```

```
% moment zero values prieto and maurer
mu0_FL=sum(pow_F_L);
mu0_HL=sum(pow_H_L);
mu0_ML=sum(pow_M_L);

%cut calculation at 95percent frequency

[mu1_FL,mu2_FL]=mu_calc(pow_F_L,FL_95_fr);
[mu1_HL,mu2_HL]=mu_calc(pow_H_L,HL_95_fr);
[mu1_ML,mu2_ML]=mu_calc(pow_M_L,ML_95_fr);

%CFREQ calculation
CFREQ_FL=sqrt(mu2_FL/mu0_FL);
CFREQ_HL=sqrt(mu2_HL/mu0_HL);
CFREQ_ML=sqrt(mu2_ML/mu0_ML);

%FREQD calculation
FREQD_FL=sqrt(1-(mu1_FL^2/(mu0_FL*mu2_FL)));
FREQD_HL=sqrt(1-(mu1_HL^2/(mu0_HL*mu2_HL)));
FREQD_ML=sqrt(1-(mu1_ML^2/(mu0_ML*mu2_ML)));



% ********************* RIGHT FOOT FFT *************************

FR_new=detrend(FR,1);
HR_new=detrend(HR,1);
MR_new=detrend(MR,1);

coeff_FR=fft(FR_new);
coeff_HR=fft(HR_new);
coeff_MR=fft(MR_new);

magnitude_FR=abs(coeff_FR(1:4500))/4500;
magnitude_HR=abs(coeff_HR(1:4500))/4500;
magnitude_MR=abs(coeff_MR(1:4500))/4500;

% calculation of powers
pow_F_R=(magnitude_FR.^2);
pow_H_R=(magnitude_HR.^2);
pow_M_R=(magnitude_MR.^2);

powFR=sum(pow_F_R);
powHR=sum(pow_H_R);
powMR=sum(pow_M_R);

[pow50_FR,FR_50_fr]=pow_50(pow_F_R,freq);
```

```
[pow50_HR,HR_50_fr]=pow_50(pow_H_R,freq);
[pow50_MR,MR_50_fr]=pow_50(pow_M_R,freq);

[pow95_FR,FR_95_fr]=pow_95(pow_F_R,freq);
[pow95_HR,HR_95_fr]=pow_95(pow_H_R,freq);
[pow95_MR,MR_95_fr]=pow_95(pow_M_R,freq);


% calc of moment zero

mu0_FR=sum(pow_F_R);
mu0_HR=sum(pow_H_R);
mu0_MR=sum(pow_M_R);

[mu1_FR,mu2_FR]=mu_calc(pow_F_R,FR_95_fr);
[mu1_HR,mu2_HR]=mu_calc(pow_H_R,HR_95_fr);
[mu1_MR,mu2_MR]=mu_calc(pow_M_R,MR_95_fr);


CFREQ_FR=sqrt(mu2_FR/mu0_FR);
CFREQ_HR=sqrt(mu2_HR/mu0_HL);
CFREQ_MR=sqrt(mu2_MR/mu0_MR);

FREQD_FR=sqrt(1-(mu1_FL^2/(mu0_FL*mu2_FL)));
FREQD_HR=sqrt(1-(mu1_HL^2/(mu0_HL*mu2_HL)));
FREQD_MR=sqrt(1-(mu1_ML^2/(mu0_ML*mu2_ML)));



% ************ COHERENCE AND OTHER RELATIONS **************

% ***************** RIGHT/LEFT F-H RELATION *******************

freq2=0:0.0244:25; %upto 25 Hz freq. range

% Cross Pwer Spectral Density Estimates

Cxy_L_FH=cpsd(FL_new,HL_new);
Cxy_R_FH=cpsd(FR_new,HR_new);

% Coherencee
Cxy_L_FH_coher=mscohere(FL_new,HL_new);
Cxy_R_FH_coher=mscohere(FR_new,HR_new);

% Magnitude or Gain
Cxy_L_FH_mag=abs(Cxy_L_FH)/128;
Cxy_R_FH_mag=abs(Cxy_R_FH)/128;
```

```
%Phase Angles calculation
phase_Cxy_L_FH=angle(Cxy_L_FH);
phase_Cxy_R_FH=angle(Cxy_R_FH);

% find coherence above 80% and their freqs
% F_H Coherence
[LFH_coh]=find(Cxy_L_FH_coher>=0.80);
[RFH_coh]=find(Cxy_R_FH_coher>=0.80);

frq_LFH_coh=freq2(LFH_coh)';
frq_RFH_coh=freq2(RFH_coh)';


L_FH=[LFH_coh,frq_LFH_coh,Cxy_L_FH_coher(LFH_coh),Cxy_L_FH_mag(LF
H_coh),phase_Cxy_L_FH(LFH_coh)*180/pi];

R_FH=[RFH_coh,frq_RFH_coh,Cxy_R_FH_coher(RFH_coh),Cxy_R_FH_mag(RF
H_coh),phase_Cxy_R_FH(RFH_coh)*180/pi];


% ******************** RIGHT/LEFT F-M RELATION ***************
Cxy_L_FM=cpsd(FL_new,ML_new);
Cxy_R_FM=cpsd(FR_new,MR_new);

Cxy_L_FM_coher=mscohere(FL_new,ML_new);
Cxy_R_FM_coher=mscohere(FR_new,MR_new);

Cxy_L_FM_mag=abs(Cxy_L_FM)/1025;
Cxy_R_FM_mag=abs(Cxy_R_FM)/1025;

phase_Cxy_L_FM=angle(Cxy_L_FM);
phase_Cxy_R_FM=angle(Cxy_R_FM);

[LFM_coh]=find(Cxy_L_FM_coher>=0.85);
[RFM_coh]=find(Cxy_R_FM_coher>=0.85);

frq_LFM_coh=freq2(LFM_coh)';%transpose
frq_RFM_coh=freq2(RFM_coh)';


L_FM=[LFM_coh,frq_LFM_coh,Cxy_L_FM_coher(LFM_coh),Cxy_L_FM_mag(L
FM_coh),phase_Cxy_L_FM(LFM_coh)*180/pi];

R_FM=[RFM_coh,frq_RFM_coh,Cxy_L_FM_coher(RFM_coh),Cxy_R_FM_mag(
RFM_coh),phase_Cxy_R_FM(RFM_coh)*180/pi];
```

```
% ******************* RIGHT/LEFT H-M RELATION ****************

Cxy_L_HM=cpsd(HL_new,ML_new);
Cxy_R_HM=cpsd(HR_new,MR_new);

Cxy_L_HM_coher=mscohere(HL_new,ML_new);
Cxy_R_HM_coher=mscohere(HR_new,MR_new);

Cxy_L_HM_mag=abs(Cxy_L_HM)/1025;
Cxy_R_HM_mag=abs(Cxy_R_HM)/1025;

phase_Cxy_L_HM=angle(Cxy_L_HM);
phase_Cxy_R_HM=angle(Cxy_R_HM);

% H-M Coherence
[LHM_coh]=find(Cxy_L_HM_coher>=0.85);
[RHM_coh]=find(Cxy_R_HM_coher>=0.85);

frq_LHM_coh=freq2(LHM_coh)';
frq_RHM_coh=freq2(RHM_coh)';


L_HM=[LHM_coh,frq_LHM_coh,Cxy_L_HM_coher(LHM_coh),Cxy_L_HM_mag
(LHM_coh),phase_Cxy_L_HM(LHM_coh)*180/pi];

R_HM=[RHM_coh,frq_RHM_coh,Cxy_L_HM_coher(RHM_coh),Cxy_R_HM_ma
g(RHM_coh),phase_Cxy_R_HM(RHM_coh)*180/pi];

%********* Write to text file ****************

Cellarr(1,1:32)={leftf,'L',powFL, pow50_FL, FL_50_fr,pow95_FL,FL_95_fr,
mu0_FL, mu1_FL, mu2_FL, powHL, pow50_HL,HL_50_fr, pow95_HL,HL_95_fr,
mu0_HL, mu1_HL, mu2_HL, powML,pow50_ML, ML_50_fr,
pow95_ML,ML_95_fr,mu0_ML, mu1_ML,
mu2_ML,CFREQ_FL,CFREQ_HL,CFREQ_ML,FREQD_FL,FREQD_HL,FREQD
_ML};


Cellarr(2,1:32)={rightf,'R',powFR,pow50_FR, FR_50_fr,
pow95_FR,FR_95_fr,mu0_FR, mu1_FR, mu2_FR,powHR,pow50_HR, HR_50_fr,
pow95_HR,HR_95_fr,mu0_HR, mu1_HR, mu2_HR, powMR,pow50_MR,
MR_50_fr, pow95_MR,MR_95_fr, mu0_MR, mu1_MR, mu2_MR,
CFREQ_FR,CFREQ_HR,CFREQ_MR,FREQD_FR,FREQD_HR,FREQD_MR};

dlmcell('Freq-domain-results.csv',Cellarr,',','-a');

% ********* Write Coherence values to file ******
```

% end

% ** pow_50 function *****

```
function [sum5,frekans]=pow_50(cins,frk)
sum50=0;
k=1;
   while ~(sum50 >= (sum(cins)/2));
    sum50=sum50+cins(k);
    k=k+1;
   end;
   frekans=frk(k);
   sum5=sum50;
```

% * pow_95 function *****

```
function [frekans,mu0,sum9]=pow_95(cins,frk)
sum95=0;
K=1;
   while ~(sum95 >= (0.95*sum(cins)));
    sum95=sum95+cins(K,1);
    K=K+1;
   end;
   frekans=frk(K);
   mu0=sum(cins);
   sum9=sum95;
```

% ** mu_calc function ***

```
function [mu1,mu2]=mu_calc(sinyal,f95)
delta_f=1/180;


for i=1:1:round(f95/delta_f)
   mu_1d(i)=(i*delta_f)*sinyal(i);
   mu_2d(i)=(i*delta_f)^2*sinyal(i);
end
mu1=sum(mu_1d);
mu2=sum(mu_2d);
```

B-3 Frequency Domain Special Metrics Above Threshold “0.80”

```
clear all; close all;
pathname='//Pressure_Pad_Exp/male_mat/';

cd(pathname);
files=dir('*.mat');
```

%read mat files into matlab

```
%
file_header(1,:)={'Filename','Foot','Region','coher_low_mean', 'coher_low_var',
'coher_mid_mean', 'coher_mid_var', 'coher_high_mean',
'coher_high_var','phase_mean'};
dlmcell('Freq-domain-coherence_freq_band_mean_results.csv',file_header,',');

 for i=1:2:size(files)

 filename = (files(i).name);
 filelength=length(files(i).name);
 k=filename(1:filelength-8);

 k=filename(1:filelength-5);

 leftfile=strcat(pathname,k,'L.mat');
 leftf=strcat(k,'L.mat');
 rightfile=strcat(pathname,k,'R.mat');
 rightf=strcat(k,'R.mat');

 load(leftfile);
   load(rightfile);
```

%********************** LEFT FOOT FFT *************************

```
freq_2=1/180:1/180:9000*1/180;

freq=freq_2(1:4501); %25 Hz freq.

FL_det=detrend(FL);
HL_det=detrend(HL);
ML_det=detrend(ML);

FR_det=detrend(FR);
HR_det=detrend(HR);
MR_det=detrend(MR);
```

% ********** COHERENCE AND OTHER RELATIONS **************

% **************** RIGHT/LEFT F-H RELATION ******************

% nooverlap 9000 points at 50 Hz

```
Cxy_L_FH=cpsd(FL_det,HL_det,[],0,9000,50);
Cxy_R_FH=cpsd(FR_det,HR_det,[],0,9000,50);
```

% Coherencee

```
Cxy_L_FH_coher=mscohere(FL_det,HL_det,[],0,9000,50);
```

```
Cxy_R_FH_coher=mscohere(FR_det,HR_det,[],0,9000,50);

%Gain
Cxy_L_FH_mag=abs(Cxy_L_FH)/8; % divide 8 for accurate result
Cxy_R_FH_mag=abs(Cxy_R_FH)/8;

%Phase
phase_Cxy_L_FH=angle(Cxy_L_FH);
phase_Cxy_R_FH=angle(Cxy_R_FH);



% find coherence above 80% and their freqs
% ------------------------ F_H Coherence over 80% -------------------

LFH_coh=find(Cxy_L_FH_coher>=0.80); %array index numbers of coherence
RFH_coh=find(Cxy_R_FH_coher>=0.80);

frq_LFH_coh=freq(LFH_coh)'; frq_LFH_coh=check_empty(frq_LFH_coh);
frq_RFH_coh=freq(RFH_coh)'; frq_RFH_coh=check_empty(frq_RFH_coh);
 %respective freqs


Cxy_LFH_target_coher=Cxy_L_FH_coher(LFH_coh);
Cxy_LFH_target_coher=check_empty(Cxy_LFH_target_coher);
Cxy_RFH_target_coher=Cxy_R_FH_coher(RFH_coh);
Cxy_RFH_target_coher=check_empty(Cxy_RFH_target_coher);

Cxy_L_FH_target_mag=Cxy_L_FH_mag(LFH_coh);
Cxy_L_FH_target_mag=check_empty(Cxy_L_FH_target_mag);
Cxy_R_FH_target_mag=Cxy_R_FH_mag(RFH_coh);
Cxy_R_FH_target_mag=check_empty(Cxy_R_FH_target_mag);

phase_Cxy_L_FH_target=check_empty(phase_Cxy_L_FH(LFH_coh));
phase_Cxy_R_FH_target=check_empty(phase_Cxy_R_FH(RFH_coh));

Cxy_L_FH_coher_start_frq=frq_LFH_coh(1); %start freq
Cxy_L_FH_coher_start_value=Cxy_LFH_target_coher(1); %starting value
Cxy_L_FH_coher_end_frq=frq_LFH_coh(end); %end freq
Cxy_L_FH_coher_end_value=Cxy_LFH_target_coher(end); %end value


Cxy_R_FH_coher_start_frq=frq_RFH_coh(1); %start freq
Cxy_R_FH_coher_start_value=Cxy_RFH_target_coher(1); %starting value
Cxy_R_FH_coher_end_frq=frq_RFH_coh(end); %end freq
Cxy_R_FH_coher_end_value=Cxy_RFH_target_coher(end); %end value
```

```
Cxy_L_FH_coher_low=
freq_range_chk(frq_LFH_coh,Cxy_LFH_target_coher,'low');

Cxy_L_FH_coher_mid=
freq_range_chk(frq_LFH_coh,Cxy_LFH_target_coher,'mid');

Cxy_L_FH_coher_high=
freq_range_chk(frq_LFH_coh,Cxy_LFH_target_coher,'high');


Cxy_R_FH_coher_low=
freq_range_chk(frq_RFH_coh,Cxy_RFH_target_coher,'low');
 Cxy_R_FH_coher_mid=
freq_range_chk(frq_RFH_coh,Cxy_RFH_target_coher,'mid');

 Cxy_R_FH_coher_high=
freq_range_chk(frq_RFH_coh,Cxy_RFH_target_coher,'high');

%**** mean and var of above target value ***********

Cxy_L_FH_coher_low_mean=mean(Cxy_L_FH_coher_low);
Cxy_L_FH_coher_low_var=std(Cxy_L_FH_coher_low);

Cxy_L_FH_coher_mid_mean=mean(Cxy_L_FH_coher_mid);
Cxy_L_FH_coher_mid_var=std(Cxy_L_FH_coher_mid);

Cxy_L_FH_coher_high_mean=mean(Cxy_L_FH_coher_high);
Cxy_L_FH_coher_high_var=std(Cxy_L_FH_coher_high);

Cxy_R_FH_coher_low_mean=mean(Cxy_R_FH_coher_low);
Cxy_R_FH_coher_low_var=std(Cxy_R_FH_coher_low);

Cxy_R_FH_coher_mid_mean=mean(Cxy_R_FH_coher_mid);
Cxy_R_FH_coher_mid_var=std(Cxy_R_FH_coher_mid);

Cxy_R_FH_coher_high_mean=mean(Cxy_R_FH_coher_high);
Cxy_R_FH_coher_high_var=std(Cxy_R_FH_coher_high);


% ----- max-min of coherence -------------

[Cxy_L_FH_coher_max,idx]=max(Cxy_LFH_target_coher);

Cxy_L_FH_coher_max_frq=frq_LFH_coh(idx);

phase_Cxy_L_FH_coher_max=abs(phase_Cxy_L_FH(idx))*180/pi;

[Cxy_L_FH_coher_min,idx]=min(Cxy_LFH_target_coher);
```

```
Cxy_L_FH_coher_min_frq=frq_LFH_coh(idx);

phase_Cxy_L_FH_coher_min=abs(phase_Cxy_L_FH(idx))*180/pi;

[Cxy_R_FH_coher_max,idx]=max(Cxy_RFH_target_coher);

Cxy_R_FH_coher_max_frq=frq_RFH_coh(idx);

phase_Cxy_R_FH_coher_max=abs(phase_Cxy_R_FH(idx))*180/pi;

[Cxy_R_FH_coher_min,idx]=min(Cxy_RFH_target_coher);
Cxy_R_FH_coher_min_frq=frq_RFH_coh(idx);

phase_Cxy_R_FH_coher_min=abs(phase_Cxy_R_FH(idx))*180/pi;
```

%------------ magnitude or gain ----

```
[Cxy_L_FH_mag_max,idx]=max(Cxy_L_FH_target_mag);

Cxy_L_FH_mag_max_frq=frq_LFH_coh(idx);

phase_Cxy_L_FH_mag_max=abs(phase_Cxy_L_FH(idx))*180/pi;

[Cxy_L_FH_mag_min,idx]=min(Cxy_L_FH_target_mag);

Cxy_L_FH_mag_min_frq=frq_LFH_coh(idx);

phase_Cxy_L_FH_mag_min=abs(phase_Cxy_L_FH(idx))*180/pi;

[Cxy_R_FH_mag_max,idx]=max(Cxy_R_FH_target_mag);

Cxy_R_FH_mag_max_frq=frq_RFH_coh(idx);

phase_Cxy_R_FH_mag_max=abs(phase_Cxy_R_FH(idx))*180/pi;

[Cxy_R_FH_mag_min,idx]=min(Cxy_R_FH_target_mag);

Cxy_R_FH_mag_min_frq=frq_RFH_coh(idx);

phase_Cxy_R_FH_mag_min=abs(phase_Cxy_R_FH(idx))*180/pi;

phase_Cxy_L_FH_mean=mean(abs(phase_Cxy_L_FH(LFH_coh)))*180/pi;
phase_Cxy_R_FH_mean=mean(abs(phase_Cxy_R_FH(RFH_coh)))*180/pi;
```

% ------- ** ---------

```
% L_FH=[LFH_coh,frq_LFH_coh,Cxy_L_FH_coher(LFH_coh),Cxy_L_FH_mag(LFH_coh),phase_Cxy_L_FH(LFH_coh)*180/pi];
% R_FH=[RFH_coh,frq_RFH_coh,Cxy_R_FH_coher(RFH_coh),Cxy_R_FH_mag(RFH_coh),phase_Cxy_R_FH(RFH_coh)*180/pi];


% ******************* RIGHT/LEFT F-M RELATION ***************

Cxy_L_FM=cpsd(FL_det,ML_det,[],0,9000,50);
Cxy_R_FM=cpsd(FR_det,MR_det,[],0,9000,50);


%Coherence
Cxy_L_FM_coher=mscohere(FL_det,ML_det,[],0,9000,50);
Cxy_R_FM_coher=mscohere(FR_det,MR_det,[],0,9000,50);

%Gain
Cxy_L_FM_mag=abs(Cxy_L_FM)/8;
Cxy_R_FM_mag=abs(Cxy_R_FM)/8;

%Phase
phase_Cxy_L_FM=angle(Cxy_L_FM);
phase_Cxy_R_FM=angle(Cxy_R_FM);

% ******************** target values of above 0.80 ******************

LFM_coh=find(Cxy_L_FM_coher>=0.80);
RFM_coh=find(Cxy_R_FM_coher>=0.80);

frq_LFM_coh=freq(LFM_coh)'; frq_LFM_coh=check_empty(frq_LFM_coh);

%transpose exist
frq_RFM_coh=freq(RFM_coh)'; frq_RFM_coh=check_empty(frq_RFM_coh);

Cxy_LFM_target_coher=check_empty(Cxy_L_FM_coher(LFM_coh));
Cxy_RFM_target_coher=check_empty(Cxy_R_FM_coher(RFM_coh));

Cxy_L_FM_target_mag=check_empty(Cxy_L_FM_mag(LFM_coh));
Cxy_R_FM_target_mag=check_empty(Cxy_R_FM_mag(RFM_coh));

phase_Cxy_L_FM_target=check_empty(phase_Cxy_L_FM(LFM_coh));
phase_Cxy_R_FM_target=check_empty(phase_Cxy_R_FM(RFM_coh));

Cxy_L_FM_coher_start_frq=frq_LFM_coh(1); %start freq
```

```
Cxy_L_FM_coher_start_value=Cxy_LFM_target_coher(1); %starting value
Cxy_L_FM_coher_end_frq=frq_LFM_coh(end); %end freq
Cxy_L_FM_coher_end_value=Cxy_LFM_target_coher(end); %end value

Cxy_R_FM_coher_start_frq=frq_RFM_coh(1); %start freq
Cxy_R_FM_coher_start_value=Cxy_RFM_target_coher(1); %starting value
Cxy_R_FM_coher_end_frq=frq_RFM_coh(end); %end freq
Cxy_R_FM_coher_end_value=Cxy_RFM_target_coher(end); %end value

Cxy_L_FM_coher_low=
freq_range_chk(frq_LFM_coh,Cxy_LFM_target_coher,'low');

 Cxy_L_FM_coher_mid=
freq_range_chk(frq_LFM_coh,Cxy_LFM_target_coher,'mid');
Cxy_L_FM_coher_high=
freq_range_chk(frq_LFM_coh,Cxy_LFM_target_coher,'high');

Cxy_R_FM_coher_low=
freq_range_chk(frq_RFM_coh,Cxy_RFM_target_coher,'low');

Cxy_R_FM_coher_mid=
freq_range_chk(frq_RFM_coh,Cxy_RFM_target_coher,'mid');

Cxy_R_FM_coher_high=
freq_range_chk(frq_RFM_coh,Cxy_RFM_target_coher,'high');

%**** mean and var of above target value ***********

Cxy_L_FM_coher_low_mean=mean(Cxy_L_FM_coher_low);
Cxy_L_FM_coher_low_var=std(Cxy_L_FM_coher_low);
% Cxy_L_FM_coher_mid_mean=mean(Cxy_L_FM_coher_mid);
Cxy_L_FM_coher_mid_var=std(Cxy_L_FM_coher_mid);
% Cxy_L_FM_coher_high_mean=mean(Cxy_L_FM_coher_high);
Cxy_L_FM_coher_high_var=std(Cxy_L_FM_coher_high);

Cxy_R_FM_coher_low_mean=mean(Cxy_R_FM_coher_low);
Cxy_R_FM_coher_low_var=std(Cxy_R_FM_coher_low);
% Cxy_R_FM_coher_mid_mean=mean(Cxy_R_FM_coher_mid);
Cxy_R_FM_coher_mid_var=std(Cxy_R_FM_coher_mid);
% Cxy_R_FM_coher_high_mean=mean(Cxy_R_FM_coher_high);
Cxy_R_FM_coher_high_var=std(Cxy_R_FM_coher_high);
%

% ----- max-min of coherence -------------


[Cxy_L_FM_coher_max,idx]=max(Cxy_LFM_target_coher);
Cxy_L_FM_coher_max_frq=frq_LFM_coh(idx);
```

```
[Cxy_L_FM_coher_min,idx]=min(Cxy_LFM_target_coher);
Cxy_L_FM_coher_min_frq=frq_LFM_coh(idx);

[Cxy_R_FM_coher_max,idx]=max(Cxy_RFM_target_coher);
Cxy_R_FM_coher_max_frq=frq_RFM_coh(idx);
[Cxy_R_FM_coher_min,idx]=min(Cxy_RFM_target_coher);
Cxy_R_FM_coher_min_frq=frq_RFM_coh(idx);

%------------ magnitude or gain ----
[Cxy_L_FM_mag_max,idx]=max(Cxy_L_FM_target_mag);
Cxy_L_FM_mag_max_frq=frq_LFM_coh(idx);
[Cxy_L_FM_mag_min,idx]=min(Cxy_L_FM_target_mag);
Cxy_L_FM_mag_min_frq=frq_LFM_coh(idx);

[Cxy_R_FM_mag_max,idx]=max(Cxy_R_FM_target_mag);
Cxy_R_FM_mag_max_frq=frq_RFM_coh(idx);
[Cxy_R_FM_mag_min,idx]=min(Cxy_R_FM_target_mag);
Cxy_R_FM_mag_min_frq=frq_RFM_coh(idx);


phase_Cxy_L_FM_mean=mean(abs(phase_Cxy_L_FM(LFM_coh)))*180/pi;
phase_Cxy_R_FM_mean=mean(abs(phase_Cxy_R_FM(RFM_coh)))*180/pi;

%
L_FM=[LFM_coh,frq_LFM_coh,Cxy_L_FM_coher(LFM_coh),Cxy_L_FM_mag(L
FM_coh),phase_Cxy_L_FM(LFM_coh)*180/pi];
%
R_FM=[RFM_coh,frq_RFM_coh,Cxy_R_FM_coher(RFM_coh),Cxy_R_FM_mag(
RFM_coh),phase_Cxy_R_FM(RFM_coh)*180/pi];

phase_Cxy_L_FM_coher_max=abs(phase_Cxy_L_FM(idx))*180/pi;
phase_Cxy_L_FM_coher_min=abs(phase_Cxy_L_FM(idx))*180/pi;
phase_Cxy_R_FM_coher_max=abs(phase_Cxy_R_FM(idx))*180/pi;
phase_Cxy_R_FM_coher_min=abs(phase_Cxy_R_FM(idx))*180/pi;

phase_Cxy_L_FM_mag_max=abs(phase_Cxy_L_FM(idx))*180/pi;
phase_Cxy_L_FM_mag_min=abs(phase_Cxy_L_FM(idx))*180/pi;
phase_Cxy_R_FM_mag_max=abs(phase_Cxy_R_FM(idx))*180/pi;
phase_Cxy_R_FM_mag_min=abs(phase_Cxy_R_FM(idx))*180/pi;

% ***************** RIGHT/LEFT H-M RELATION ****************

Cxy_L_HM=cpsd(HL_det,ML_det,[],0,9000,50);
Cxy_R_HM=cpsd(HR_det,MR_det,[],0,9000,50);


%Coherence
Cxy_L_HM_coher=mscohere(HL_det,ML_det,[],0,9000,50);
```

```
Cxy_R_HM_coher=mscohere(HR_det,MR_det,[],0,9000,50);

%Gain
Cxy_L_HM_mag=abs(Cxy_L_HM)/8;
Cxy_R_HM_mag=abs(Cxy_R_HM)/8;

%Phase
phase_Cxy_L_HM=angle(Cxy_L_HM);
phase_Cxy_R_HM=angle(Cxy_R_HM);

% H-M Coherence
LHM_coh=find(Cxy_L_HM_coher>=0.80);
RHM_coh=find(Cxy_R_HM_coher>=0.80);

frq_LHM_coh=freq(LHM_coh)';      frq_LHM_coh=check_empty(frq_LHM_coh);
frq_RHM_coh=freq(RHM_coh)';      frq_RHM_coh=check_empty(frq_RHM_coh);


Cxy_LHM_target_coher=Cxy_L_HM_coher(LHM_coh);
        Cxy_LHM_target_coher=check_empty(Cxy_LHM_target_coher);
Cxy_RHM_target_coher=Cxy_R_HM_coher(RHM_coh);
        Cxy_RHM_target_coher=check_empty(Cxy_RHM_target_coher);

Cxy_L_HM_target_mag=Cxy_L_HM_mag(LHM_coh);
        Cxy_L_HM_target_mag=check_empty(Cxy_L_HM_target_mag);
Cxy_R_HM_target_mag=Cxy_R_HM_mag(RHM_coh);
        Cxy_R_HM_target_mag=check_empty(Cxy_R_HM_target_mag);

phase_Cxy_L_HM_target=check_empty(phase_Cxy_L_HM(LHM_coh));
phase_Cxy_R_HM_target=check_empty(phase_Cxy_R_HM(RHM_coh));

Cxy_L_HM_coher_start_frq=frq_LHM_coh(1); %start freq
Cxy_L_HM_coher_start_value=Cxy_LHM_target_coher(1); %starting value
Cxy_L_HM_coher_end_frq=frq_LHM_coh(end);%end freq
Cxy_L_HM_coher_end_value=Cxy_LHM_target_coher(end); %end value


Cxy_R_HM_coher_start_frq=frq_RHM_coh(1); %start freq
Cxy_R_HM_coher_start_value=Cxy_RHM_target_coher(1); %starting value
Cxy_R_HM_coher_end_frq=frq_RHM_coh(end);%end freq
Cxy_R_HM_coher_end_value=Cxy_RHM_target_coher(end); %end value

Cxy_L_HM_coher_low=
freq_range_chk(frq_LHM_coh,Cxy_LHM_target_coher,'low');

Cxy_L_HM_coher_mid=
freq_range_chk(frq_LHM_coh,Cxy_LHM_target_coher,'mid');
```

```
 Cxy_L_HM_coher_high=
freq_range_chk(frq_LHM_coh,Cxy_LHM_target_coher,'high');

Cxy_R_HM_coher_low=
freq_range_chk(frq_RHM_coh,Cxy_RHM_target_coher,'low');

Cxy_R_HM_coher_mid=
freq_range_chk(frq_RHM_coh,Cxy_RHM_target_coher,'mid');

Cxy_R_HM_coher_high=
freq_range_chk(frq_RHM_coh,Cxy_RHM_target_coher,'high');



%**** mean and var of above target value ***********

Cxy_L_HM_coher_low_mean=mean(Cxy_L_HM_coher_low);
Cxy_L_HM_coher_low_var=std(Cxy_L_HM_coher_low);

Cxy_L_HM_coher_mid_mean=mean(Cxy_L_HM_coher_mid);
Cxy_L_HM_coher_mid_var=std(Cxy_L_HM_coher_mid);

Cxy_L_HM_coher_high_mean=mean(Cxy_L_HM_coher_high);
Cxy_L_HM_coher_high_var=std(Cxy_L_HM_coher_high);

Cxy_R_HM_coher_low_mean=mean(Cxy_R_HM_coher_low);
Cxy_R_HM_coher_low_var=std(Cxy_R_HM_coher_low);

Cxy_R_HM_coher_mid_mean=mean(Cxy_R_HM_coher_mid);
Cxy_R_HM_coher_mid_var=std(Cxy_R_HM_coher_mid);

Cxy_R_HM_coher_high_mean=mean(Cxy_R_HM_coher_high);
Cxy_R_HM_coher_high_var=std(Cxy_R_HM_coher_high);


% ----- max-min of coherence -------------
[Cxy_L_HM_coher_max,idx]=max(Cxy_LHM_target_coher);
Cxy_L_HM_coher_max_frq=frq_LHM_coh(idx);
[Cxy_L_HM_coher_min,idx]=min(Cxy_LHM_target_coher);
Cxy_L_HM_coher_min_frq=frq_LHM_coh(idx);

[Cxy_R_HM_coher_max,idx]=max(Cxy_RHM_target_coher);
Cxy_R_HM_coher_max_frq=frq_RHM_coh(idx);
[Cxy_R_HM_coher_min,idx]=min(Cxy_RHM_target_coher);
Cxy_R_HM_coher_min_frq=frq_RHM_coh(idx);

%------------ magnitude or gain ----
```

```
[Cxy_L_HM_mag_max,idx]=max(Cxy_L_HM_target_mag);
Cxy_L_HM_mag_max_frq=frq_LHM_coh(idx);
[Cxy_L_HM_mag_min,idx]=min(Cxy_L_HM_target_mag);
Cxy_L_HM_mag_min_frq=frq_LHM_coh(idx);

[Cxy_R_HM_mag_max,idx]=max(Cxy_R_HM_target_mag);
Cxy_R_HM_mag_max_frq=frq_RHM_coh(idx);
[Cxy_R_HM_mag_min,idx]=min(Cxy_R_HM_target_mag);
Cxy_R_HM_mag_min_frq=frq_RHM_coh(idx);

phase_Cxy_L_HM_mean=mean(abs(phase_Cxy_L_HM(LHM_coh)))*180/pi;
phase_Cxy_R_HM_mean=mean(abs(phase_Cxy_R_HM(RHM_coh)))*180/pi;

phase_Cxy_L_HM_coher_max=abs(phase_Cxy_L_HM(idx))*180/pi;
phase_Cxy_L_HM_coher_min=abs(phase_Cxy_L_HM(idx))*180/pi;
phase_Cxy_R_HM_coher_max=abs(phase_Cxy_R_HM(idx))*180/pi;
phase_Cxy_R_HM_coher_min=abs(phase_Cxy_R_HM(idx))*180/pi;

phase_Cxy_L_HM_mag_max=abs(phase_Cxy_L_HM(idx))*180/pi;
phase_Cxy_L_HM_mag_min=abs(phase_Cxy_L_HM(idx))*180/pi;
phase_Cxy_R_HM_mag_max=abs(phase_Cxy_R_HM(idx))*180/pi;
phase_Cxy_R_HM_mag_min=abs(phase_Cxy_R_HM(idx))*180/pi;

%
L_HM=[LHM_coh,frq_LHM_coh,Cxy_L_HM_coher(LHM_coh),Cxy_L_HM_mag
(LHM_coh),phase_Cxy_L_HM(LHM_coh)*180/pi,Cxy_L,FH_coher_max,Cxy_L_
FH_coher_min,phase_Cxy_L_FH_mean,Cxy_L,FM_coher_max,Cxy_L_FM_coher
_min,phase_Cxy_L_FM_mean,Cxy_L_HM_coher_max,Cxy_L_HM_coher_min,ph
ase_Cxy_L_HM_mean];
%
R_HM=[RHM_coh,frq_RHM_coh,Cxy_R_HM_coher(RHM_coh),Cxy_R_HM_ma
g(RHM_coh),phase_Cxy_R_HM(RHM_coh)*180/pi,Cxy_R,FH_coher_max,Cxy_R
_FH_coher_min,phase_Cxy_R_FH_mean,Cxy_R,FM_coher_max,Cxy_R_FM_coh
er_min,phase_Cxy_R_FM_mean,Cxy_R_HM_coher_max,Cxy_R_HM_coher_min,
phase_Cxy_R_HM_mean];

% Before writing to a text file arrays filled with calculated data
Cellarr(1,:)={leftf,'L','FH',Cxy_L_FH_coher_low_mean,
Cxy_L_FH_coher_low_var, Cxy_L_FH_coher_mid_mean,
Cxy_L_FH_coher_mid_var, Cxy_L_FH_coher_high_mean,
Cxy_L_FH_coher_high_var,phase_Cxy_L_FH_mean, phase_Cxy_L_FH_mean};

Cellarr(2,:)={rightf,'R','FH',Cxy_R_FH_coher_low_var,
Cxy_R_FH_coher_mid_mean, Cxy_R_FH_coher_mid_var,
Cxy_R_FH_coher_high_mean,  Cxy_R_FH_coher_high_var,
phase_Cxy_R_FH_mean};
% %
```

```
Cellarr(3,:)={leftf,'L','FM',Cxy_L_FM_coher_low_mean,
Cxy_L_FM_coher_low_var, Cxy_L_FM_coher_mid_mean,
Cxy_L_FM_coher_mid_var, Cxy_L_FM_coher_high_mean,
Cxy_L_FM_coher_high_var,phase_Cxy_L_FM_mean};

Cellarr(4,:)={rightf,'R','FM',Cxy_R_FM_coher_low_mean,
Cxy_R_FM_coher_low_var, Cxy_R_FM_coher_mid_mean,
Cxy_R_FM_coher_mid_var, Cxy_R_FM_coher_high_mean,
Cxy_R_FM_coher_high_var,phase_Cxy_R_FM_mean};

Cellarr(5,:)={leftf,'L','HM',Cxy_L_HM_coher_low_mean,
Cxy_L_HM_coher_low_var, Cxy_L_HM_coher_mid_mean,
Cxy_L_HM_coher_mid_var, Cxy_L_HM_coher_high_mean,
Cxy_L_HM_coher_high_var,phase_Cxy_L_HM_mean};
Cellarr(6,:)={rightf,'R','HM',Cxy_R_HM_coher_low_mean,
Cxy_R_HM_coher_low_var, Cxy_R_HM_coher_mid_mean,
Cxy_R_HM_coher_mid_var, Cxy_R_HM_coher_high_mean,
Cxy_R_HM_coher_high_var,phase_Cxy_R_HM_mean};
%%
```

% ******** Write Coherence values to file *********

```
%
dlmcell('Freq-domain-coherence_freq_band_mean_results.csv',Cellarr,',','-a');


 end
```

% end of file

*****Check_empty function block********

```
function chk=check_empty(argch)
if isempty(argch)
	chk=0;
else
	chk=argch;
end
```

***** freq_range_chk function block ********

```
function [chk]=freq_range_chk(frekans,coh,level)

switch (level)
	case 'low';
		target_fr=check_empty(frekans(frekans>=0 & frekans<=3));
		target_coh=check_empty(coh(frekans>=0 & frekans<=3));
	case 'mid';
		target_fr=check_empty(frekans(frekans>3 & frekans<=10));
		target_coh=check_empty(coh(frekans>3 & frekans<=10));
	case 'high';
```

```
                target_fr=check_empty(frekans(frekans>10 & frekans<=25));
                target_coh=check_empty(coh(frekans>10 & frekans<=25));
end
                if (target_fr & target_coh)==1;
                        chk=horzcat(target_fr,target_coh);
                elseif xor(target_fr,target_coh)==0;
                        if target_fr==0
                                target_fr=zeros(size(target_coh));
                        else
                                target_coh=zeros(size(target_fr));
                        end
                        chk=horzcat(target_fr,target_coh);
                end
end

%******end of function*****
```

B-4 Calculation of ANOVA Values

```
varnames = {'Gender';'Subject';'Region';'Foot';'Eyes'};
[p,table,stats] = anovan(Maxgain_frq,{Gender Subject Region Foot
Eyes},'model','full','varnames',varnames);

ana='Maxgain_frq';


[c1,m1] = multcompare(stats,'dim', [1]);
% saveas(gcf,strcat(ana,'_dim1'),'fig');
[c2,m2]= multcompare(stats,'dim', [2]);
% saveas(gcf,strcat(ana,'_dim2'),'fig');
[c3,m3] = multcompare(stats,'dim', [3]);
% saveas(gcf,strcat(ana,'_dim3'),'fig');
[c4,m4] = multcompare(stats,'dim', [4]);
% saveas(gcf,strcat(ana,'_dim4'),'fig');
[c5,m5] = multcompare(stats,'dim', [5]);
% saveas(gcf,strcat(ana,'_dim5'),'fig');
[c12,m12]= multcompare(stats,'dim', [1 2]);
% saveas(gcf,strcat(ana,'_dim12'),'fig');
[c13,m13] = multcompare(stats,'dim', [1 3]);
% saveas(gcf,strcat(ana,'_dim13'),'fig');
[c14,m14] = multcompare(stats,'dim', [1 4]);
% saveas(gcf,strcat(ana,'_dim14'),'fig');
[c15,m15] = multcompare(stats,'dim', [1 5]);
% saveas(gcf,strcat(ana,'_dim15'),'fig');
[c23,m23]= multcompare(stats,'dim', [2 3]);
```

```
% saveas(gcf,strcat(ana,'_dim23'),'fig');
[c24,m24] = multcompare(stats,'dim', [2 4]);
% saveas(gcf,strcat(ana,'_dim24'),'fig');
[c25,m25] = multcompare(stats,'dim', [2 5]);
% saveas(gcf,strcat(ana,'_dim25'),'fig');
[c34,m34] = multcompare(stats,'dim', [3 4]);
% saveas(gcf,strcat(ana,'_dim34'),'fig');
[c35,m35] = multcompare(stats,'dim', [3 5]);
% saveas(gcf,strcat(ana,'_dim35'),'fig');
[c134,m134] = multcompare(stats,'dim', [1 3 4]);
% saveas(gcf,strcat(ana,'_dim134'),'fig');
[c135,m135] = multcompare(stats,'dim', [1 3 5]);
% saveas(gcf,strcat(ana,'_dim135'),'fig');
[c123,m123]= multcompare(stats,'dim', [1 2 3]);
% saveas(gcf,strcat(ana,'_dim123'),'fig');
[c124,m124] = multcompare(stats,'dim', [1 2 4]);
% saveas(gcf,strcat(ana,'_dim124'),'fig');
[c125,m125] = multcompare(stats,'dim', [1 2 5]);
% saveas(gcf,strcat(ana,'_dim125'),'fig');
```

VITA

PERSONAL INFORMATION

Surname, Name: Alkan, Okan

Nationality: Turkish (TC)

Date and Place of Birth: 05 August 1970, Bartın

Marital Status: Married

Phone: +90 533 469 99 38

Fax: +90 312 210 44 62

Email: okanalk@gmail.com

EDUCATION

Degree	Institution	Year of Graduation
MS	METU Mechanical Engineering	1996
BS	METU Mechanical Engineering	1993
High School	Cumhuriyet Lisesi, Ankara	1987

WORK EXPERIENCE

Year	Place	Enrollment
1996 -	Başbakanlık	Dept. Manager
1993 -1996	METU Mechanical Engineering Dept.	Research Assistant

FOREIGN LANGUAGES

English

PUBLICATIONS

1. Kaftanoğlu, B., Alkan, O., "Computer Aided Design of Rotary Screen and Conveyor for Solid Waste Processing", Journal of Machine Design and Manufacturing, Vol. 3, No 4, September 1998, 154-160,
2. Okan Alkan · Akbarifar R · Gurses Senih, "Role of the human foot in the erect posture" Poster Presentation, International Society for Posture & Gait Research, Akita-Japan, June 2013

HOBBIES

Scouting, gardening, 3D printing, ballroom dancing